Photomultiplier Handbook

Contents

Page

1. Introduction 3

Early development, photoemitter and secondary-emitter development, applications development, photomultiplier and solid-state detectors compared

2. Photomultiplier Design 10

Photoemission, practical photocathode materials, opaque and semitransparent photocathodes, glass transmission and spectral response, thermionic emission, secondary emission, time tag in photoemission and secondary emission

3. Electron Optics of Photomultipliers 26

Electron-optical design considerations, design methods for photomultiplier electron optics, specific photomultiplier electron-optical configurations, anode configurations

4. Photomultiplier Characteristics 36

Photocathode-related characteristics, gain-related characteristics, dark current and noise, time effects, pulse counting, scintillation counting, liquid scintillation counting, environmental effects

5. Photomultiplier Applications 80

Summary of selection criteria, applied voltage considerations, mechanical considerations, optical considerations, specific photomultiplier applications

Appendix A. Typical Photomultiplier Applications and Selection Guide 119

Appendix B. Glossary of Terms Related to Photomultiplier lubes and Their Applica- 125

Appendix C. Spectral Response Designation Systems 132

Appendix D. Photometric Units and Photometric-to-Radiant Conversion 137

Appendix E. Spectral Response and Source-Detector Matching 143

Appendix F. Radiant Energy and Sources 148

Appendix G. Statistical Theory of Noise in Photomultiplier Tubes 160

Index 177

information furnished by BURLE INDUSTRIES, INC. is believed to be accurate and reliable. However, no responsibility of liability is assumed by BURLE for its use, nor for any infringement of patents or other rights of third parties which may result from its use. No license is granted by implication or otherwise under any patent or other rights of BURLE INDUSTRIES, INC.

BURLE ® and BURLE INDUSTRIES, INC.® are registered trademarks of BURLE TECHNOLOGIES, INC. Marca(s) Registrada(s).

Copyright © 1980 by BURLE TECHNOLOGIES, INC. All rights reserved. No part of this book may be copied or reproduced in any form or by any means -- graphic, electronic, or mechanical or incorporated into any information storage or retrieval system, without the written permission of the copyright owner.

Supersedes PMT-62, 8-80 Printed in U.S.A./ 10-89

TP-136

1 Introduction

The photomultiplier is a very versatile and sensitive detector of radiant energy in the ultraviolet, visible, and near infrared regions of the electromagnetic spectrum. A schematic diagram of a typical photomultiplier tube is given in Fig. 1. The basic radiation sensor is the **photocathode** which is located inside a vacuum envelope. Photoelectrons are emitted and directed by an appropriate electric field to an electrode or **dynode** within the envelope. A number of secondary electrons are emitted at this dynode for each impinging primary photoelectron. These secondary electrons in turn are directed to a second dynode and so on until a final gain of perhaps 10^6 is achieved. The electrons from the last dynode are collected by an **anode** which provides the signal current that is read out.

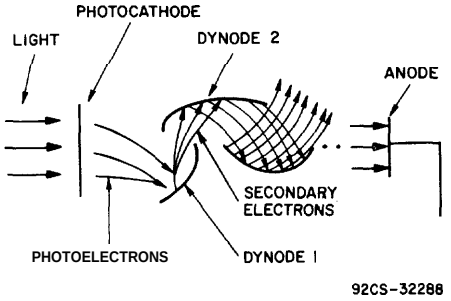

Fig. 1 - Schematic representation of a photomultiplier tube and its operation

For a large number of applications, the photomultiplier is the most practical or sensitive detector available. The basic reason for the superiority of the photomultiplier is the secondary-emission amplification that makes it possible for the tube to approach "ideal" device performance limited only by the statistics of photoemission. Amplifications ranging from 10^3 to as much as 10^8 provide output signal levels that are compatible with auxiliary electronic equipment without need for additional signal amplification. Extremely fast time response with rise times as short as a fraction of a nanosecond provides a measurement capability in special applications that is unmatched by other radiation detectors.

EARLY DEVELOPMENT

The development (history) of the photomultiplier is rooted in early studies of secondary emission. In 1902, Austin and Starke[1] reported that the metal surfaces impacted by cathode rays emitted a larger number of electrons than were incident. The use of secondary emission as a means for signal amplification was proposed as early as 1919.[2] In 1935, Iams and Salzberg[3] of RCA reported on a single-stage photomultiplier. The device consisted of a semicylindrical photocathode, a secondary emitter mounted on the axis, and a collector grid surrounding the secondary emitter. The tube had a gain of about eight. Because of its better frequency response the single-stage photomultiplier was intended for replacement of the gas-filled phototube as a sound pickup for movies. But despite its advantages, it saw only a brief developmental sales activity before it became obsolete.

Multistage Devices

In 1936, Zworykin, Morton, and Malter, all of RCA[4] reported on a multistage photomultiplier. Again, the principal contemplated application was sound-on-film pickup. Their tube used a combination of electrostatic and magnetic fields to direct electrons from stage to stage. A photograph of a developmental sample is given in Fig. 2. Although the magnetic-type photomultiplier provided high gain, it had several difficulties. The adjustment of the magnetic field was very critical, and to change the gain by reducing the applied voltage, the magnetic field also had to be adjusted.

Another problem was that its rather wide open structure resulted in high dark current because of feedback from ions and light developed near the output end of the device. For these reasons, and because of the development of electrostatically focused photomultipliers, commercialization did not follow.

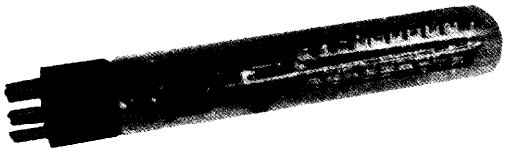

Fig. 2 - Magnetic-type multistage ***photomultiplier*** *reported by Zworykin, Morton, and* ***Malter*** *in 1936.*

The design of multistage electrostatically focused photomultipliers required an analysis of the equipotential surfaces between electrodes and of the electron trajectories. Before the days of high-speed computers, this problem was solved by a mechanical analogue: a stretched rubber membrane. By placing mechanical models of the electrodes under the membrane, the height of the membrane was controlled and corresponded to the electrical potential of the electrode. Small balls were then allowed to roll from one electrode to the next. The trajectories of the balls were shown to correspond to those of the electrons in the corresponding electrostatic fields. Working with the rubber-dam analogue, both J.R. **Pierce**[5] of Bell Laboratories and J.A. **Rajchman**[6] of RCA devices linear arrays of electrodes that provided good focusing properties. Although commerical designs did not result immediately from the linear dynode array, The Rajchmann design with some modifications eventually was, and still is, used in photomultipliers-particularly for high-gain wide-bandwidth requirements.

First Commercial Devices

The first commercially successful photomultiplier was the type 931. This tube had a compact circular array of nine dynodes using electrostatic focusing. The first such arrangement was described by Zworykin and **Rajchman.**[7] Modifications were later reported by Rajchmann and Snyder[8] and by Janes and **Glover**[9], all of RCA. The basic electron-optics of the circular cage was thus well determined by 1941 and has not changed to the present time although improvements have been made in processing, construction, and performance of the 931A product.

The success of the 931 type also resulted from the development of a much improved photocathode, Cs_3Sb, reported by Gorlich[10] in 1936. The first experimental **photo**multipliers had used a Ag-O-Cs **photocath**ode having a typical peak quantum efficiency of 0.4% at 800 nm. (The Ag-O-Cs layer was also used for the dynodes.) The new **Cs_3Sb** photocathode had a quantum efficiency of 12% (higher today) at 400 nm. It was used in the first 931's, both as a photocathode and as a secondary-emitting material for the dynodes.

PHOTOEMITTER AND SECONDARY-EMITTER DEVELOPMENT

Photocathode Materials

Much of the development work on photomultiplier tubes has been concerned with their physical configuration and the related electron optics. But a very important part of the development of photomultiplier tubes was related to the photocathode and secondary-emission surfaces and their processing. RCA was very fortunate during the 1950's and 60's in having on its staff, probably the world's foremost photocathode expert, Dr. A.H. Sommer. His treatise on **Photoemissive Materials**[11] continues to provide a wealth of information to all photocathode process engineers.

Sommer explored the properties of numerous photocathode materials-particularly alkali-antimonides. Perhaps his most noteworthy contribution was the multialkali photocathode (S-20 spectral response). This photocathode, **$Na_2KSb:Cs$,** is important because of its high sensitivity in the red and near infrared; the earlier Cs_3Sb photocathode spectral response barely extends through the visible, although it is very sensitive in the blue where most scintillators emit.

Bialkali photocathodes were also developed by Sommer and have proven to be

better in some applications than the Cs_3Sb photocathode. Thus, the Na_2KSb photocathode has been found to be stable at higher temperatures than Cs_3Sb and, in addition, has a very low dark (thermal) emission. It has been particularly useful in oil-well-logging applications. Another bialkali photocathode, K_2CsSb, is more sensitive than Cs_3Sb in the blue and is, therefore, used by RCA to provide a better match to the NaI:Tl crystals used in scintillation counting.

Dynode Materials

The first secondary-emission material used practically by RCA was the Ag-O-Cs surface. But with the development of the Cs_3Sb material for photocathodes, it was found that this material was also an excellent secondary emitter. Other practical secondary emitters developed during the early years of photomultiplier development were MgO:Cs (often referred to as "silver-magnesium") and BeO:Cs ("copper-beryllium").

In the early 1960's, R.E. Simon[12] while working at the RCA Laboratories developed his revolutionary concept of Negative Electron Affinity (NEA). Electron affinity is the energy required for an electron at the conduction-band level to escape to the vacuum level. By suitably treating the surface of a p-type semiconductor material, the band levels at the surface can be bent downward so that the effective electron affinity is actually negative. Thermalized electrons in the conduction band are normally repelled by the electron-affinity barrier; the advantage of the NEA materials is that these electrons can now escape into the vacuum as they approach the surface. In the case of secondary emission, secondary electrons can be created at greater depths in the material and still escape, thus providing a much greater secondary-emission yield. In the case of photoemission, it has been possible to achieve extended-red and infrared sensitivities greater than those obtainable with any other known materials. The first practical application of the NEA concept was to secondary emission. An early paper by Simon and Williams[13] described the theory and early experimental results of secondary-emission yields as high as 130 at 2.5 kV for GaP:Cs.

APPLICATIONS DEVELOPMENT

Astronomy and Spectroscopy

Early applications of the photomultiplier were in astronomy and spectroscopy. Because the effective quantum efficiency of the photomultiplier was at least ten times that of photographic film, astronomers were quick to realize the photomultiplier tube's advantage. Furthermore, because the output current of the photomultiplier is linear with incident radiation power, the tube could be used directly in photometric and spectrophotometric astronomy. The type 1P28, a tube similar to the 931 but having an ultraviolet-transmitting envelope was particularly useful in spectroscopy. The size and shape of the photocathode were suitable for the detection and measurement of line spectra and the very wide range of available gain proved very useful.[14]

Radar Jammer

A totally unexpected application for the new photomultiplier tube occurred during World War II. The development of radar for detecting and tracking aircraft led to the simultaneous need for wideband electronic-noise sources as radar jammers. Although other sources of noise were tried, the photomultiplier proved to be most successful. The advantage of the tube was its high gain (10^7) and wide band width (several hundred MHz). As a noise source the tube was operated with a non-modulated input light source and with high gain. The output amplifier photoelectric shot noise was "white" and thus indistinguishable from natural noise sources. This application of photomultiplier tubes resulted in production of thousands per month compared with previous production measured in only hundreds per year.

Scintillation Counting

A proliferation of photomultiplier designs followed the invention of the scintillation counter shortly after World War II.[15,16] The photomultiplier tubes were designed with semitransparent photocathodes deposited on an end window which could be coupled directly to the scintillator. The principal scintillator used, NaI doped with thallium, was discovered by Hofstadter[17]. Much of the development work on photomultiplier

tubes during this period was reported by RCA and its competitors in the biannual meetings of the **Scintillation Counter Symposium.** These symposia were reported fully in the IRE (and later the IEEE) **Transactions on Nuclear Science** beginning with the meeting in Washington, January 1948. The scintillation counter became the most important measurement instrument in nuclear physics, nuclear medicine, and radioactive tracer applications of a wide variety.

Headlight Dimmer

During the 1950's, RCA collaborated with the General Motors Company (Guide-Lamp Division) on a successful headlight dimmer. The photoelectric headlight dimmer-first made available only on Cadillacs and Oldsmobiles-basically used a tube similar to the 931A, but redesigned and tested to the auto manufacturer's particular requirements. The optical engineering problem was to sense the oncoming headlights or taillights being followed without responding to street and house lights. Vertical and horizontal angular sensitivity was designed to match the spread of the high beams of the automobile. A red filter was installed in the optical path to provide a better balance between sensitivity to oncoming headlights and to taillamps being followed. The device achieved a remarkable success, probably because of the novelty, and thousands of photomultiplier tubes were used. But today, one rarely sees a headlight dimmer.

Medical Diagnostic Equipment

In recent years two medical applications have used large numbers of photomultiplier tubes and have spurred further developments and improvements. The gamma camera[18] is a sophisticated version of the scintillation counter used medically for locating tumors or other biological abnormalities. A radioactive isotope combined in a suitable compound is injected into the blood stream or ingested orally by the patient. The radioactive material disintegrates and gamma rays are ejected from preferential locations such as tumors or specific organs. A large crystal intercepts the gamma rays and scintillates. Behind the crystal are photomultiplier tubes, perhaps 19, in hexagonal array. The location of the point of scintillation origin is obtained by an algorithm depending upon the individual signals from each of the photomultipliers. Counting is continued until several hundred thousand counts are obtained and the organ in question is satisfactorily delineated. The location of each scintillation is represented by a point on a cathode-ray-tube presentation.

The Computerized Axial Tomographic (CAT) scanner was introduced to this country in 1973. The device uses a pencil or fan-beam of X-rays which rotates around the patient providing X-ray transmission data from many directions. A scintillator coupled to a photomultiplier detects the transmitted beam-as an average photomultiplier current-and a computer stores and computes the cross-section density variation of the patient's torso or skull. The photomultipliers are 1½-inch or 3/4-inch end-on tubes which couple to the scintillator, commonly BGO (bismuth germanate). Each unit is equipped with as many as 600 photomultipliers.

PHOTOMULTIPLIERS AND SOLID-STATE DETECTORS COMPARED

In some applications either a photomultiplier or solid-state detector could be used. The user may make his choice on the basis of factors such as cost, size, or previous experience. In other applications, the choice may be dictated by fundamental properties of the photomultiplier or the solid-state detector. A discussion follows of some of the common applications favoring one or the other detector with reasons for the choice. A summary presents the principal considerations the user must apply in making a choice in an application for which he requires a photodetector. This information should be particularly useful to the designer who is not well acquainted in this field.

Photomultiplier Features

The photomultiplier is unique in its ability to interface with a scintillation crystal and not only count the scintillations but measure their magnitude and time their arrival. Most scintillators emit in the blue and near ultraviolet. This spectral output obviously favors the photomultiplier having a photocathode with high quantum efficiency in the short wavelength range. On the other hand a silicon p-i-n diode is relatively poor in this part of the spectrum but does best in the red and near infrared. The most important factor,

probably, is the gain of the photomultiplier which permits the measurement of the very small signals from individual scintillations with a good signal-to-noise ratio, limited primarily by the statistics of the number of photoelectrons per pulse. Finally, the short rise time of the photomultiplier using fast scintillators permits time-of-flight measurements to be made in nuclear physics.

Although the CAT scanner equipment also uses photomultipier tubes to detect the scintillations in bismuth germanate (BGO) crystals, the situation is somewhat different from the scintillation counting applications discussed above. In the CAT scanner the X-rays produce a broad band of pulse heights and no attempt is made to single out and detect single scintillation events. The photomultiplier is used in an analog mode to detect the level of radiation incident on the crystal. In the CAT scan operation the typical machine scans the patient in a few seconds and the level of irradiance from the crystal onto the photomultiplier is relatively high so that only a relatively low gain photomultiplier is required. Furthermore, the speed of response requirement for the photomultiplier is relatively modest-perhaps a few hundred microseconds. Still, the principal advantage of using a photomultiplier in this application for the detection of the radiant signal is its good signal-to-noise ratio. This ratio is very important to the patient because a reduction in its signal-to-noise ratio would have to be made up for with an increased X-ray dose. Nevertheless, there is interest and development activity aimed at replacing the photomultiplier with silicon p-i-n detectors. Two factors could favor the alternate use of a silicon cell: (1) a better scintillator (BGO is almost an order of magnitude less sensitive than NaI:Tl; (2) a faster scanning machine (a very desirable technological advance because is would minimize effects of body motions). Both of these factors would result in a larger photocurrent and could bring the signal level for the silicon detector to the point where the fundamental signal-to-noise ratio from the X-ray source would not be degraded. Such developments may be anticipated because the silicon detector would also have the advantage of smaller size and perhaps lower cost.

As a result of increasing concern about environment, pollution monitoring is becoming another important application for photomultiplier tubes. For example, in the monitoring of NO_X the gas sample is mixed with O_3 in a reaction chamber. A chemiluminescence results which is measured using a near-infrared-pass filter and a photomultiplier having an S-20 spectral response. Although the radiation level is very low, NO can be detected down to a level of 0.1 ppm. The advantage of the photomultiplier in this application is again the high gain and good signal-to-noise ratio (the photomultiplier is cooled to 0°C to reduce dark-current noise) even though the radiation spectrum is observed near the threshold of the S-20 spectral range.

In another pollution-monitoring application, SO_2 is detected down to a level of 0.002 ppm. Here, the sample containing SO_2 is irradiated with ultraviolet and the excited SO2 molecules fluoresce with blue radiation that is detected with a combination of a narrow-band filter and photomultiplier. Very weak signals are detected and again it is the high gain, good signal-to-noise ratio and, in addition, good blue sensitivity which makes the detection and measurement of small contaminations of SO_2 possible.

Spectroscopy is one of the very early applications for photomultipliers. The wide range of radiation levels encountered is readily handled by the approximately logarithmic gain variation of the photomultiplier with voltage. At very low signal levels, the signal-to-noise capability of the photomultiplier is essential. Because photomultiplier spectral response (with quartz or ultraviolet-transmitting-glass windows) covers the range from ultraviolet to near infrared, the photomultiplier is the logical choice for spectroscopic applications, except in the infrared region of the spectrum.

Photocell* Features

Because of their small size and low cost, CdSe and CdS type photocells are the logical selection for applications such as automatic exposure control in photographic cameras or various inspection and counting requirements.

*"Photocell" is used here to indicate a photosensitive device in which the charge transport takes place through a solid as compared with "photo*tube*" in which the charge transport is through a vacuum.

Many p-i-n silicon cells are used in combination with lasers or LED's (light emitting diodes). Here, one of the principal advantages of the silicon cell is its good response in the near infrared out to 1100 nm. In combination with the Nd:YAG laser emitting at 1060 nm, the silicon cell is used widely in laser ranging and laser tracking. A similar application utilizes an LED emitting near 900 nm with a silicon cell for automatic ranging for special camera equipment. Size and infrared sensitivity are again the important qualifications.

A rapidly growing application for photocells is for fiber-optic communication systems. LED's are coupled to the fibers and the detector may be a p-i-n diode or, for a better signal-to-noise ratio, a silicon avalanche diode. The qualifying attributes for the choice of detector are size, near infrared sensitivity, adequate speed of response, and good signal-to-noise ratio.

Smoke detectors now use large numbers of LED's and p-i-n silicon cells. Again size, cost, and infrared sensitivity are the important qualifications.

Characteristics Comparison Summary

Spectral Response. Photomultipliers can be obtained with good spectral sensitivity in the range 200 to 900 nm. Silicon cells have rather poor blue sensitivity, but are excellent out to 1100 nm. In general, then, the photomultiplier is to be preferred for applications involving the shorter wavelengths, although other factors may override this consideration.

Speed of Response. If very fast response is required, the photomultiplier is usually the best choice of a detector. Photomultipliers are available with rise times (10 to 90%) of 1 or 2 nanoseconds using a **50-ohm** load. The inherent rise time of silicon cells may be in the range 10 to 20 nanoseconds, depending upon the area of the cell. However, because of the cell's capacitance, the effective rise time is much longer depending upon the choice of load resistance. For example, with a **1-megohm** load resistance, the rise time may be of the order of 20 microseconds. A fairly large load resistance must be chosen to maintain good signal-to-noise characteristics for the silicon cell. Silicon avalanche photodiodes can have rise times as short as 2 nanoseconds. Gain for an avalanche photodiode can be of the order of 100, but the sensitive area is small-about 0.5 square millimeter.

Sensitive Area. Photomultiplier tubes are made in a variety of sizes so that many different optical configurations can be accommodated. The largest photocathode area available in commercial RCA **photomultiplier** tubes has a nominal diameter of 5 inches and a minimum useful area of 97 square centimeters. By way of contrast, the $^1/_2$-inch side-on photomultiplier has a projected **photocathode** area of 0.14 square centimeter. Silicon p-i-n diodes are available with sensitive areas generally not larger than 1 square centimeter; and avalanche silicon cells, 0.005 square centimeter. In many applications, a fairly large area is required, e.g., coupling to a cathode-ray tube or a large scintillator. This requirement generally indicates the use of a photomultiplier tube. Silicon cells are at an advantage when the source is small for direct coupling or for lens imaging.

Temperature. Photomultipliers are generally not rated for operation at temperatures higher than 75° C. Exceptions are **photomultipliers** having a Na_2KSb photocathode. This bi-alkali photocathode can tolerate temperatures up to 150° C or even higher for short cycles. In oil-well logging measurements this consideration is important. Photocathode sensitivities and gain change very little with temperature, but dark current does increase rapidly. Dark currents at room temperature are of the order of 10^{-15} ampere at the **photocathode** and double about every 10° C. Silicon cells are rated from – 50 to 80° C. Sensitivities are also relatively independent of temperature. But dark current which may be 10^{-7} ampere at room temperature, also tends to double about every 10° C.

Signal-to-Noise Ratio. At very low light levels, the limitation to detection and measurement is generally the signal-to-noise ratio. One way of describing the limit to detection is to state the Equivalent Noise Input **(ENI)** or the Noise Equivalent Power **(NEP).** The NEP is the power level into the device which provides a signal just equal to the noise. Most often the bandwidth is specified as 1 hertz and the wavelength of the measurement is at the peak of the spectral responsivity. ENI is the same type of specification except the unit instead of power may

be luminous flux.

For a photomultiplier such as one used for spectroscopy, the NEP at room temperature at 400 nm is about 7 x 10^{-16} watts, or the EN1 is about 7 x 10^{-13} lumens. Both specifications are for a l-hertz ban
For a p-i-n silicon photocell, the NEP at 900 nanometers may be of the order of 2 x 10^{-13} watts, or the EN1 of 1.5 x 10^{-11} lumens. Both values are for a l-hertz bandwidth. Thus, the photomultiplier is clearly superior in this category. Also it should be pointed out that the silicon diode must be coupled into a load resistance of about 5 megohms in order to avoid noise domination from the coupling resistor. Unfortunately, this large resistance then increases the effective rise time of the silicon device to about 100 microseconds. The NEP of a silicon avalanche photodiode is about 10^{-14} watt at 900 nanometers or the ENI is 8 x 10^{-13} lumens, both for a l-Hz bandwidth. The lumen in these descriptions is that from a tungsten source operating at 2856 K color temperature. Peak emission for such a source is near 1000 nm and thus closely matches the spectral peak of the silicon devices.

Gain. A photomultiplier can have a gain factor, by which the fundamental photocathode signal is multiplied, of from 10^{3} to 10^{8}. Silicon avalanche photodiodes have a gain of about 100. Silicon p-i-n diodes have no gain. The high gain of the photomultiplier frequently eliminates the need of special amplifiers, and its range of gain controlled by the applied voltage provides flexibility in operation.

Stability. Photomultiplier tubes are not noted for great stability although for low anode currents and careful operation they are satisfactory. When the light level is reasonably high, however, the very good stability of the silicon p-i-n cell is a considerable advantage. The silicon cell makes a particularly good reference device for this reason. In fact, the National Bureau of Standards has been conducting special calibration transfer studies using p-i-n silicon diodes.

REFERENCES

1. H. Bruining, **Physics and applications of secondary electron emission, (McGraw-**Hill Book Co., Inc.; 1954).
2. J. Slepian, U.S. Patent 1, 450, 265, April 3, 1923 (Filed 1919).
3. H. E. Iams and B. Salzberg, "The secondary emission phototube," **Proc. IRE,** Vol. 23, pp. 55-64 (1935).
4. V.K. Zworykin, G.A. Morton, and L. Malter, "The secondary-emission multipli - er-a new electronic device," **Proc.** IRE, Vol. 24, pp. 351-375 (1936).
5. J.R. Pierce, "Electron-multiplier design," **Bell Lab. Record,** Vol. 16, pp. 305-309 (1938).
6. J.A. Rajchman, "Le courant residue1 dans les multiplicateurs d'electrons **elec**trostatiques," These L'Ecole Polytechnique Federale (Zurich, 1938).
7. V.K. Zworykin and J.A. Rajchman, "The electrostatic electron multiplier, **Proc. IRE,** Vol. 27, pp. 558-566 (1939).
8. J.A. Rajchman and R.L. Snyder, "An electrostatically focused multiplier phototube," Electronics, Vol. 13, p. 20 (1940).
9. R.B. Janes, and A.M. Glover, "Recent developments in phototubes," **RCA Review,** Vol. 6, pp. 43-54 (1941). Also, A.M. Glover, "A review of the development of sensitive phototubes," **Proc. IRE,** Vol. 29, pp. 413-423 (1941).
10. P. Gorlich, "Uber zusammengesetzte, durchsichtige Photokathoden," **2. Physik,** Vol. 101, p. 335 (1936).
11. A.H. Sommer, **Photoemissive materials,** John Wiley and Sons; 1968.
12. R.E. Simon, **Research in electron emission from semiconductors,** Quarterly Report, Contract DA 36-039-AMC-02221 (E) (1963).
13. R.E. Simon and B.F. Williams, "Secondary-electron emission," **IEEE Trans. Nucl. Sci.,** Vol. NS-15, pp. 166-170 (1968).
14. M.H. Sweet, "Logarithmic photomultiplier tube photometer," **JOSA,** Vol. 37, p. 432 (1947).
15. H. Kallmann, **Natur u Technik** (July 1947).
16. J.W. Coltman and F.H. Marshall, "A photomultiplier radiation detector," **Phys. Rev.,** Vol. 72, p. 582 (1947).
17. R. Hofstadter, "Alkali halide scintillation counters," **Phys. Rev.,** Vol. 74, p. 100 (1948).
18. H.O. Anger, "Scintillation camera", **Rev. Sci. Instr.,** Vol. 29, pp. 27-33 (1958).

2. Photomultiplier Design

PHOTOEMISSION

The earliest observation of a photoelectric effect was made by Becquerel in 1839. He found that when one of a pair of electrodes in an electrolyte was illuminated, a voltage or current resulted. During the latter part of the 19th century, the observation of a photovoltaic effect in selenium led to the development of selenium and cuprous oxide photovoltaic cells.

The emission of electrons resulting from the action of light on a photoemissive surface was a later development. Hertz discovered the photoemission phenomenon in 1887, and in 1888 Hallwachs measured the photocurrent from a zinc plate subjected to ultraviolet radiation. In 1890, Elster and Geitel produced a forerunner of the vacuum phototube which consisted of an evacuated glass bulb containing an alkali metal and an auxiliary electrode used to collect the negative electrical carriers (photoelectrons) emitted by the action of light on the alkali metal.

Basic Photoelectric Theory

The modern concept of photoelectricity stems from Einstein's pioneer work for which he received the Nobel Prize. The essence of Einstein's work is the following equation for determining the maximum kinetic energy E of an emitted photoelectron:

$$E = mv^2/2 = h\nu - \phi \qquad (1)$$

Eq. (1) shows that the maximum energy of the emitted photoelectron $mv^2/2$ is proportional to the energy of the light quanta $h\nu$ less the energy ϕ (the work function) which must be given to an electron to allow it to escape the surface of a metal. For each metal, the photoelectric effect is characterized by a value of ϕ, which is usually expressed in electron-volts.

In the energy diagram for a metal shown in Fig. 3, the work function represents the energy which must be given to an electron at the top of the energy distribution to raise it to the level of the potential barrier at the metal-vacuum interface.

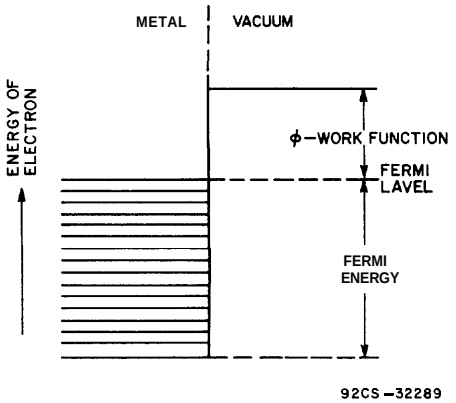

Fig. 3 - Energy mode/ for a *metal showing the relationship of the work function and the Fermi level.*

According to the quantum theory, only one electron can occupy a particular quantum state of an atom. In a single atom, these states are separated in distinct "shells"; normally only the lower energy states are filled. In an agglomeration of atoms, these states are modified by interaction with neighboring atoms, particularly for the outermost electrons of the atom. As a result, the outer energy levels tend to overlap and produce a continuous band of possible energy levels, as shown in Fig. 3.

The diagram shown in Fig. 3 is for a temperature of absolute zero; all lower energy levels are filled. As the temperature is increased, some of the electrons absorb thermal energy which permits them to occupy

scattered states above the maximum level for absolute zero. The energy distribution of electrons in a particular metal is shown in Fig. 4 for several different temperatures. At absolute zero, all the lower states are occupied up to the Fermi level. At higher temperatures, there is some excitation to upper levels. The electron density at a particular temperature is described by the Fermi-Dirac energy-distribution function, which indicates the probability of occupation f for a quantum state having energy E:

$$f = \frac{1}{1 + \exp[(E - E_f)/kT]} \qquad (2)$$

When E is equal to E_f, the value of f is 1/2. It is customary to refer to the energy of level E_f, for which there is a 50-per-cent probability of occupancy, as the Fermi level. At absolute zero, the Fermi level corresponds to the top of the filled energy distribution.

If the energy derived from the radiant energy is just sufficient to eject an electron at the Fermi level, the following relation exists:

$$h\nu_0 = \phi \qquad (3)$$

ν_0 the threshold frequency of the exciting radiation, is related to the long-wavelength limit λ_0 and the velocity of light c as follows:

$$\lambda_0 = c/\nu_0 \qquad (4)$$

The relationship may be rewritten to relate the long-wavelength limit to the work function, as follows:

$$\lambda_0 = 1240/\phi \quad \text{nm} \qquad (5)$$

Because some of the electrons occupy states slightly higher than the Fermi level, as shown in Fig. 4, excitation of these electrons produces an extended response at the red threshold of the spectral-response characteristic. As a result, there is no abrupt red threshold at normal temperatures, and the true work function cannot be obtained in a simple manner from the spectral-response measurement. However, a universal function devised by Fowler can be used to predict the shape of the spectral-response curve near the threshold; the work function can then be calculated from these data.

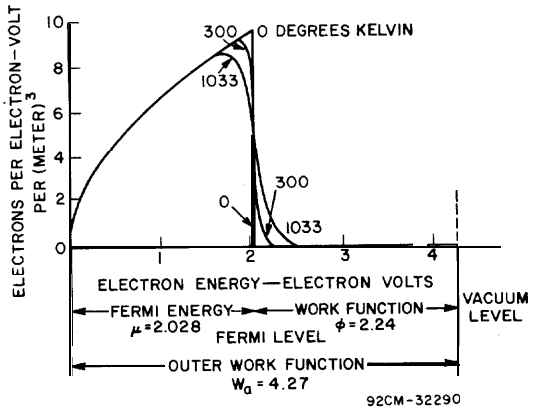

fig. 4 - Energy distribution of conduction electrons in potassium at temperatures of 0, 200, and 1033 degrees Kelvin based on elementary Sommerfeld theory. (ref. 19)

Work Function and Spectral Response

Measurement of the work function and spectral response for clean metal surfaces has been of considerable importance in the development of photoelectric theory.

Work functions for pure metals are in the range 2 to 5 electron-volts. (See A.H. Sommer, Ref. 11, Table 3.)

Fig. 5 shows spectral-response curves for the alkali metals. The curves indicate a regular progression of the wavelength for maximum response with atomic number. The most red-sensitive of these metals is cesium, which is widely used in the activation of most commercial phototubes.

The energy distribution of emitted photoelectrons has been measured for a number of metals and photosurfaces. Typical results are shown in Fig. 6 for a potassium film of 20 molecular layers on a base of silver.[20] The maximum emission energy corresponds to that predicted by the Einstein photoelectric equation.

Quantum Efficiency

Because a quantum of radiation is necessary to release an electron, the photoelectric current is proportional to the intensity of the radiation. This first law of photoelectricity has been verified experimentally over a wide range of light intensities. For most materials, the quantum efficiency is very low; on the best sensitized commercial photosurfaces, the maximum yield reported is as high as one electron for three light quanta.

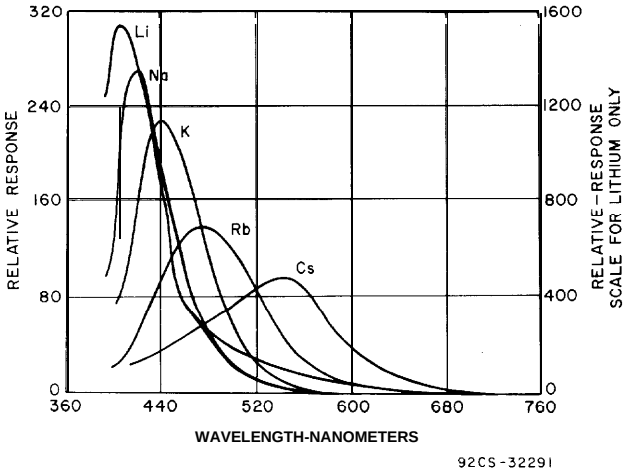

Fig. 5 - Spectral-response characteristics for the alkali metals showing ***regular progression*** *in the order of the periodic table. (ref. 19)*

An ideal photocathode has a quantum efficiency of 100 per cent; i.e., every incident photon releases one photoelectron from the material into the vacuum. All practical photoemitters have quantum efficiencies below 100 per cent. To obtain a qualitative understanding of the variations in quantum efficiency for different materials and for different wavelengths or photon energies, it is useful to consider photoemission as a process involving three steps: (1) absorption of a photon resulting in the transfer of energy from photon to electron, (2) motion of the electron toward the material-vacuum interface, and (3) escape of the electron over the potential barrier at the surface into the vacuum.

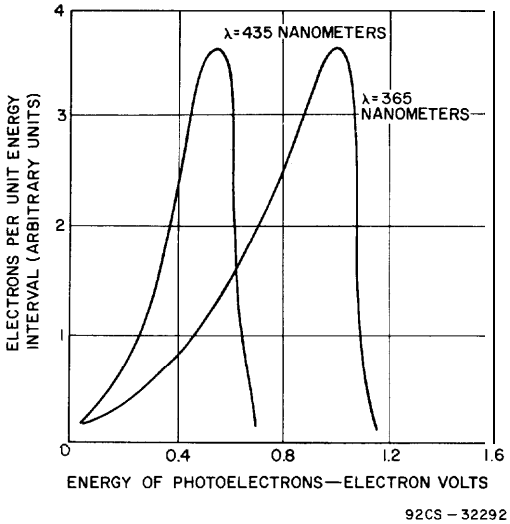

Fig. 6 - Energy distribution of photoelectrons from a potassium film. (ref. ***20****)*

Energy losses occur in each of these steps. In the first step, only the absorbed portion of the incident light is effective and thus losses by transmission and reflection reduce the quantum efficiency. In the second step, the photoelectrons may lose energy by collision with other electrons (electron scattering) or with the lattice (phonon scattering). Finally, the potential barrier at the surface prevents the escape of some electrons.

Metallic and Semiconductor Materials

The energy losses described vary from material to material, but a major difference between metallic and semiconducting materials makes separate consideration of each of these two groups useful. In metals, a large fraction of the incident visible light is reflected and thus lost to the photoemission process. Further losses occur as the photoelectrons rapidly lose energy in collisions with the large number of free electrons in the metal through electron-electron scattering. As a result, the escape depth, the distance from the surface from which electrons can reach the surface with sufficient energy to overcome the surface barrier, is small, and is typically a few nanometers. Finally, the

work function of most metals is greater than three electron-volts, so that visible photons which have energies less than three electron-volts are prevented from producing electron emission. Only a few metals, particularly the alkali ones, have work-function values low enough to make them sensitive to visible light. Because of the large energy losses in absorption of the photon and in the motion of the photoelectron toward the vacuum (the first and second steps described above), even the alkali metals exhibit very low quantum efficiency in the visible region, usually below 0.1 per cent (one electron per 1000 incident photons). As expected, higher quantum efficiencies are obtained with higher photon energies. For 12-electron-volt photons, quantum yields as high as 10 per cent have been reported.

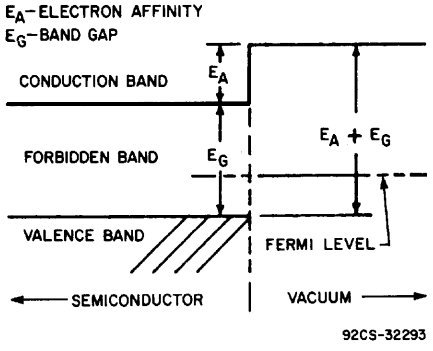

Fig. 7 - Simplified semiconductor energy band model.

The concept of the energy-band models that describe semiconductor photoemitters is illustrated in its simplest form in Fig. 7. Electrons can have energy values only within well defined energy bands which are separated by forbidden-band gaps. At 0 K, the electrons of highest energy are in the so-called valence band and are separated from the empty conduction band by the bandgap energy E_G. The probability that a given energy level may be occupied by an electron is described by Fermi-Dirac statistics and depends primarily on the difference in energy between the level under consideration and Fermi level. As a first approximation, it may be said that any energy levels which are below the Fermi level will be filled with electrons, and any levels which are above the Fermi level will be empty. At temperatures higher than 0 K, some electrons in the valence band have sufficient energy to be raised to the conduction band, and these electrons, as well as the holes in the valence band created by the loss of electrons, produce electrical conductivity. Because the number of electrons raised to the conduction band increases with temperature, the conductivity of semiconductors also increases with temperature. Light can be absorbed by valence-band electrons only if the energy of the photon is at least equal to the band-gap energy E_G. If, as a result of light absorption, electrons are raised from the valence band into the conduction band, photoconductivity is achieved. For photoemission, an electron in the conduction band must have energy greater than the electron affinity E_A. The additional energy E_A is needed to overcome the forces that bind the electron to the solid, or, in other words, to convert a "free" electron within the material into a free electron in the vacuum. Thus, in terms of the model of Fig. 7, radiant energy can convert an electron into an internal photoelectron (photoconductivity) if the photon energy exceeds E_G and into an external photoelectron (photoemission) if the photon energy exceeds $(E_G + E_A)$. As a result, photons with total energies E_p less than $(E_G + E_A)$ cannot produce photoemission.

The following statements can therefore be made concerning photoemission in semiconductors. First, light absorption is efficient if the photon energy exceeds E_G. Second, energy loss by electron-electron scattering is low because very few free electrons are present; thus, energy loss by phonon scattering is the predominant loss mechanism. The escape depth in semiconductors is therefore much greater than in metals, typically of the order of tens of nanometers. Third, the threshold wavelength, which is determined by the work function in metals, is given by the value of $(E_G + E_A)$ in semiconductors. Synthesis of materials with values of $E_G + E_A$) below 2 electron-volts has demonstrated that threshold wavelengths longer than those of any metal can be obtained in a semiconductor. Semiconductors, therefore, are superior to metals in all three steps of the photoemissive process: they absorb a much higher fraction of the incident light, photoelectrons can escape from a

greater distance from the vacuum interface, and the threshold wavelengths can be made longer than those of a metal. Thus, it is not surprising that all photoemitters of practical importance are semiconducting materials.

Negative-Electron-Affinity Materials [20a]

In recent years, remarkable improvements in the photoemission from semiconductors have been obtained through deliberate modification of the energy-band structure. The approach has been to reduce the electron affinity, E_A, and thus to permit the escape of electrons which have been excited into the conduction band at greater depths within the material. Indeed, if the electron affinity is made less than zero (the vacuum level lower than the bottom of the conduction band, a condition described as "negative electron affinity" and illustrated in Fig. **8),** the escape depth may be as much

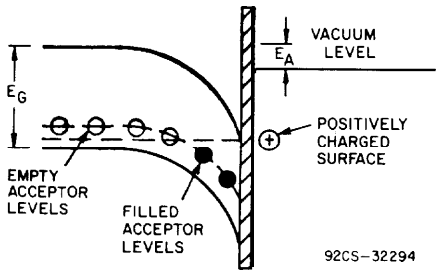

Fig. 8 - Semiconductor energy-band model showing **negative** *electron affinity.*

as 100 times greater than for the normal material. The escape depth of a photoelectron is limited by the energy loss suffered in phonon scattering. Within a certain period of time, of the order of 10^{-12} second, the electron energy drops from a level above the vacuum level to the bottom of the conduction band from which it is not able to escape into the vacuum. On the other hand, the electron can stay in the conduction band in the order of 10^{-10} second without further loss of energy, i.e., without dropping into the valence band. If the vacuum level is below the bottom of the conduction band, the electron will be in an energy state from which it can escape into the vacuum for a period of time that is approximately 100 times longer than if an energy above the bottom of the conduction band is required for escape, as in the materials represented by Fig. 7. Therefore, a material conforming to the conditions of Fig. 8 has greatly increased escape depth. Under such circumstances, the photosensitivity is significantly enhanced. Substantial response is observed even for photons with energies close to that of the band gap where the absorption is weak. Efficient photoemission in this case results only because of the greater escape depth.

The reduction of the electron affinity is accomplished through two steps. First, the semiconductor is made strongly p-type by the addition of the proper "doping" agent. For example, if gallium arsenide is the host material, zinc may be incorporated into the crystal lattice to a concentration of perhaps 1,000 parts per million. The zinc produces isolated energy states within the forbidden gap, near the top of the valence band, which are normally empty, but which will accept electrons under the proper circumstances. The p-doped material has its Fermi level just above the top of the valence band. The second step is to apply to a semiconductor a surface film of an electropositive material such as cesium. Each cesium atom becomes ionized through loss of an electron to a p-type energy level near the surface of the semiconductor, and is held to the surface by electrostatic attraction.

The changes which result in the energy-band structure are two-fold. In the first place, the acceptance of electrons by the p-type impurity levels is accompanied by a downward bending of the energy bands. This bending can be understood by observing that a filled state must be, in general, below the Fermi level; the whole structure near the surface is bent downward to accomplish this result. In the second place, the potential difference between the charged electropositive layer (cesium) and the body charge (filled zinc levels) results in a further depression of the vacuum level as a result of a dipole moment right at the surface.

Another way to describe the reduction of the electron affinity is to consider the surface of the semiconductor as a capacitor. The charge on one side of the capacitor is represented by the surface layer of cesium ions; the other charge is represented by the region of filled acceptor levels. The reduction in the electron affinity is exactly equal to the potential difference developed across the capacitor.

In a more rigorous analysis, the amount by which the energy bands are bent is found to be approximately equal to the band-gap, and the vacuum level is lowered until the absorption level of the electropositive material is essentially at the top of the valence band.

PRACTICAL PHOTOCATHODE MATERIALS

Research on commercially useful photoemitters has been directed primarily toward developing devices sensitive to visible radiation. The first important commercial photosurface was silver-oxygen-cesium. This surface, which provides a spectral response designated S-l, is sensitive throughout the entire visible spectrum and into the infrared. Although it has rather low sensitivity and high dark emission, the good response in the red and near-infrared still recommends its use in special applications although other photocathodes are more generally used in photomultipliers today.

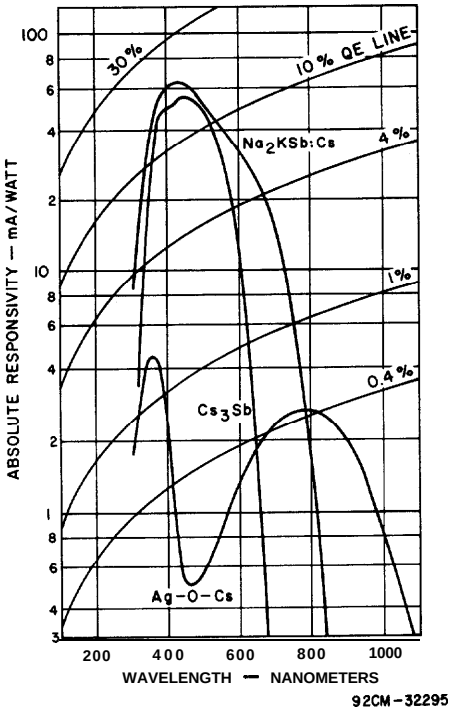

*Fig. 9 - Typical spectra/-response curves, with 0080 lime-glass window for (a) **silver**-oxygen-cesium (Ag-O-Cs), (b) **cesium**-antimony (Cs_3Sb), (c) multialkali or trialkali **(Na_2KSb:Cs***

*The terminology **":Cs"** indicates trace quantities of the element.

The photocathodes most commonly used in photomultipliers are cesium-antimony (Cs_3Sb), multialkali or trialkali (Na_2KSb:Cs),* and bialkali (K_2CsSb). Another bialkali photocathode **(Na_2KSb)** is particularly useful at higher operating temperatures because of its stability. Recently, the rubidium-cesium-antimony (probably **Rb_2** Cs Sb) photocathode has been introduced because of its favorable blue sensitivity. Typical spectral response curves for these materials are shown in Figs. 9 and 10. Additional information about these and other photocathodes of practical importance is shown in Table I.

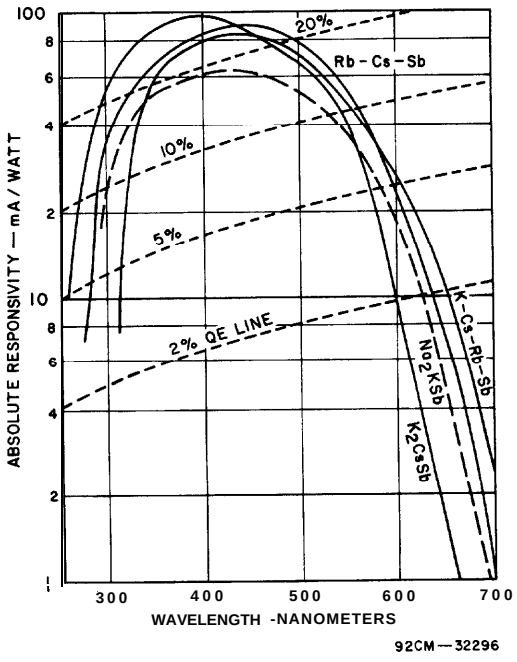

*Fig. **10** - Typical spectral-response curves for various photocathodes useful in scintillation counting applications. The variation in the cutoff at the low end is due to the use of different envelope materials.*

The long-wavelength response of the **multi**alkali photocathode has been extended by processing changes including the use of an increased photocathode-film thickness at the expense of the short-wavelength response. Fig. 11 shows two typical spectral-response curves of the ERMA types (Extended Red Multi-Alkali) II and III compared with the S-20 response of the conventionally processed multialkali photocathode.

Table I
Nominal Composition and Characteristics of Various Photocathodes

Nominal Composition	Type of Photo-cathode	Envelope Material[a]	JEDEC Response Designation	Conversion Factor[b] (lumen/ watt)	Luminous Respon-sivitv (uA/lumen)	Wave-length of Maximum Response	Respon-sivitv (mA/watt)	Quantum Efficiency (percent)	Dark Emission at 25° C (fA/cm^2)
Cs_3Sb	0	0080	S-4	950	40	380	38	12	0.2
Cs_3Sb	0	9741	S-5	1244	40	340	50	18	0.3
Cs3Sb	S	0080	S-11	857	70	400	60	19	3
Na_2KSb	S	7056	S-24	1250	40	380	50	16	.0003
Na_2KSb	S	Sapphire		1400	43	380	60	19	.0003
K_2CsSb	0	0080		938	60	380	56	18	
K_2CsSb	0	7740		1083	60	400	65	20	.02
K_2CsSb	S	B270		1111	90	380	100	33	.02
K_2CsSb	S	0080		1120	80	380	90	29	.02
K_2CsSb	S	7740		1140	71	420	82	24	
K_2CsSb	S	9741		1240	56	380	70	23	.02
Rb_2CsSb	S	0080		948	100	420	95	28	.08
Na_2KSb:Cs	0	9741		510	75	380	38	12	
Na_2KSb:Cs	S	7740	ERMA III[c]	160	180	575	29	6	.3
Na_2KSb:Cs	S	0080	ERMA II[c]	250	200	550	50	11	
Na_2KSb:Cs	S	0080	S-20	480	135	390	65	21	0.4
Na_2KSb:Cs	S[d]	0080		230	300	530	70	16	1.2
Na_2KSb:Cs	S	7056		432	117	420	51	15	
GaAs: Cs-0	O[e]	9741		115	720	800	80	12	92.

a Numbers refer to the following glasses:
0080 - Corning Lime Glass
9741 - Corning Ultraviolet Transmitting Glass
7056 - Coming Borosilicate Glass
7740 - Corning Pyrex Glass
B270 - Schott BK270

b These conversion factors are the ratio of the radiant responsivity at the peak of the spectral response characteristic in amperes per watt to the luminous responsivity in amperes per lumen for a tungsten lamp operated at a color temperature of 2856 K.

c A BURLE designation for "Extended-Red Multialkali."

d Reflecting substrate.

e Single crystal.

0 = Opaque

S = Semitransparent

The negative-electron-affinity materials described earlier are used in both opaque and semitransparent photocathodes. Spectral response curves for GaAs:Cs-O and InGaAs:Cs-O are shown in Fig. 12. There has been considerable interest in detectors for 1060 nm, the wavelength of the Nd:YAG laser. For comparison of sensitivities at this wavelength, the spectral response of the Ag-O-Cs photocathode is also shown. The InGaAs:Cs-O photocathode has the higher responsivity at 1060 nm. The NEA photocathodes are generally fairly small compared with the large semitransparent photocathodes used for scintillation counting. Stability, especially for the longer-wave-length NEA photocathodes, is a problem unless the photomultiplier output current are kept low.

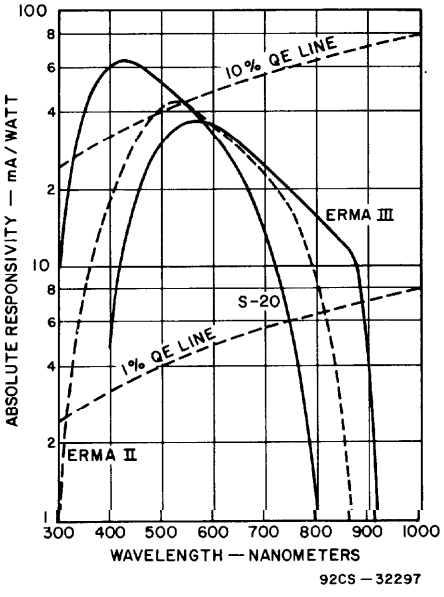

Fig. 11 - Typical spectral-response curves for Extended Red Multi-Alkali (ERMA) photocathodes ERMA II and ERMA III in comparison with the standard S-20 response.

OPAQUE AND SEMITRANSPARENT PHOTOCATHODES

Photocathodes may be classified as opaque or semitransparent. In the opaque photocathode, the light is incident on a thick photoemissive material and the electrons are emitted from the same side as that struck by the radiant energy. In the second type, the semitransparent photocathode, the photoemissive material is deposited on a transparent medium so that the electrons are emitted from the side of the photocathode opposite the incident radiation.

Because of the limited escape depth of photoelectrons, the thickness of the semitransparent photocathode film is

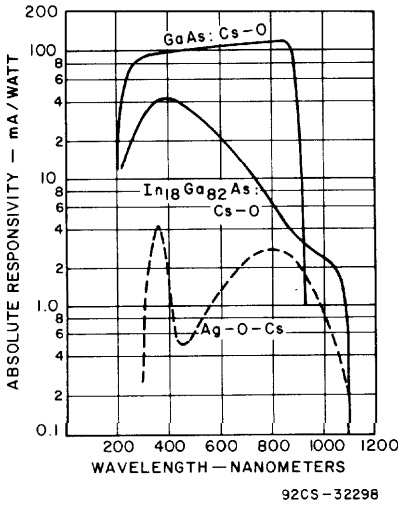

Fig. 12 - Spectra/ response characteristics for GaAs:Cs-O and $In_{18}Ga_{82}As$:Cs-O compared with the S-1 characteristic (Ag-O-Cs).

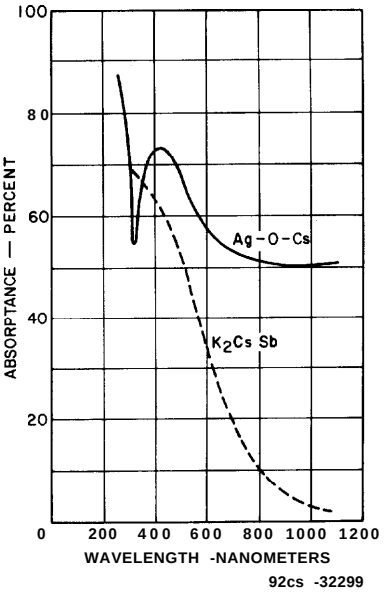

Fig. 13 - Spectral absorptance of the Ag-O-Cs and the K_2CsSb semitransparent photocathodes.

critical. If the film is too thick, much of the incident radiant energy is absorbed at a distance from the vacuum interface greater than the escape depth; if the film is too thin, much of the incident radiant energy is lost by transmission.

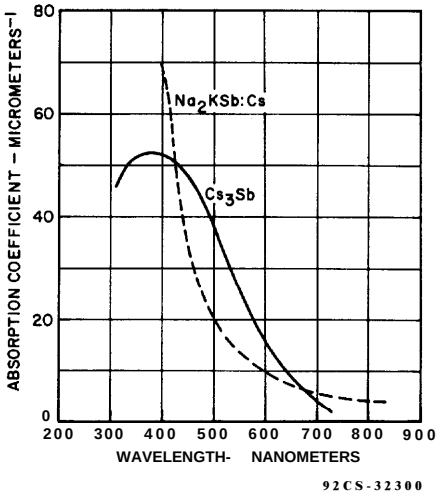

Fig. 14 - Spectral absorption coefficient data for semitransparent Cs_3 and Na_2KSb:Cs photocathodes.

The radiant spectral flux absorption of a semitransparent photocathode varies with wavelength as illustrated in Figs. 13 and 14. The ordinate in Fig. 13 is **absorptance** which is defined as the ratio of the radiant flux absorbed by the layer to that incident upon it. (**Absorptance** plus **reflectance** plus **transmittance** add to unity.) The data shown in Fig. 14 are spectral absorption coefficients. The **flux, ϕ, transmitted through a thickness, d,** of the photocathode layer is given by

$$\phi = \phi_0 e^{-\alpha d} \qquad (6)$$

where α is the absorption coefficient. Note that the data in Fig. 14 are given in units of micrometers - 1 so that in Eq. 6, d must be given in micrometers. Typical thickness of a Na_2KSb:Cs photocathode is about 0.030 μm. Thus, at 400 nm the photocathode absorbs 87% of the flux which is not reflected. The spectral response of semitransparent photocathodes can be controlled to some extent by thickness variation. With increasing thickness in the case of alkali antimonides, blue response decreases and red response increases.

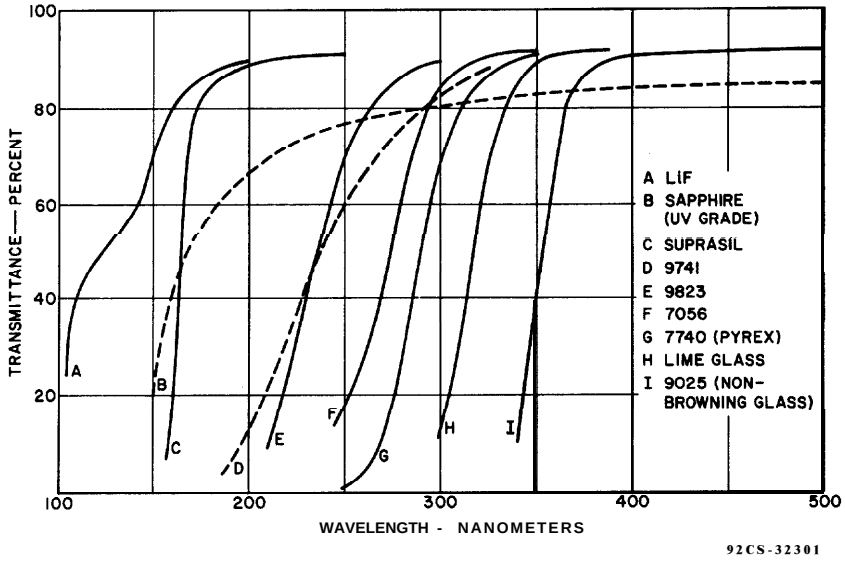

Fig. 15 - Ultraviolet transmittance cut off of various glasses and crystals used in photomultiplier photocathode windows. Data are all for 1 mm thickness.

GLASS TRANSMISSION AND SPECTRAL RESPONSE

Although photocathode spectral response is determined primarily by the nature of the photocathode surface, especially in the visible and long wavelength cut-off regions, the short-wave length cut-off characteristic of all photocathodes is determined by the transmission of the window to the photocathode. Ultraviolet cut-off characteristics of a number of glasses or crystals which have been used in photomultiplier fabrication are shown in Fig. 15.

The data presented in this figure are all for 1 mm thickness. The data also include losses from reflection. For most glasses with an index of refraction of about 1.5, the reflection loss is about 4% at each surface. The loss is higher in high index-of-refraction material such as sapphire. Although some photomultipliers, especially those of small size may have window thickness of 1 mm or less, larger face plates are generally thicker in order to provide adequate strength. The transmittance varies with thickness according to the following relationship

$$T = k\,10^{-\alpha t} \qquad (7)$$

where k is a factor (approximately 0.92 for most glasses) dependent upon the surface reflectivity, α is the coefficient of absorption, and t is the thickness.

The window extending the furthest into the ultraviolet is LiF. A few tubes are made with this material but, because its fabrication is difficult, LiF face plates are only used for special applications of spectroscopy. Transmission extends to wavelengths shorter than the Lyman-alpha limit of 121.5 nm.

Sapphire windows (ultraviolet grade) are good down to about 150 nm and are easier to use than LiF. Sapphire can be sealed to Kovar by a metalizing and brazing technique. Special photomultiplier tubes having sapphire windows were used in the HEAO program (High Energy Astronomical Observatory).

Except for the extended short wavelength cutoff of sapphire, Suprasil, an ultraviolet grade of synthetic fused quartz, has a better transmission characteristic. Sapphire suffers some loss in transmission by reflection because of its relatively high index of refraction. Photomultiplier tubes made with fused quartz windows are useful in Cerenkov counting applications where the spectral energy distribution increases with decreasing wavelength as $1/\lambda^3$ per unit-wavelength interval. Fused quartz is also a useful material in liquid scintillation counting because of its minimum contamination with ^{40}K which can cause unwanted background counts.

Less expensive than synthetic fused quartz is Corning 9741 glass, which is frequently used in photomultipliers designed for the near ultraviolet. It is a Kovar-sealing glass but has the disadvantage of possible weathering over long periods of exposure to the atmosphere.

Another glass for the near ultraviolet is Corning 9823, which seals to 0120 lead glass and which can be used with Dumet metal leads. This glass is somewhat inferior to 9741 at the shortest wavelengths, but is better for wavelengths longer than 240 nm.

Glass type 7056 is selected for its good optical quality. It is a hard glass which seals to 7052 and Kovar. Pyrex type 7740 is selected primarily for its low content of ^{40}K and is used in liquid scintillation-counting applications. Lime glass is the least expensive; it is a soft glass which seals to lead glass, type 0120.

Corning 9025 is a special non-browning glass. It is doped with cerium and resists darkening from exposure to ionizing radiation. One application is in satellites which must pass through space regions of high-intensity ionizing radiation.

THERMIONIC EMISSION

Current flows in the anode circuit of a photomultiplier tube even when it is operated in complete darkness. The dc component of this current is called the anode dark current, or simply the dark current. This current and its resulting noise component usually limit the lower level of photomultiplier light detection. As a result, the anode dark-current value is nearly always given as part of the data for any tube.

There are several sources of dark current in a photomultiplier tube: ohmic leakage, thermionic emission, and regenerative effects. **Ohmic leakage** may result from contaminations on the insulators within the tube, on the outside of the tube envelope, or

on the base. **Thermionic emission** generally originates from the photocathode itself and is amplified by the gain of the multiplier section. Some emission may also come from the secondary-emission dynode surfaces. **Regenerative effects** can occur in the tube particularly if it is operated with high voltage and high gain. (Regenerative effects are discussed in more detail in a later section on **Dark Current and** Noise.) The following discussion relates to the origin of thermionic emission current and gives practical values for this current in photomultiplier **photocathodes.**

In a metal, the electrons which escape as thermionic emission are generally from the top of the conduction band (see Fig. 3). Thus, the work functions for photoemission and for thermionic emission are the same. Thermionic emission as a function of work **function ϕ in electron volts* and temperature** T in degrees Kelvin is given by the familiar Richardson equation:

$$j = \frac{4\pi emk^2T^2}{h^3} \exp[-\phi/kT] \qquad (8)$$

where j is the thermionic current density; e, the electron charge; m, the electron mass; k, Boltzman's constant; and h, Planck's constant. If the constants before the exponential expression are given in mks units, the equation (8) expressed in amperes per meter^2 becomes

$$j = 1.2 \times 10^6 T^2 \exp[-\phi/kT] \qquad (9)$$

For semiconductor photocathodes, the work functions of photoemission and **thermionic** emission may be quite different. The work function for photoemission (see Fig. 7) is the electron energy corresponding to the height from the top of the valence band to the vacuum level, or E_A (the electron affinity) plus E_G (the forbidden gap, i.e., the separation of valence and conduction bands). For an intrinsic semiconductor, **thermionic** emission originates from the valence band, as does photoemission, but the "work function" is not the same as for **photoemission.** In the case of an intrinsic semiconductor, thermionic-emission density can be expressed as

$$j = \frac{4\pi emk^2T^2}{h^3} \exp[-(E_A + E_G/2)/kT] \qquad (10)$$

For an impurity semiconductor where thermionic emission originates from the **im-**

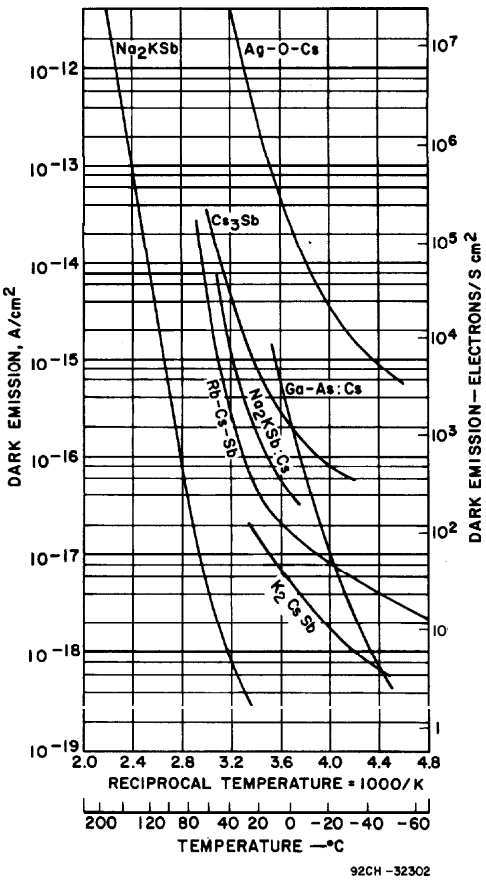

Fig. 16 - Variation of thermionic-emission current density from various photocathodes used in photomultiplier tubes as a function of reciprocal temperature. Thermionic emission multiplied by the gain of the photomultiplier is a principal source of anode dark current.

*An electron volt is the energy acquired by an electron in being accelerated through a drop in potential of one volt. In equations such as **(8),** the value of **kT** in the exponent must also be expressed in electron volts. It is the **practice elsewhere to express ϕ in volts (the same numerical value as ϕ in electron volts) and in this case ϕ** in volts must be multiplied by the electron charge, e, in coulombs (1.6 x 10 $^{-19}$) to obtain the work function in joules. The value of **kT** may then also be expressed in joules.

purity centers, the equation for thermionic emission may be written as follows[21]:

$$j = \frac{4\pi emk^2T^2}{h^3} \; n_o^{1/2} \; \frac{h^{3/2}}{(2\pi mkT)^{3/4}} \exp[-(E_A + E_G - E_F)/kT] \qquad (11)$$

where E_F is the Fermi level energy referenced from the top of the valence band, and n_o is the impurity concentration.

Typical dark-emission current-density characteristics for various photocathodes are shown in Fig. 16 as a function of reciprocal temperature. The current density is plotted on a logarithmic scale to show the exponential-like character of the emission. Anode dark current of the photomultiplier results from the cathode emission multiplied by the gain of the tube. Thermionic dark emission varies from tube to tube of the same type, probably because of the variation in n_o. Note that some of the curves show substantial curvature at the low temperature end. Some of this curvature is explained by the variation of T in the $T^2/T^{3/4} = T^{5/4}$ term. But an explanation for the greater part of the curvature may be the presence of patches of different impurity level or concentration, or it may be that the impurity concentration itself is a function of temperature. Exposure to temperatures above the normal operating range sometimes results in permanent reduction in dark current. Most photocathodes are p-type semiconductors one result of which is a lower dark emission than for n-type semiconductors because of the reduced Fermi-level energy.

SECONDARY EMISSION

When electrons having sufficient kinetic energy strike the surface of a material, secondary electrons are emitted. The **secondary-emission ratio or yield, δ, is** defined as follows:

$$\delta = N_s/N_e \qquad (12)$$

where N_s is the average number of secondary electrons emitted for Ne primary electrons incident upon the surface.

Fundamentals of Secondary Emission

The physical processes involved in secondary emission are in many respects similar to those already described under **Photoemission.** The main difference is that the impact of primary electrons rather than incident photons causes the emission of electrons. The steps involved in secondary emission can be stated briefly as follows:

1. The incident electrons interact with electrons in the material and excite them to higher energy states.

2. Some of these excited electrons move toward the vacuum-solid interface,

3. Those electrons which arrive at the surface with energy greater than that represented by the surface barrier are emitted into the vacuum.

When a primary beam of electrons impacts a secondary-emitting material, the primary-beam energy is dissipated within the material and a number of excited electrons are produced within the material. The numbers of excited electrons produced are indicated in Fig. 17 for primary energies varying from 400 to 2200 electron-volts. The total number of excited electrons produced by a primary is indicated by the area of the individual rectangles in the figure. These approximate data are based on experimental data assuming that the range of primary electrons varies as the 1.35 power of the primary energy and that the number of electrons excited is uniform throughout the primary range.

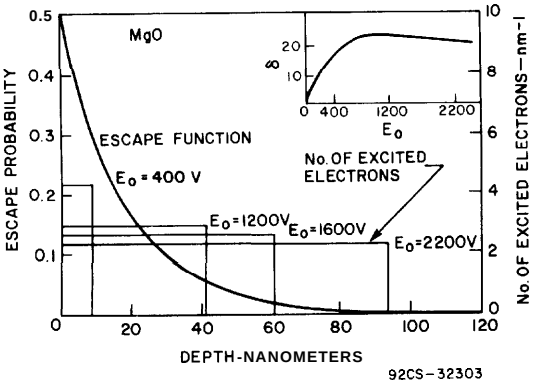

Fig. 17 - The processes of secondary emission. See text for explanation.

As an excited electron in the bulk of the material moves toward the vacuum-solid interface, it loses energy as a result of collisions with other electrons and optical phonons. The energy of the electron is very rapidly dissipated as a result of these collisons, and it is estimated that the energy of such an electron will decay to within a few times the mean thermal energy above the bottom of the conduction band within 10^{-12} second. If the electron arrives at the vacuum-solid interface with energy below that required to traverse the potential barrier, it cannot escape as a secondary electron. Therefore, only those electrons excited near the surface of the material are likely to escape as secondary electrons. The probability of escape for an excited electron is assumed to vary exponentially with the excitation depth, as indicated in Fig. 17. If the product of the escape function and the number of excited electrons (which is a function of primary energy and depth) is integrated, a secondary-emission-yield function δ may be obtained, as indicated in the insert at the top of Fig. 17. The model which has been assumed thus explains the general characteristics of secondary emission as a function of primary energy. Secondary-emission yield increases with primary energy, provided the excited electrons are produced near the surface where the escape probability is high. As the primary-electron energy increases, the number of excited electrons also increases, but the excitation occurs at greater depths in the material where escape is much less probable. Consequently, the secondary-emission yield eventually reaches a maximum and then decreases with primary energy.

Secondary Emitter Materials

Experimental secondary-emission-yield values are shown as a function of primary-electron energy in Fig. 18 for MgO, a traditional secondary-emission material, and for GaP:Cs, a recently developed negative-electron-affinity material. Also shown is a calculated curve from Simon and Williams[13] based on their model of the GaP:Cs emitter. Although both MgO and GaP:Cs display the general characteristics of secondary emission as a function of primary energy, as expected from the model illustrated in Fig. 17, the secondary-emission yield for GaP:Cs increases with voltage to much higher values. Even though electrons are excited rather deep in the negative-electron-affinity material and lose most of their excess energy as a result of collisions, many still escape into the vacuum because of the nature of the surface barrier.

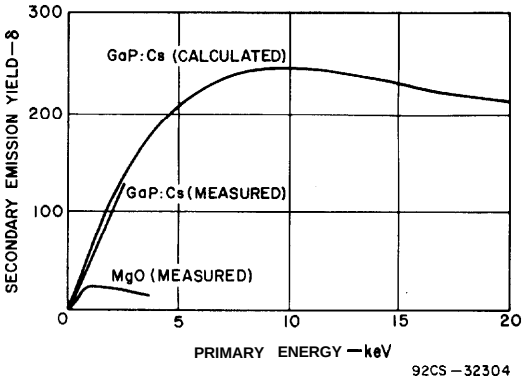

Fig. 18 - Typical experimental curve of secondary-emission yield as a function of primary-electron energy in GaP:Cs and MgO. Also shown in calculated curve for GaP:Cs from Simon and Williams.[13]

Because the GaP:Cs material is more difficult to handle than more conventional secondary emitters, and, therefore, results in higher cost, its use as a dynode has been restricted to applications where the very high secondary emission is particularly advantageous. It is used as, for example, in photomultiplier applications benefitting by the reduction in statistical noise, or in the design of photomultipliers having fewer stages for a given amplification. The use of fewer stages also reduces the variation of gain with voltage changes.

In the development of photomultiplier tubes it has been found that the photocathode material may also be useful as a secondary emitter[22]. Such was the case in some of the first photomultipliers developed which used a Ag-O-Cs photocathode and Ag-O-Cs dynodes. Because of its high dark-emission current and its instability, especially at moderate current-density levels, this material is no longer used.

Other photocathode materials which also serve as secondary emitters are Cs_3Sb, Rb-Cs-Sb, K_2CsSb, and Na_2KSb:Cs. Because the processing of these secondary emitters is

not identical in most cases to that of the corresponding photocathode, the particular chemical formulations specified here may not be accurate. Secondary emission ratios for these and other materials are shown in Fig. 19.

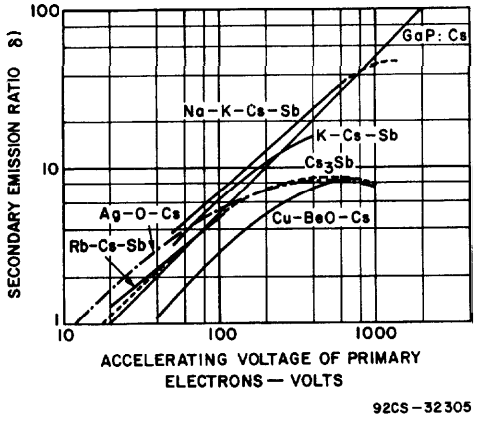

Fig. 19 • Secondary emission ratios for a number of **materials** *which have been used* **as** *dynodes in photomultipliers as a function of accelerating voltage of the primary electrons.*

Very high secondary-emission yields have been reported[23,24] for Na_2KSb:Cs, the multi-alkali **photocathode** (S-20 response). Some photomultiplier with this material as the secondary emitter although its processing is complex. The very high yields, particularly at high primary energies, would suggest that the material has an effective negative electron affinity similar to that of GaP:Cs. This explanation may also hold true for K-Cs-Sb, which is used is some tubes having this type of photocathode. A material that has been very commonly used is Cs_3Sb corresponding to the photocathodes with S-4 or S-l1 spectral responses. It has good secondary emission in the practical working range near 100 volts. Rb-Cs-Sb is a rather new material which is just coming into use because the corresponding photocathode has good properties. All of the alkali **antimonides** mentioned here have limitations. They cannot tolerate exposure to air and they are damaged by temperatures in excess of 75 degrees C. In addition, stability suffers **at current densities in excess of 100** μA cm^{-2}.

A very practical secondary emitter can be made from an oxidized silver-magnesium alloy[25,26] containing approximately 2 per cent of magnesium. Although silver-magnesium dynodes do not have as high a secondary-emission ratio as some of the materials mentioned above (see Fig. **18),** the material is easily processed and is more stable at relatively high currents. In addition, it can tolerate higher temperatures. This surface has a low thermionic background emission which is important in applications requiring detection of low-level light. When it is activated with cesium, gain is somewhat higher. Without the cesium activation, the oxygen-activated silver-magnesium layer has been used effectively in demountable systems for detecting ions and other particles.

A material having characteristics very similar to those of silver-magnesium is an oxidized layer of copper-beryllium alloy[27,28,29] in which the beryllium component is about 2 per cent of the alloy. Secondary emission is usually enhanced by the bake-out in cesium vapor. A **secondary-**emission characteristic of the cesium-activated copper-beryllium material is shown in Fig, 19. Because of the advantages in handling and the manufacturing cost, the copper-beryllium is largely taking the place of silver-magnesium in applications requiring low dark emission and stability at relatively high current densities. The lower secondary-emission yield is usually compensated for in photomultiplier design by application of higher voltage or by an increase in the number of dynode stages.

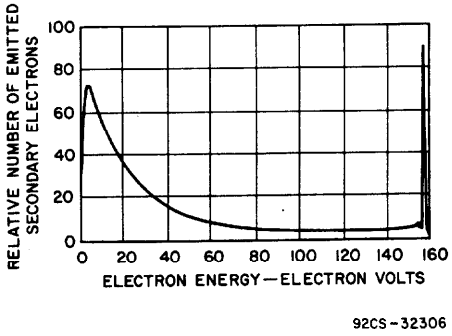

Fig. 20 • Typical secondary-electron energy distribution; peak at right is caused by reflected primary electrons.

When secondary electrons are emitted into the vacuum, the spread of emission energies may be quite large, as illustrated in the curve of Fig. 20 for a positive-electron-affinity emitter. The peak at the right of the curve does not represent a true secondary, but rather a reflected primary. Data are not available for the emission energies from a negative-electron-affinity material, but they are expected to be considerably less than for positive-affinity materials.

TIME LAG IN PHOTOEMISSION AND SECONDARY EMISSION

Because both photoemission and secondary emission can be described in terms of the excitation of electrons within the volume of the solid and the subsequent diffusion of these electrons to the surface, a finite time interval occurs between the instant that a primary (photon or electron) strikes a surface and the emergence of electrons from the surface. Furthermore, in the case of secondary emission, the secondaries can be expected to reach the surface over a period of time. Within the limitations of a mechanistic approach to a quantum phenomenon, time intervals for metals or insulators of the order of 10^{-13} to 10^{-14} second may be estimated from the known energy of the primaries, their approximately known range, and the approximately known diffusion velocities of the internal electrons. In negative-electron-affinity semiconductors, it is known that the lifetime of internal "free" electrons having quasi-thermal energies (i.e., electrons near the bottom of the conduction band) can be of the order of 10^{-10} second.

Thus far, experiments have provided only upper limits for the time lag of emission. In the case of secondary emission, a variety of experiments have established limits. Several investigators[30,31,32] have deduced limits from the measured performance of electron tubes using secondary emitters. Others, making direct measurements of these limits, have determined the time dispersion of secondary emission by letting short electron bunches strike a target and comparing the duration of the resulting secondary bunches with the measured duration of the primary bunch. By this means an upper limit of 6×10^{-12} second was determined for platinum[33] and an upper limit of 7 x 10^{-11} second for an MgO layer[34] formed on the surface of an AgMg alloy.

The upper limit for the time lag in photoemission, however, is not well established. From careful measurements of the time performance of fast photomultipliers it can be inferred that the limit must be less than 10^{-10} seconds.

While these limits are a useful guide to the type of time performance to be expected in present photomultipliers, they will probably have less significance as photomultipliers using new semiconducting photoemitters and secondary emitters are developed. Semiconductors having minority-carrier lifetimes of the order of microseconds are now available. Probably, by combination of this characteristic with negative electron affinity, higher gains and quantum efficiencies can be achieved, but at a sacrifice of time response or band width. However, the first generation of negative-electron-affinity emitters (e.g., GaP) has actually resulted in photomultipliers having better time performance because a smaller number of stages operating at higher voltage can be used. At this time it can only be concluded that in the future photomultipliers will probably be designed to match in more detail the requirements of a particular use.

REFERENCES

19. V.K. Zworykin, and E.G. Ramberg, **Photoelectricity and its Application,** John Wiley and Sons, Inc., New York, (1949).

20a. H. Rougeot and C. Baud, "Negative Electron Affinity Photoemitters," **Advances in Electronics and Electron Physics,** Vol. 48, Edited by L. Marton, Academic Press, 1979.

20. J.J. Brady, "Energy Distribution of Photoelectrons as a Function of the Thickness of a Potassium Film," **Phys. Rev.,** Vol. 46, (1934).

21. D.A. Wright, **Semi-conductors,** Methuen and Co., New York (1955).

22. A.H. Sommer, "Relationship between photoelectric and secondary electron emission, with special reference to the Ag-O-Cs (S-l) photocathode," **J. Appl. Phys.,** Vol. **42,** pp. 567-569, (1971).

23. A.A. Mostovskii, G.B. Vorobeva, and G.B. Struchinskii, **Soviet Physics-Solid State,** Vol. 5, p. 2436, (1964).

24. C. Ghosh and B.P. Varma, "Secondary emission from multialkali photocathodes," **J. Appl. Phys.,** Vol. 49, pp. 4554-4555, (1978).
25. V.K. Zworykin, J.E. Ruedy, and E.W. Pike, "Silver-magnesium alloy as a secondary emitting material," **J. Appl. Phys.,** Vol. 12, (1941).
26. P. Rappaport, "Methods of processing silver-magnesium secondary emitters for electron tubes," **J. Appl. Phys.,** Vol. 25, pp 288-292, (1954).
27. J.S. Allen, "An improved electron multiplier particle counter," **Rev. Sci. Instr.,** Vol. 18, (1947).
28. A.M. Tyutikov, "Structure and secondary emission of emitters of activated beryllium bronze, " **Radio Engineering and Electronic Physics,** (Translated from the Russian and published by the IEEE), Vol. 8 No. 4, pp. 725-734, (1963).
29. A.H. Sommer, "Activation of silver-magnesium and copper-beryllium dynodes," **J. Appl. Phys.,** Vol. 29, pp. 598-599, (1958).
30. G. Diemer and J.L.H. Jonker, "On the time delay of secondary emission," **Philips Research Repts.,** Vol. 5, p. 161 (1950).
31. M.H. Greenblatt and P.A. Miller, Jr., "A microwave secondary-electron multiplier," **Phys. Rev.,** Vol. 72, p. 160 (1947).
32. C.G. Wang, "Reflex Oscillators using. secondary-emission current," **Phys. Rev.,** Vol. 68, p. 284 (1945).
33. I.A.D. Lewis and F.H. Wells, **Milli-Microsecond Pulse Techniques,** Pergamon Press (1959).
34. K.C. Schmidt and C.F. Hendee, "Continuous-channel electron multiplier operated in the pulse saturated mode," **IEEE Trans. Nucl. Sci.,** Vol. NS-13, No. 3, p. loo (1966).

3. Electron Optics of Photomultipliers

ELECTRON-OPTICAL DESIGN CONSIDERATIONS

One of the primary design considerations in a photomultiplier tube is the shaping and positioning of the dynodes (usually in a recurrent geometrical pattern) so that all the stages are properly utilized and no electrons are lost to support structures in the tube or deflected in other ways. Although it is not necessary that the electrons come to a sharp focus on each succeeding stage, the shape of the fields should be such that electrons tend to return to a center location on the next dynode, even though the emission point is not at the optimum location of the preceding dynode. If this requirement is not met, the electrons increasingly diverge from the center of the dynode in each successive dynode stage. This effect in turn can lead to the skipping of stages and loss of gain. Magnetic fields may be combined with electrostatic fields to provide the required electron optics, although today most photomultipliers are electrostatically focused. In addition to providing good collection of secondary electrons from stage-to-stage, it is important for some applications to minimize the time spread of electron trajectories. For this purpose is is useful to provide strong electric fields at the surfaces of the dynodes to assure high initial acceleration of the electrons. Also important may be the design of configurations which provide nearly equal transit times between dynodes regardless of the point of emission on the dynode.

In scintillation counting applications, fairly large photocathode areas are required for efficient scintillator coupling. Ideally, the photocathode should be semitransparent and located on the flat window of the tube. This requirement poses a special problem in design of efficient photocathode-to-first-dynode electron optics. If all of the emitted photoelectrons are not guided properly to the first dynode, the signal-to-noise ratio of the photomultiplier is degraded and poorer pulse-height-resolution characteristics result.

The region between the last dynode and the anode is also of special electron-optical concern. The withdrawal field at the last dynode should be large to minimize space charge effects which limit the linearity and magnitude of output current pulses. Another consideration in high-speed photomultipliers is to provide a structure which is matched to appropriate transmission lines.

The complete electron-optical configuration of the photomultiplier must also be such as to avoid regenerative effects. For example, there should not be an open path in the tube through which occasional ions or light could feed back from the output end to the photocathode.

DESIGN METHODS FOR PHOTOMULTIPLIER ELECTRON OPTICS

Before the days of high-speed computers, photomultiplier electron-optical problems were often solved by means of mechanical analogues such as a stretched rubber membrane. When mechanical models of the electrodes were placed under such a membrane and their height adjusted to correspond to the desired electrical potential, the height of the membrane in the spaces between the electrodes corresponded to the equivalent electrical potential. Small balls were then allowed to roll from one electrode to the next. The trajectories of the balls corresponded to those of the electrons in the photomultiplier structure. With appropriate model design, friction and depression of the membrane by

the ball were made negligible. This model, however, was only valid for geometries in which the electrodes could be assumed to be cylindrical surfaces (generated by a line parallel to a fixed direction and moving along a fixed curve) sufficiently long to be considered infinite in extent. Application was made to numerous dynode configurations.

Another useful analogue was the resistance network such as a two-dimensional array of connectors having equal spacing vertically and horizontally. This array represented a cross-section plane through cylindrical surfaces again assumed to be infinite in length. Resistors of equal value were connected between adjacent connectors both vertically and horizontally. Points in the array corresponding to an electrode were all connected to the same potential. Equipotential lines between electrodes could then be determined by observing the potential values on the connectors between the electrodes. When the equipotential lines had been determined, electron trajectories could be readily calculated between closely spaced equipotential surfaces.

In another variation of the resistance network, the vertical distribution of resistance values was made logarithmic instead of uniform. This array then corresponded to an axially symmetrical system with the axis approximated across the top of the board. An example of a relevant problem is the region between the photocathode and first dynode for end-on-type photomultipliers where the axis passes through the center of the photocathode.

Only very simple electron-optical systems can be solved in closed form, which requires the solution of Laplace's equation, $\nabla^2 V = 0$. However, by using relaxation techniques with a computer, the potential distribution on a set of points confined within defined boundary conditions can be determined. Secondly, using the force equations, electron paths can be traced. Computer programs exist for solving various cases with or without symmetry and with irregular potential boundaries.

An electron-optical design for a photomultiplier may be arrived at from computer-developed equipotential lines and electron trajectories plotted on a plan showing the electrode configurations. Collection efficiency and time response may be predicted from an analysis of the electron trajectories. Collection efficiency at the first dynode is defined as the ratio of the number of photoelectrons which land upon a useful area of the dynode to the number of emitted photoelectrons. If all the photoelectrons begin their trajectories at the surface of the photocathode with zero velocity, 100% collection would be possible. Because of the finite initial velocities, however, some electrons begin their trajectories with unfavorable angles of launch and are not collected on a useful area.

In modern photomultiplier structures, first-dynode collection efficiencies range from 85 to 98 per cent. Ideally, the emitted photoelectrons should converge to a very small area on the first dynode. In practice, this electron-spot diameter is usually less than 1/4 of the cathode diameter, depending upon the tube type and focusing structure.

SPECIFIC PHOTOMULTIPLIER ELECTRON-OPTICAL CONFIGURATIONS

Circular-Cage Structure with Side-On Photocathode

The first commercially successful photomultiplier design was based on a circular array of photocathode and dynodes-as in the 931A. This design is depicted schematically in Fig. 21. The photocathode is of the "opaque" type; i.e., electrons are emitted from the same side as the photocathode is illuminated. This particular type of tube is relatively inexpensive and is useful for applications such as spectroscopy where high sensitivity is required but the photocathode area need not be large. In this case the best collection is from the side of the photocathode near the first dynode. In the part of the photocathode near the apex formed by the grill and the photocathode, the electrostatic fields are small and collection efficiency is poor. The time of response of the tube is short because of its small size and high interdynode field strengths, and there is relatively small feedback from the anode end of the tube back to the photocathode.

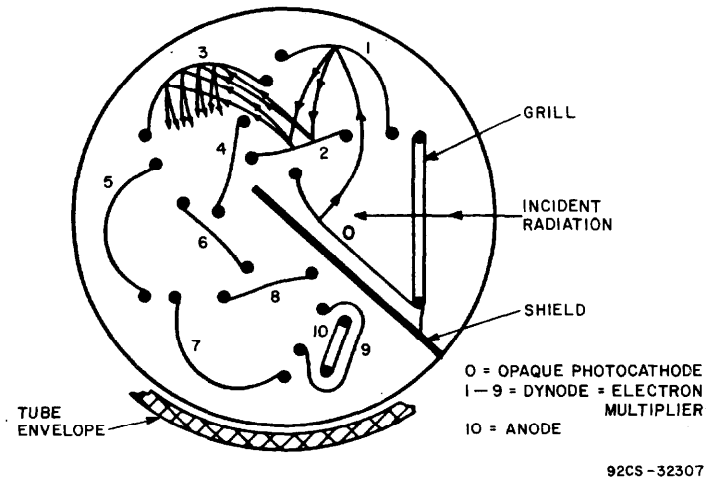

Fig. 21 - The circular-cage multiplier structure.

Circular-Cage Structure with End-On Photocathode

Fig. 22 illustrates the use of a circular cage coupled to a flat semi-transparent photocathode. Such a configuration is useful in scintillation counting where the flat photocathode is coupled to the scintillating crystal. In order to improve the collection efficiency of photoelectrons by the first dynode, the electrode which was the photocathode in Fig. 21 has been modified to provide a larger useful first-dynode area in the end-on construction. In addition, a skewed field is provided by the focusing electrode which results in a more favorable pattern of impacting photoelectrons on the first dynode. This end-on construction still has a relatively short time response because of the focused dynode arrangement, although the transit-time spread of electrons traversing the photocathode-to-first-dynode space increases the time of response as compared with that of the simple circular side-on structure of Fig. 21.

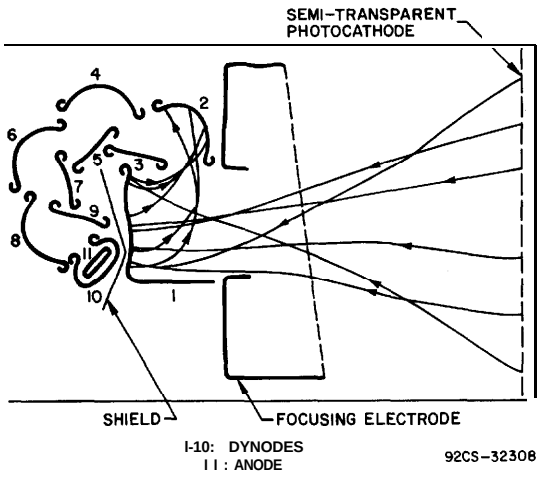

fig. 22 - An end-on photomultiplier structure utilizing a circular dynode arrangement. This type of tube would be useful as a detector for scintillation counting.

Box-and-Grid Structure with End-On Photocathode

The box and grid dynode structure shown in Fig. 23 is also useful in scintillation counting because of the relatively large flat semi-transparent photocathode. This configuration has the advantage of providing a rather large entrance area to collect photoelectrons so that collection efficiency is very nearly 100%. This feature is important in providing good pulse-height resolution in scintillation counting. The individual dynode boxes are open at the exit end and have a grid at the entrance. The grid provides an electric field which penetrates the preceding dynode region and aids in the withdrawal of secondary electrons. The grid also eliminates a retarding field that would be caused by the potential of the preceding dynode. Because the field penetration is rather weak, the electron

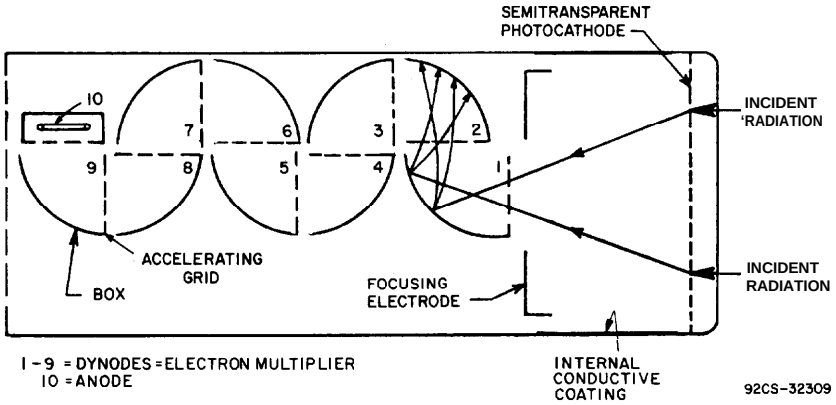

Fig. 23 - The box-and-grid multiplier structure.

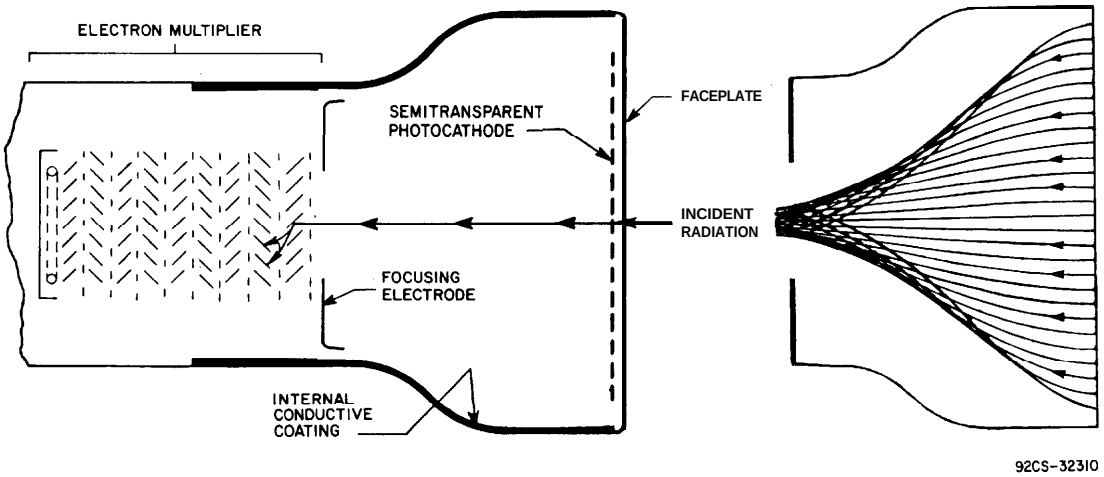

Fig. 24 - The Venetian-blind multiplier structure.

transit time between dynodes is relatively slow and has a rather large time spread.

Venetian-Blind Structure

Another structure which provides good collection of photoelectrons, but again is rather slow in response time, is the venetian-blind photomultiplier shown in Fig. 24. Good collection of photoelectrons is aided by the size of the photoelectron collecting area which can be even larger than that of the box-and-grid construction. The relatively slow time response is the result of the weak electric field at the surfaces of the dynode vanes. The structure is very flexible as to the number of stages. Some of the secondary electrons are lost because of the interposition of the grids between stages, as with the box-and-grid construction.

Tea-Cup Structure

A recent innovation in front-end design is the so-called "tea-cup" photomultiplier, named after its large first dynode. Secondary electrons from the first dynode are directed to an opening in the side of the tea-cup and thence to the second dynode. Fields between the photocathode region and the first dynode region are separated by a very fine grid structure. The particular advantage of this design is that the collection efficiency of the large first dynode is good not only for

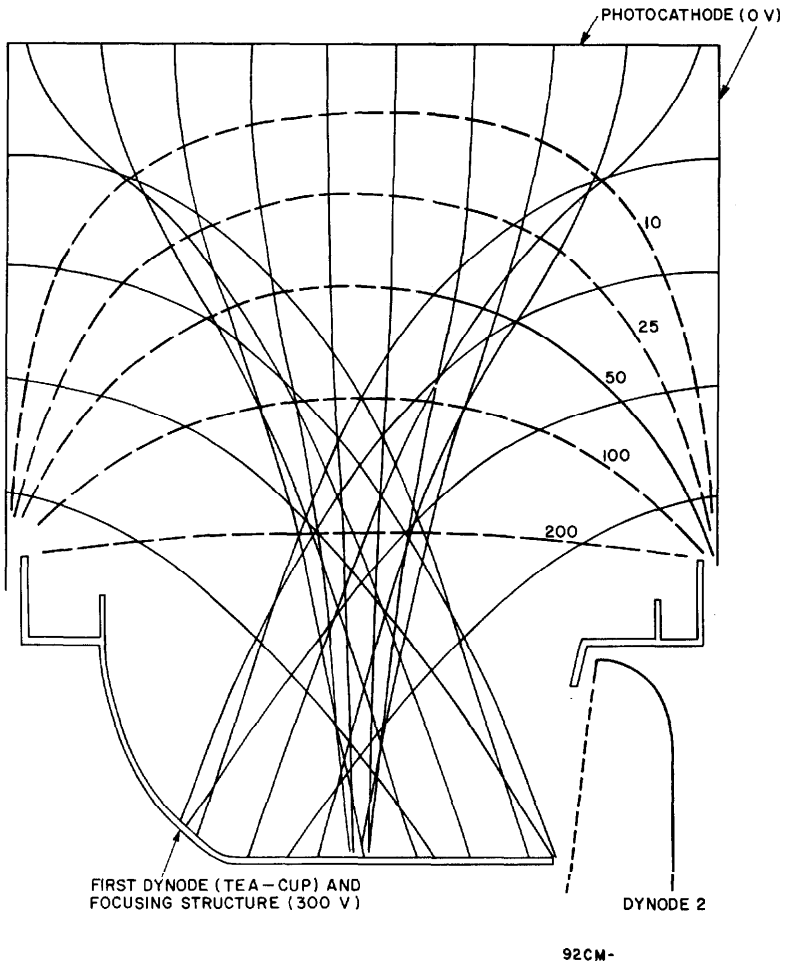

Fig. 25 - Tea-cup photomultiplier showing photoelectron paths directly from the photocathode and those initiated by light transmitted through the photocathode and striking the side wall which also ***has*** *an active photoemissive layer. Also indicated are equipotential lines in the region between photocathode and first* ***dynode.***

photoelectrons emitted from the photocathode but for photoelectrons emitted from the activated side walls between the first dynode and the photocathode as shown in Fig. 25. The side-wall photoemission results from light which passes through the front semitransparent photocathode. The increased photoemission and collection efficiency improves the pulse-height resolution in scintillation counting applications. Indicated on the diagram are equipotential lines and photoelectron paths showing the collection of electrons from the front surface and from the side walls.

In-Line Dynode Structure with Curved Photocathode

The planar-photocathode design, such as that shown in Figs. 22-25, provides excellent coupling to a scintillation crystal, but its time response is not as good as that of a spherical-section-photocathode design. The spherical-section photocathode shown in Fig. 26 when coupled to a high-speed electron multiplier provides a photomultiplier having a very fast time response. Some tube types utilize a spherical-section photocathode on a plano-concave faceplate to facilitate scintillator coupling. This design is

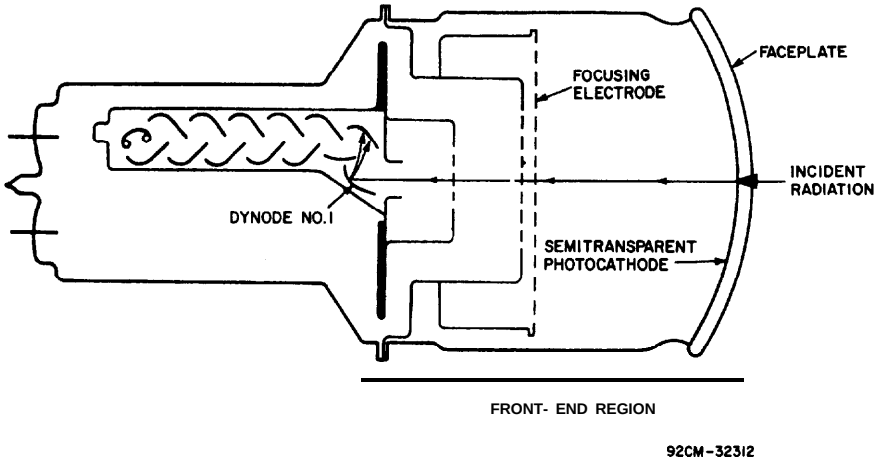

Fig. 26 - Photomultiplier design with curved faceplate and in-line dynode structure to provide a minimum transit time and transit-time spread.

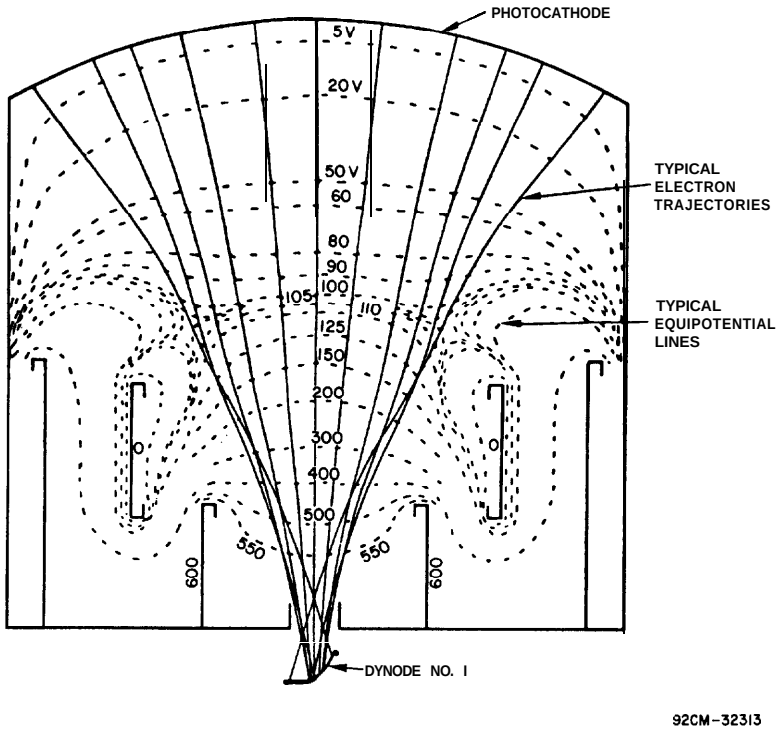

Fig. 27 - Cross section of a photomultiplier showing equipotential lines and electron trajectories that were plotted by computer.

usually limited to faceplate diameters of two inches or less because of the excessive thickness of the glass at the edge. The plano-concave faceplate may also contribute to some loss in uniformity of sensitivity because of internal reflection effects near the thick edge of the photocathode.

The performance of the front-end structure shown in Fig. 26 has been determined by the use of a computer to trace equipotential lines and electron trajectories which have then been superimposed on a schematic diagram of the tube structure as shown in Fig. 27.

A time parameter of interest is the photocathode transit-time difference, the time difference between the peak current outputs for simultaneous small-spot illumination of different parts of the photocathode. In a planarcathode design, the transit time is longer for edge illumination than for center illumination because of the longer edge trajectories and the weaker electric field near the edge of the photocathode. The center-to-edge transit-time difference may be as much as 10 nanoseconds. The spherical-section photocathode affords more uniform time response than the planar photocathode because all the electron paths are nearly equal in length; however, the transit time is slightly longer for edge trajectories than for axial trajectories because of the weaker electric field at the edge.

The photocathode transit-time difference is ultimately limited by the initial-velocity distribution of the photoelectrons; this distribution causes time-broadening of the electron packet during its flight from the photocathode to the first dynode. The broadening effect can be minimized by increasing the strength of the electric field at the surface of the photocathode.

Because the energy spread of secondary electrons is even larger than that of photoelectrons, initial-velocity effects are the major limitation on the time response of the electron multiplier. Multiplier time response is usually improved by the use of high electric-field strengths at the dynode surfaces and compensated design geometries. In a compensated design, such as that shown in Fig. 28 and as used in the type of photomultiplier shown in Fig. 26, longer electron paths and weaker fields alternate with shorter electron paths and stronger fields from dynode to dynode to produce nearly equal total transit time.

Certain materials have advantages over other materials in providing good multiplier time performance. For example, a standard dynode material, copper beryllium, has a maximum gain per stage of 8 at a 600-volt interstage potential difference. In contrast, gallium phosphide exhibits a gain of 60 or more at a 1200-volt interstage potential difference. The advantage in time performance of the GaP dynode over one of the CuBe type is that the number of stages, and thus the total transit time may be reduced, and that the energy spread of the secondary electrons is less.

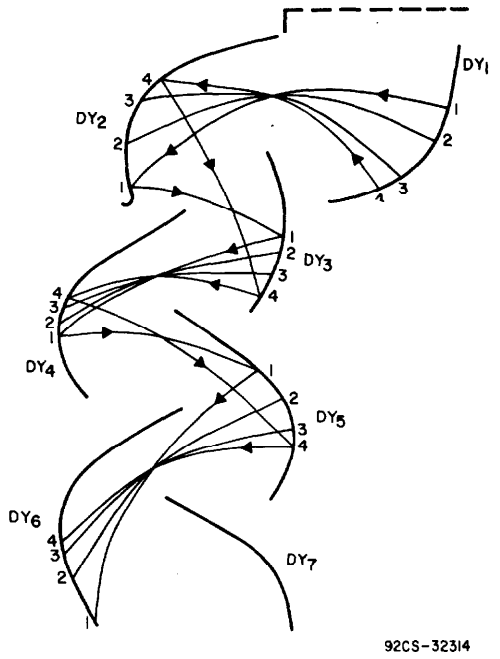

Fig. 28 - A compensated-design multiplier.

Continuous-Channel Multiplier Structure

The continuous-channel multiplier structure[35] shown in Fig. 29 is very compact and utilizes a resistive emitter on the inside surface of a cylinder rather than a discrete number of dynodes. The lack of discrete dynodes causes the electron-multiplication statistics to be poor because of the variable path lengths and the variable associated voltages. The gain of a continuous-channel multiplier is determined by the ratio of the

channel length to inside diameter; a typical value of this ratio is 50 but it may range from 30 to 100.

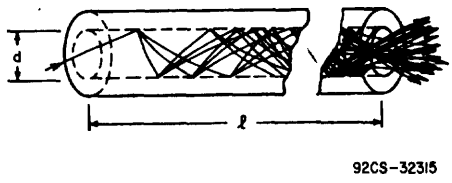

Fig. 29 - The continuous-channel multiplier structure.

Very high gain can be achieved with such a single-channel multiplier, provided the channel is curved or bent to avoid line-of-sight feed-back paths. Numerous special purpose photomultiplier tubes have been built using this concept.

Recently,[36] very-high-speed photomultiplier tubes have been designed utilizing microchannel plates in proximity with the photocathode and anode. Such a device is illustrated in Fig. 30. A microchannel plate is an array of parallel channels, each perhaps 40 μm or less in diameter. A fairly large array is mounted close to the photocathode with the plane of the channel plate parallel to the photocathode. A high voltage, 1 kilovolt, may be applied between photocathode and microchannel plate, and similar voltages applied across the microchannel sandwich and between the plate and the anode. These voltages assure short transit times. Time resolution for pulses initiated by single photoelectrons measured at full width at half maximum (FWHM) is less than 300 picoseconds.[37] Because of the construction and high electric fields employed, the sensitivity to external magnetic fields is much reduced, a fact which is important in some nuclear physics experimentation.

Crossed-Field Multiplier Structure

As mentioned earlier, a crossed-field photomultiplier was first reported in early 1936 by Zworykin, Morton and Malter.[38] Their tube, shown schematically in Fig. 31, used a combination of electrostatic and magnetic fields to direct electrons to repeated stages of secondary emission. Above each emitter was a field plate whose potential was set to be equal to that of the next emitter down the line. As a result of this configuration, electrons emitted from the photocathode or from one of the secondary emitters, were caused to follow approximately cycloidal paths to the next electrode. This early development was not carried into large-scale manufacture because of the critical magnetic-field adjustments needed to change the gain. Also, the rather wide open structure resulted in high dark current because of feedback from ions and light developed near the output end of the device.

Recently, however, similar, but improved crossed-field photomultipliers[39] have been designed to provide perhaps the fastest rise time of any photomultiplier. The electron trajectories are essentially isochronous in the crossed magnetic and electric fields so that a very short rise time, 250 picoseconds[40], is

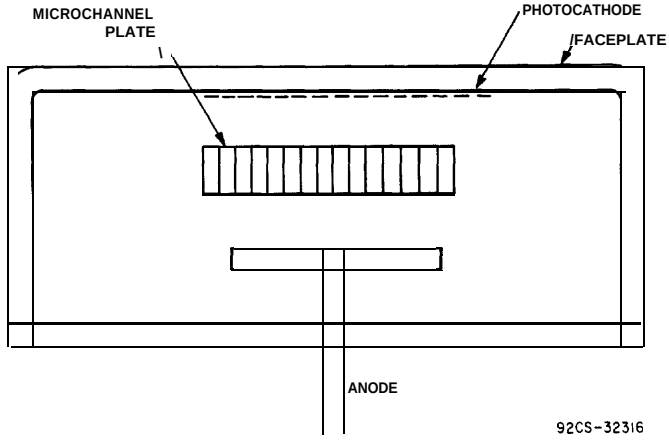

Fig. 30 - Microchannel-plate photomultiplier.

achieved. Unfortunately, the photocathode is rather small and inaccessible by the nature of the design. A schematic drawing of the recent crossed-field photomultiplier is shown in Fig. 32. Note the single field electrode in contrast to the multiple field the plates of the Zworykin tube. The stepped arrangement is required in order to provide uniform electric field. A **50-ohm** coaxial output connector provides coupling to the high-speed **photo**multiplier.

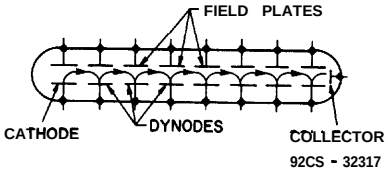

*Fig. 31 - Schematic of the Zworykin **crossed**-field photomultiplier reported in 1936. A mag**netic** field, perpendicular to the plane of the **drawing,** and an electrostatic field, produced by the upper fieldplates, combine to bend the electron paths in the cycloidal trajectories illustrated.*

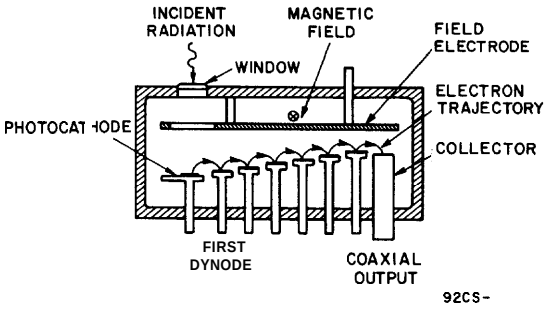

Fig. 32 - Schematic arrangement of a modern static crossed-field photomultiplier.

ANODE CONFIGURATIONS

The primary function of the anode is to collect secondary electrons from the last dynode. The anode should exhibit a constant-current characteristic of the type shown in Fig. 33. The simplest anode structure, shown in Fig. 34, is a grid-like collector used in some Venetian-blind structures. The secondary electrons from the next-to-last dynode pass through the grid to the last dynode. Secondary electrons leaving the last dynode are then collected on the grid-like anode.

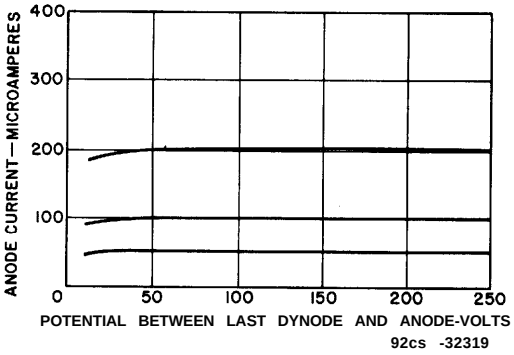

Fig. 33 - Constant-current characteristics of a photomultiplier anode.

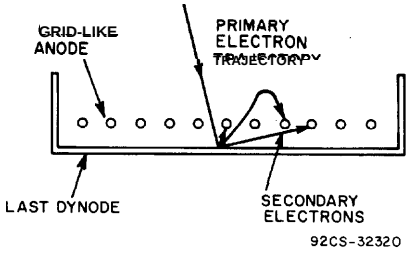

*Fig. 34 - **The** simplest anode structure, a grid-like collector.*

In applications where large output pulse currents are required it is important to provide a design having reasonably high withdrawal fields to avoid space-charge development which could limit the output current. Space charge may actually limit the output at the next to the last dynode, which is the case in the circular-cage structure, Fig. 21, because the withdrawal field at the last dynode is significantly higher than at the eighth dynode. In special applications a tapered divider network may be used to provide higher inter-stage voltages in the last several stages of the tube (see Chapter **5—Photomultiplier Applications).**

Where fast time response is important, the type of design shown in Fig. 34 may be at a disadvantage because electrons from the last dynode are not necessarily collected on the first pass through the anode grid structure. It is also important for fast time response that the anodes be designed with **matched**-impedance transmission lines or with short connecting support leads. Most high-speed circuits are designed to utilize a **50-ohm** im-

pedance, which requires a suitable connector or lead geometry outside the tube to permit proper impedance matching.

Anode configurations and internal transmission lines may be analyzed by use of the standard methods of cavity and transmission-line analysis. These methods yield approximate design parameters[41], which are optimized experimentally by means of time-domain reflectometry, TDR[42,43]. TDR provides information about the discontinuities in the characteristic impedance of a system as a function of electrical length and is an extremely useful approach in the design of voltage-divider circuits and mating sockets which do not readily lend themselves to mathematical analysis.

Certain anode structures in fast-rise-time photomultipliers exhibit a small-amplitude pulse (prepulse) that can be observed a nanosecond or two before the true signal pulse. In grod-like anode structures this prepulse is induced when electrons from the next-to-last dynode pass through the anode grid. In more sophisticated photomultiplier designs this phenomenon may be suppressed by auxiliary grids that shield the anode from the effects of the impinging electron cloud.

REFERENCES

35. K.C. Schmidt and C.F. Hendee, "Continuous-Channel Electron Multiplier Operated in the Pulse-Saturated Mode," **IEEE Trans. Nucl. Sci.,** Vol. NS-13, No. 3, p. 100 (1966).

36. Ph. Chevalier, J.P. Boutot and G. Pietri, "PM of new design for high speed physics," **IEEE Trans. Nucl. Sci.,** Vol. NS-17, No. 3, pp. 75-78 (June, 1970); G. Pietri , "Contribution of the channel electron multiplier to the race of vacuum tubes towards picosecond resolution time," **IEEE Trans. Nucl. Sci. ,** Vol. NS-24, No. 1, pp. 228-232, (Feb. , 1977).

37. C.C. Lo, P. Lecomte and B. Leskovar, "Performance studies of prototype microchannel plate photomultipliers," **IEEE Trans. Nucl. Sci.,** Vol. NS-24, No. 1 , pp. 302-311 , (Feb. , 1977).

38. V.K. Zworykin, G.A. Morton, and L. Malter , "The secondary emission multiplier-a new electronic device"' **Proc. I.R.E.** Vol. 24 p. 351-375 (1936).

39. R.S. Enck and W.G. Abraham, "Review of high speed communications photomultiplier detectors," **Proc. Soc. Photo Optical Instrumentation Engineers,** Vol. 150; Laser and Fiber Optics Communications' San Diego CA; 28-29 Aug. , 1978 (Bellingham , WA; Soc. Photo-Optical Instrumentation Engineers , 1978) , p 3 l-8.

40. B. Leskovar and C.C. Lo, "Time Resolution Performance Studies of Contemporary High Speed Photomultipliers," **IEEE Trans. Nucl. Sci.,** Vol. NS-25, No. 1, pp. 582-590, (Feb. 1978).

41. I.A.D. Lewis and F.H. Wells, **Millimicrosecond Pulse Techniques,** Pergamon Press (1959).

42. "Time-Domain Reflectometry," Hewlett Packard Application Note 62.

43. "Time-Domain Reflectometry," Tektronix Publication 062-0703-00.

4. Photomultiplier Characteristics

PHOTOCATHODE-RELATED CHARACTERISTICS

Current-Voltage Characteristics

Photomultiplier tubes may be operated as photodiodes by utilizing the first dynode and focusing electrode (if present) tied together as an anode. In this mode of operation the photocurrent is linear with light flux except that, for semitransparent photocathodes, the resistivity of the thin photocathode layer limits the current which can be drawn. In the case of a resistive photocathode, when the light is directed to the center of the sensitive area, there is a drop in potential between the outer conductive ring and the illuminated area. Because the illuminated area becomes positively charged with respect to the photocathode contact, only the more energetic photoelectrons emitted will overcome the slightly repelling electric field near the photocathode surface.

Fig. 35 shows a pair of current-voltage characteristics for 75-mm-diameter photomultipliers operated as photodiodes. In both cases the illuminated area is approximately 5 mm in diameter and located at the center of the photocathode. The multialkali photocathode (S-20 response) layer is fairly conductive so that even for a photocurrent of over 200 nanoamperes, good collection efficiency is achieved for a collection voltage as low as 50 volts. On the other hand, the bialkali photocathode , K_2CsSb , is very resistive causing poor collection efficiency over a wide range of voltage even for photoemission currents as low as 10 nanoamperes.

For resistive photocathodes it is thus necessary to limit the maximum photocathode current to avoid non-linear operation. Resistivity characteristics of several types of photocathode are shown in Fig. 36. Here, the resistance per square is shown as a function of temperature. The increase in resistivity with decreasing temperature is expected because of the semiconductor nature of photocathode materials. Resistance per square is the resistance of a surface layer between conductors at opposite sides of a square of the layer. Note that, if the resistivity of the photocathode material is ρ, for a square of side dimension **d,** and thickness **t,**

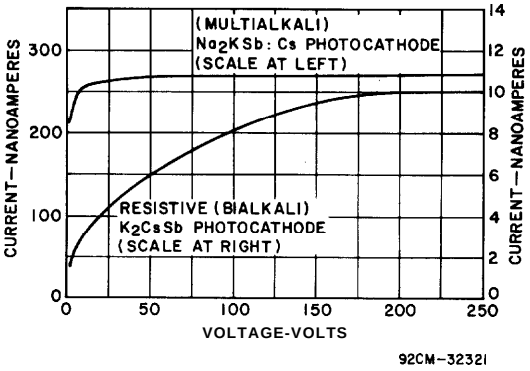

Fig. 35 - Current-voltage characteristics for 75-mm diameter photomultiplier tubes operated as photodiodes. The poor collection efficiency shown for the tube with the resistive photocathode is caused by the voltage drop from the edge of the photocathode to the center illuminated spot and the resulting electrostatic field distortion between the photocathode and the first dynode and focus electrode used together as an anode.

the resistance **R** is given by

$$R = \frac{\rho d}{d \bullet t} \qquad (13)$$

where d • t is the cross-section area. Thus, the resistance per square is independent of the side dimension. On photocathode types that are very resistive , it is advisable to maintain operating temperatures above -100° C depending upon photocathode diameter , the light-spot diameter, and the photocathode current. The larger the photocathode diameter and the smaller the light-spot diameter, the more severe the effect.

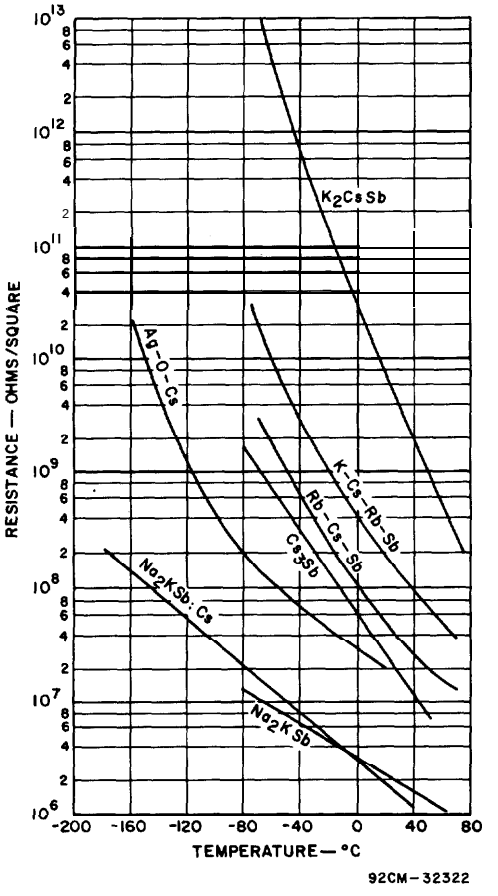

Fig. 36 - Resistance per square as a function of temperature for various semitransparent photocathodes.[44,45] *These data were obtained with special* **tubes** *having connections to parallel conducting lines or between concentric conducting circular rings on the surface of the photocathode.*

Photocathode resistive effects can be avoided at manufacture by the use of nearly transparent conductive undercoatings. Opaque types of photocathode, such as Cs3Sb on a solid substrate of nickel, do not have a resistivity problem. Table II provides guidance as to the maximum dc current that can be utilized with various semitransparent photocathodes at room temperature. It should be realized that these data are only typical; individual photocathodes may vary considerably from the guideline provided in their capability of delivering current without resistive blocking.

Table II - Maximum Recommended Pbotocathode DC Currents for Various Semitransparent Photocathode Types as Determined by Surface Resistivity.

Photocathode	Maximum Recommended Current for T = 22°C
K_2CsSb	1 nA
Na_2KSb	1 μA
Na_2KSb:Cs	10 μA
Ag-O-Cs	1 μA
Cs_3Sb	1 μA
Rb_2CsSb	1 μA

In the case of pulsed photocathode currents, the peak current values may be higher than those shown in Table II. Average currents, however, are still limited, as shown, by the resistance of the photocathode layer. For a current pulse, the local surface potential of the cathode is sustained for a time by the electrical charge associated with the photocathode capacitance. Thus, a square centimeter of photocathode may have a capacitance of about 0.5 picofarad. A 5-volt change in potential is about the maximum that could occur without blocking of the photoemission current. The equivalent charge is therefore 2.5 picocoulombs. For a pulse duration of **t** seconds, a pulse current of 2.5/t picoamperes could be maintained. For t = 1 microsecond, the current maximum could be 2.5 microamperes, as determined by stored charge alone.

Pulse current maximum can be increased by the capacitance of the photocathode layer. For example, if a ground plane is provided in contact with the outside of the

photocathode faceplate, the capacitance of a square centimeter of photocathode may be increased to about 2 picofarads (assuming a dielectric constant 6.75 and a glass thickness of 3 mm). The ground plane must, of course, be reasonably transparent to the light signal. A conducting mesh is a suitable solution. The ground plane should also be set at or near photocathode potential, or noisy operation and deterioration of the photocathode may result. See the section below under "Dark Current and Noise."

Variations in Spectral Response with Temperature.

Minor variations in the spectral response characteristics of photocathodes occur with changes in temperature. Data are presented here on the typical variations which can be expected. Deviations from these data may be expected on individual photocathodes because of variations in thickness and processing.

When the temperature is decreased, the response of photocathodes usually improves in the shorter-wavelength region and worsens in the longer-wavelength region near the threshold. An illustration of this trend is provided in Fig. 37 in which the

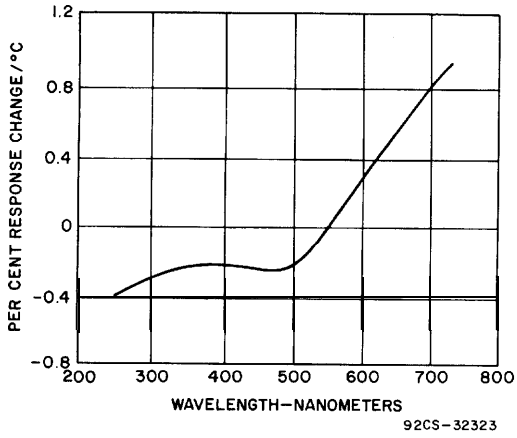

*Fig. 37 - Temperature coefficient of **cesium**-antimony cathodes as a function of wavelength at 20 "C. Note the large positive effect near the threshold.*

temperature coefficient of responsivity of a cesium-antimony photocathode is plotted as a function of wavelength.[46] The difference in spectral response from room to liquid-air temperature is illustrated in Fig. 38, also for **Cs_3Sb.** According to Spicer and **Wooten[47],** the increase in response in the blue at low temperatures is the result of a decrease in energy loss from lattice scattering; the decrease in the red at low temperatures results from a decrease in occupied defect levels in the forbidden energy band because of an increase in band gap and possibly because of an unfavorable change in band bending. It may also be the case that, in photocathodes having significant impurity levels, the extended red sensitivity at higher temperatures is partly the result of thermally assisted photoemission. The change of slope at the elevated temperature in Fig. 38 is suggestive of this mechanism.

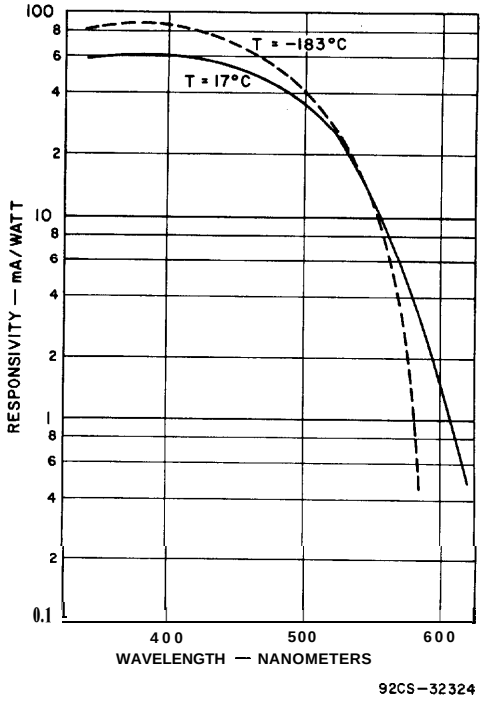

*Fig. 38 - Dependence of responsivity of a **Cs_3Sb** photocathode on temperature; taken from Spicer and **Wooten.**[47]*

The data shown in Fig. 39 is of the same type as that in Fig. 38, but for a GaAs:Cs photocathode. Note, again, the increase in sensitivity with decrease in temperature except for the shift in the long wavelength threshold. In GaAs:Cs the photoexcitation is from the valence band; there is essentially no excitation from the forbidden energy band. Note the sharp long-wavelength cutoff.

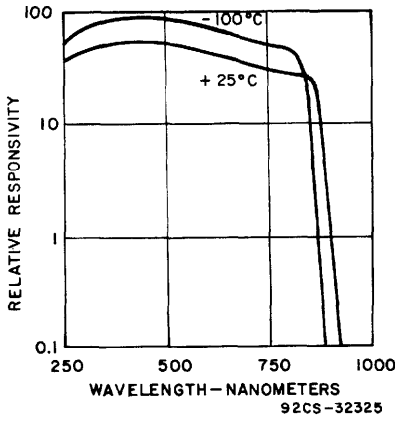

Fig. 39 - Relative spectral responsivity shift with temperature for a GaAs:Cs photocathode.[48]

Variation of Photocathode Response with Angle of Incidence and Angle of Polarization.

In a theoretical paper[49] **Ramberg** has evaluated the optical factors which determine the variation of photoresponse as a function of polarization angle and angle of incidence. One interesting conclusion of Ramberg's work is that for normal incidence and for a certain regime of cathode thickness and escape depth, the photoemission "may be expected to be about 1.4 times as great for illumination from the glass side as for illumination from the vacuum side." Photomultiplier tubes with semitransparent photocathodes such as are used in typical scintillation counting applications are all designed for radiation incident on the glass substrate which supports the photocathode. The two curves of Fig. 40 are calculated from Ramberg's formulae for incidence through the glass faceplate, and for polarization perpendicular and parallel to the plane of incidence. (i.e. "parallel" implies that the electric vector lies in the plane defined by the incident ray and the normal to the glass surface.) These curves assume an index of refraction for the glass of 1.5, for the photosensitive layer of 3.25, and the absorption index for the photosensitive layer, K, of 3.25. The photocathode layer is assumed to be thin with respect to the wavelength of light—taken as 550 nanometers for Fig. 40.

Note that Ramberg's prediction is that response should be greater for perpendicular polarization, especially at large angles of incidence. This conclusion is at odds with some reported measurements. Experimental measurements for a semitransparent Cs_3Sb

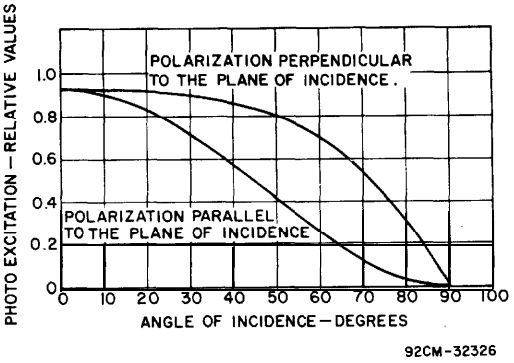

Fig. 40 - Theoretical photoexcitation determined by optical factors for different polarization orientation as a *function of angle of incidence. Radiation is incident on a semitransparent photocathode such as Cs_3Sb through a* glass *substrate of index of refraction 1.5. Data are taken from* **Ramberg.**[49]

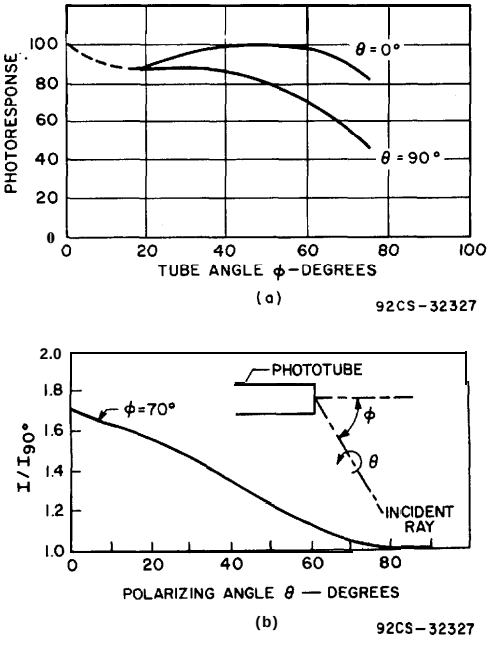

Fig. 41 - (a) Photoresponse for a semitransparent Cs_3Sb photocathode as a function of angle of incidence, Φ, for polarization parallel (0°) and perpendicular (90°) to the plane of incidence. (b) Photoresponse ratio for polarization angle, Θ, to the response at 90° measured at an angle of incidence of 70°(from Hoenig and **Cutler**[50]).

photocathode on Corning 9741 glass are reported by Hoenig and Cutler[50]. Their data, are shown in Fig. 41 **a** and b. Their curve, **a,** shows the variation of photosensitivity as a function of angle of incidence, ϕ, for two different angles of polarization. The subscript, $\Theta = 0°$ represents polarization parallel to the plane of incidence. The curve, **b,** shows the ratio of the photoresponse for polarization angle 0° to the photoresponse for perpendicular polarization ($\Theta = 90°$), both measured at 70° angle of incidence. Note that the response is greater for polarization **parallel** to the plane of incidence.

Measurements at RCA support the general conclusion that the response is higher for **parallel** polarization for Cs_3Sb, **K_2CsSb** and **Na_2KSb:Cs** semitransparent photocathodes at large angles of incidence. On the other hand, Hora[51] finds the response for a "trialkali antimonide" to be higher for perpendicular polarization.

It is likely that the discrepancies noted above are related to the differences in photocathode substrates (between the glass and the photocathode), photocathode thickness, and photocathode processing which may result in non-isotropic and structured layers, in contrast, for example, to the assumption by **Ramberg** of a very thin and isotropic photocathode layer.

Optical Devices to Enhance Photoresponse

Numerous optical devices have been devised to enhance photoresponse by utilizing multiple paths in the faceplate and photocathode. Experimental data and theoretical analyses have been reported by a number of different authors.[52-56] Fig. 42 shows a typical arrangement permitting the light beam to enter the glass substrate so that reflected rays approach the glass-air interface at an angle greater than the critical angle and thus do not permit a refracted ray to escape the glass. In this manner multiple excitations of the photosensitive layer are possible. Enhancement of the quantum efficiency for an alkali-antimonide photocathode may be something less than 2:1 in the blue where the absorption of the photocathode layer is high, but may be as high as 4: 1 in the red where the absorption is low.

An interesting series of measurements and theoretical predictions have been reported by

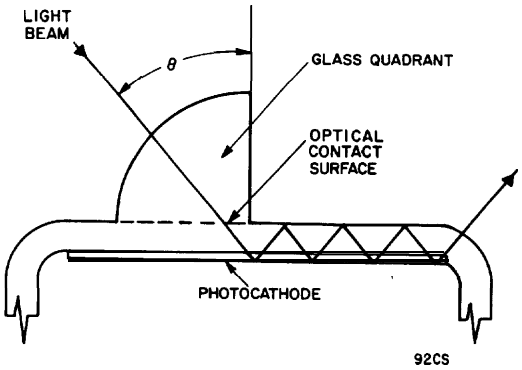

Fig. 42 - A glass quadrant in optical contact with the photocathode window, permitting incoming radiation to approach the glass-photocathode interface at any angle of incidence. When the angle, Φ, exceeds the critical angle for the glass-air interface (about 42°) all of the radiation is reflected, permitting multiple excitations of the photosensitive surface.

D.P. Jones[56] on the behavior of a semitransparent **Na_2KSb:Cs** photocathode with angle of incidence, wavelength, and polarization angle. The optical arrangement is similar to that shown in Fig. 42 except that a full 180° cylindrical lens is cemented to the faceplate and half of the surface is coated with aluminum to reflect the rays back to the photocathode. His data and theory favor perpendicular polarization, particularly at longer wavelengths.

Photocathode Uniformity

The uniformity of photocathode response over its area may be of importance in some applications. For example, in scintillation counting, light pulses which excite different areas of a non-uniform photocathode would then result in variations in measured pulse height. Such an effect would be more apparent in the case where the scintillating crystal is thin. In flying-spot scanners, nonuniform photocathode sensitivity would result in picture shading unless precaution is taken to avoid even approximate imaging on the photocathode surface.

Photocathode non-uniformity may result from a variety of causes. Fig. 43 shows some tests of photocathode uniformity. These curves represent photoresponse for a small focused (l/16-inch) spot as it is scanned across the diameter of a semitransparent photocathode. Curve (a) represents the

uniformity (± 3%) typical of a well-processed photocathode in a **2-inch** photomultiplier designed for scintillation counting. In curve **(b),** the variation (1) across the photocathode is the result of a non-uniform evaporation of antimony during the processing of the photocathode. Curve (c) shows some peculiar non-uniformities in a 3-inch photocathode. The peaks (2) are the result of light entering the rounded corner of the tube envelope and increasing emission by reflections in the glass faceplate. The peaks (3) result when light, which is transmited through the photocathode, strikes the reentry shoulder of the glass envelope. The inside shoulder of the envelope is aluminized as part of the photocathode contact. Some light striking the shoulder may be reflected back to the photocathode and cause **increased** emission, or there may actually be some photosensitivity on the shoulder because of the presence of processing materials.

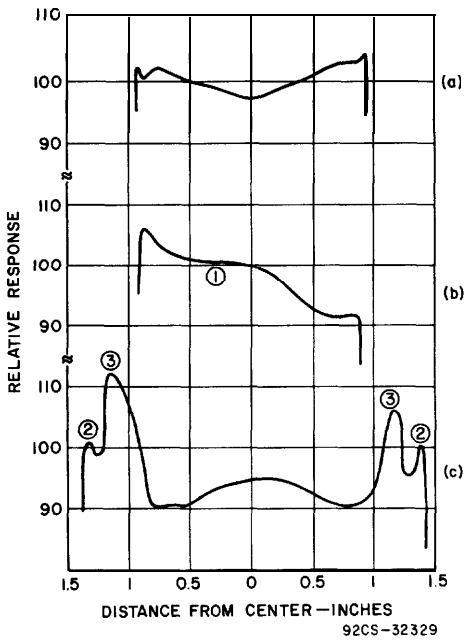

*Fig. 43 - Photocathode uniformity patterns observed by scanning a 1/16-inch **spot** across a diameter of a semitransparent photocathode in **2-inch** and **3-inch** photomultiplier tubes used in scintillation counting. (a), scan on a typical well-processed **2-inch** tube; **(b),** scan on a tube with non-uniform antimony evaporation on the faceplate (1); (c), scan on a typical **3-inch** tube showing peaks (2) due to entry of light on the edge of the faceplate and (3) peaks due to reflection or photoemission from transmitted radiation through the photocathode onto the shoulder of the bulb.*

Anomalies in the photocathode uniformity such as shown in Fig. 43(c) can be largely eliminated by a fabrication technique[57] creating a diffusing layer on the photocathode substrate. The fabrication of a diffusing layer can be easily accomplished by sandblasting the inside surface of the photomultiplier faceplate. The effect of the diffusing layer is to scatter the incoming light so that light transmitted through the photocathode is spread out in many directions, thus avoiding direct correlation between the position of the incoming light spot and any internal reflections. The diffusing layer also has a desirable effect of enhancing the photocathode sensitivity.

Uniformity of photocathode response, however, is not sufficient to assure a uniform output response from the photomultiplier. All of the emitted photoelectrons may not be properly directed to the first dynode by the electron optics. In the case of a Venetian-blind dynode structure, some of the photoelectrons may strike parts of the dynode which do not provide good collection fields to the second dynode. Fig. 44 is a

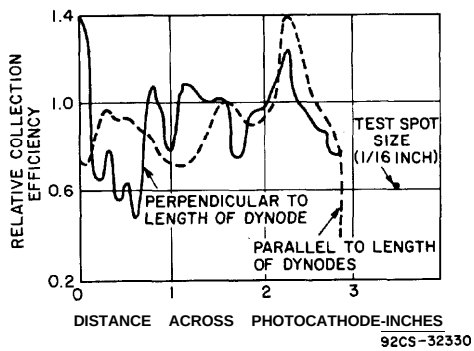

Fig. 44 - Relative collection efficiency for photoelectrons in a venetian-blind type photomultiplier tube.[58]

plot of collection uniformity in a 3-inch Venetian-blind photomultiplier tube. The structure in the pattern for the scan perpendicular to the length of the dynode is related to the individual slats in the Venetian-blind structure. By way of contrast, Fig. 45 shows similar collection uniformity plots for a 3-inch "teacup" design where the large

open structure of the "tea-cup" first dynode eliminates the electron-optical effects observed in the Venetian-blind type tube.

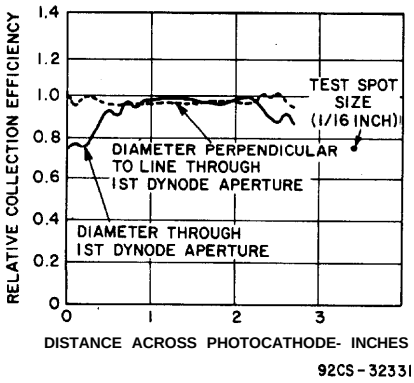

Fig. 45 - Relative collection efficiency for photoelectrons in a "teacup" type RCA photomultiplier tube.[58]

Uniformity of response of a photomultiplier may also be affected by the voltage at which the focusing electrode is operated. Many photomultipliers are equipped with a focusing electrode, between the photocathode and the first dynode to provide optimum collection of the photoelectrons emitted from the photocathode. The focusing-electrode voltage is usually set at the point at which maximum anode output current is obtained. In some applications, spatial uniformity i.e., the variation of anode current with position of photocathode illumination, may be more important than maximizing output current. In such cases, however, the final adjustment of the focusing-electrode potential should not differ significantly from the adjustment that provides optimized collection efficiency. Fig. 46 shows a typical focusing-electrode characteristic.

Photocathode Stability

Stability and life of a photocathode is usually related approximately inversely to the current drawn from it. More stable and reliable performance results if small areas of concentrated illumination on the cathode surface are avoided. In normal operation of photomultipliers, of course, the photocathode current is usually small and damage to the tube is more likely to be caused by the amplified secondary emission currents in the latter dynode stages.

If a photomultiplier were to contain any significant trace of gas, ionization of the gas could occur , depending upon the applied voltages and level of photocurrent. Ion bombardment of the photocathode can readily cause damage and loss of sensitivity in proportion to the ion current. Photomultiplier tubes, however, are generally so well evacuated that ion damage is essentially only a theoretical possibility.

Electrolytic effects can bring about serious fatigue in Cs_3Sb photocathodes (Ref. 11, p. 79) and presumably in other alkali-antimonide photocathodes. An electrolytic effect is caused when a potential gradient is maintained across the cathode surface. Photocathodes generally only have one physical contact, but a gradient can be developed because of the resistive nature of the photocathode layer if a large photocurrent is drawn, for example, from a center spot on the cathode. Actual electrolytic decomposition takes place, which can be recognized by a color change in the cathode material.

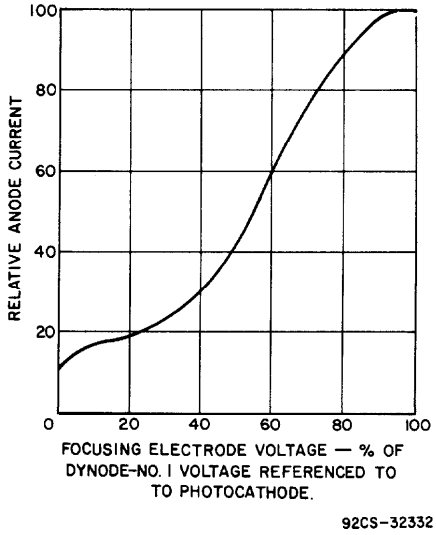

Fig. 46 - A typical focusing-electrode characteristic.

It is also possible to damage a photocathode by maintaining a difference in potential through the faceplate supporting the photocathode, particularly at elevated temperatures. For example, if the photocathode in a photomultiplier is maintained at − 1000

volts and a ground plane at 0 volts is established on the outside surface of the glass, ionic conduction takes place through the glass. Photocathode sensitivity will be gradually deteriorated by the ionic reaction.[69]

Photomultiplier tubes should be stored in the dark when not in use. Blue and ultraviolet radiation, especially, can cause photochemical changes in the photocathode which result in changes in sensitivity. It is especially important to avoid exposure to intense illumination such as sunlight even when no voltage is applied to the tube. Permanent damage may also result if the tube is exposed to radiation so intense that it causes excessive heating of the photocathode. Tubes should not be stored for long periods at temperatures near the maximum rating of the tube; high temperatures almost always result in loss of sensitivity in the photocathode.

A photomultiplier having a multialkali photocathode (S-20 spectral response) tends to lose sensitivity especially in the red portion of its spectral response upon extended exposure to high ambient room lighting; the change is usually permanent. Contrary to this behavior, photocathodes of the extended red multi-alkali (ERMA) type apparently do not exhibit this loss.

The Ag-O-Cs photocathode (S-l) spectral response) also suffers a decrease in sensitivity, particularly during operation, when exposed to high radiant-energy levels normally not harmful to other types of photocathode materials. The decreased sensitivity occurs primarily in the infrared portion of the spectrum. Loss of infrared sensitivity may also occur following long periods of storage.

The GaAs:Cs photocathode is particularly sensitive to responsivity loss even for photocurrents as small as 0.1 μA.

Another effect related to the exposure of photocathodes to excessive blue or ultraviolet radiation, as from fluorescent room lighting, is a temporary increase in photocathode dark emission current. The increase may be as much as three orders of magnitude even from relatively short exposure. This increase in dark current occurs even though voltage is not applied to the tube and may persist for a period of from 6 to 24 hours after such irradiation. Fig. 47 illustrates the recovery after exposure to fluorescent-lamp radiation for several photocathode types. Some of this effect is the result of phosphorescence in the glass faceplate of the photomultiplier, but a larger part of the effect is apparently an excitation phenomena in the photocathode itself.[68]

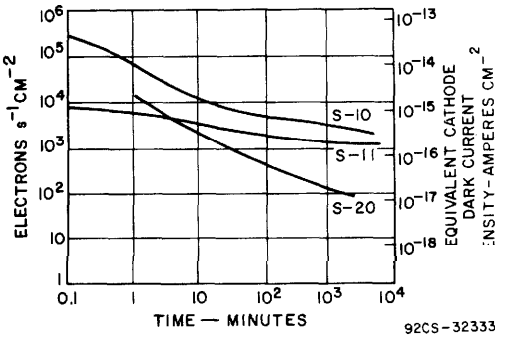

Fig. 47 - Variation of dark current following exposure of photocathode to cool white fluorescent-lamp radiation. The various photocathodes are identified by their spectral-response symbols.

When semitransparent photocathodes such as Cs_3Sb and Ag-Bi-O-Cs (and probably others) are kept in the dark for many hours, they become very resistive[59], especially at reduced temperatures. The effect may be so great that the photomultiplier may appear to have lost sensitivity. Apparently, passage of current through the photosensitive layer as a result of normal operation restores the photocathode conductivity. At reduced temperatures, the process may require minutes or hours of operation to return the photocathode to a reasonable conductivity.

Photomultiplier tubes have been exposed to gamma and X-radiation to an intensity of 10^{10} roentgens per hour by the Naval Radiological Defense Laboratory.[60] No photocathode damage was noted except that faceplate discoloration was observed for exposure in excess of 10^4 roentgens. Glass fluorescent effects were also noted during the tests. For applications where excessive radiation may be present, it may be noted that Corning has developed a non-browning glass, Ce-doped No. 9025, which has been used for special photomultipliers.

As a result of enhanced dark count rates observed in photomultiplier tubes used in various earth-orbiting satellites, an in-

vestigation was made by Viehmann et al[61] on fluorescent and phosphorescent effects in windows used in photomultiplier tubes when bombarded by beta rays. Source of the beta rays was an 0.8 millicurie beta emitter, $^{90}Sr-^{90}Y$, with beta energies in a range up to 2.23 MeV (megaelectron volts). A number of special windows were tested. For Coming 9741 glass, two decay constants were observed in the phosphorescense: 4.2 and 57 minutes. For an exposure of 9.5 x 10^{10} electrons per square centimeter in 30 minutes, an initial count of more than 3×10^4 s^{-1} (2π steradian)$^{-1}$ was observed in a photomultiplier with an S-20 response, closely coupled to the glass plate.

GAIN-RELATED CHARACTERISTICS

Gain vs. Voltage

When several secondary-emission stages are coupled together, so that the secondary electrons from one become the primary electrons of the next, the total gain μ of the multiplier phototube is given by

$$\mu = \delta^n \qquad (14)$$

where δ is the secondary emission per stage (assumed to be equal for each stage) and n is the number of stages. It is also assumed in this expression that all the secondary electrons are collected at the next stage.

In practice, some of the electrons may skip stages, or become lost to the amplification process by impinging upon nonproductive secondary-emission areas.

It is customary to describe the gain of the multiplier phototube as a function of the applied voltage. Fig. 48 shows two such curves on a semilog scale. These curves illustrate the wide range of amplification in a multiplier phototube. They also indicate the necessity of providing a well regulated voltage supply for the dynode stages.

It is possible to operate a four-to-six stage photomultiplier so that each stage is at the voltage required for maximum secondary emission, as shown in Fig. 19. In such cases, the gain could be made practically independent of voltage over a small range. However, such a condition would require approximately 500 volts per stage; thus the total voltage required would be very high for the amount of gain achieved.

In the design or operation of a multiplier phototube having a fixed supply voltage, the number of stages can be chosen so that the gain of the tube is maximum. For this purpose, the optimum voltage per stage is that value at which a line through the origin (unity gain on the log-gain scale) is tangent to the curve, as shown in Fig. 48. This point is

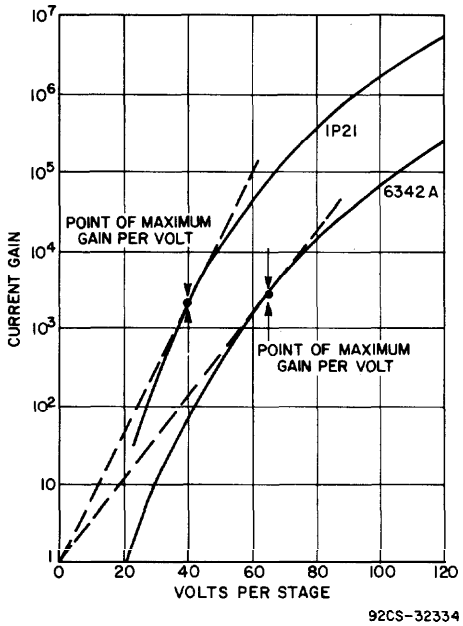

Fig. 48 - Log of gain as a function of volts per stage for a tube (1P21) with Cs-Sb dynodes and for a tube (6342A) with Cu-Be dynodes.

identified on the graph as the point of maximum gain per volt. (Note that this argument neglects the voltage used between the last dynode and the anode and any discrepancy resulting from nonuniform distribution of voltage per stage). In most applications of multiplier phototubes, the tubes are operated above the point of maximum gain per volt. When both the gain and the voltage are presented on a logarithmic scale, the resultant curve is then closely approximated by a straight line. Fig. 49 describes the anode sensitivity in amperes per lumen and the typical amplification characteristics of a photomultiplier as a function of the applied voltage. Curves of minimum and maximum sensitivity are also shown.

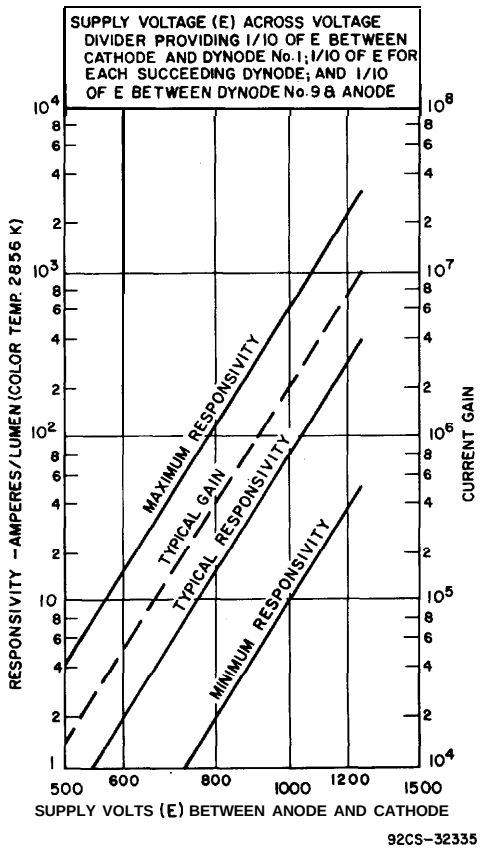

Fig. 49 - Typical anode sensitivity and amplification characteristics of a photomultiplier tube as a function of applied voltage. Note the log-log scaling.

External Magnetic and Electrostatic Fields

All photomultipliers are to some extent sensitive to the presence of external magnetic and electrostatic fields. These fields may deflect electrons from their normal path between stages and cause a loss of gain. Tubes designed for scintillation counting are generally very sensitive to magnetic fields because of the relatively long path from the cathode to the first dynode; consequently, such tubes ordinarily require electrostatic and magnetic shielding. Magnetic fields may easily reduce the anode current by a much as 50 per cent or more of the "no-field" value.

The three curves in Fig. 50 show the effect on anode current of magnetic fields parallel to the main tube axis and perpendicular to the main axis in the directions parallel and perpendicular to the dynodes. The curves are

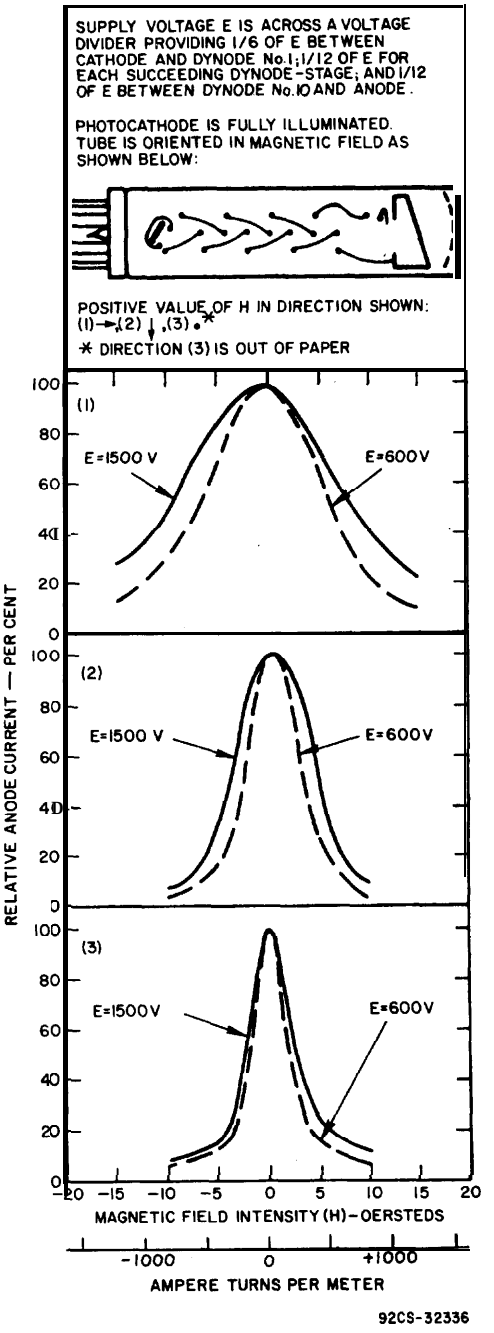

Fig. 50 - Curves for 3/4-inch diameter type 4516 photomultiplier showing the effect on anode current of magnetic fields parallel to the main axis of the tube and perpendicular to the main axis in the directions parallel and perpendicular to the dynodes. (Units for magnetic field intensity are shown in both SI units, ampere turns per meter, and conventional cgs units, oersteds. Note that 1 oersted

= $10^3/4\pi$ ampere turns per meter. Photomultiplier tubes contain some parts which have magnetic properties, but if they are neglected, the magnetic induction-or magnetic flux density B-measured in units of gauss would be numerically the same as the oersted values. in the case of SI units for magnetic induction, 1 weber per square meter = 1 tesla = 10^4 gausses.)

usually provided for one or more values of over-all applied voltage and indicate the relative anode current in per cent as a function of magnetic field intensity. Fig. 51 shows the variation of output current of several photomultiplier tubes as a function of magnetic-field intensity directly parallel to the major axis of the tube. The magnitude of the effect depends to a great extent upon the structure of the tube, the orientation of the field, and the operating voltage. In general, the higher the operating voltage, the less the effect of these fields.

High-mu material in the form of foils or preformed shields is available commercially for most photomultipliers. When such a shield is used, it must be at cathode potential. The use of an external shield may present a safety hazard because in many applications the photomultiplier is operated with the anode at ground potential and the cathode at a high negative potential. Adequate safeguards are therefore required to prevent personnel from coming in contact with the high potential of the shield.

It is possible to modulate the output current of a photomultiplier with a magnetic field. The application of a magnetic field generally causes no permanent damage to a photomultiplier although it may magnetize those internal parts of a tube that contain ferromagnetic materials (tubes are available which contain practically no ferromagnetic materials). If tube parts do become magnetized, the performance of the tube may be

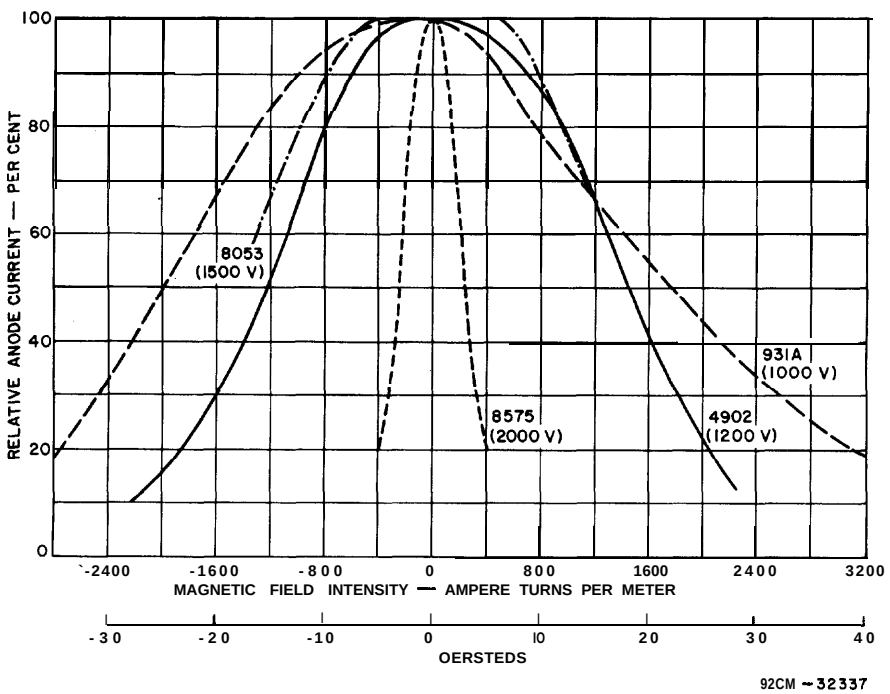

Fig. 51 - Variation of output current of several photomultiplier tubes as a function of magnetic-field intensity directly parallel to the major axis of the tube. Positive values of magnetic field are in the direction of the tube base. Operating voltages are indicated. The 931A is a circular-cage, side-on type. The 4902, 8053 and 8575 are 2-inch end-on types: teacup; Venetian-blind dynode; and in-line dynode structure, respectively.

degraded somewhat; however, the condition is easily corrected by degaussing, a process in which a tube is placed in and then gradually withdrawn from the center of a coil operated at an alternating current of 60 Hz with a maximum field strength of 8000 ampere turns per meter (100 oersteds).

Linearity

Because the emission rate of photoelectrons is proportional to the incident radiant flux, and the yield of secondary electrons for a given primary electron energy is proportional to the number of primary electrons, the anode current of a photomultiplier is proportional to the magnitude of the incident radiant flux. A linearity plot over a wide range of light level is shown in Fig. 52

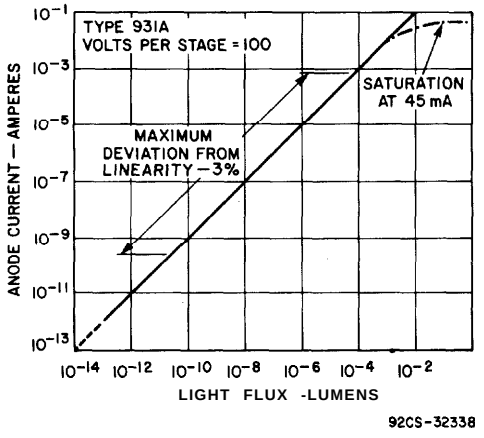

Fig. 52 - Range of anode-current linearity as a function of light flux for a 931A photomultiplier.

for a type 931A. The limit of linearity occurs when space charge begins to form. Space-charge-limiting effects usually occur in the space between the last two dynodes. The voltage gradient between anode and last dynode is usually much higher than between dynodes and, therefore, results in a limitation at the previous stage, even though the current is less. The maximum output current, at the onset of space charge, is proportional to the 3/2 power of the voltage gradient in the critical dynode region. By use of an unbalanced dynode-voltage distribution increasing the interstage voltages near the output end of the multiplier, it is possible to increase the linear range of output current.

Table III provides guidance as to the maximum pulse current which can be drawn from the anode of various types of photomultipliers before spacecharge effects limit linearity. Note that the type 8575, which has a focused dynode structure, provides the highest withdrawal fields and highest linear output current. On the other hand, venetian-blind or box-and-slot dynodes have relatively low withdrawal fields. Higher currents can be obtained from all types of photomultipliers by unbalancing the voltage distribution to provide higher fields at the critical last stages.

Some photomultipliers used in applications requiring high output pulse current use an accelerating grid between the last dynode and the anode to reduce the effects of space-charge limiting. The potential of such a grid is usually between that of the last and the next-to-last dynode and is adjusted by observing and maximizing the value of the anode output current.

Another factor that may limit anode-output-current linearity is cathode resistivity; cathode resistivity is a problem only in tubes with semitransparent photocathodes, particularly of the Cs-Sb or bialkali type.

Linear behavior is not always obtained from photomultipliers even at low current levels. For example, if the test light spot on a 931A is not directed close to the center of the active area of the photocathode, disturbing effects may arise from the proximity of the ceramic end plates. Near the end plates, the fields are not uniform and are affected by charge patterns on the insulator spacers, which change with the current level. An exterior negative shield placed around the bulb wall may improve tube linearity by eliminating bulb charging effects. The passage of excessive current may change the sensitivity of the tube and cause an apparent nonlinearity.

Some photomultipliers exhibit a temporary instability in anode current and change in anode sensitivity for several seconds after voltage and light are applied. This instability, sometimes called hysteresis because of cyclic behavior, may be caused by electrons striking and charging the dynode support spacers and thus slightly changing the electron optics within the tube. Sensitivity may overshoot or undershoot a few per

cent before reaching a stable value. The time to reach a stable value is related to the resistance of the insulator, its surface capacitance, and the local photomultiplier current. This instability and non-linear behavior may be a problem in applications such as photometry where a photomultiplier is used in a constant-anode-current mode by varying the photomultiplier voltage as the light input changes.

Table III

Maximum Anode Currents That Can be Utilized in Various Photomultiplier Types Without Serious Loss of Linearity from Space-Charge Build-up.

Tube Type	Supply Volts	Voltage Distribution*	Maximum Output Current (mA) with Linearity Loss Less Than 10%
931A (side-on, circular cage)	1000	1,1,1,1,1,1,1,1,1,1	
4524 (3-inch, venetian-blind dynodes)	1500	2,1,1,1,1,1,1,1,1,1,1	5
4900 (3 -inch, Tea-cup type)	1200	2,1,1,1,1,1,1,1,1,1,1	5
8575 (2-inch, linear focused dynode structure)	1760	4,1,1.4,1,1,1,1,1,1,1,1,1,1	30
8575	2100	4,1,1.4,1,1,1,1,1,1,1.5,2,4,2	120
C-31059 (1 1/8-inch, box and slot dynodes)	1050	2,1,1,1,1,1,1,1,1,1,2,1	4
C-31059	1150	2,2.5,1,1,1,1,1,1,1,2,3,2	12

*These number series represent the relative voltage applied between cathode and first dynode, first dynode and second dynode,. . . . . , last dynode and anode. Note that in the case of the 8575 and the C-31059, a second voltage distribution is given with increased voltage drop in the last stages providing higher output currents before the onset of space-charge-limiting conditions.

Hysteresis has been eliminated in many tubes by coating the dynode spacers with a conductive material in the manufacturing process and maintaining the coating at a fixed potential. Tubes treated by this method assume final sensitivity values almost immediately upon application of light and voltage.

Peak linear and saturation currents are usually measured by pulsed methods. One common method makes use of a cathode-ray tube with a P15 or P16 phosphor. The grid is double-pulsed with pulses of unequal amplitudes but fixed amplitude ratio. As the amplitude of the two pulses is increased, a point is observed at which the amplitude of the larger of the anode pulses does not increase in the same proportion as the smaller pulse. At this point the tube is assumed to become non-linear. The current value at this point is then measured by means of an oscilloscope and load resistor. The maximum saturation current is found when a further increase in radiation level yields no further increase in output.

Although very high anode current can be drawn from photomultiplier tubes, it should be emphasized that stability cannot be expected at such levels. These high current levels are principally of interest in **light-**pulse applications. In this case, the stability of the tube is approximately that of the tube operated at the integrated average current level.

Gain Variation with Temperature

It is often advisable to reduce the ambient temperature of a photomultiplier in order to reduce dark emission from the photocathode and improve the signal-to-noise ratio of the measurement. Variations of the spectral characteristics of photocathodes with temperature have been noted in the previous section on **Photocathode Stability.** There are numerous reports on the over-all variation of the photomultiplier output current with temperature including the effect of temperature on photocathode **sensitivity**[62-64]. Fig. 53 is a typical characteristic for type 8571 photomultiplier having Cs-Sb dynodes showing the variation of gain with temperature. These data do not include the variation of photocathode response with temperature which has been described in the section on **Variations in Spectral Response with Temperature.** The gain data were obtained by measuring both the anode response variation and the photocathode response variation with temperature and dividing out the latter to obtain only the gain variation. It is probable that the increase in gain at low temperatures is the result of a decrease in energy loss from lattice scattering. Although the variation in over-all gain is fairly large, it should be remembered that the variation results from a small variation in each stage compounded by the 9 stages. At room temperature, the average gain per stage for the 8571 is 4.5 at 100 V per stage and the percentage change in stage gain with temperature is approximately -0.06% per °C. Thus the secondary emission temperature coefficient is generally less that the photoresponse temperature coefficient, both for Cs-Sb surfaces. See Fig. 37.

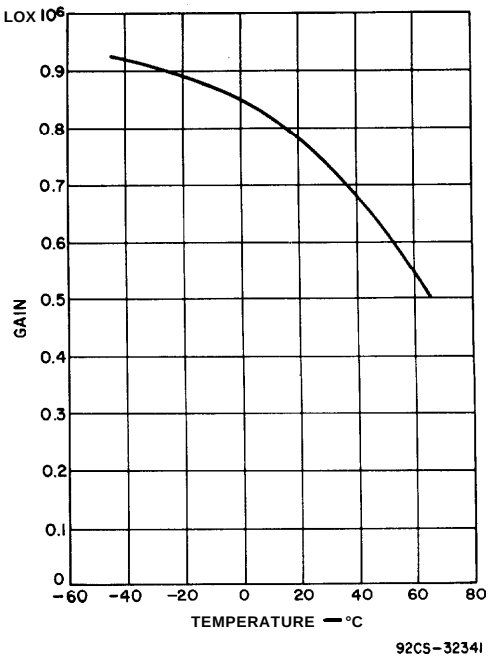

*Fig. 53 - Typical variation of gain with temperature for a **9-stage** photomultiplier tube (type 8571) with Cs-Sb dynodes operating at 100 volts per stage.*

A few words of caution regarding the ambient temperature of photomultipliers are pertinent. A maximum ambient temperature, and in some instances a minimum temperature, is specified for all **photo-**

multipliers. The specification of maximum ambient temperatures reduces the possibility of heat damage to the tube. Cesium, for example, is very volatile and may be redistributed within the tube causing loss of secondary emission gain or loss of cathode sensitivity.

It is recommended that photomultipliers be operated at or below room temperature so that the effects of dark current are minimized. The variation of dark current, or noise, is most important because of its effect on ultimate low-light-level sensitivity. Various cryostats and solid-state thermionic coolers have been designed that reduce dark current at low temperatures in low-light-level applications. An important consideration in the use of these devices is to prevent condensation of moisture on the photomultiplier window. A controlled low-humidity atmosphere or special equipment configuration may be necessary to prevent such condensation.

Another reason for avoiding the operation of photomultipliers at extremely low temperatures is the possible phase change that this type of operation may cause in some of the metal parts. These changes are particularly probable when Kovar is used in metal-to-glass seals. Tubes utilizing Kovar in their construction should not be operated at temperatures below that of liquid nitrogen (-196°C).

In some tubes, particularly those with multialkali photocathodes, it is sometimes observed that the noise actually increases as the temperature of the photocathode is reduced below about -40°C. The reason for this noise increase is not understood. However, most of the dark-current reduction has already been achieved at temperatures above -40°C.

In general, it is recommended that all wires and connections to the tube be encapsulated for refrigerated operation. Encapsulation minimizes breakdown of insulation, especially that caused by moisture condensation.

Stability and Gain

All photomultipliers have a maximum anode current rating. The primary reason for such a rating is to limit the anode power dissipation to approximately one-half watt or less. Consequently, the magnitude of the maximum anode current is restricted to a few milliamperes when the tube is operated at 100 to 200 volts between the last dynode and the anode. Many photomultipliers are rated for only 0.1 mA or less.

Operating a photomultiplier at an excessively high anode current results in an increased fatigue that occurs as the average anode current increases. The loss in sensitivity occurs as a result of a reduction in the secondary emission, particularly in the last stages of the photomultiplier where the currents are the highest.

Tube fatigue or loss of anode sensitivity is a function of output-current level, dynode materials, and previous operating history. The amount of average current that a given photomultiplier can withstand varies widely, even among tubes of the same type; consequently, only typical patterns of fatigue may be cited.

The sensitivity changes are thought to be the result of erosion of the cesium from the dynode surfaces during periods of heavy electron bombardment, and the subsequent deposition of the cesium on other areas within the photomultiplier. Sensitivity losses of this type, illustrated in Fig. 54 for a 1P21

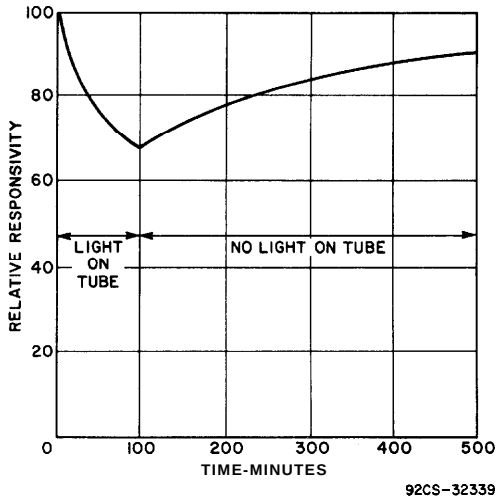

Fig. 54 - Short-time fatigue and recovery characteristics of a typical 1P21 operating at 100 volts per stage and with a light source adjusted to give 100 microamperes initial anode current. At the end of 100 minutes the light is turned off and the tube allowed to recover sensitivity. Tubes recover approximately as shown, whether the voltage is on or off.

operated at an output current of 100 microamperes, may be reversed during periods of non-operation when the cesium may again return to the dynode surfaces. This process of recovery may be accelerated by heating the photomultiplier during periods of non-operation to a temperature within the maximum temperature rating of the tube; heating above the maximum rating may cause a permanent loss of sensitivity.

Sensitivity losses for a given operating current normally occur rather rapidly during initial operation and at a much slower rate after the tube has been in use for some time. Fig. 55 shows this type of behavior for a

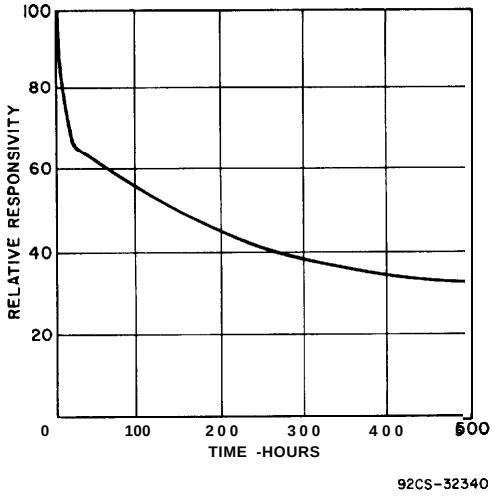

Fig. 55 - Typical sensitivity loss for a 1P21 operating at 100 volts per stage for a period of 500 hours. Initial anode current is 100 microamperes and is readjusted to this operating value at 48, 168, and 360 hours.

1P21 having Cs-Sb dynodes, operating at an output current of 100 microamperes. Tubes operated at lower current levels, of the order of 10 microamperes or less, experience less fatigue than those operated at higher currents, and, in fact, may actually recover from high-current operation during periods of low-current operation.

Fatigue rates are also affected by the type of dynode materials used in a tube. Copper beryllium or silver magnesium dynodes are generally more stable at high operating currents than the cesium antimony types. The sensitivity for tubes utilizing these dynodes very often increases during initial hours of

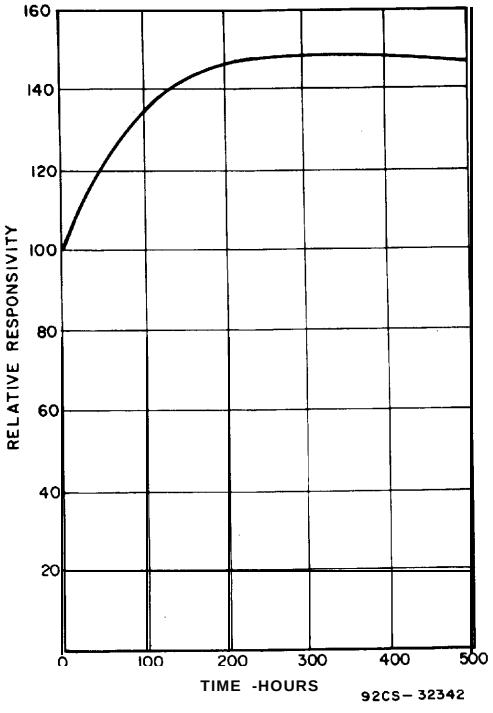

Fig. 56 - Typical responsivity variation on life for a photomultiplier having silver-magnesium dynodes. Initial anode current was 2 milliamperes and was readjusted to this operating value at 48, 168, and 360 hours.

operation, after which a very gradual decrease takes place, as illustrated in Fig. 56.

The operating stability of a photomultiplier depends on the magnitude of the average anode current; when stability is of prime importance, the use of average anode currents of 1 microampere or less is recommended.

In addition to the life characteristics, which are probably the result of changes in the dynode layer itself, other changes of a temporary nature also occur. Not all these changes are well understood; some are charging of insulators in the tube.

Fig. 57 illustrates one of the peculiar instabilities which are sometimes observed in photomultiplier tubes. When the light is first turned on, the current apparently overshoots and then decays to a steady value. This particular phenomenon is probably the result of the charging of the supporting insulator for the dynodes. The effect is observed to occur more rapidly at higher currents, presumably

because of the greater charging current. Electrons striking the insulator probably result in secondary emission and a resultant positive charge. The change in potential affects the electron optics in the space between dynodes. The effect is observed as an increase in some tubes and as a decrease in others. When the photomultiplier is designed with metal shields or with conductive coatings on the critical areas of the insulators, this effect is eliminated.

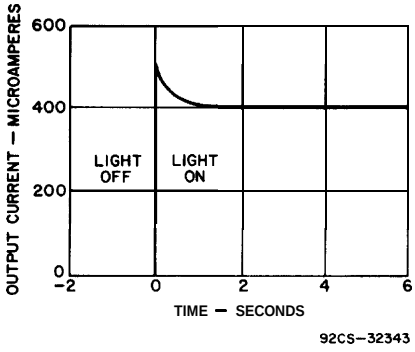

Fig. 57 - Sudden shift in anode current probably as the result of insulator spacer charging. Observation was made using an experimental photomultiplier in which the effect was unusually large.

A related phenomenon is the variation of pulse height with pulsecount rate in scintillationcounting applications. Thus, when a radio-active source is brought closer to a scintillating crystal a greater rate of scintillations should be produced, all having the same magnitude. In a particular photomultiplier a few per cent change in amplitude may result and cause problems in measurement. Fig. 58 shows the typically minor variation of pulse height with pulse-count rate for a type 6342A multiplier phototube.

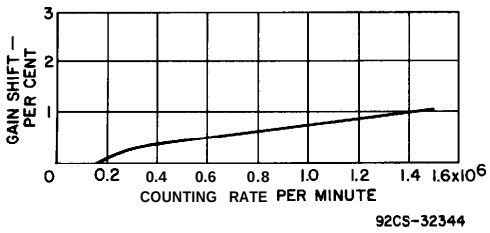

Fig. 58 - Typical variation of pulse height with pulsecount rate for a 6342A. (^{137}Cs source with a NaI:Tl source).

In order to investigate the phenomena of pulse-height variation with pulsecount rate, a purposely exaggerated experiment was devised. Instead of a scintillating crystal, a pulsed cathode-ray tube was used as a light source. Two pulse rates were studied: 100 and 10,000 pulses per second. Pulse duration was one microsecond; decay time to 0.1 maximum was 0.1 microsecond. The experiment was devised to study the rate at which the photomultiplier tube output response changed when the pulse rate was suddenly switched between the two rates. Tubes such as the **6342A,** and especially the 8053 and 8054, showed practically no effect (of the order of one per cent or less). Fig. 59 shows

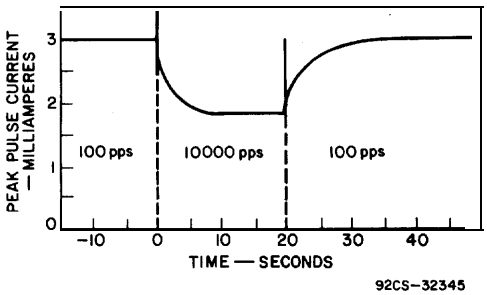

Fig. 59 - Variation of output pulse height as the rate of pulsing is changed in a poorly designed experimental tube. Light pulses were provided from a cathode-ray tube. At the left of the graph, which shows the pulse-amplitude envelope with time for the output of the photomultiplier tube, the pulses are at 100 per second. The pulse rate is increased suddenly to 10,000 per second and again reduced as indicated. Changes in amplitude are probably the result of insulator charging.

the pulses during the switching procedure for an experimental tube. The phenomena were completely reversible and were observed (to a lesser extent) on many different tube types. The time-decay period of several seconds suggests the charging of an insulator spacer to a new potential as the result of the increased charge flow and the subsequent modification of interdynode potential fields.

In scintillation counting it is particularly important that the photomultiplier have very good stability. There are two types of gain stability tests which have been used to evaluate photomultipliers for this **applica-**

tion: (1) a test of long-term drift in pulse-height amplitude measured at a constant counting rate; and (2) a measure of short-term pulse-height amplitude shift with change in counting rate.

In the **time stability test,** a pulse-height analyzer, a ^{137}Cs source, and a NaI(T1) crystal are employed to measure the pulse height. The 137Cs source is located along the major axis of the tube and crystal so that a count-rate of 1000 counts per second is obtained. The entire system is allowed to warm up under operating conditions for a period of one-half to one hour before readings are recorded. Following this period of stabilization, the pulse height is recorded at one-hour intervals for a period of 16 hours. The drift rate in per cent is then calculated as the mean gain deviation (MGD) of the series of pulse-height measurements, as follows:

$$MGD = \frac{\sum_{i=1}^{i=n} | p - p_i |}{n} \cdot \frac{100}{p} \qquad (15)$$

where p is the mean pulse height, pi is the pulse height at the i^{th} reading, and n is the total number of readings. Typical maximum mean-gain-deviation values for photomultipliers with high-stability Cu-Be dynodes are usually less than 1 per cent when measured under the conditions specified above. Gain stability becomes particularly important when photopeaks produced by nuclear disintegrations of nearly equal energy are being differentiated.

In the **count-rate stability test,** the photomultiplier is first operated at 10,000 counts per second. The photopeak counting rate is then decreased to 1000 counts per second by increasing the source-to-crystal distance. The photopeak position is measured and compared with the last measurement made at a counting rate of 10,000 per second. The count-rate stability is expressed as the percentage gain shift for the count-rate change. It should be noted that count-rate stability is related to the hysteresis effect discussed above. Photomultipliers designed for counting stability may be expected to have a value of no greater than 1 per cent gain shift as measured by this count-rate stability test.

Life Expectancy

The life expectancy of a photomultiplier, although related to fatigue, is very difficult to predict. Most photomultipliers will function satisfactorily through several thousand hours of conservative operation and proportionally less as the severity of operation increases. Photomultipliers do not have elements which "burn out" as in the case of a filament in a vacuum tube. Furthermore, loss of sensitivity which occurs with operation tends to recover during idle periods or during conservative operation.

Factors which are known to affect life adversely are high-current operation, excessive-voltage operation, high photocathode illumination, and high temperature.

Operation of photomultipliers in regions of intense nuclear radiation or X-rays may result in an increase in noise and dark current as a result of fluorescence and scintillation within the glass portions of the tubes. Continued exposure may cause darkening of the glass and a resultant reduction in transmission capability.

DARK CURRENT AND NOISE

The lower limit of light detection for a photomultiplier tube is determined in many cases by the electrical noise associated with the anode dark current. There are several sources of dark current in a photomultiplier. These sources are described below,

Sources of Dark Current

Dark current in a photomultiplier tube may be categorized by origin into three types: ohmic leakage, dark or "thermionic" emission of electrons from the cathode and other elements of the tube, and regenerative effects .

Ohmic leakage, which results from the imperfect insulating properties of the glass stem, the supporting members, or the plastic base, is always present. This type of leakage is usually negligible, but in some tubes it may become excessive because of the presence of residual metals used in the processing of the photocathode or the dynodes. Condensation of water vapor, dirt, or grease on the outside of the tube may increase ohmic leakage beyond reasonable limits. Simple precautions are usually sufficient to eliminate this sort of leakage. In unfavorable environmental conditions, however, it may be necessary

to coat the base of the tube with moisture-resisting materials, which may also prevent external arc-overs resulting from high voltage.

Ohmic leakage is the predominant source of dark current at low-voltage operating condition. It can be identified by its proportionality with applied voltage. At higher voltages, ohmic leakage is obscured by other sources of dark current.

Fig. 60 shows the typical variation of dark

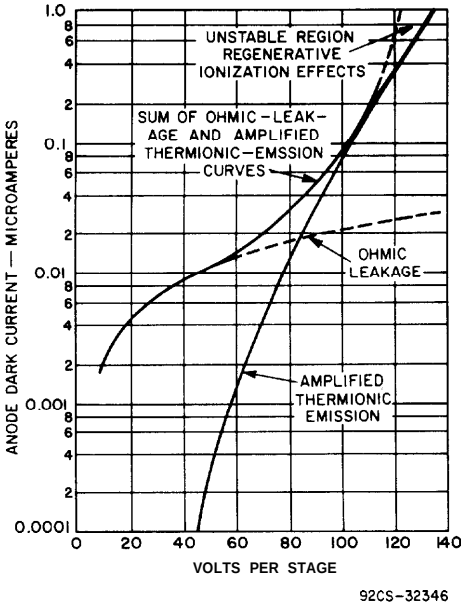

Fig. 60 - Typical variation of dark current with voltage for a multiplier phototube.

current of a photomultiplier tube as a function of applied voltage. Note that in the mid-range of voltage, the dark current follows the gain characteristic of the tube. The source of the gain-proportional, dark current is the dark or **thermionic emission** of electrons primarily from the photocathode. Because each electron emitted from the photocathode is multiplied by the secondary-emission gain of the tube, the result is an output pulse having a magnitude equal to the charge of one electron multiplied by the gain of the tube. (There are statistical amplitude variations which will be discussed later.) Because the emission of thermionic electrons is random in time, the output dark current consists of random unidirectional pulses. The time average of these pulses, which may be measured on a dc meter, is usually the principal dc component of the dark current at normal operating voltages. The limitation to the measurement of very low light levels is the variable character of the thermionic dark-current component. It is not possible to balance out this wide-band noise component of the photomultiplier tube, as it might be to balance out a steady ohmic-leakage current. Nevertheless, it is usually advantageous to operate the photomultiplier tube in the range where the thermionic component is dominant. In this range, the relationship between sensitivity and noise is fairly constant as the voltage is increased because both the photoelectric emission and the thermionic emission are amplified by the same amount.

Typical dark emission current densities for various photocathodes are given in Table I (page 16). The resulting anode dark current may be estimated by multiplying the dark emission per unit area at the photocathode by the photocathode area and by the gain of the photomultiplier tube at the desired operating voltage.

The **thermionic component** of the dark current varies in a regular way with temperature as illustrated in Fig. 16, and because the thermionic component of the dark current is a source of electronic noise in the anode circuit, it is frequently advantageous to cool the photomultiplier and take advantage of the reduced dark current and noise. Various cryostats have been designed[62,66] providing low temperature operation of photomultipliers. One practical consideration is the prevention of condensation of moisture on the window. In a Dewar-type arrangement, condensation may not be a problem; in simpler set-ups moisture condensation may be prevented by a controlled low-humidity atmosphere at the external window. On some types of photocathode, too cool a temperature may result in the photocathode becoming so resistive that the photoemission is blocked by a drop in potential across the photocathode surface. See earlier section on **Current-Voltage Characteristics.** Commercial cryostats or cooled photomultiplier chambers are available designed especially for photomultiplier operation[67].

At higher dynode voltages, a **regenerative type of** dark current develops, as shown in

Fig. 60 . The dark current becomes very erratic, and may at times increase to the practical limitations of the circuit. Continued flow of large dark currents may cause damage to the sensitized surfaces. Some possible causes of the regenerative behavior will be discussed in more detail later. All photomultiplier tubes eventually become unstable as the gain is increased.

Dark-Current Specification

Dark-current values are often specified at a particular value of anode sensitivity rather than at a **fixed** operating voltage. Specifications of dark current in this manner are more closely related to the actual application of the photomultiplier.

The best operating range for a given photomultiplier can usually be predicted from the quotient of the anode dark current and the luminous sensitivity at which the dark current is measured. This quotient is identified as the **Equivalent Anode Dark Current Input** (EADCI) in the Technical Data for individual photomultiplier tubes; and is the value of radiant flux incident on the photocathode required to produce an anode current equal to the dark current observed. The units used in specifying **EAD-**CI are either lumens or watts at the wavelength of maximum cathode responsivity or watts at a specified wavelength.

The curves in Fig. 61 shows both typical anode dark current and equivalent anode dark current input (EADCI) as functions of luminous sensitivity. The optimum operating range occurs in the region of the minimum on the EADCI curve, the region in which the signal-to-noise ratio is also near its maximum. The increase in the EADCI curve at higher values of sensitivity indicates the onset of a region of unstable and erratic operation. Many curves of this type also include a scale of anode-to-cathode supply voltage corresponding to the sensitivity scale.

Equivalent Noise Input-The dark current in a photomultiplier is the average current value of the output pulses occurring at random intervals plus the dc leakage current. Fluctuations or noise associated with these pulses limit precision of measurement, rather than the particular dark current value. Noise from a photomultiplier may be evaluated in terms of a signal-to-noise-ratio measurement. If the type of modulation and bandwidth used in the measurement is known, an equivalent noise input, **ENI,** can be calculated from the signal-to-noise ratio, Equivalent noise input is defined as the value of incident luminous or radiant flux which, when modulated in a stated manner, produces an rms output current equal to the rms noise current within a specified bandwidth, usually 1 Hz.

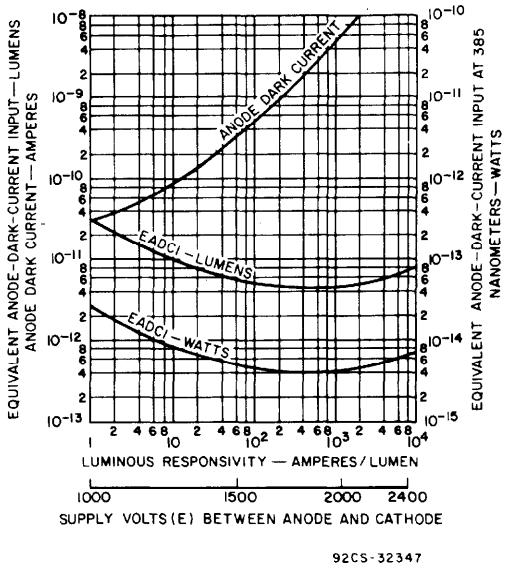

Fig. 61 - Illustrative data showing the variation of anode dark current and the equivalent anode-dark current input (EADCI) as *a function of luminous sensitivity for a* type 8575. *Operation of the tube at voltages higher than that for the minimum of the EADCI characteristic does not provide the best signal-to-noise ratio.*

Noise Equivalent Power-Another way to categorize the limit of detection of a photomultiplier is by noise equivalent power **(NEP)** which is essentially the same as EN1 except the units are always in watts. NEP is the radiant flux in watts at a specified wavelength incident on the detector which gives a signal-to-noise ratio of unity. The frequency bandwidth (usually 1 Hz) and the frequency at which the radiation is chopped must be specified as well as the spectral content of the radiation (most often, monochromatic radiation at the peak of the detector response). It should be noted that NEP is

frequently specified in units of watts Hz-1/2. The numerical value of this formulation of NEP is the same as that given in units of watts but with a specified bandwidth of 1 Hz.

Detectivity-Detectivity **(D)** is the reciprocal of NEP; it is expressed in W^{-1}. Detectivity is a figure of merit providing the same information as NEP but in the reverse sense so that the lower the radiation level to which the photodetector responds, the higher the **detectivity.**

Regenerative Effects

Dynode Glow. Although photomultipliers are designed to minimize regenerative effects, at some high voltage and gain almost all photomultipliers exhibit breakdown phenomena. One source of regeneration in photomultipliers is the glowing of the dynodes under electron bombardment.[68] The glow has a blue spectral emission and of course is most prominent in the latter stages where the current is highest. The regenerative effect occurs when the light from the dynode glow is scattered and reflected back to the photocathode. Dynode cage shields and opaque support wafers minimize this effect .

Glass Charging Effects. Regenerative **photomultiplier** currents may also be triggered by the electrostatic potential of the bulb walls surrounding the dynode or **photocathode** structure. Particularly when the potential of the bulb is near anode potential, stray electrons may be attracted to the bulb and cause the emission of light on impact, depending upon the nature of the glass surface and the presence of contamination. Secondary electrons resulting from the impact of stray electrons on the glass surface are collected by the most positive elements in the tube and help maintain the positive potential of the inner surface of the glass. Under these circumstances, it is possible to observe the formation of glowing spots on the inside of the glass bulb, provided the eye is dark adapted and the applied voltage is sufficiently high. Some of this fluorescent light may be reflected back to the photocathode and result in an increase in the photocathode dark (or light) emission.

Shielding. The effect just described can be minimized by controlling the external potential of the glass envelope. Fig. 62 shows the effect of various voltages applied to an external shield around the tube envelope of a 1P21 photomultiplier. The graph shows the equivalent noise input decreasing as the shield is made negative toward the-potential of the photocathode. It should be noted also that an actual contact is not always required to produce the effects noted in Fig. 62. The proximity of a positive potential near the glass bulb can cause a noisy operation.

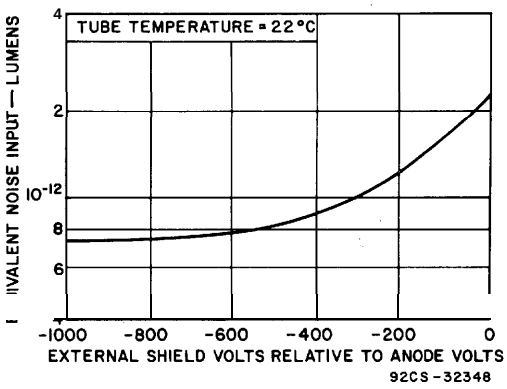

Fig. 62 - Effect of external-shield potential on the noise of a 1P21 photomultiplier. Note the desirability of maintaining a negative bulb potential.

Operation of a photomultiplier tube with an improper external shield may not only cause an increase in noise or lead to an electrical breakdown of the tube, but can result in damage to the photocathode and reduced tube life. In order to prevent these effects, the envelope wall should be maintained near photocathode potential by wrapping or painting it with conductive material and connecting this material to cathode potential. The connection is usually made through a high impedance to reduce the shock hazard. If a cathode potential shield is not provided, the glass surface in the vicinity of the **photocathode** must be insulated from any source of potential difference so that leakage currents to the bulb are less than 10^{-12} ampere.

In photomultiplier tubes in which the -tocathode is of a transmission type, on the inside surface of the glass bulb, it is particularly important to avoid a positive voltage contact on the external surface of the photocathode window. In this case, ionic currents can flow through the glass and produce a **fluoresence** and an accompanying noisy photocathode current.

It should also be noted that continued operation of a photomultiplier tube with a positive voltage contact to the glass in the photocathode area can cause a permanent damage to the photocathode. The damage is reported to be the result of ionic conduction through the glass and poisoning of the photocathode by sodium ions.[69]

Afterpulsing. Afterpulses,[70] which may be observed when photomultipliers are used to detect very short light flashes as in scintillation counting or in detecting short laser pulses, are identified as minor secondary pulses that follow a main anode-current pulse. There are two general types of afterpulses; both are characterized by their time of occurrence in relation to the main pulse. The first type results from light feedback from the area of the anode, or possibly certain dynodes, to the photocathode; the intensity of the light is proportional to the tube currents. When this light feedback reaches the cathode, the afterpulse is produced. Afterpulses of this type, characterized by a delay in the order of 40 to 50 nanoseconds, may be a problem in many older photomultipliers having open dynode structures. The time delay experienced with this type of afterpulse is equal to the total transit time of the signal through the photomultiplier plus the transit time of the light that is fed back.

The second type of afterpulse has been shown to be the result of ionization of gas in the region between the cathode and first dynode. The time of occurrence of the afterpulse depends upon the tube dimensions, the type of residual gas involved and the mass of the gas ion, but usually ranges from 200 nanoseconds to well over 1 microsecond after the main pulse. When the ion strikes the photocathode, several secondary electrons may be emitted; thus, the resulting afterpulse has an amplitude equal to several electron pulse-height equivalents. These pulses appear to be identical to the larger dark-current pulses, and it is suspected that many of the dark-current pulses are the result of photocathode bombardment by gas ions.

Several gases, including N_2^+ and H_2^+, are known to produce afterpulses. Each gas produces its own characteristic delay following the main pulse. The most troublesome, perhaps, is the afterpulse caused by the H_2^+ ion; this afterpulse occurs approximately 300 nanoseconds after the main pulse in a tube of type 7850 construction. One source of hydrogen in the tube is water vapor absorbed by the multiplier section before it is sealed to the exhaust system. Other gases which may cause afterpulsing may be present as a result of outgassing of the photomultiplier parts during processing or operation. Present photomultiplier processing techniques are designed to eliminate or at least to minimize the problem of afterpulsing.

Helium Penetration[71,72] Another effect must be considered in relation to the sources of dark current-the penetration of helium through the glass of photomultiplier tubes. When the photomultiplier is operated or stored in an environment where helium is present, helium will gradually permeate through the glass envelope. Because helium is inert, it does not react with the photocathode or dynode surfaces. But tubes subjected to such an environment will exhibit a noise increase and an increase in afterpulsing because of the ionization of the helium by electron impact. Depending upon the degree of permeation, a point will be reached at which complete ionization and electrical breakdown occurs making the tube unusable.

Other Noise Sources

Excess noise or dark current can also result from field emission occurring within the tube and from scintillations in the glass envelope of the tube caused by radioactive elements within glass (most glasses contain some radioactive ^{40}K). Fused silica is sometimes utilized in photomultiplier faceplates to minimize these effects.

Noise in photomultiplier tubes can also result from the proximity of nuclear sources or from cosmic rays which result in glass scintillations. Andrew T. Young[73,*] has identified large pulses which originate from Cerenkov light flashes produced by cosmic rays traversing the window of end-on photomultipliers. The flashes correspond to

*Andrew T. Young also has written a chapter, "Photomultipliers: Their Cause and Cure," in Volume 12 of **Methods of Experimental Physics:** Astrophysics, L. Marton, Editor, Academic Press, 1974. As well as being a good general reference on photomultipliers, this chapter contains a further discussion of the Cerenkov-light-flash effect.

photoemission pulses of **50** electrons and larger. The number of pulses is greater when the face of the photomultiplier is upward rather than downward because the Cerenkov radiation is emitted in a conical pattern away from the direction of entry. Young reports the total number of pulses from this source to be about 1.2 $\min^{-1} \mathrm{cm}^{-2}$.

Another phenomenon which deserves mention in connection with dark current is the effect of previous exposure to light, especially blue or near ultraviolet. Large increases in photocathode dark emission may occur as discussed in section on **Photocathode Stability** with rather slow recovery, as illustrated in Fig. 47. It is advisable, therefore, that photomultipliers be kept in the dark at all times, or at least for many hours before they are used for making low-level measurements.

Noise Output of a Photomultiplier

The output current of a photomultiplier consists of a train of unidirectional electrical pulses whether the tube is in the dark or with illumination on its photocathode. Each pulse is the result of an electron emitted from the photocathode and amplified by the secondary emission of the tube. (Some pulses may originate also from light striking the first dynode or from thermionic emission from the first or other dynodes.) In a system having a wide bandwith, the individual pulses may be measured and counted. Their spacing in time will have a statistical variation as will their height. There variations constitute noise and limit the precision of measurements.

If the bandwidth is not sufficient to resolve the individual pulses, particularly when the light level is relatively high, the output will exhibit noise or rapid variation in signal level about an average value. The noise level relative to the signal level will decrease with increasing signal level or with decreasing bandwidth. The noise may be described by giving the rms value of the current variation in a specified bandwidth.

Dark-Current and Noise Reduction

Dark-Current Reduction. If care is taken to avoid damage to the photomultiplier by operation with excessive current, the dark current can often be reduced by a process of operating the photomultiplier in the dark at or near the maximum operating voltage. This process, called **dark aging,** may require several hours to several days. After such a process of aging, it is recommended that a photomultiplier be operated for several minutes at the reduced voltage before measurements are attempted.

Dark Noise Reduction with Cooling. Because the dark emission is reduced as the temperature of the photocathode is reduced, the dark noise output of the photomultiplier may also be reduced by cooling. Fig. 63

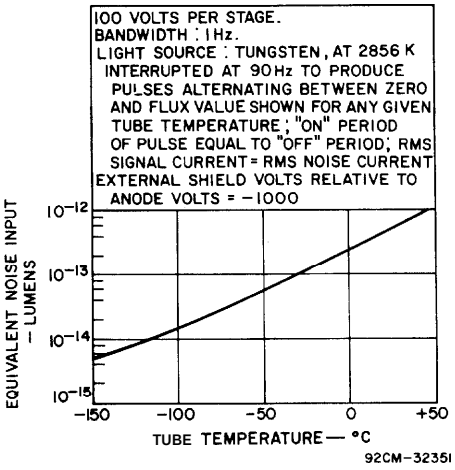

Fig. 63 - Equivalent noise input in lumens for a 1P21 photomultiplier as a function of temperature.

shows the variation of equivalent noise inputs, **ENI,** for a 1P21 (opaque Cs_3Sb photocathode) over a wide range of temperature. The implication of these data is that by cooling from room temperature to – 150 °C the low light level limit of detection can be reduced by two orders of magnitude.

Photomultiplier Noise Characteristics

The following paragraphs describe the noise and signal levels from both a pulse and a dc point of view. The noise frequency spectrum is also described and data are presented showing the dark noise spectrum.

At very low signal levels, the detection limit will be shown to be determined by the dark current of the photomultiplier and its associated noise. At high levels, the precision of measurement is limited by the statistical variation in the signal pulses-or the noise which is always present to some degree in the dc signal level. The signal-to-noise ratio can

be improved by decreasing the bandwidth in dc measurements or by the equivalent of increasing the time in pulse-counting applications.

Noise Spectrum. The width of an output current pulse initiated by an electron from the photocathode is determined by the variations in transit time through the tube. The noise associated with these pulses of electron current is flat with frequency out to frequencies corresponding to the width of the individual pulses. (The frequency spectrum of a delta function is flat.) A power spectrum of the noise from type 931 has been calculated by R. D. Sard[74] and is shown in Fig. 64. Sard's calculation was done by considering

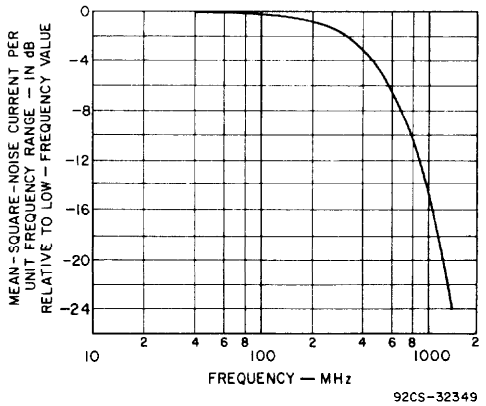

Fig. 64 - Spectral energy distribution of the noise from type 931A operated at 100 volts per stage, as calculated by R. D. Sard.[74]

the anode current from a single electron traversing the space between the last two dynodes and anode and the distribution of electron arrival times due to differences in transit time between stages; then, the Fourier transform of the pulse shape was taken to obtain the frequency spectrum.

The bandwidth of the noise spectrum differs in different tube designs, depending upon transit-time variations. Usually, high-speed photomultipliers are characterized by rise and fall times of the output pulses rather than by bandwidth. This subject is discussed in more detail in a later section.

Dark Noise Pulse Spectrum. Because of the statistical nature of the secondary emission gain at each stage of the photomultiplier, the output pulses have a fairly wide distribution of heights even though each pulse is initiated by a single electron. Fig. 65

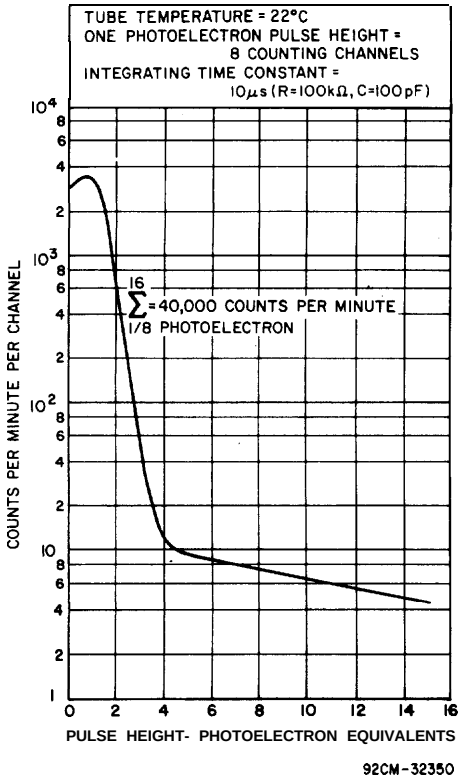

Fig. 65 - Typical Dark-Pulse Spectrum

shows a differential dark-noise pulse spectrum-the number of pulses counted per unit of time as a function of their height.

A differential dark-noise spectrum is obtained with a multichannel pulse-height analyzer. The calibration of the single-photoelectron pulse height is determined by illuminating the photocathode with a light level so low that there is a very low probability of coincident photoelectron emission. The dark-pulse distribution is then subtracted from the subsequent combination of dark pulses and single-photoelectron pulses, so that the remainder represents only that distribution resulting from single-photoelectron events. By adjusting the gain of the pulse-height analyzer, the single-electron photopeak can be placed in the desired channel to provide a normalized distribution.

The dark-pulse spectrum of Fig. 65 is characteristic of photomultipliers intended for use in scintillation counting and other

low-light-level pulse applications. The curve shown is idealized and represents an average or typical spectrum. An actual spectrum shows statistical variations depending upon the length of the count.

The slope of the curve for the pulse-height region between 1 and 4 photoelectrons is as expected for single-electron emission, when the statistical nature of secondary-emission multiplication is considered. The number of pulses in this region may be reduced by cooling the photomultiplier. Below a pulse height of one photoelectron equivalent, the curve is determined partly by the statistical spread due to the multiplication process and partly from emission from some of the dynode surfaces.

The slope of the curve for the pulse-height region greater than 4 photoelectrons is presumed to be caused by multiple-electron-emission events. These multiple pulses are caused by processes such as ionic bombardment of the photocathode. Other mechanisms contributing to the noise spectrum include cosmic rays, field emission, and radioactive contaminants that produce scintillations within the glass envelope. Cooling has little effect upon reduction of the number of these multiple electron pulses, but extended operation of the tube may improve performance. Operation of the tube may result in erosion of sharp points and reduce the possible contribution of field effects. In addition, improvement occurs because residual gases are absorbed within the tube, ion bombardment of the photocathode is reduced, and the resulting multiple electron emission is lessened.

For many applications it is useful to have a summation of the total number of dark pulses. In Fig. 65, for example, the sum of dark-pulse counts from 1/8th electron equivalent height to 16 electron equivalent heights is 4 x 10^4 counts per minute.

Analytical Model of Noise and Signal-to-Noise Ratio-Consider the lower limit of light detection capability of a photomultiplier as determined by the fluctuation in the thermionic dark emission. If the dark emission current from the photocathode is i_d, the rms shot noise associated with this current is given by

$$i_{rms} = (2ei_dB)^{1/2} \quad (16)$$

where e is the charge on the electron and **B** is the bandwidth of the observation,

The photocathode dark emission and its associated noise are both amplified by the gain, μ, of the photomultiplier. Assuming for the moment that the amplification process is noise free, and that all of the current emitted from the photocathode is collected by the first dynode, the anode dark current is given by

$$I_d = \mu i_d \quad (17)$$

and the anode rms noise current is given by

$$I_{rms} = \mu(2ei_dB)^{1/2} \quad (18)$$

Actually, noise is introduced by the secondary emission process. (This subject is discussed at length in Appendix G.) If one assumes Poisson statistics for the secondary emission process, the anode noise current shown in Eq. 18 should be increased by a factor $[1 + 1/(\delta - 1)]^{1/2}$ where δ is the secondary emission ratio per stage, assumed to be the same for all stages. If a typical value of $\delta = 4$ is assumed, the noise is increased by a factor of 1.15. Actual measurements indicate a somewhat higher figure. On the other hand, higher voltage on the first stage, or the use of a GaP:Cs first dynode having a very high secondary-emission ratio would reduce this factor. For the purpose of the present discussion, this increased noise from secondary emission will be neglected and the photomultiplier anode noise will be taken as the amplified photocathode shot noise as given by Eq. 18.

A fundamental advantage of a photomultiplier as compared with a photodiode, is the high gain and the fact that the secondary emission process contributes very little to the relative noise output of the tube. The high gain of the photomultiplier permits the use of a relatively small load resistance (R) without deterioration of the photomultiplier signal-to-noise ratio by the Johnson thermal noise of the load resistance. The small load resistance permits an operation of the photomultiplier with the very high bandwidths inherent in the photomultiplier design. A large load resistance shunted by the finite tube and lead capacitance would otherwise seriously limit the effective bandwidth of the system.

In order to maintain the fundamental signal-to-noise capability of the **photomultiplier**, the Johnson noise of the load resistance must be less than the photomultiplier output noise. Johnson noise (rms) is given by

$$V_{rms} = (4kTRB)^{1/2} \quad (19)$$

where **k** is Boltzmann's constant and T is the temperature in Kelvin units. In order to compare this noise with the photomultiplier output noise we may convert it to an equivalent current noise by dividing by the load resistance:

$$I_{rms} = (4kTB/R)^{1/2} \quad (20)$$

Fig. 66 illustrates the relative magnitudes

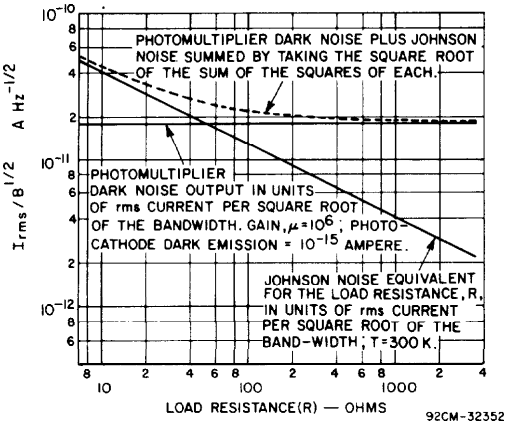

Fig. 66 • Comparison of the magnitudes of Johnson noise in the load resistance and of the output photomultiplier dark noise, both in units of rms amperes per square root hertz. For the case illustrated, both sources of noise are equal for a load resistance of 50 ohms.

of dark noise output from a photomultiplier and of the Johnson noise in the load resistance. The horizontal line independent of the load resistance is the rms anode current per square root bandwidth for a photomultiplier as calculated from equation 18, assuming a gain, $\mu = 10^6$ and a photocathode dark emission of 1 fA (10^{-15}A). The equivalent Johnson noise current per square root bandwidth calculated from Eq. 20 decreases as the square root of the load resistance, R. Temperature was chosen as 300 K. For a 50-ohm load—a value typical of the termination and cable used in pulse applications-the two noise sources are about equal. Therefore, at this point in the example chosen there is some, but not a serious, reduction of signal-to-noise ratio.

Noise in **Signal.** When the photocathode current representing the signal is larger than the photocathode dark emission, the dominant noise is the noise in the signal. For a photocathode signal current, i_s, the anode signal current I_s, is given by

$$I_s = \mu i_s \quad (21)$$

and, paralleling equation 18, the anode rms noise current associated with the signal current is given by

$$I_{rms} = \mu(2ei_sB)^{1/2} \quad (22)$$

But, one must consider both the dark emission noise and the noise in the signal current. Because there is no correlation between the two sources, the noises may be added by summing their squares, or for **total** rms noise current:

$$I_{rms} = \mu[2e(i_d + i_s)B]^{1/2} \quad (23)$$

An expression for the signal-to-noise ratio may now be written:*

$$SNR = \frac{i_s}{[2e(i_d + i_s)B]^{1/2}} \quad (24)$$

Fig. 67 illustrates the variation of **signal**-to-noise according to equation 24 as a function of bandwidth and photocathode signal current. The cathode dark emission is assumed to be 10^{-15} ampere. For signal currents less than the dark emission, the dark noise is the limit to the signal-to-noise ratio. In this case, a narrow bandwidth is a requirement for detection. When dark noise is the limit to detection, it is useful to reduce dark emission by cooling. At wider bandwidths and higher photocathode signal levels, the limit to the signal-to-noise ratio is in the

*In this discussion, the signal is treated as though it were dc. In an actual application, the signal may be modulated and signal-to-noise figures would involve the rms value of the modulated signal. Note also that the noise calculation neglects the factor by which the noise is increased by the secondary emission statistics.

noise of the signal so that cooling would not be advantageous. In Fig. 67, it has been assumed that the load resistance is sufficient (greater than 50 ohms) so that Johnson noise is not a factor.

In applying these signal-to-noise concepts to an actual case, the photocathode dark current may differ greatly from the 10^{-15} ampere figure assumed. (See the data, Fig. 16.) The photocathode signal currents may be calculated from a knowledge of the photocathode responsivity as published in a tube data sheet. For example, a photocathode may have a responsivity of 160 microamperes per lumen for tungsten irradiation, or 70 milliamperes per watt at the wavelength of maximum responsivity (i.e., 420 nanometers). A photocathode current of 1 femtoampere would then correspond to $10^{-15}/160 \times 10^{-6} = 6.25 \times 10^{-12}$ lumen or $10^{-15}/70 \times 10^{-3} = 1.43 \times 10^{-14}$ watt flux incident on the photocathode.

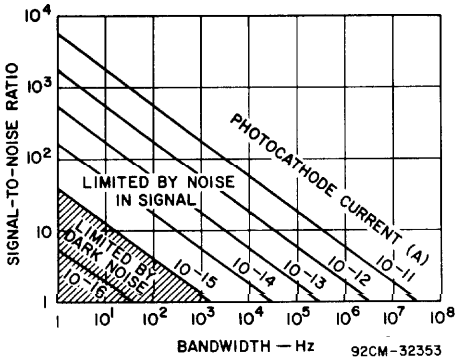

Fig. 67 - Illustrating how the signal-to-noise ratio in a photomultiplier varies with bandwidth and photocathode signal level. Photocathode dark emission assumed to be 10^{-15} ampere. Load resistance greater than 50 ohms.

TIME EFFECTS

Terminology

Photomultiplier tubes may be characterized for time response in various ways. The terms used in these time characterizations are defined below. In these definitions it is assumed that the photomultiplier is activated with a delta-function light pulse. Fig. 68 illustrates the definitions of some of the more common terms. *

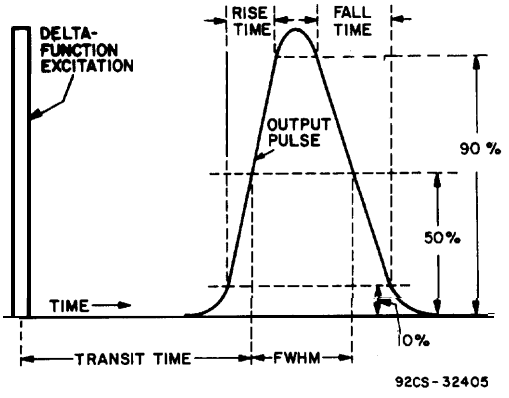

Fig. 68 - The various time relationships in a photomultiplier output pulse, assuming a delta excitation function. Illustrated are transit time, rise time, fall time, and full width at half maximum (FWHM).

Transit time† "is the mean time difference between the incidence of the light upon the photocathode (full illumination) and the occurrence of the half-amplitude point on the output-pulse leading edge."

Rise time "is the mean time difference between the 10- and 90-percent amplitude points on the output waveform for full cathode illumination and delta-function excitation."

Fall time "is the mean time difference between the 90- and 10-percent amplitude points on the trailing edge of the output-pulse waveform for full cathode illumination and delta-function excitation."

*These definitions follow the standards appearing in "IEEE Standard Test Procedures for Photomultipliers for Scintillation Counting and Glossary for Scintillation Counting Field." ANSI N 42.9 - 1972; IEEE Std 398 -1972. Published by The Institute of Electrical and Electronics Engineers, Inc., 345 East 47 St., New York, N.Y. 10017.

†This definition differs from the definition appearing in the **IEEE Standard Dictionary of Electrical and Electronics Terms** (ANSI/IEEE Std. 100-1977: "The time interval between the arrival of a delta-function light pulse at the entrance window of the tube and the time at which the output pulse at the anode terminal reaches peak amplitude."). This latter definition is closer to the actual transit time which might be defined to the average time of arrival of the electrons at the output. However, the definition given to the half-amplitude point may be more useful in an application where the half-amplitude point is used for timing purposes.

Full-width-at-half-maximum (FWHM) is the mean elapsed time between the half-amplitude points on the output waveform for full cathode illumination and delta-function excitation.

Delta-function light pulses. In tests related to time characterization of photomultiplier tubes it is useful to have light pulse sources available which approach characterization as a delta-function pulse. A delta-function pulse is one whose duration is significantly shorter than that of the output pulse to be measured. It approaches the mathematical concept of a function whose area is finite but whose width approaches zero.

Various light sources have been used to generate delta-function pulses for time-testing of photomultipliers.

A reverse-biased light-emitting diode (Ferranti type XP-23) has been used by Leskovar[75] to obtain light pulse widths of as short as 200 ps. Mercury-wetted relay spark sources have also been used and have provided pulses having rise times of 500 ps. Pulses of radiation having a duration of 50 ps or less can be obtained with a mode-locked Nd:YAG laser. The laser wavelength is 1.06 μm, but it can be utilized to produce radiation at 532 nm by means of a nonlinear crystal. Random pulses can be produced with fast scintillators. A rise time of 400 ps can be obtained for Naton 136 and a ^{60}Co source.[81]

Transit Time

Transit Time is expected to increase as the inverse half power of the applied voltage, provided the effects of initial velocities and secondary-emission delay are negligible. Fig. 69 shows the transit time measurements for an 8053 photomultiplier plotted so as to display the reciprocal square root voltage relationship. The intercept of the line on the time axis is probably due to the distortion of the simple relationship by the magnitude of the initial secondary emission velocities.

Fig. 70 shows the transit times for a number of photomultiplier tubes plotted over a range of operating voltages. The larger part of the transit time is just the accumulation of times for electrons to traverse from stage to stage. Usually, the time for the photocathode-to-first-dynode transit is the largest component, especially for photomultipliers with large photocathode areas. The large photocathode necessitates a fairly long path to the first dynode to provide good photoelectron collection from the entire photocathode.

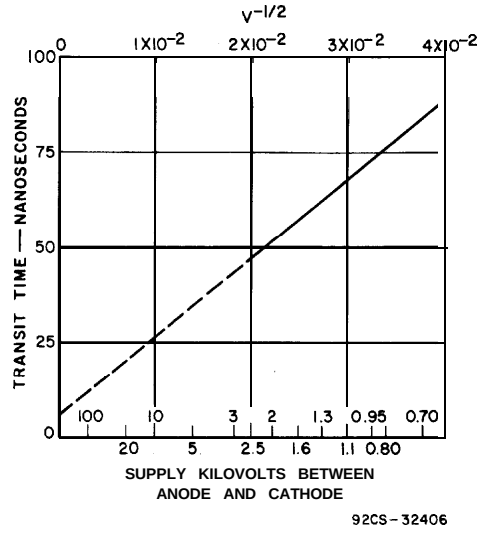

Fig. 69 - Transit time as a function of the square foot of reciprocal applied voltage for a type 8053 photomultiplier tube.

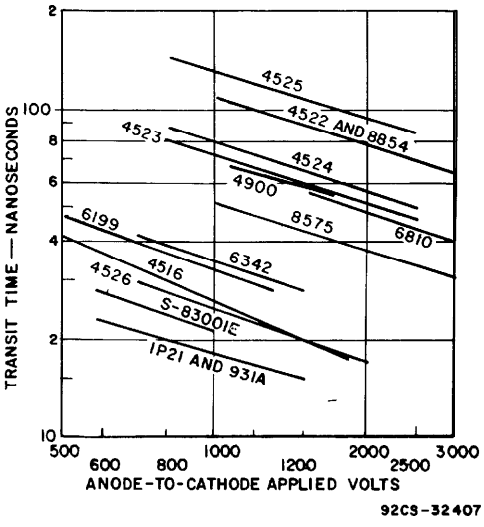

Fig, 70 - Transit time as a function of supply voltage (log scales) for a number of photomultiplier tubes.

Photo- and secondary-emission times may be as short as 10 ps, although for negative-electron-affinity (NEA) materials, the times may be as long as 100 ps. One reason for the

high performance of NEA materials is that long diffusion paths for electrons are obtained. Although this increase in diffusion path length also increases the emission time, emission time is not a significant part of the transit time in most commercial photomultipliers. In general, the transit time of a photomultiplier is not as important as its rise time or as variations in the transit time which would cause uncertainty in time measurements made with the photomultiplier. A fixed delay time is easily compensated for by circuit design.

Rise Time

Fig. 71 shows the rise time-from the 10

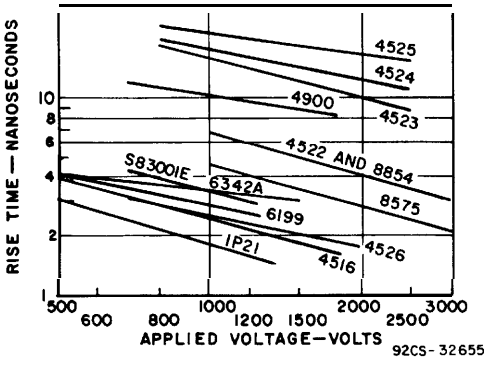

Fig. 71 - Anode-pulse rise times as a function of anode-to-cathode applied **voltage (log** *scales) for a number of photomultipliers.*

to 90% amplitude points-for a number of photomultipliers plotted over a range of typical operating voltages. No correction was made for the finite rise time of the light pulse and measuring equipment, which is estimated to be of the order of 0.8 ns. In using photomultipliers for high-resolution-time spectroscopy, the ideal point on the output pulse to use as an indicator would be at the half maximum of the rising characteristic. The rising characteristic is generally faster than the fall and thus provides the highest precision in timing. However, because output pulse heights vary, a fixed discriminator level results in a loss of precision. When a fixed discriminator level is used, the highest precision is obtained by use of a discriminator level between 10 and 20% of maximum. A superior method is the use of a constant fraction of the pulse height as a trigger .[76]

Pulse Width

The width of the output pulse is determined by the variation in transit time through the secondary emission chain of the photomultiplier. The variations arise because of variations in emission energies and directions of the secondary electrons as related to the tube structure. The measurement of pulse width is generally the full width at half maximum. The output pulse width follows the inverse half power of the applied voltage as does the average transit time. Fig. 72 illustrates the pulse width (FWHM) for an 8053. For timing experiments, it is generally desirable to have a narrow pulse width for good timing precision capability.

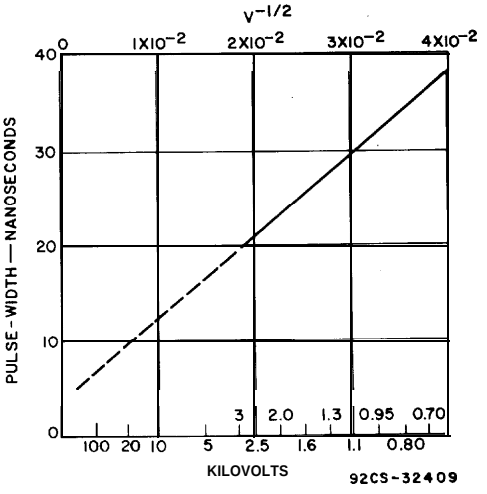

Fig. 72 - Pulse width (full width at half maximum) for a type 8053 as a function of the inverse half power of the applied **voltage.**

Pulse Jitter (Time Resolution)

Although pulse timing is done on the rising characteristic of the output pulse and is more precise for a fast rise time, the ultimate limit to time measurement is the variation in pulse timing, or pulse jitter. Suppose single photoelectrons initiate pulses. Variations in transit time of photoelectrons to the first dynode will occur because of variations in the initial velocity and electric field resulting from the electrode geometry. The same considerations apply to the secondary electrons. If a number of pulses initiated by single electrons are observed, a histogram can be developed showing the number of pulses having a

given transit-time difference. Such a histogram, measured by Birk, Kerns, and Tusting,[77] is shown in Fig. 73. The time of each pulse was measured by using the leading-edge half-height point. The full width at half maximum of this distribution is about 360 ps and is a measure of the time resolution capability of this particular tube.

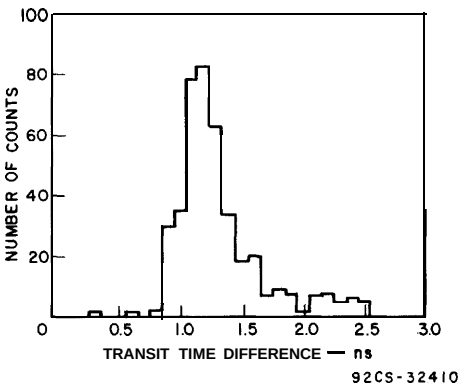

Fig. 73 - Histogram of transit-time difference for single-photoelectron pulses from an **RCA** *developmental type photomultiplier. (From* ***Birk****, Kerns, and Tusting[77].)*

If a number, N, of simultaneous photoelectrons is emitted, the pulse jitter is reduced by the square root of N, simply by the statistical averaging process. This relationship has been demonstrated by Leskovar and Lo[75] for a microchannel-plate photomultiplier as shown in Fig. 74.

Data on time resolution for single photoelectrons for a variety of photomultipliers are given in Table IV. Values are given for full photocathode illumination as well as for illumination at the center point. The time spread for full photocathode illumination is larger than for a single point because it includes the difference in transit time from the photocathode to the first dynode for different photocathode locations.

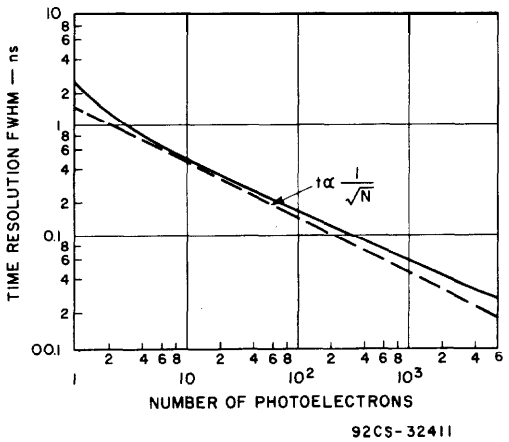

Fig. 74 - Time resolution of a ***microchannel****-plate photomultiplier as a function of the number of photoelectrons per pulse, measured with light pulse width of 2.6 ns, for full photocathode illumination. Data are from Leskovar and Lo[75] The dashed* **line** *showing the inverse square root relationship has been added.*

Table IV - Time Resolution (FWHM)* for Single Photoelectrons for Various Photomultipliers

Tube Type	Nominal Diameter, Inches	No. of Stages	First Dynode Material	Photocathode Type	Photocathode Area, cm^2	Time Resolution, Emission from the Center Point, ns	Time Resolution, Emission from the Whole Photocathode, ns
8575	2	12	copper-beryllium	K_2CsSb	14	0.90[78]	1.03[78]
8852	2	12	GaP:Cs	Na_2KSb:Cs	16	0.59[79]	0.81[79]
8850	2	12	GaP:Cs	K_2CsSb	16	0.59[79]	0.64[79]
C-31024	2	5	GaP:Cs**	K_2CsSb	16	0.48[79]	0.57[79]
8854***	5	14	GaP:Cs	K_2CsSb	100	1.70[79]	2.42[79]

*The full width at half maximum is related to the variance as follows, assuming a gaussian distribution: FWHM = 2.355 σ. (Variance = σ^2.)

**All the dynodes of this type are GaP:Cs, providing high gain with few stages and consequent good time response.

***Formerly developmental type C-70133B.

The improvement of the 8852 over the 8575 is the result of the use of the high-gain first dynode. The difference between the 8850 and the 8852 may be due to the larger photoelectron emission energies of the multialkali photocathode. The poorer time resolution of the 8854 is caused by the very large cathode area and the consequent reduced electric field strengths and increased path lengths.

A general treatment of single photoelectron detection and timing has been provided by Poultney[80]. The analysis of time resolution for a photomultiplier is very similar to that for noise in a photomultiplier as given in Appendix G. Variations in transit time in the early stages of the photomultiplier are most important to the over-all time resolution. The large number of electrons in the latter stages bring about an averaging process which reduces the time variation.

Summary of Time-Resolution Statistics

The summary of time resolution statistics below follows the work of Gatti and Svelto[81].

If the secondary emission of each stage is taken as a constant, δ, the total variance in electron flight times including all of n stages is given by

$$\sigma_a^2 = \sigma_0^2 + \sigma_1^2\delta^{-1} + \sigma_2^2\delta^{-2} + \ldots\sigma_n^2\delta^{-n} \quad (25)$$

Here σ_0^2 is the variance of the flight time from cathode to first dynode, and σ_i^2 is the variance of the flight time from the i^{th} dynode to the $(i + 1)^{th}$ dynode. The last term represents the variance in flight time from the last dynode to the anode. This expression is actually a simplification because of the induction effect of the electrons in flight between the last stage and anode. Because of the δ^{-n} term, however, the error is negligible. If n is large and the variances of flight times for each stage are assumed to be equal to σ_d^2, Eq. 25 may be approximated as follows:

$$\sigma_a^2 = \sigma_0^2 + \sigma_d^2/(\delta - 1) \quad (26)$$

When variations in secondary emission are taken into account, assuming all stages have the same average secondary emission, δ, with a Poisson distribution, the total variance in time of flight for the over-all tube is given by

$$\sigma_a^2 = \sigma_0^2 + \sigma_d^2\,\delta/(\delta - 1)^2. \quad (27)$$

Eq. 27 refers to the variance of the centroid of the output pulse from a single photoelectron input. If timing is done by a point on the rising characteristic, an additional time variance might be included, that for the variation in pulse width. Gatti and Svelto[81] have shown that this term would add a negligible amount to the variance as given by Eq. 27.

PULSE COUNTING

One effective way to use a photomultiplier for measuring very weak signals is to detect and count pulses resulting from single photoelectrons-sometimes referred to as "photon counting". (Actually, the highest quantum efficiencies for photocathodes are such that at best one in every three photons would be detected, assuming a spectral match to the peak quantumefficiency wavelength.) Counting of single electrons assumes that the rate of arrival of photons is such that it would be unusual for more than one photoelectron to be emitted in a time equivalent to the output pulse width for a single electron input to the multiplier. Single-electron pulse counting is an important technique in applications such as Raman spectroscopy, astronomical photometry, and bio-luminescent measurements. Baum[82] has shown that in some cases pulse counting has an advantage equivalent to a factor of 1.2 in quantum efficiency over current-measurement techniques.

Output Pulse Height Distribution

An important consideration in photon counting is the distribution of pulse heights at the output of the photomultiplier. Statistics of the variation in pulse heights for single electron inputs is discussed in Appendix G. (See Fig. G-6). Pulse height distributions are obtained with a multichannel pulse-height analyzer. Fig. 75 shows (1) a differential pulse-height distribution in which the number of pulses in a given time interval and in a given channel (between height, h and h + $\triangle$h) is plotted as a function of h; and (2) an integral pulse-height distribution in which the total number of pulses occurring in the given time interval with a height of h or

greater is plotted.[83] Also shown on the graph is a rectangle whose intercept on the abscissa is the equivalent of the output pulse associated with one photoelectron and an average photomultiplier gain of $\overline{G}$. The rectangle is determined by setting its height equal to the intercept of the integral-pulse-height distribution curve on the ordinate axis, and by setting the area of the rectangle equal to the area under the integral-pulse-height curve. This area is equal to the total charge of all the pulses counted: the total number of pulses multiplied by the average multiplier gain and the charge of one electron. This equality may be demonstrated by integrating the integral-pulse-height curve along the ordinate axis and comparing the result with the integral of the product of the differential pulse-height-distribution ordinate (number of pulses) and the abscissa value (pulse height or charge associated). The pulse-height resolution for single electrons in this case is FWHM = 1.6 electron equivalents. Note that the data of Fig. 75

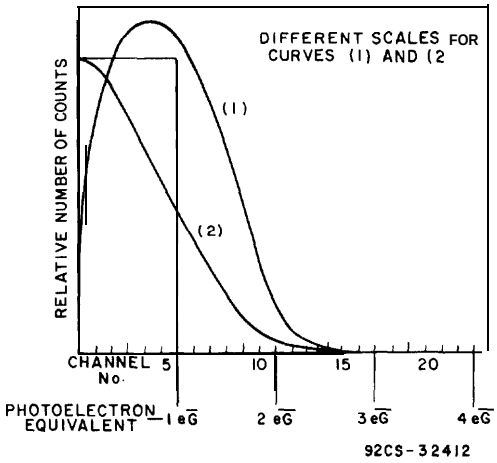

Fig. 75 - Single electron (1) differential and (2) integral pulse-height distribution curves. Type 4501, photocathode K^2CsSb, counting time 10 minutes (from G. A. Morton[83]). Different scales for (1) and (2).

were taken on a tube, 4501, that has copper-beryllium dynodes and a modest secondary-emission gain. The pulse-height resolution for single electrons in the case of gallium-phosphide dynodes is much better, as will be discussed below.

When a very low light flux is measured by the pulse-counting technique, it is also necessary to measure the count in the dark and to subtract the rates to obtain that due to the light alone. The optimum time which should be spent on each measurement is discussed in Appendix G-see for example, Eq. G-103. If the signal count is much less than the dark count, however, about equal times should be spent on both measurements. At higher signal levels, more time should be spent on the signal count.

Copper-Beryllium Dynodes

Differential pulse-height distributions are shown in Fig. 76 on a developmental photo-

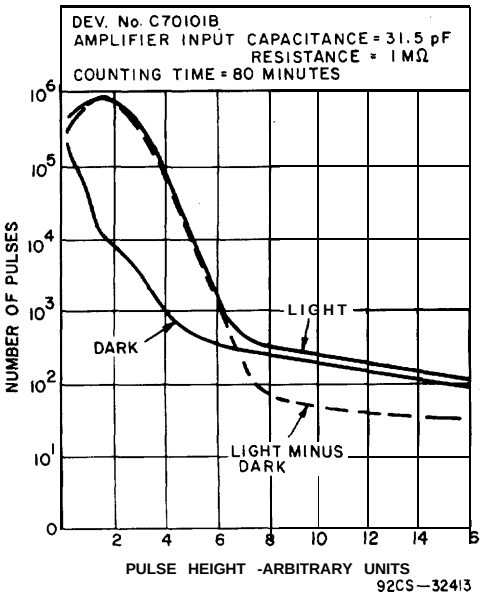

Fig. 76 - Differential pulse-height distributions obtained with type Dev. No. C-70101B. (Similar to type 8575, but having an S-20 response. From R. M. Matheson[84].)

multiplier having copper-beryllium dynodes. Note that the dark pulse-height distribution does not show a peak representing single electrons. The probable explanation is that dark emission originates not only from the photocathode, but from the dynodes as well. Electrons originating from the first dynode would show a distribution similar to that of the photoelectrons, but with a pulse height lower by the secondary-emission ratio of the first dynode. Pulse-height distributions also usually show an extended foot, as in Fig. 76, for heights greater than 7 on the figure's arbitrary scale. These counts represent pulses

of more than one electron per pulse and are probably caused by secondary mechanisms such as ion feedback, scintillations in the glass envelope initiated by cosmic rays or by radioactive traces in the glass or in the tube environment. Note that the numbers of these large pulses are usually several orders of magnitude less than the numbers in the single-electron distribution. When a single-electron integral count is made, the upper discriminator level could be set to exclude these larger pulses.

In setting the lower level of the discriminator, an optimum level is determined by the different character of the light and dark pulse distributions. Morton[83] has shown that the minimum error in determining the signal pulse count is obtained by adjusting the lower-level discriminator setting so that for an integral count distribution

$$\frac{d}{dh}(\ln N_s) = \frac{1}{2}\frac{d}{dh}(\ln N_d) \qquad (28)$$

where N_s represents the number of signal pulses counted and N_d represents the number of dark pulses counted. In Fig. 77, the value of the pulse height that satisfies the relation shown in Eq. 28, is given by h_1.

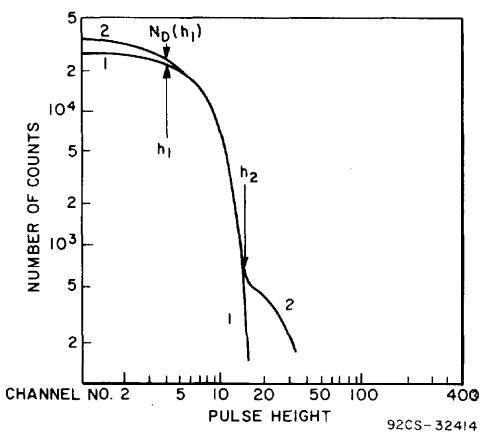

Fig. 77 - Single electron response (I) and dark pulse distribution (2) of tube type 4501 for counting time of 10 minutes; integral distribution curves. h_1 and h_2 are discriminator settings (From G. A. Morton[83]).

Gallium-Phosphide Dynodes

For tubes having the high-gain GaP:Cs first dynodes, the statistics of multiplication are much improved. Consequently, such tubes are particularly advantageous for single-electron pulse counting. The improvement in multiplication is demonstrated by the differential pulse-height distribution for single electrons shown in Fig. 78. Note the

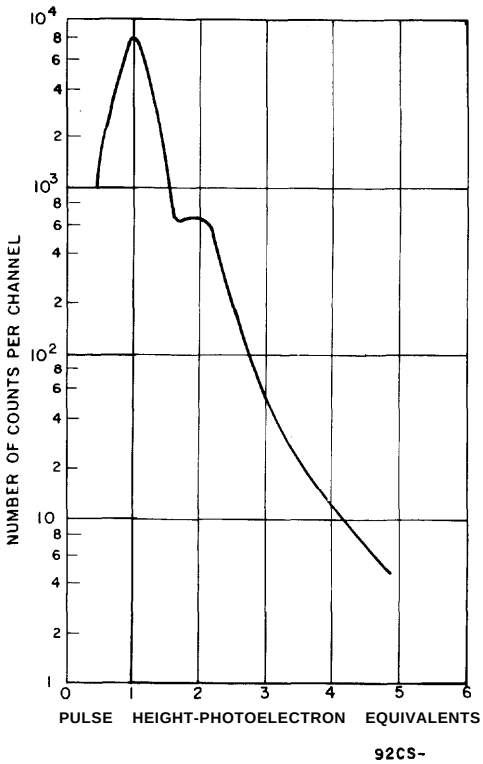

Fig. 78 - Resolution of a single electron peak having a measured FWHM of 63%. The first dynode is GaP:Cs. (Data from Morton, Smith, and Krall[85].)

improvement in resolution as compared with that of Figs. 75 or 76. When the intensity of the light flashes is increased, a pulse-height spectrum such as illustrated in Fig. 79 results, again for a GaP:Cs first dynode. In this case the light level has been adjusted so that the peak counts are nearly equal for one, two, and three electron pulses. The small pulse distribution to the left of the single-electron peak distribution is probably an artifact caused by equipment noise at the lower channel settings.

Peak-to-Valley Ratio

Another important consideration for a photomultiplier used in pulse counting is the **peak-to-valley** ratio. Referring to Fig. 79,

for single electrons, the peak-to-valley ratio is the value of the peak of the single-electron distribution divided by the minimum value of the count distribution between the first and second peaks-in this case a ratio of about 2.3.

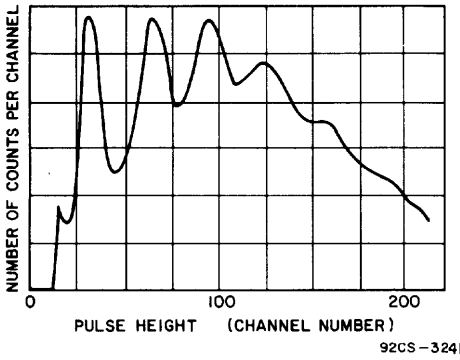

Fig. 79 - Pulse-height spectrum showing peaks corresponding to one, two, and up to five electrons. The first dynode is **GaP:Cs.** ***(Data from Morton, Smith, and Krall[85].)***

SCINTILLATION COUNTING

Pulse Magnitude

In scintillation counting, the problems are similar to those of counting single photoelectrons but the numbers of equivalent photoelectrons per pulse can vary from a few to a fairly large number. For example, in the case of a soft-beta emitter, using a coincidence liquid scintillation counter (for an unquenched standard, PPO and POPOP in toluene), the total number of photoelectrons developed in the pair of photomultipliers having K_2CsSb photocathode is approximately 2.5 per keV of beta-ray energy. Because dark noise from single electrons can be effectively discriminated against by using coincidence techniques, a relatively efficient count of low-energy beta emission can be made. On the other hand, in the case of a NaI:Tl crystal coupled to a photomultiplier having a K2CsSb photocathode, the number of photoelectrons developed is approximately 8 per keV of gamma-ray energy. Thus, for the isotope ^{137}Cs, where the gamma-ray energy is 662 keV, the pulse height would be the equivalent of 5300 photoelectrons.

Isotope 137Cs Sources

Fig. 80 shows the pulse-height distribution for ^{137}Cs using a NaI:Tl crystal scintillator.

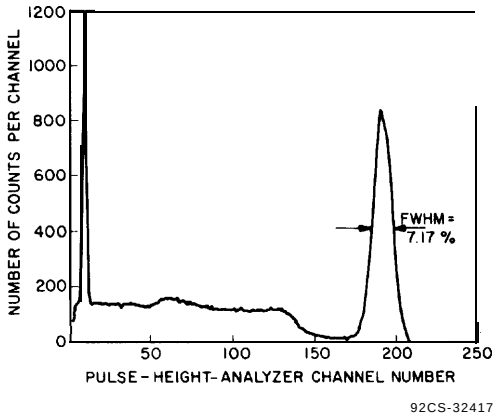

Fig. 80 - Pulse-height distribution for ^{137}Cs taken with a NaI:Tl crystal and a two-inch "teacup" photomultiplier (type 4902).

Pulse-height resolution is illustrated for full width at half maximum. The peak at the extreme left is the barium K X-ray peak at 32 keV. The region between the two peaks is the result of Compton scattering.

From Appendix G, Eq. G-111, the pulse-height resolution is given by

$$\text{FWHM} = 2.355\left[\frac{1-\eta+\frac{1}{\delta-1}}{m_c\eta}+\frac{\sigma_c^2}{m_c^2}\right]^{1/2}$$

The following values may be assumed:

η = photocathode quantum efficiency = 0.25
δ = secondary emission gain per stage = 4
m_c = number of photons corresponding to the photopeak = 21200 for ^{137}Cs
σ_c^2 = variance in the number of photons per photopeak pulse

For the case illustrated in Fig. 80, the FWHM = 7.17%. Substituting the above values in G-111, and solving for σ_c^2 gives 325,000. The FWHM related to the crystal statistics alone is 6.33%. The FWHM related to the photomultiplier alone is 3.37%.

Isotope 55Fe Sources

Fig. 81 shows a pulse-height distribution for ^{55}Fe which emits a gamma ray with an energy of 5.9 keV. Note that for this spectrum, the FWHM is approximately 40%. Following the same type of analysis as used above to evaluate the relative contributions to FWHM for ^{137}Cs, the FWHM (for ^{55}Fe) for the photomultiplier alone is 36% and for the scintillator, 18%.

Narayan and Prescott[86] have presented data illustrating a trend in which the photomultiplier statistics dominate the pulse-height resolution at low gamma-ray energies and the scintillator statistics dominate at high gamma-ray energies. This trend is illustrated in the above analysis of the data in Figs. 80 and 81.

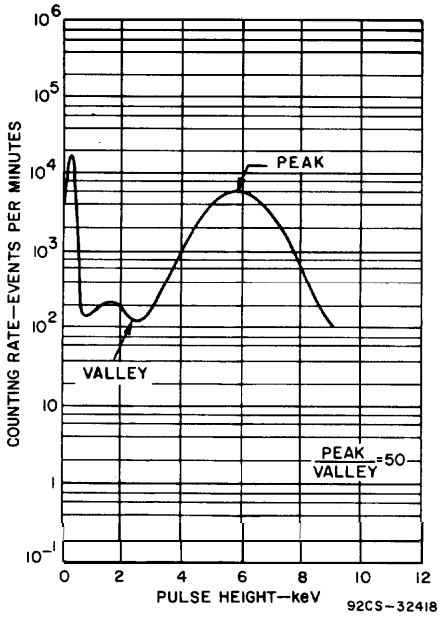

Fig. 81 - Pulse-height distribution for ^{55}Fe taken with type 8850 photomultiplier and NaI:Tl crystal.

As the gamma ray energy is increased, of course, the relative pulse-height resolution attributable to the photomultiplier decreases as the square root of the number of photoelectrons per pulse or as the square root of the gamma ray energy. The relative pulse-height resolution attributable to the crystal also decreases with gamma ray energy, but not as rapidly. The light-pulse statistics of the crystal also varies from crystal to crystal.

Key Photomultiplier Characteristics for Good Pulse-Height Resolution

Several characteristics of a **photomultiplier** tube determine its suitability for obtaining good pulse-height resolution. Of prime importance is the **quantum efficiency** of the photocathode, especially as it matches the generally blue spectrum of scintillators. Secondly, of course, the photomultiplier must have a suitable **electron-optical configuration** so that all or nearly all of the emitted photoelectrons effectively impact the first dynode. The statistics of secondary emission, especially in the first stage, also affect the ultimate resolution. It is desirable, therefore, to provide a fairly **high secondary-emission yield** either by the nature of the dynode surface material or by applying a rather high voltage between the **photocathode** and the first dynode. Finally, it is generally advantageous that the **photoemission be uniform** across the photocathode and that a **uniform collection** of all the photoelectrons be provided. This latter characteristic is particularly important in the case of thin scintillators where the light from a scintillation is more localized on the photocathode than it would be for thicker scintillators. Light pipes may be used to improve the uniformity of light on the photocathode and therefore improve the pulse-height resolution in the case of thin scintillators. For a crystal whose length is comparable to its diameter, the output **light-flux** distribution is generally uniform so that photocathode uniformity becomes statistically less significant.

Peak-to-Valley Ratio

As in pulse-counting applications, another way of classifying the performance of photomultipliers in scintillation counters is by the peak-to-valley ratio of the distribution. This way is illustrated in Fig. 81. The peak will be higher, of course, if the resolution of the tube is better. Good resolution also results in a lower valley point before the pulse-height distribution increases on the low energy side as a result of photomultiplier dark current. The peak-to-valley ratio is a particularly valuable parameter for measurements with sources characterized by low emission energy.

Plateau Concept

A plateau curve for a scintillation counter is illustrated in Fig. 82. The curve is developed by using a source such as ^{137}Cs and counting all pulses higher than a fixed discriminator level. The total counts are then plotted as a function of the photomultiplier voltage. The development of the curve in Fig. 82 may be understood by referring to the pulse-height distribution curve of Fig. 80. At the lowest value of photomultiplier

voltage, the pulse heights are less than the equivalent of the discriminator setting. As the voltage is increased, the discriminator setting moves in effect from right to left on Fig. 80. The rising portion of Fig. 82 then corresponds to the discriminator moving through the photopeak, through the Compton scattering region of the distribution, and through the barium X-ray peak. The plateau corresponds to the dark background[87] of the photomultiplier which would appear at the extreme left of Fig. 80 except for the scale-the barium X-ray peak at 32 keV corresponds to about 250 photoelectrons. The dark background pulse distribution of a photomultiplier is shown in Fig. 76. As the voltage on the photomultiplier is increased, the dark current of the tube increases because various regenerative effects increase, and the plateau is terminated at the upper end of Fig. 82.

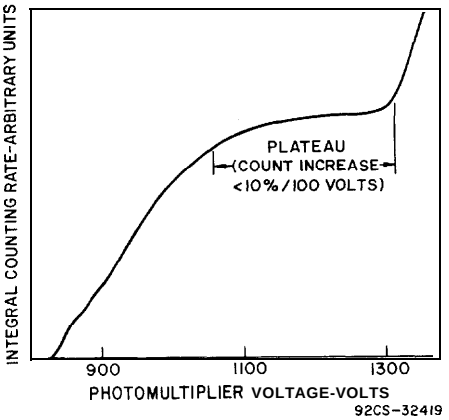

Fig. 82 - Typical plateau is defined as portion of integral-bias characteristic in which change of counting rate per 100-volt interval is less than a selected value (Engstrom and Weaver[87]).

The concept of utilizing a plateau characteristic probably stemmed from the plateau of Geiger-Muller tubes. In the case of photomultipliers, the length of the plateau is determined by the stability of the tube at high gain (a minimum of regenerative effects) and by the characteristic variation of gain with voltage. That is, a tube having Cs-Sb dynodes would generally have a shorter plateau than one having Cu-Be dynodes simply because of the more rapid increase in gain with voltage for the Cs-Sb dynodes. The plateau would also be shorter as the number of stages is increased.

Photomultiplier plateau is of particular interest in the application to oil-well logging. A rather intense gamma-ray source such as ^{137}Cs is mounted in the sonde near the photomultiplier and crystal assembly, but shielded from it. The gamma-rays result in Compton scattering in the materials near the probe. The scattered radiation is detected and measured with an integral count with the discriminator set to correspond to a point on the plateau so that essentially all of the intercepted radiation is counted. As the depth of the measurement in the drill hole increases, the temperature does also. It is, therefore, important that the counting characteristic of the scintillation detector be essentially independent of temperature. But, as the temperature increases, both the dark background count and the instability of the photomultiplier increases and, as a result, the length of the plateau decreases. Fig. 83 illustrates plateau characteristics taken at 22°C and 150°C for a photomultiplier having a Na_2KSb photocathode. The curves indicate a range of photomultiplier voltage that would be satisfactory for this range of temperature.

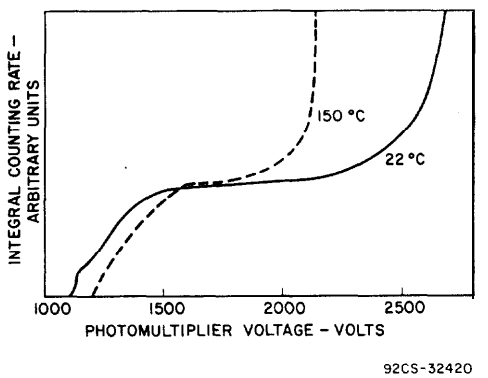

Fig. 83 - Plateau characteristics at room temperature and at 150 °C for a photomultiplier having a Na_2KSb photocathode. The photomultiplier's principal application is in oil-well-logging.

In scintillation counting applications where gamma-ray energy resolution is important, the plateau concept is not particularly applicable. Direct measurement of pulse-height resolution would be more use-

ful. But in special applications such as the oil-well logging, the plateau characterizes the useful range of operating voltage.

LIQUID SCINTILLATION COUNTING

Liquid scintillators are most commonly used for the evaluation of low-energy beta emitters because of the generally short range of beta particles and the need to provide an intimate contact between the source and the scintillator .[88,89] There are numerous fluors or solutes which may be used, such as PPO (2,5 diphenyloxazole). A common solvent is toluene which must be miscible with the liquid radioactive sample. The emission of the typical liquid scintillator is in the near ultraviolet and blue spectrum so that a photomultiplier having a "bialkali" photocathode (K_2CsSb) provides a good spectral match.

Counting Techniques

When liquid-scintillation counting was first introduced, the technique involved the use of a single photomultiplier to observe the liquid scintillator . Because of the low energies involved and the need to measure samples of relatively low activity, the background count of the photomultiplier was a severe limitation. An improved approach is the use of a pair of photomultiplier tubes facing a common scintillator chamber. Because of the number of photons involved when a scintillation occurs in the sample, it is quite likely that both photomultipliers will sense the flash, thus permitting the use of coincidence circuitry. Events that initiate background counts in one photomultiplier are only infrequently coincident with those in the second tube and so a high degree of discrimination against background counts is possible.

The three most commonly used radioisotopes in liquid-scintillation counting are tritium, ^3H; carbon, ^{14}C; and phosphorus, ^{32}P. The beta-ray energies from these radioisotopes may vary over a fairly broad range; for example, ^3H emits betas having energies varying from zero to a maximum of 18.6 keV. Maximum beta-ray energies for ^{14}C and ^{32}P are 156 keV and 1.71 MeV respectively. Fig. 84 illustrates the distribution of pulse heights (which are proportional to energy) for tritium. (The average energy is about 6 keV.)

A block diagram of a liquid-scintillation spectrometer is shown in Fig. 85. If a photomultiplier having a fast time characteristic is used in the spectrometer, the coincidence resolving time may be as small as 10 nanoseconds.

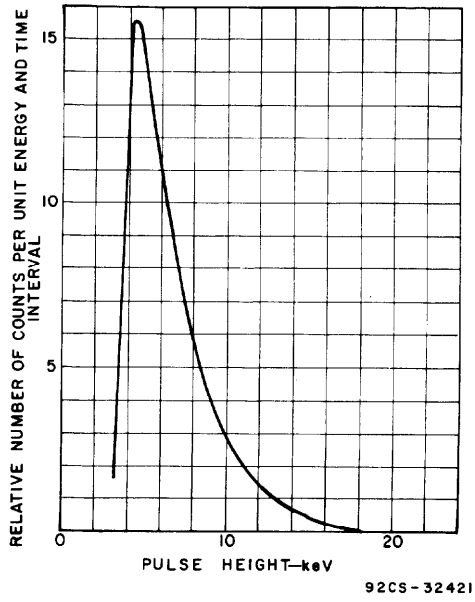

Fig. 84 - Pulse-height spectrum representing the beta energy for tritium (18.6 keV maximum) from a liquid-scintillation counter. Maximum and minimum discriminator levels are indicated (From E.D. Bransome[88]).

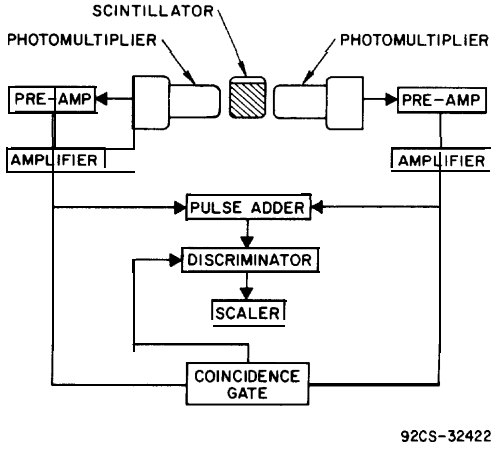

Fig. 85 - Block diagram of a liquid-scintillation spectrometer.

Counter Efficiency

A conventional figure of merit for a liquid scintillation coincidence counter is the ratio, E_2/B, where E is the counting efficiency expressed in per cent, and B is the number of background coincident counts per minute. The efficiency, E, is measured utilizing a standard sample whose disintegration rate is known. The recorded count rate is compared with that of the standard, taking into account the exponential decay in the disintegration rate. The background count value, B, is measured by utilizing a blank sample of the scintillator .

Note that E_2/B is proportional to the square of a signal-to-noise figure for the system. Thus, the efficiency E is proportional to the signal; and the square root of B is the expected standard deviation in the statistical count.

Efficiencies of the scintillators and the photomultipliers in liquid-scintillation-counting equipment (using the most efficient liquid scintillator and photocathodes) are such that about 2.5 photoelectrons are emitted per keV of energy of the beta ray. The best counting efficiency for a given radioisotope is obtained when a highly efficient scintillator and a photomultiplier having a high quantum efficiency in the spectral emissivity range of the scintillator are used. The optical system containing the two photomultipliers and the counting vial is also of major importance. The system should be designed so that, as far as possible, the photons produced in a scintillation are equally divided between the photomultipliers. This division assures that a coincidence pulse results from as many scintillations as possible. In some cases two or more different isotopes may be counted simultaneously. It is desirable, therefore, that the photomultipliers have matched gains and good energy (pulse-height) resolution capability to provide best isotope separation. A typical value for E is about 60%. Quantum efficiency of the bialkali photocathode for the scintillation radiation is approximately 25 %.

Sources of Background Counts

There are various sources of the coincident background counts. One source is the random dark-noise pulses in each of the two photomultipliers which are occasionally coincident. The coincident rate may be predicted by the following equation:

$$C = \frac{2N_1N_2\tau}{60} \qquad (29)$$

where C is the chance coincidence rate per minute, N_1 is the dark-noise count rate in counts per minute from tube No. 1, N_2 is the dark-noise count rate in counts per minute from tube No. 2, and τ is the resolving time of the coincidence circuit in seconds. In a liquid-scintillation spectrometer employing two tubes each having dark-noise rates of 30,000 counts per minute each and a coincidence circuit having a resolving time of 10 nanoseconds, the number of accidental coincidences is approximately 0.3 count per minute.

Another source of background count is cross talk between the two photomultipliers as a result of light flashes in one tube which are sensed by the other.

Cosmic rays and other natural radiation can result in flashes in the scintillator or possibly in the photomultiplier envelope. Shielding the equipment with lead can reduce the background from these sources. However, the photomultipliers themselves also contain radioactive isotopes. A common contaminant is ^{40}K, a naturally occurring isotope of potassium (0.1 %), that is present in many glasses. Photomultipliers designed for use in liquid-scintillation counters may utilize quartz face plates or thin face plates of a glass having a minimum potassium content and with a low yield of scintillations from gamma rays.

When a vial filled only with a scintillator is placed between the photomultipliers, and the output from the coincidence circuit is examined by use of a multichannel analyzer, a pulse-height distribution such as that shown in Fig. 86 is obtained. Clearly, not many of the background pulses shown are caused by the accidental coincidences of dark-noise pulses from the photomultipliers, but are caused by cosmic rays of scintillations in the material of the vial and photomultiplier envelope resulting from the presence of radioisotopes in the materials of which they are constructed.

Typical values for B, the number of background counts, in coincidence liquid-

scintillation counters are in the range 15 to 20 counts per minute, and E^2/B values are typically in the range 150 to 250 for tritium.

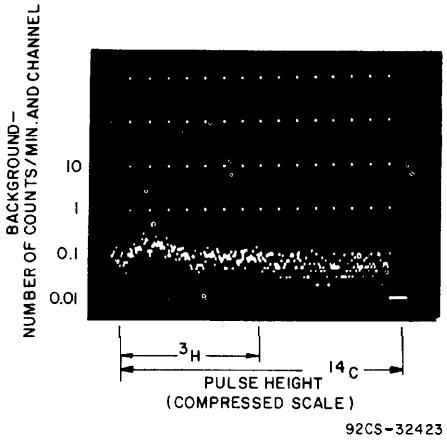

Fig. 86 - Background distribution obtained from a liquid scintillator using a coincidence system.

Photomultiplier Selection for Liquid Scintillators

The E^2/B figure of merit is, however, not necessarily the best way of evaluating all systems. It is valid at very low counting rates where the background count is the dominant factor, but is not of great help at high-counting rates where the background count of the system becomes less important than the efficiency in determining the merit of the system.

In selecting a photomultiplier tube for a liquid-scintillation application, the following items are of major importance: high photocathode quantum efficiency, low dark-noise count rate, minimum internal-light generation, low scintillation-efficiency envelope, fast time response, and good energy resolution. The 4501V3 photomultiplier has been specifically designed to meet these requirements.

ENVIRONMENTAL EFFECTS

Although photomultiplier tubes are not overly sensitive to their environment and can be handled without exercising undue caution, there are various considerations the user should be aware of in order to maximize tube life, avoid permanent damage, and provide the optimum performance. This section provides guidance relating to specific environmental limitations or to means for optimizing performance under adverse conditions.

Temperature

The maximum temperature to which a photomultiplier should be exposed during either operation or storage is determined primarily by the characteristics of the photocathode. Temperature ratings vary with tube type depending upon the particular photocathode. For a specific type, its published data should be consulted. In general, however, a temperature of 75 °C should not be exceeded. Excessive exposure to higher temperatures will alter the delicate balance of chemicals of the photocathode and result in a loss of responsivity and/or a shift in spectral response. Another reason for avoiding operation of photomultipliers at elevated temperatures is that it causes an increase in the dark current. (See Fig. 16.)

There are also hazards in cooling photomultiplier tubes to reduce the dark emission from the photocathode. Rapid cooling should be avoided to minimize thermal shock which could result in cracking of the bulb or stem. Temperatures below – 50°C should be avoided because the difference in expansion between the glass and the base material could result in cracking of the glass. This hazard is also present for photomultiplier tubes having metal envelopes or for tubes having stiff lead glass stems when socketed in a material of different expansion coefficient.

In the cooling of photomultiplier tubes care must also be taken to avoid moisture condensation. One method is to provide a dry atmosphere for the tube and, especially, its base and socket. Another method is to cover the critical areas of the tube with a silicone rubber such as General Electric RTV-11. The tube should first be cleaned and then primed (4004 primer for RTV-11) before the silicone rubber coating is applied.

Differential cooling in which only the photocathode end of the tube is cooled is not recommended. This practice may result in loss of photocathode sensitivity because of the vapor transport of alkali metals from the dynodes to the photocathode.

Voltage

The published data for photomultiplier

tubes contain information on the maximum supply voltage as well as information on the specific maxima for voltages between adjacent electrodes such as between dynode No. 1 and the photocathode. Too high a voltage between closely spaced electrodes can result in electrical breakdown, particularly across insulator surfaces. The over-all tube voltage maximum is determined by considerations of the maximum gain which a tube can tolerate. Depending upon the construction of the photomultiplier, at some gain in excess of 10^7 or 10^8, there may be sufficient feedback-perhaps by light generated in the output section of the tube-to result in a sustained electrical current. This current breakdown, if sufficiently large, can permanently damage the tube by causing an increase in the dark current and a decrease in responsivity .

Ground potential and shielding of the photomultiplier can also be a problem. In order to minimize regenerative effects it is generally recommended that the wall of the photomultiplier envelope be maintained at a potential at or near cathode potential. This recommendation offers no problem in a circuit in which the cathode is at ground potential. But when the anode is at ground potential, it may be advisable for safety reasons to provide a double shield: the inner shield at cathode potential, surrounded by an insulator, and an outer shield at ground potential. The inner shield should be maintained at cathode potential through a high resistance (usually 5 to 10 megohms) to avoid hazard through accidental contact or breakdown of the insulation.

It is strongly recommended that no difference of potential be maintained between the semitransparent photocathode layer of a photomultiplier and its outer glass faceplate. A potential on the outside of the glass that is positive with respect to that of the photocathode can result in damage to the photocathode by ionic transport through the glass faceplate.[69] (See section on "Shielding" earlier in this Chapter.)

In supplying the tube voltage by means of a resistive voltage divider, care must be taken to avoid physical contact between any of the resistors. Such contact can cause miniature electrostatic discharges resulting in noise spikes in the photomultiplier output.

Light Level

It is generally advisable to store photomultiplier tubes in the dark and to avoid excessive exposure of the tubes to any light rich in blue or ultraviolet such as that from fluorescent lamps or sunlight. Exposure of the photocathode to such radiation will generally cause a very substantial increase in the dark current originating from the photocathode. Complete recovery from this effect may take as long as several days. See Fig. 47. Exposure of the photocathode to sunlight even though no voltage is being applied may also result in photocathode response changes such as loss of infrared response in a tube having a multialkali photocathode.

Before a photomultiplier tube is used for critical low-light-level measurements, it is recommended that it be aged for a period of 24 hours in the dark with voltage applied. This precaution is particularly recommended after a long period of idleness even if the tube has not been exposed to ambient lighting.

When the photomultiplier has the appropriate voltage applied, it is of course prudent to avoid any excessive light exposure. Particularly, if the voltage divider has a substantial current flow, an excessive current may flow in the photomultiplier which could result in loss of gain and an increase in dark current. Photomultiplier data sheets generally contain ratings of the maximum anode current which may be drawn.

Some semitransparent photocathodes are very resistive. See Fig. 36. Even though the light flux on the photocathode may be relatively small, it is possible that the drop in voltage across the photocathode between the electrical contact and the light spot may inhibit the photoelectron current flow and cause a non-linear behavior that could upset careful measurements.

When measurements are made at very low light levels, it is important that the tube be totally shielded from unwanted stray light to avoid an increase in background noise output. A person's photopic vision is not a good judge of the presence of light leakage that the photomultiplier might sense readily. For example, light may leak through an open-ended coaxial cable connector such as BNC or through certain bases or sockets. It may be noted that light-tight caps are generally

commercially available to terminate unusual coaxial connectors.

Magnetic Fields

Care should be exercised to keep the magnetic field environment of a photomultiplier to a minimum. The electron optical operation of a photomultiplier can be considerably altered by magnetic fields, as shown in Fig. 51. It is also possible to induce a permanent magnetization of some photomultiplier parts such as dynodes or dynode side rods constructed of nickel. If magnetization occurs, degaussing may readily be accomplished by placing the tube at the center of a coil operated at an alternating current of 60 Hz with a maximum field strength of 8000 ampere turns per meter and then gradually withdrawing the tube from the coil.

Magnetic shields are generally available commercially for photomultiplier tubes of various constructions. In providing such protection, it may be important to use a shield which extends beyond the semitransparent photocathode a distance of at least half the diameter of the photocathode.

Atmosphere

In some applications it may be necessary to operate the photomultiplier in other than normal atmospheric pressure. Most photomultipliers will tolerate pressures to three atmospheres. For the larger tubes, however, this pressure may present an implosion hazard. In these special cases, it would be well to check with the tube manufacturer. Pressures less than one atmosphere also present a problem in that electrical breakdown can more readily occur. In such cases it may be necessary to coat all exposed connections and wiring with an insulator such as silicone rubber.

Corrosive atmospheres must be avoided, especially on photomultipliers having metal envelopes. Corrosion could destroy the glass-to-metal seal and result in loss of vacuum.

High-humidity conditions should be avoided if possible because condensation on the base and socket can result in additional electrical leakage or even breakdown. If the moisture situation is unavoidable, it may again be advisable to coat exposed connections with an insulator such as silicone rubber as described earlier under "Temperature."

Again, a word of caution about the problem of helium penetration of glass. Even at room temperature, if there is a significant helium content in the ambient photomultiplier atmosphere, some helium will penetrate the glass envelope. The result is an increase in dark current and after pulsing because of ionization of the helium gas. Eventually, with sufficient helium pressure a complete electrical breakdown can occur with voltage applied to the photomultiplier tube.

If helium cannot be avoided, it may be desirable to use a separate enclosure for the photomultiplier through which a small flow of purging gas such as dry nitrogen is provided. It is also reported[90] that helium penetration can be blocked by a thin layer of an epoxy-Epon 828 resin (registered trademark of Shell Chemical Company) and Belsamid 125 hardening agent (registered trademark of General Mills Incorporated).

Shock and Vibration

Most photomultipliers will survive only a reasonable amount of shock or vibration (less than 10-g shock, depending on shock duration and direction). Although special photomultipliers have been designed to survive in extreme environments (shock values from 30 to 1500 g), the user should make every effort to avoid excessive shock or vibration, possibly by the use of special vibration-isolation fixtures. The photomultiplier tube should be handled as the delicate instrument that it is. Excessive shock or vibration can actually cause physical damage to the tube to the point of shorting out some of the elements or even resulting in breakage of the envelope and loss of vacuum. A lesser degree of shock may cause deformation of the tube elements and can result in loss of gain or deterioration of other performance parameters. If measurements are being made while a tube is vibrated, it is likely that the output will be modulated by the vibration not only because the light spot may be deflected to different positions on the photocathode but also because some of the dynodes may actually vibrate and cause modulation of the secondary-emission gain.

Many photomultipliers have been designed for use under severe conditions of shock and vibration and, in many cases, spe-

cifically for use in missile and rocket applications. Such tubes, however, find uses in many other applications including oil-well logging or other industrial control applications where the tube may be subjected to rough usage. These tubes are available with most of the electrical and spectral characteristics typical of the more general-purpose types. These types differ primarily in mechanical construction in that additional supporting members may be employed and an improved cathode connection may be used to assure positive contact when the tube is subjected to these environments. Ruggedization of tubes using the glass envelope has also been accomplished by moving the dynode cage close to the stem (thereby drastically shortening the lead lengths and raising their mechanical resonant frequency), by using heavier leads and extra spacers to hold the dynode cage in place, and by a special heavy-duty welding process on the metal-to-metal joints.

Tubes recommended for use under severe environmental conditions are usually designed to withstand environmental tests equivalent to those specified in the applicable portions of MIL-E-5272C or MIL-STD-810B in which the specified accelerations are applied directly to the tubes. Sinusoidal vibration tests are performed on apparatus that applies a variable sinusoidal vibration to the tube. The sinusoidal frequency is varied logarithmically with time from a minimum to a maximum to a minimum value. Each tube is vibrated in each of the three orthogonal axes.

Random vibration tests are performed by subjecting the tube to a specified spectral density (g^2/Hz) in a specified frequency band.

Shock tests are performed on an apparatus that applies a half-wave sinusoidal shock pulse to the photomultiplier tube. The tube is subjected to the shock in each of the three orthogonal axes. The shock pulse is expressed in terms of the peak acceleration of the pulse and the time duration of the pulse. The tubes may receive more than one shock pulse in each of the orthogonal axes.

Nuclear Radiation

In specialized applications such as the use of photomultiplier tubes in satellites, the tubes may be subjected to high levels of radiation such as occur in the Van Allen belts. A summary of the effects of radiation on photomultiplier tubes may be found in a paper by S.M. Johnson, Jr.[90a]. Temporary effects of intense radiation are principally an increase in background current and noise. Continued exposure, however, will also cause permanent damage to the face-plate glass, and to a much lesser extent the photocathode, and the dynodes.

The origin of the increased background current in photomultipliers exposed to nuclear radiation is a fluorescence or scintillation in the glass faceplate that causes electron emission from the photocathode. For example, irradiation with ^{60}Co gamma rays produces the equivalent of 10^{-12} W/cm2 of 420-nm flux for an input of 10^{-3} rad/s.

The major damage to a photomultiplier is the browning of the faceplate glass. Significant changes in transmission are observed for 9741 and 7056 glass with an exposure of 10^5 rads of ^{60}Co gamma radiation. Fused silica shows much less change for the same irradiation. Lime glass is reported to be very susceptible to browning. Sapphire is the least degraded by gamma radiation of windows used in photomultipliers. Of the far-ultraviolet windows, LiF is reported to be very susceptible to radiation damage. MgF_2 is recommended down to the Lyman-alpha wavelength level in the presence of high radiation exposures.

Although most of the damage to photomultipliers from nuclear radiation is in the faceplate, some change may be expected in the photocathode. The damage is not great compared with that to the glass, probably because of the very small absorption of the very thin photocathodes. The same may be said for dynode material where, again, the surface layer is most important.

REFERENCES

44. W.J. Harper and W.J. Choyke, "The resistance of semitransparent photocathodes," **Jour. Appl. Phys.,** Vol. 27, p. 1358 (1956).

45. R.W. Engstrom, R.G. Stoudenheimer, H.L. Palmer, and D.A. Bly, "Recent Work on photoemission and dark emission problems," **IRE Trans. Nucl. Sci.,** Vol. NS 5,

No. 3, p. 120-124, (Dec. 1958).
46. M. Lontie-Bailliez and A. Messen, "L'influence de la temperature sur les photomultiplicateurs," **Annales de la Scoiete Scientifique de Bruxelles,** Vol. 73, Series 1, p. 390 (1959).
47. W.E. Spicer and F. Wooten, "Photoemission and photomultipliers," **Proc. IEEE,** Vol. 51, p. 1119-1126, (Aug. 1963).
48. H. Martin, Cooling photomultipliers with III-V photocathodes," **Electro-Optical Systems Design,** Vol. 8, No. 11, p. 16-20 (Nov. 1976).
49. E.G. Ramberg, "Optical factors in the photoemission of thin films," **Appl. Opt.,** Vol. 6, No. 12, p. 2163-2170 (Dec. 1967).
50. S.A. Hoenig and A. Cutler III, "Polarization sensitivity of the RCA 6903 photocathode tube," **Appl. Opt.,** Vol. 5, No. 6, p. 1091-2 (June 1966).
51. H. Hora, "Experimental evidence of angular dependence of electron excitation in photoemission", **Phys. Stat. Sol.,** Vol. (a) 5, p. 159-166 (1971).
52. W.D. Gunter, Jr., E.F. Erickson, and G.R. Grant, "Enhancement of photomultiplier sensitivity by total internal reflection," **Appl. Opt.,** Vol. 4, No. 4, p. 512 (April 1965).
53. J.R. Sizelove and J.A. Love, III, "Analysis of a multiple reflective translucent photocathode," **Appl. Opt.,** Vol. 6, No. 3, p. 443-446, (March 1967).
54. J.B. Oke and R.E. Schild, "A practical multiple reflection technique for improving the quantum efficiency of photomultiplier tubes," **Appl. Opt.,** Vol. 7, No. 4, p. 617-622 (Apil 1968).
55. W. D. Gunter, Jr., G.R. Grant, and S.A. Shaw, "Optical devices to increase photocathode quantum efficiency," **Appl. Opt.,** Vol. 9, No. 2, p. 25 l-257 (Feb. 1970).
56. D.P. Jones, "Photomultiplier sensitivity variation with angle of incidence on the photocathode," **Appl. Opt.,** Vol. 15, No. 4, p. 910-914 (April 1976).
57. F.A. Helvy and R.M. Matheson, "Photosensitive cathode with closely adjacent light-diffusing layer," U.S. Patent 3 242,626, (Mar. 29, 1966).
58. R.W. Engstrom, "Improvement in photomultiplier and TV camera tubes for nuclear medicine," **IEEE Trans. Nucl. Sci.,** Vol. NS-24, No. 2, p. 900-903 (Apil 1977).
59. W. Widmaier and R.W. Engstrom, "Variation of the conductivity of the semitransparent cesium-antimony photocathode," **RCA Rev.,** Vol. 16, No. 1, p. 109-115 (March 1955).
60. H.A. Zagorites and D.Y. Less, "Gamma and X-ray effects in multiplier phototubes," Naval Radiological Defense Laboratory, USNRDL-TR-763, (7 July 1964).
61. W. Viehmann, A.G. Eubanks, G.F. Pieper, and J.H. Bredekamp, "Photomultiplier window materials under electron irradiation: fluorescence and phosphorescence" **Appl. Opt.,** Vol. 14, No. 9, p. 2104-2115 (Sept. 1975).
62. R.B. Murray and J.J. Manning, "Response of end-window photomultiplier tubes as a function of temperature," **IRE Trans. Nucl. Sci.,** Vol. NS-7, No. 2-3, p. 80-86 (June-Sept . 1960).
63. A.T. Young, "Temperature effects in photomultipliers and astronomical photometry," **Appl. Opt.,** Vol. 2, No. 1, p. 5 l-60-(Jan. 1963).
64. R.E. Rohde, "Gain vs. temperature effects in NaI(Tl) photomultiplier scintillation detectors using 10 and 14 stage tubes," **Nucl. Intr. and Methods,** Vol. 34, p. 109-115 (1965).
65. D.F. Cove11 and B.A. Euler, "Gain shift versus counting rate in certain multiplier phototubes," USNRDL-TR-521, U.S. Naval Radiological Defense Laboratory, San Francisco (1961).
66. C.S. Wiggins and K. Earley, "Photomultiplier refrigerator," **Rev. Sci. Instr.,** Vol. 33, p. 1057-8 (1962).
67. For example, among others: Products for Research, Inc., 78 Holten Street, Danvers, Massachusetts 01923 (617-774-3250).

Pacific Precision Instruments, 1040 Shary Court, Concord, California 945 18 (415-827-9010).

68. H.R. Krall, "Extraneous light emission from photomultipliers," **IEEE Trans. Nucl. Sci.** Vol. NS-14, No. 1, p. 455-9 (Feb. 1967).
69. Louis Lavoie, "Photomultiplier cathode poisoning," **Rev. Sci. Instr.,** Vol. 38, No. 6, pp 833-4, (1967).
70. G.A. Morton, H.M. Smith and R. Wasserman, "Afterpulses in photomulti-

pliers," IEEE Trans. Nucl. Sci., Vol. NS-14, No. 1, pp 443-448, (1967).
71. V.O. Altemose, "Helium diffusion through glass," J. Appl. Phys., Vol. 32, No. 7, pp 1309-1316, (1961).
72. W.C. Paske, "He + afterpulses in photomultipliers: Their effect on atomic and molecular lifetime determinations," Rev. Sci. Instr., Vol. 45, No. 8, p. 1001-3 (1974).
73. A.T. Young, "Cosmic ray induced dark current in photomultipliers," Rev. Sci. Instr., Vol. 37, No. 11, pp 1472-1481 (1966).

74. D. Sard, "Calculated frequency spectrum of the shot noise from a photomultiplier tube," J. Appl. Phys., Vol. 17, p. 768-777 (1946).
75. B. Leskovar and C.C. Lo, "Transit time spread measurements of microchannel-plate photomultipliers," European Conference on Precise Electrical Measurements, Brighton, Sussex, England, 5-9 Sept. 1977 (London, England: IEEE (1977), pp 41-3.)
76. D.A. Gedcke and W.J. McDonald, "Design of the constant fraction of pulse height trigger for optimum time resolution," Nucl. Instr. and Meth., Vol. 58, No. 2, pp 253-60 (1968).
77. M. Birk, Q.A. Kerns, and R.F. Tusting, "Evaluation of the C-70045A high-speed photomultiplier," IEEE Trans. Nucl. Sci. Vol. NS-11, No. 3, pp 129-138 (1964).
78. F. de la Barre, "Influence of transit time differences on photomultiplier time resolution," IEEE Trans. Nucl Sci., Vol. NS-19, No. 3, pp 119-121 (1972).
79. B. Leskovar, C.C. Lo, "Performance studies of photomultipliers having dynodes with GaP(Cs) secondary emitting surface," IEEE Trans. Nucl. Sci., Vol. NS-19, No. 3, pp 50-62 (1972).
80. S.K. Poultney, "Single Photon Detection and Timing: Experiments and Techniques," Advances in Electronics and Electron Physics, Vol. 31, Academic Press, Inc., New York, (1972).
81. E. Gatti and V. Svelto, "Review of theories and experiments of resolving time with scintillation counters," Nucl. Instr. and Methods, Vol. 43, pp 248-268, (1966).
82. W.A. Baum, "The detection and measurement of faint astronomical sources," Astronomical Techniques, Edited by W .A. Hiltner, The University of Chicago Press, (1962).
83. G.A. Morton, "Photon Counting," Appl. Opt., Vol. 7, No. 1, pp l-10, (1968).
84. R.M. Matheson, "Recent photomultiplier developments at RCA," IEEE Trans. Nucl. Sci. Vol. NS-11, No. 3, pp 64-7 1, (1964).
85. G.A. Morton, H.M. Smith, and H.R. Krall, "Pulse-height resolution of high gain first dynode photomultipliers," Appl. Phys. Lett., Vol. 13, No. 10, pp 356-7, (1968).
86. G.H. Narayan and J.R. Prescott, "Line-widths in NaI(Tl) scintillation counters for low energy gamma-rays," IEEE Trans. Nucl. Sci., Vol. NS-13, No. 3, pp 132-7, (1966).
87. R.W. Engstrom and J.L. Weaver, "Are plateaus significant in scintillation counting?" Nucleonics, Vol. 17, No. 2, pp 70-74, (1959).
88. The Current Status of Liquid-Scintillation Counting, Edited by Edwin D. Bransome, Grune and Stratton, New York and London, (1970).
89. Liquid-Scintillation Counting, Recent Developments, Edited by Philip E. Stanley and Bruce A. Scoggins, Academic Press (1974).
90. Yasunori Nikaido et al, "Electron tube for photoelectric conversion," Patent Publication No. SHO 42-16002 (Shimizu Patent Office, Fukiai-Ku, Kobe, Japan).
90a. S.M. Johnson, Jr., "Radiation effects on multiplier phototubes," IEEE Trans. Nucl. Sci., Vol. NS-20, No. 1, pp 113-124, Feb. 1973.

5. Photomultiplier Applications

SUMMARY OF SELECTION CRITERIA

A comparison of the relative advantages of photomultipliers and solid-state detectors is given in the introductory chapter of this manual. The following is a summary of the application requirements that indicate when, in general, a photomultiplier is the most suitable detector.

The most important consideration is the light or radiation level to be detected. The use of photomultipliers is recommended when the level of light flux is very low. If levels are relatively high, it may be simpler to use a solid-state detector. Furthermore, a high level of light flux could overload and damage the photomultiplier. A photomultiplier may be used if the light flux is 100 microlumens or less or of the order of 0.1 microwatt or less at the peak of the spectral response.

When a fairly large detector area is required, a photomultiplier is also recommended, as is the case in scintillation counting where a crystal scintillator may be several centimeters in diameter. Silicon avalanche photodiodes have good low-light-level capability but their area is generally limited to a few square millimeters.

Spectral response of the photomultiplier, of course, must be a reasonable match to that of the source of radiation. Photomultipliers are useful in the range 120 nanometers to 1100 nanometers, depending upon the type of photocathode and window material. Responses further in the infrared than 1100 nanometers require an infrared photoconductive detector or some other infrared-sensitive device.

When a fast response time is an important requirement, the photomultiplier is usually the most suitable detector. Photomultiplier tubes have response-time capability down to the nanosecond range and even better in the case of specially designed tubes.

APPLIED VOLTAGE CONSIDERATIONS

Proper operation of a photomultiplier depends critically upon the applied voltage and the voltage distribution to the dynode stages. A small variation in voltage can result in a much larger percentage change in the tube gain. For example, see Fig. 49 which shows the log of the gain as a function of the log of the voltage. For a 9-stage tube the slope of the log-gain vs log-voltage curve is approximately 7; for a 14-stage tube the slope is about 12. (If the secondary emission ratio were linear with voltage, see Fig. 19, one would expect the slope of the log-gain vs log-voltage curves to be equal to the number of stages.) For a 12-stage tube, a 1% change in voltage results in a 10% change in gain. Thus, there is need for more than ordinary precaution to provide a well-regulated power supply.

Power Supply, Regulation, Polarity, and Shielding

Commercial power supplies are generally available that have a line-regulation of 0.005% with some available at 0.001% for a 10% change in line voltage when working into a fixed divider network. Voltage variation with temperature might be of similar magnitude for a 1 °C change in temperature. It would not be too difficult, therefore, to provide voltage supplies that would result in gain stability of the photomultiplier tube due to line voltage and temperature changes of better than 0.1%. For requirements not this critical, BURLE manufactures a simplified compact power supply that includes a socket and voltage-divider network for 1-l/8inch diameter, 9-stage, side-on photomultipliers. Also manufactured by BURLE are Integrated Photodetection Assemblies (IPA's) that package a photomultiplier tube, optical filter, power supply, signal-conditioning

amplifier, and electrostatic/magnetic shielding. The IPA operates from a 12-volt dc supply.

The recommended polarity of the photomultiplier power-supply voltage with respect to ground depends largely on the application intended. Of course, the cathode is always negative with respect to the anode. In some pulsed application, however, such as scintillation counting, the cathode should be grounded and the anode operated at a high positive potential with a capacitance-coupled output. In this case the scintillator and any magnetic or electrostatic shields should also be connected to ground potential.

In applications in which the signal cannot be passed through a coupling capacitor, the positive side of the power supply should be grounded. The cathode is then at a high negative potential with respect to ground. When this arrangement is used, extra precautions must be taken in the mounting and shielding of the photomultiplier. If there is a potential gradient across the tube wall, scintillations occurring in the glass will increase dark noise. If this condition continues for a sufficiently long period of time, the photocathode will be permanently damaged by the ionic conduction through the glass. To prevent this situation when a shield is used, the shield is connected to photocathode potential. Light-shielding or supporting materials used in photomultipliers must limit leakage currents to 10^{-12} ampere or less. Fig. 62 shows a curve of the effect of external-shield potential on photomultiplier noise.

To reduce the shock hazard to personnel, a very high resistance should be connected between the shield and the negative high voltage.

Voltage Divider Design

The interstage voltage gradients for the photomultiplier elements may be supplied by individual voltage sources. The usual source, however, is a resistive voltage divider placed across a high-voltage source, as shown in Fig. 87.

A resistive voltage divider must be designed to divide the applied voltage equally or unequally among the various stages as required by the electrostatic system of the tube. The most common voltage between stages is usually referred to as the stage voltage and the voltage between other stages as

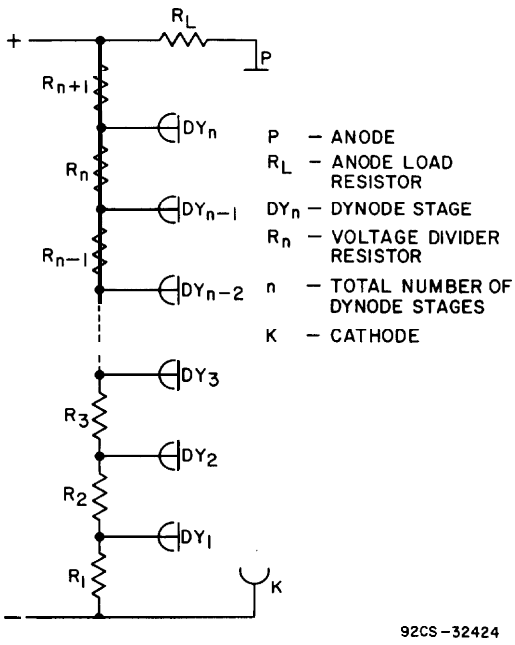

Fig. 87 - Schematic diagram of a resistive voltage divider.

relative to the most common stage voltage.

The voltage distribution is normally specified in the following way:

Between	Relative Voltage
K - Dy_1	r_1
Dy_1 - Dy_2	r_2
Dy_{n-1} - Dy_n	r_n
Dy_n - Anode	r_{n+1}

where n represents the number of the dynode stage and r_j ($j = 1$ to $n+1$) represents the relative interstage voltage. There is always one more interstage voltage than there are dynode stages.

The following formula may be used to calculate the voltage between stages:

$$V_j = \frac{(E_{supply})\, r_j}{r_t}$$

where $r_t = \sum_{j=1}^{n+1} r_j$.

The voltage-divider resistor values required for each stage can be determined from the value of the total resistance required of the voltage divider and the voltage-divider ratios of the particular tube type.

The interstage resistance values are in proportion to the voltage-divider ratios as follows:

$$R_j = R_t \frac{r_j}{r_t}$$

where R_j is the resistance between elements Dy_{j-1} and Dy_j. The recommended resistance values for a photomultiplier voltage divider range from 20,000 ohms per stage to 5 megohms per stage; the exact values are usually the result of a compromise. If low values of resistance per stage are utilized, the power drawn from the regulated power supply may be excessively large. The resistor power rating should be at least twice the calculated power dissipation to provide a safety margin and to prevent a shift in resistance values as a result of overheating. The highest suitable value of stage resistance (after consideration has been given to average anode current as described below) is dictated by leakage currents in the photomultiplier and socket wiring.

One criterion for the selection of a suitable range of voltage-divider resistance values is the expected maximum anode current that may be drawn from the photomultiplier. When the anode current is of the same order of magnitude as the divider current, nonlinear response results. This non-linearity is illustrated in Fig. 88 which shows the response of a 931A photomultiplier as a function of light level using a conventional voltage divider such as shown in Fig. 87 with equal voltage per stage.[91] (The value of R_L was essentially zero for this measurement.) The anode current is shown relative to the divider current at zero light level. The superlinearity region is explained by a change which takes place in the voltage distribution between stages from uniform to non-uniform as the light level is increased. Thus, the electron current flow from the last dynode to the anode causes less current to flow through the voltagedivider resistor, $R_{10} = R_{n+1}$. The result is an increase in voltage between dynodes and a decrease in the collection voltage between the last dynode and the anode. The reduced collection voltage tends to reduce the output current slightly, but the increased dynode voltages more than compensate for this reduction by an increased gain.

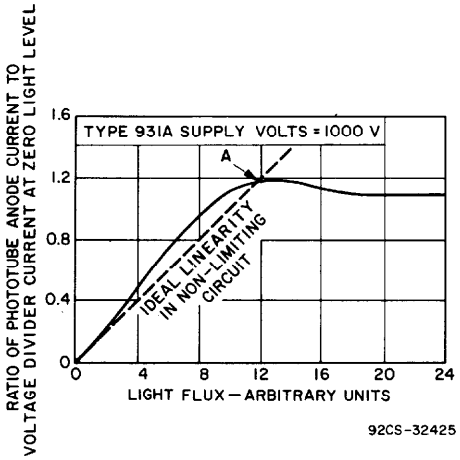

Fig. 88 - The relative response of a 931A photomultiplier as a function of the light flux using the circuit of Fig. 87 with equal stage voltage (at zero light level). (From Engstrom and Fischer[91])

The decrease in sensitivity that occurs beyond region A of Fig. 88 results from the extension of voltage losses to the last two or three dynode resistors causing defocusing and skipping in the associated dynode stages. In order to prevent this loss and assure a high degree of linearity, the current through the voltage-divider network should be at least ten times the maximum average anode current required. In calculating the voltage-divider current, the average anode current must first be estimated; this estimate requires knowledge of the value of the input (light) signal and the required output (electrical) signal.

Photo-multiplier noise or a shift in gain may result from heat emanating from the voltage-divider resistors. The divider network and other heat-producing components, therefore, should be located so that they will not increase the tube temperature. Resistance values in excess of five megohms should be avoided because current leakage between the photomultiplier terminals could cause a variation of the interstage voltage.

The type of resistor used in a divider depends on the dynode structure with which the divider will be used. Close-tolerance resistors, such as the laser-trimmed metal-film types, are normally required with the focused structures. On the other hand, interdynode voltages in the Venetian-blind structures can vary widely with but little effect on

the photomultiplier. For this reason, the resistors used with a Venetian-blind structure can be of a less stable variety, such as composition.

Cathode-to-First-Dynode Region

The over-all performance of a tube that has a cathode-to-first-dynode region essentially electrostatically isolated from the remaining dynode region can be improved by maintaining a high electric field, in the cathode-to-first-dynode region to reduce the transit-time spread of photoelectrons arriving at the first dynode and minimize the effect of magnetic fields. A high first-dynode gain, which implies a high cathode-to-first-

have the disadvantage of reducing the gain in

Intermediate Stages

In applications in which it is desirable to control the anode sensitivity without changing the over-all voltage, the voltage of a single dynode may be varied. Fig. 89 shows the variation of anode current for a 931A photomultiplier when one of the dynode voltages is varied while the total supply voltage is held constant. The dynode should be selected from the middle of the dynode string because a variation of dynode potentials near the cathode or anode would have a detrimental effect on photomultiplier operation.

Operation with Fewer Stages

A photomultiplier need not be operated with all dynode stages, although the design of the tube has been optimized for this condition. In some situations where the light level being detected is so high that it would overload the output stages of the photomultiplier, it is possible to eliminate these stages from the circuit. For example, the last several stages of the tube and the anode may be tied together electrically to form an anode. The tube is then operated with the reduced gain of the remaining stages. In an extreme case, the photomultiplier may be operated just as a photodiode using only the photocathode and several or all of the remaining elements together as an anode. It must be realized in operating the photomultiplier in such a manner that many photocathode types are very resistive (see Figs. 35 and 36) and, therefore, the photocurrent will not be linear with light at the high level which may be available. Photocathodes of the opaque type with a conductive substrate, or the semitransparent type with a conductive undercoating will tolerate a much higher light level without loss of linearity.

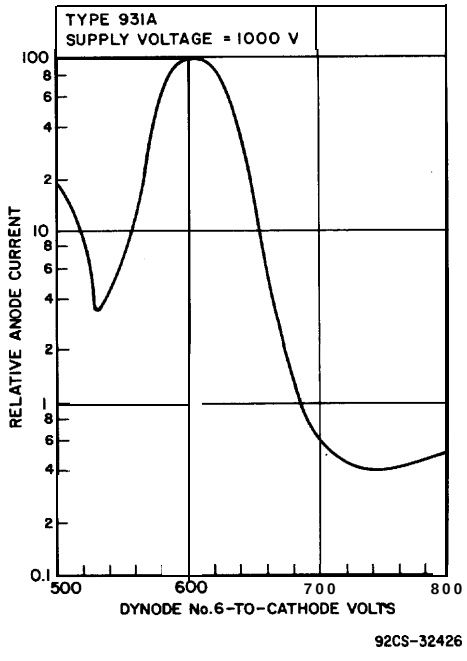

Fig. 89 - The output-current variation of a 931A when the voltage on one dynode (No. 6) is varied while the total supply voltage remains fixed.

Voltage Dividers for Pulsed Operation

In applications in which the input signal is in the form of pulses, the average anode current can be determined from the peak pulse current and the duty factor. The total resis-

tance of the voltage-divider network is calculated for the average anode current.

In cases in which the average anode current is much less than a peak pulse current, dynode potentials can be maintained at a nearly constant value during the pulse duration by use of charge-storage capacitors at the tube socket. The voltage-divider current need only be sufficient to provide the average anode current for the photomultiplier. The high peak currents required during the large-amplitude light pulses are supplied by the capacitors.

The capacitor values depend upon the value of the output charge associated with the pulse or train of pulses. The value of the final-dynode-to-anode capacitor C is given by

$$C = 100 \frac{q}{V}$$

where C is in farads, q is the total anode charge per pulse in coulombs, and V is the voltage across the capacitor. The factor 100 is used to limit the voltage change across the capacitor to a l-per-cent maximum during a pulse. Capacitor values for preceding stages should take into account the smaller values of dynode currents in these stages. Conservatively, a factor of approximately 2 per stage is used. Capacitors are not required across those dynode stages at which the peak dynode current is less than 1/10 of the average current through the voltage-divider network. For pulse durations in the 1 to 100 ns range, consideration should be given to the inherent stage-to-stage capacitances which are in the order of 1 to 3 pF.

Medium-Speed Pulse Applications

In applications in which the output current consists of pulses of short duration, the capacitance C_L of the anode circuit to ground becomes very important. The capacitance C_L is the sum of all capacitances from the anode to ground: photomultiplier-anode capacitance, cable capacitance, and the input capacitance of the measuring device. For pulses having a duration much shorter than the anode time constant $R_L C_L$, the output voltage is equal to the product of the charge and $1/C_L$ because the anode current is simply charging a capacitor. The capacitor charge then decays exponentially through the anode load resistor with a time constant of $R_L C_L$. To prevent pulses from piling up on each other, the maximum value of $R_L C_L$ should be much less than the reciprocal of the repetition rate.

An important example of this type of operation is scintillation counting, for example with NaI:Tl. The time constant of the scintillations is 0.25 microsecond and, because the integral of the output current pulse is a measure of the energy of the incident radiation, the current pulse is integrated on the anode-circuit capacitance for a period of about 10 microseconds. Because the scintillations occur at random, the maximum average counting rate is limited to about 10 kHz. If circumstances require a higher counting rate, the integration time must be reduced accordingly.

Fast-Pulse Applications

In fast-pulse light applications, it is recommended that the photomultiplier be operated at negative high voltage with the anode at ground potential. A typical voltage-divider circuit with series-connected capacitors is shown in Fig. 90. The parallel configuration of capacitors may also be used, as shown in Fig. 91. The parallel arrangement requires capacitors of higher voltage ratings. Regardless of the configuration, the capacitors must be located at the socket. The capacitor arrangements just described may also be applied to negative-ground applications.

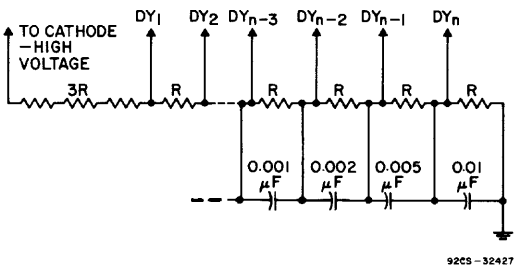

Fig. 90 - Series-connected capacitors in voltage-divider circuit using positive ground for pulse-light applications.

The wiring of the anode or dynode "pick-off" circuit is very critical in pulse applications if pulse shape is to be preserved. Most pulse circuitry uses 50-ohm characteristic impedance cables and connectors because of

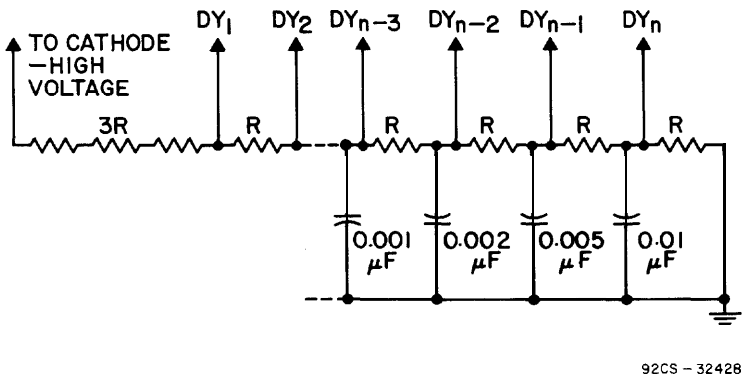

Fig. 91 - Parallel-connected capacitors in voltage-divider circuit for pulsed-light application.

their ready availability, although 75- and **92-ohm** components are also used. Careful wiring is required. Figs 92 and 95 illustrate schematically and pictorially the best location of pulse bypass capacitors that return the anode pulse current to Dy_n and Dy_{n-1} by paths of minimum residual inductance. It should be noted that these bypass capacitors also serve the function of charge-storage capacitors, as shown in Fig. 91.

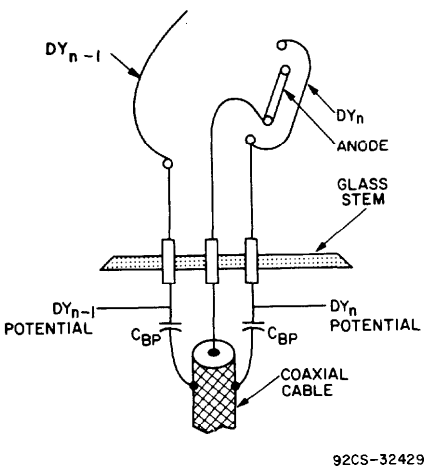

Fig. 92 - Bypass capacitors used to make the **last** *two dynodes appear as a ground plane to a fast-pulsed signal.*

Wiring Techniques

Good high-frequency wiring techniques must be employed in wiring photomultiplier sockets and associated voltage dividers if pulse-shape distortion is to be minimized. Fig. 93 illustrates the pulse shape obtained from an 8575 photomultiplier excited by a **0.5-nanosecond** rise-time light pulse. The pulse shape is most easily seen with the aid of a repetitive light pulser and a high-speed real-time oscilloscope. Fig. 94 indicates the general type of distortion encountered with the use of improperly wired or excessively inductive capacitors. The output pulse illustrates the ringing that may occur in an improperly wired socket.

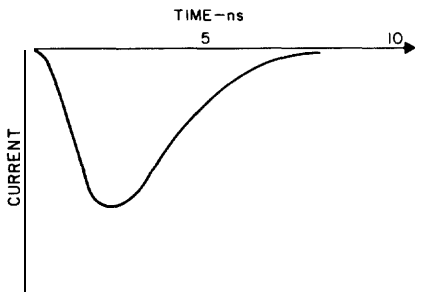

Fig. 93 - Pulse shape obtained from photomultiplier excited by a light pulse having an 0.5-nanosecond rise time.

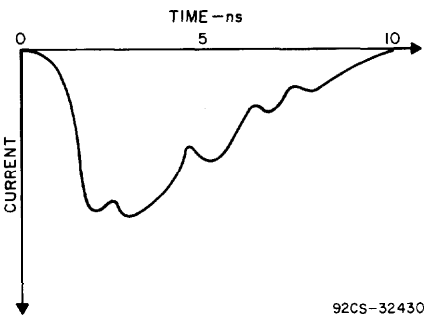

Fig. 94 - Pulse shape distortion (ringing) encountered with improperly wired or excessively inductive capacitors.

Fig. 95 shows a socket wired for a negative high-voltage application. The disk-type bypass capacitors are mounted in series with minimum lead length because the self-inductance of the lead wires becomes critical in nanosecond-pulse work. Care should also be taken in dressing the bypass capacitors and coaxial cable. The resistors for the voltage divider are shown mounted on the socket. In applications requiring minimum dark current, the resistors should be remote from the photomultiplier to minimize heating effects.

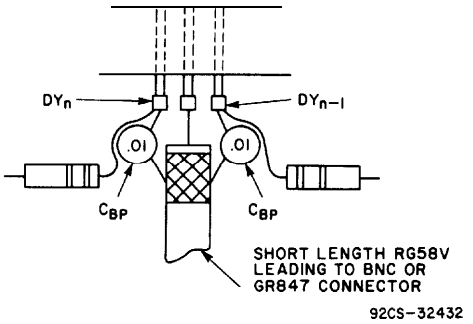

Fig. 95 - Anode detail of socket wired for a negative high-voltage application showing location of charge-storage capacitors.

Checking Socket and Tube Performance

Some photomultipliers typically display a reflected-pulse rise time of the order of 1.5 nanoseconds for an initiating pulse of the order of 50 picoseconds when the tube and socket are tested with a time-domain reflectometer, the instrument used to test the anode-pin region of the socket.

During tube operation, the output pulse can be viewed with a real-time high-speed oscilloscope. The pulse shape can be inspected for signs of clipping or ringing.

The effectiveness of the charge-storage capacitors can be verified with a simple linearity test. The output of a photomultiplier varies as V^{α}, where V is the applied voltage and alpha (α) is a constant. Thus, a plot of pulse amplitude as a function of the logarithm of the voltage value should yield a straight line.

A two-pulse technique may be employed to test linearity at constant operating voltage. Consider two sequential pulses having amplitude ratios in the range from 2:1 to 10:1. The ratio of the amplitude of the two photomultiplier current pulses is established at low pulse amplitudes where linear operation is assured. Next, the light flux is increased in a series of increments. A constant-current pulse amplitude ratio indicates linear operation. A pair of light-emitting diodes may be used to provide the two light pulses. The over-all control of the light levels may be done with a series of neutral-density filters. Exact filter calibration is not required because the system is self-calibrating in the pulse current measurements.

Tapered Dividers

Some applications require that photomultipliers sustain high signal currents for short time intervals, tens of nanoseconds or less. In general, photomultipliers are capable of supplying 0.2 ampere or more into a 50-ohm load for short durations. However, the voltage divider must be tailored to the application to allow a photomultiplier to deliver these high currents.

The principal limitation on current output (into a 50-ohm system) is space charge at the last few stages. This space charge can be overcome if the potential difference across the last few stages is increased by use of a tapered divider rather than an equal-volts-per-stage divider. The tapered divider places 3 to 4 times the normal interstage potential difference across the last stage. The progression leading to the 4-times potential difference should be gradual to maintain proper electrostatic focus between stages; a progression of 1, 1 . . . 1, 1, 1.5, 2.0, 3, 4.2 is recommended.

Another application of the tapered divider is to provide a large signal voltage across a high-impedance load. Voltage excursions of 400 to 500 volts can be obtained from photomultipliers. A possible application is in driving an electro-optical modulator. Because the photomultiplier is nearly an ideal constant current source, its output voltage signal is limited only by the potential difference between the last dynode and the anode. If the potential difference is 100 volts, the anode cannot swing through more than a 100-volt excursion. By impressing a much higher potential difference between the anode and last dynode by means of a tapered divider, greater voltage swings can be obtained. Tube data sheets should be consulted for maximum voltage ratings.

Dynamic Compression of Output Signal

Most photomultipliers operate linearly over a dynamic range of six or seven orders of magnitude, a range few monitor devices can accommodate without requiring range changes. When compression of the dynamic range is desired, a logarithmic amplifier is sometimes used. The photomultiplier may also be operated in a compressed-output mode, however, without the need for additional compression circuitry.

For example, in liquid scintillation counting where several different isotopes may be present, the output pulse height might normally vary by as much as 100: 1. By limiting the potential difference between the last dynode and anode to, for example, 10 volts, space charge will limit the maximum current that can be drawn. The anode pulse can then be used for the coincidence timing with a more convenient range of pulse heights. Energy measurements can then be made using the current at an earlier dynode where space-charge saturation is not present.

Current Protection of Photomultiplier

If a photomultiplier is accidentally exposed to an excessive amount of light, it may be permanently damaged by the resultant high currents. To reduce this possibility, the resistive voltage-divider network may be designed to limit the anode current. The average anode current of a photomultiplier cannot much exceed the voltage-divider current; therefore, the zero-light level voltage-divider network serves as an overload protection for the tube. If overexposure is expected frequently, interdynode currents, which can be quite excessive, may cause loss of gain. In some applications it may be worthwhile to protect against dynode damage by using resistors in series with each dynode lead .[91]

Active Divider Network

Although normally, the divider network current should exceed the maximum photomultiplier output current by a factor of 10 or more, it is possible by using the emitter-follower characteristics of transistors to provide a power supply requiring much less divider current. Fig. 96 is an example of such an active divider network devised by C. R. Kerns[92] As the dynode current increases, the added current is diverted from the high-beta transistors rather than from the divider-resistor string, thus improving the voltage regulation by a large factor. The capacitors shown are the usual ones for high-frequency bypassing. The circuit also retains a current-limiting action that prevents damage to the photomultiplier.

MECHANICAL CONSIDERATIONS

Handling

Because most photomultipliers have glass envelopes, they should be handled with care to avoid damage to the tube seals and other parts. This caution is especially important for tube types having graded-seal envelope construction. The pins or leads of the tube should also be treated with care.

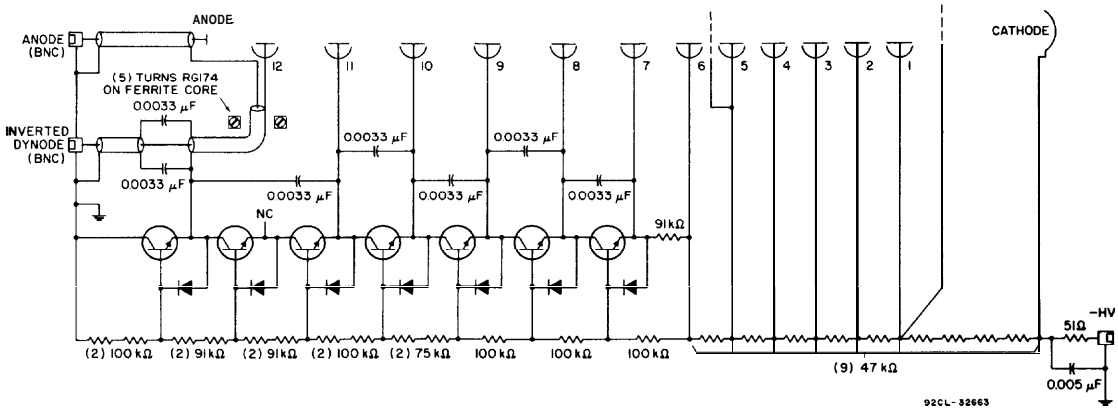

Fig. 96 - An active divider network for an 8575 photomultiplier designed to minimize voltage changes at the dynodes. (From C.R. Kerns[92])

Basing

Photomultiplier tubes may have either a temporary or a permanently attached base. Dimensional outline diagrams such as those shown in Fig. 97 are provided in the published technical data for individual tubes. Indicated on the diagrams are the type of base employed, maximum mechanical dimensions, radii of curvature where applicable, pin/lead details, location and dimensions of magnetic parts used (in tubes utilizing minimum number of magnetic materials), and notes regarding restricted mounting areas, again where applicable.

Photomultiplier tubes intended to be soldered directly to circuit boards or housings are supplied with semiflexible or "flying" leads and a temporary base, intended for testing purposes only, that should be removed prior to permanent installation.

A lead-terminal diagram that shows photomultiplier-tube lead orientation with the temporary base removed, shown in Fig. 98, provides a lead indexing reference. A lead-connection diagram, such as the one shown in Fig. **99,** relates terminal to electrode. Care must be exercised in interpreting basing and lead-terminal diagrams to insure against possible damage to the photomultiplier resulting from incorrect connections.

Terminal Connections

BURLE photomultipliers are supplied with either semiflexible leads, semiflexible leads attached to temporary bases, permanently attached bases, or stiff leads. Semiflexible leads may be soldered, resistance (spot) welded, or crimp connected into the associated circuitry. When soldering or welding is employed for such connections, care should be taken to prevent tube destruction due to thermal stress of the seals at the stem. A heat sink, such as locking forceps, should be placed in contact with the **semi-**flexible leads between the point being soldered or welded and the tube seals. If soldering is employed, only a soft solder (e.g., 60% Sn, 40% Pb) should be used. Heat should be applied only long enough to permit the solder to flow freely. By the term semiflexible, it is implied that excessive bending may break the leads, most commonly at the stem surface. Some photomultipliers are supplied with insulating wafers attached to the stem to prevent such an occurrence. The semiflexible leads are normally made of dumet or Kovar and are usually plated to facilitate soldering.

Photomultipliers supplied with permanently attached bases or stiff leads should use only high-grade, low-leakage sockets to minimize leakage currents between adjacent electrode terminals. Teflon and mica-filled sockets should be used.

Mounting and Support

Photomultipliers having permanently attached bases normally require no special mounting arrangements. When special mounting arrangements are used, however,

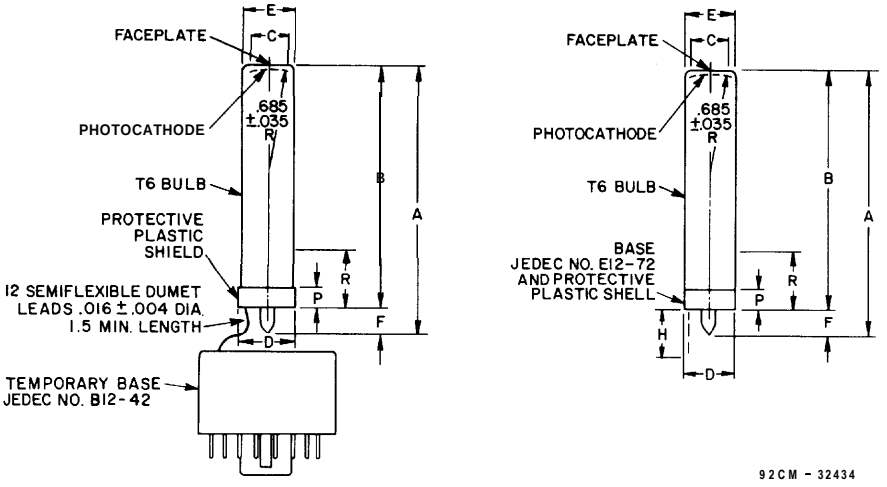

Fig. 97 - Typical dimensional-outline drawings showing the type of base supplied with each tube and pertinent notes.

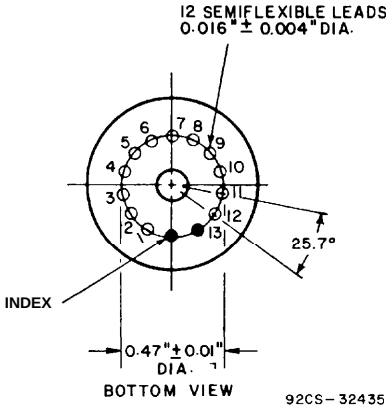

Fig. 98 - Lead-orientation diagram.

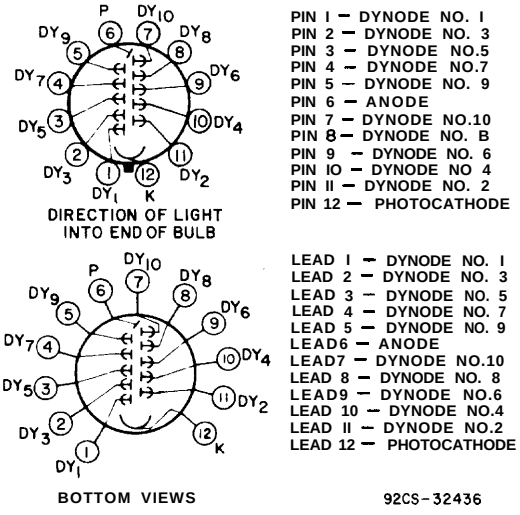

Fig. 99 - Lead-connection diagram: (a) with base connected, (b) with temporary base removed.

the envelope, especially that region near the photocathode, must be maintained at cathode potential. Care should also be taken so that tube performance is not affected by extraneous electrostatic or magnetic fields. Side-on photomultipliers should be mounted to allow rotation of the tube about its major axis to obtain maximum anode current for a given direction of incident radiation. An angular tolerance with respect to incident light direction is normally specified in tube data sheets.

Direct clamping with non-resilient materials to the envelope of tubes not having permanently attached bases is not recommended nor should clamping be made to any metal flanges employed in the construction of a tube. Such flanges, when present, are part of the tube's vacuum enclosure and any undue force or stress applied to them can damage the seals and destroy the tube.

The use of resilient potting compounds or rubber washers is recommended when photomultipliers are clamp-mounted. If a potting compound is used, its characteristics-over the temperature range in which the tube is to be operated-must be such that its resilience is maintained at low temperature and its expansion, in confined space, is not excessive at high temperature.

The electrical insulation properties of any materials supporting or shielding the photomultiplier should be considered. If such materials come into contact with high voltage with respect to photocathode, minute leakage currents can flow through the material and the tube envelope to the photocathode. Not only does this condition introduce excessive noise at the tube output but it can also permanently damage the photocathode sensitivity of the tube through electrolysis of the glass envelope. This caution is only true when the tube is operated at high negative potential with respect to ground. Under this operating condition, a decrease in sensitivity can occur if the faceplate of the tube comes into contact with ground. Cathode sensitivity does not recover after such an occurrence. Photocathode "poisoning" due to envelope electrolysis can destroy the usefulness of a photomultiplier in a very short time. Therefore, the insulating property of materials supporting the tube should be such that leakage current to the tube envelope is limited to 1×10^{-12} ampere, or less.

Shielding

Electrostatic and/or magnetic shielding of most photomultipliers is usually required. When such shields are used and are in contact with the tube envelope, they must always be connected to photocathode potential.

In applications where the dc component of the signal output is of importance, the cathode is normally operated at high negative voltage with respect to ground. As a result, the shield is at high negative voltage and precautions must be taken to avoid shorts to ground and to prevent shock

hazard to personnel. A 10-megohm resistor should be placed between the negative high voltage and shields to avoid such hazards.

In scintillation counting applications, it is recommended that the photocathode be operated at ground potential. In this case, the shields should be operated at ground potential.

Magnetic shielding of most photomultipliers is highly desirable. Characteristic curves showing the effects of magnetic fields on anode current are provided in many data sheets.

Storage

Photomultipliers should be stored in the dark. Storage of tubes in areas where light is incident on the tube results temporarily in a higher than normal dark-current level when the tubes are placed in operation. This increase in dark current is primarily due to phosphorescence of the glass and can persist for about 24 hours. Additionally, storage of tubes designed for operation in the near IR region of the spectrum (above 700 nanometers) in illuminated areas may decrease the "red" sensitivity of the tube.

The phototube should never be stored or operated in areas where there are concentrations of helium because helium readily permeates glass. The composition of the envelope material is a major factor governing the rate of helium permeation. As the silica content in the glass is reduced, the rate of permeation decreases. Accordingly, the rate of permeation is greatest for fused silica and decreases to a minimum in lime glass. It is also to be noted that the rate of permeation is proportional to temperature and varies directly with pressure.[69, 92a 92b]

Moisture Condensation

A very small anode current is observed when voltage is applied to the electrodes of a photomultiplier in darkness. Among the components contributing to this dark current are pulses produced by thermionic emission, ohmic leakage between the anode and adjacent elements, secondary electrons released by ionic bombardment of the photocathode, cold emission from the electrodes, and light feedback to the photocathode. Other conditions contributing to anode dark current include external leakage caused by condensation on the tube base and/or socket when conditions of high humidity exist and contamination of the tube base and/or socket by handling.

Moisture condensation can be minimized by potting the tube socket assembly in silicone rubber compounds such as RTV-11, or equivalent. If a tube is suspected of having high ohmic leakage as a result of handling, it is recommended that it and its socket be washed with a solution of alkaline cleaner such as Alconox*, or equivalent, and de-ionized or distilled water having a temperature not exceeding 60 °C. The base or the socket should then be thoroughly rinsed in de-ionized or distilled water (60 °C) and then air-blown dry.

*Distributed by Arthur H. Thomas Company, Vine Street and 3rd, Philadelphia, PA 19105.

OPTICAL CONSIDERATIONS

Incident Light Flux

Photomultiplier tubes are capable of operating usefully over a very wide range of incident light flux. At the very lowest levels, the limit is determined by the useable signal-to-noise ratio. Upper range of usefulness is determined by the saturation of the photocathode or by the magnitude of the output current levels which either result in space-charge limitations or cause damage to the secondary emission dynodes.

The lower limit of detection is discussed in detail in Chapter **4, Photomultiplier Characteristics,** in the section "Dark Current and Noise." See in particular Fig. 67. The lower limit in a current-measurement mode is determined by dark emission and bandwidth. Photocurrent levels as low as 10^{-16} ampere (625 photoelectrons per second) can be measured. This photocurrent level corresponds to 5×10^{-13} lumens for a 200-microampere/lumen photocathode. In a photoelectron-counting mode (see Appendix G), the limit is determined by the statistics of discriminating between photoelectrons and thermally emitted electrons. For a Na_2KSb photocathode, the dark emission from the photocathode at room temperature may be of the order of 10^{-17} ampere or 62 electrons per second. Counting for one minute in the dark and one minute in the light, one should be able to detect a photocurrent of only a few photoelectrons per second.

For resistive photocathodes (See Table II

in Chapter IV, **Photomultiplier Characteristics**, in the section "Photocathode-Related Characteristics.") such as K_2CsSb, the maximum recommended photocurrent is only of the order of 10^{-9} ampere which corresponds to a flux of the order of 10^{-5} lumen.

When the photocathode resistivity does not limit the input light flux, the maximum light flux is determined by output currents in the photomultiplier. For example, the 931A maximum average anode current is 1.0 milliampere which corresponds to an input light flux of about 10^{-5} lumen with a total applied voltage of 1000 volts. If the over-all voltage were reduced to 500 volts, the tube could tolerate an input flux of 10^{-3} lumen.

At times it may be useful to reduce the light level on the photomultiplier by a calibrated amount. Neutral-density filters can be useful for this purpose. It should be appreciated, however, that such filters are frequently not neutral and their stated density may be only an approximation. A comparison of the spectral transmittance of a metalized filter and a gelatin type is shown in Fig. 100. Wratten filters are reasonably

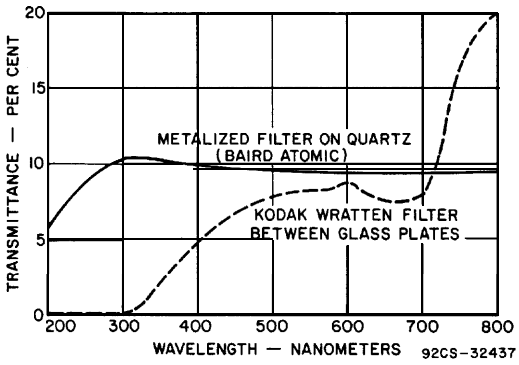

Fig. 100 - Comparison of spectral transmittance of metalized- and organic-type neutral-density filters (ND 1.0).

neutral in the visible range but become transparent in the infrared, which could cause a problem when they are used with a photomultiplier having a near-infrared response. This effect is much more pronounced for the more dense neutral-density filters.

Another method for reducing light level is by the use of a mesh or screen. This method has the advantage of providing a reduction factor that is essentially independent of wavelength. Such neutral density screens can be obtained from the Varian Instrument Division. **

Large reduction factors can be achieved by the use of opal glass, which scatters transmitted light in an approximate Lambertian (cosine) distribution (although a bit more concentrated near the normal angles than the cosine prediction). Unfortunately, the scattered flux is not neutral, providing more red than blue. See Fig. 101.

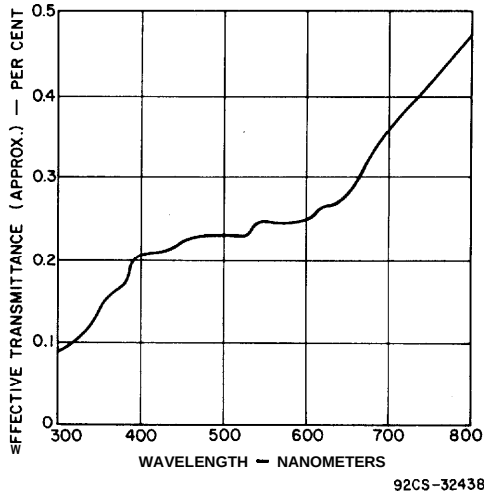

Fig. 101 - The effective spectral transmittance (for scattered light) of an opal-glass filter, 3-mm thickness, into a solid angle of approximately 0.01 steradian.

Convex front-surface spherical aluminum mirrors can also be used to provide a calibrated light-reduction factor. Aluminum mirrors have the advantage of having a reasonably flat spectral reflectance-from 92.3% at 300 nanometers to 86.7% at 800 nanometers.[93] If a lamp of CP **candelas** is located at a distance **a** from the surface of the mirror having a reflectivity ϱ and a radius **r,** the flux (L) in lumens through a test aperture of area A located at a distance **b** from the mirror surface is given **by**[94]

$$L = \frac{CP\, r^2 A\, \varrho}{4a^2b^2\left[1 + \frac{r\cos\phi}{2}\left(\frac{1}{a}+\frac{1}{b}\right)\right]\left[1 + \frac{r\sec\phi}{2}\left(\frac{1}{a}+\frac{1}{b}\right)\right]} \qquad (30)$$

● *670 E. **Arques** St., Sunnyvale, **Calif.** 94086

where ϕ is the angle of incidence of the pertinent rays on the mirror.

Calibration

For some purposes it may be useful to provide a calibration of the photomultiplier anode or photocathode responsivity. A convenient test source is the tungsten lamp (see Appendix F). Lamps with candle power and color temperature (2856 K) traceable to the National Bureau of Standards can be obtained from BURLE, Lancaster, PA (Type AJ2239). Some method of reducing the light flux such as discussed above would normally be required.

Spectral response measurements generally require a sophisticated monochromator setup. Reasonably good results, however, can be obtained by use of calibrated narrow-band-pass color filters and a calibrated tungsten lamp. The power through a particular filter may be obtained by integrating the product of the filter transmission and the tungsten irradiance over the wavelength band of the filter. Spectral irradiance for a tungsten lamp calibrated to a color temperature of 2856 K may be obtained from Appendix F, Table F-I, with a multiplying factor appropriate to the particular total luminous flux. Details are given in the footnote accompanying Table F-I.

Spot Size

It is generally advisable to utilize a large part of the photocathode area rather than to focus a small spot of the light flux on the photocathode. If the light flux is fairly high, concentrating it on a small area could cause damage to the photocathode or result in non-linearity effects because of the resistivity of the photocathode layer. Furthermore, variations in photocathode sensitivity across the surface area could cause some uncertainty in the measurement if the light spot is too small. In scintillation-counting applications, spot size is not generally a problem because of the diffuse nature of the flux and the size of the crystal. But, in flying-spot-scanner applications it is particularly important that the image being scanned should not be in focus on the surface of the photomultiplier because any non-uniformities of photocathode sensitivity would cause fixed pattern modulation.

Angle of Incidence

Photocathode response varies somewhat with the angle of incidence (see Fig. 41). It is also possible to increase the effective quantum efficiency of a photocathode by the use of a specially constructed optical coupling to the photocathode window that utilizes at the glass-air interface angles of incidence greater than the critical angle. (See Fig. 42).

Light Modulation

For some purposes, it may be advantageous to modulate the light signal with a light chopper. A synchronous motor may be used to rotate a chopper disk which could then provide an approximate square-wave modulation. The output signal could then be analyzed with a narrow-band-pass amplifier tuned to the chopper frequency. When the modulated signal is in the presence of an unmodulated background whether from the dark current of the tube itself or from an external source of light, a significant improvement in signal-to-noise may be achieved.

Regarding the testing of photomultiplier tubes with delta-function light pulses, see the section on "Time Effects" in Chapter 4, **Photomultiplier Characteristics.** Cerenkov radiation also provides very short pulses of light.

SPECIFIC PHOTOMULTIPLIER APPLICATIONS

This section discusses various applications of photomultipliers and some of the special considerations for each application. This catalogue of applications is not complete even for presently known applications, and new ones are being continually devised. The applications discussed, however, are some of the major ones and the information given can be readily adapted to other applications or to new ones.

Scintillation Counting

A scintillation counter is a device used to detect and register individual light flashes caused by ionizing radiation, usually in the form of an alpha particle, beta particle, gamma ray, or neutron, whose energy may be in the range from just a few thousand electron-volts to many million electron-volts. The most common use of scintillation counters is in gamma-ray detection and spectroscopy.

The gas, liquid, or solid in which a scintillation or light flash occurs is called the scintillator. A photomultiplier mounted in contact with the scintillator provides the means for detecting and measuring the scintillation. Fig. 102 is a diagram of a basic

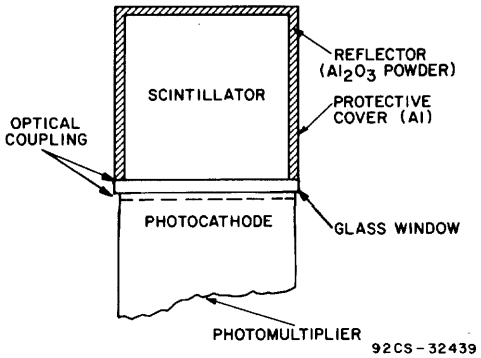

Fig. 102 - Diagram of a scintillation counter.

scintillation counter. The three most probable ways in which incident gamma radiation can cause a scintillation are by the photoelectric effect, Compton scattering, or pair production. The reaction probabilities associated with each of these-types of interaction are a function of the energy of the incident radiation as well as the physical size and atomic number of the scintillator material. In general, for a given scintillator, the photoelectric effect predominates at small quantum energies, the Compton effect at medium energies, and pair production at energies above 1.02 MeV.

Scintillation Processes. In the photoelectric effect, a gamma-ray photon collides with a bound electron in the scintillator and imparts virtually all its energy to the electron. In the Compton effect a gamma-ray photon with energy $E = h\nu$ interacts with a free electron in the scintillator and transmits only part of its energy to the electron, as shown in Fig. 103. A scattered photon of lower energy

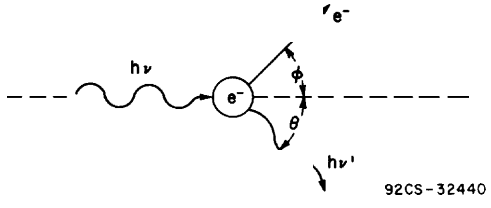

Fig. 103 - Compton-effect mechanism.

also results. To satisfy the conditions of conservation of energy and momentum, there is a maximum energy that can be transferred to the electron. This maximum energy, known as the Compton edge, occurs when θ in Fig. 103 is 180 degrees and ϕ is 0 degrees; it is given by

$$T_{CM} = \frac{E}{1 + \frac{1}{2\alpha}} \qquad (31)$$

where E is the photon energy, $\alpha = E/m_0c^2$, m_0 is the rest mass of an electron, and c is the speed of light. The resultant energy imparted to the electron can then range from zero to a maximum of T_{CM}.

In pair production, the energy of a gamma ray is converted to an electron-positron pair in the field of a nucleus. The gamma ray must have energy at least equal to two times the rest-mass-energy equivalent of an electron, 2 (m_0c^2), or 1.02 MeV; any additional energy is transferred as kinetic energy. When the positron is annihilated, two photons are produced 180 degrees apart, each with an energy of 0.51 MeV. The photons are then subject to the normal probabilities of interaction with the scintillator .

In neutron detection, unlike alpha- or beta-particle or gamma-ray detection, the primary interaction is with the nuclei of the scintillator atoms rather than its atomic electrons. The interaction may consist of scattering or absorption; in either case, some or all of the energy of the neutron is transferred to the recoil nucleus which then behaves similarly to an alpha particle.

In each interaction between a form of ionizing radiation and a scintillator, an electron having some kinetic energy is produced. A secondary process follows which is independent of both the kind of ionizing radiation incident on the scintillator and the type of interaction which occurred. In this secondary process, the kinetic energy of the excited electron is dissipated by exciting other electrons from the valence band in the scintillator material into the conduction band. When these excited electrons return to the valence band, some of them generate light or scintillation photons. The number of photons produced is essentially proportional to the energy of the incident radiation. In the photoelectric interaction described above, all

of the incident photon energy is transferred to the excited electrons; therefore, the number of photons produced in this secondary process, and hence the brightness of the scintillation, is proportional to the energy of the incident photon.

Scintillation Mechanism. The exact mechanism of the scintillation or light-producing process is not completely understood in all types of materials; however, in an inorganic scintillator, the phenomenon is known to be caused by the absorption of energy by a valence electron in the crystal lattice and its subsequent return to the valence band. Fig. 104 shows a simplified energy-band diagram

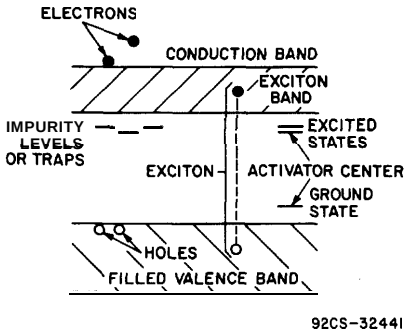

Fig. 104 - A simplified energy diagram of a scintillation crystal: ionized electron-hole pairs; an ***exciton;*** *an activator center through which an electron may return to the ground state causing fluorescence; or through which an electron may return to the ground state by a thermal, non-radiative process; impurity levels that can trap an electron for a time causing phosphorescence.*

of a scintillation crystal. The presence of energy levels or centers between the valence and conduction bands is the result of imperfections or impurities in the crystal lattice. Three types are important: (1) fluor**escence** centers in which an electron, after excitation, quickly returns to the valence band with the emission of a photon; (2) **quenching** centers in which the excited electron returns to the valence band with the dissipation of heat without emission of light; and (3) **phosphorescence** centers in which the excited electron can be trapped in a metastable state until it can absorb some additional energy and return to the valence band with the emission of a photon. An important process in the transfer of energy to the fluorescence, or activator, centers in the generation of **excitons** or bound **hole**-electron pairs. These pairs behave much like hydrogen atoms and, being electrically neutral, can wander freely through the crystal until captured by fluorescence centers. The emission of a photon from a phosphorescence center is a relatively slow or delayed process. Of the three types of centers through which an excited electron can return to the valence band, the first, fluorescence, is that sought for in the preparation of scintillators. The second type, quenching, tends to lessen the efficiency of the scintillator because it does not cause the emission of photons, and the third, phosphorescence, produces an undesirable background glow.

Scintillator Materials. The most popular scintillator material for gamma-ray energy spectrometry is thallium-activated sodium iodide, **NaI:Tl.** This material is particularly good because its response spectrum contains a well-defined photoelectric peak; i.e., the material has a high efficiency or probability of photoelectric interaction. In addition, the light emitted by the material covers a spectral range from approximately 350 to 500 nanometers with a maximum at about 410 nanometers, a range particularly well matched to the spectral response of conventional photomultipliers, NaI:Tl does not, however, have a fast decay time in comparison to other scintillators, and, therefore, is generally not used for fast-time resolution. **As** a comparison, the decay time constant for **NaI:Tl** is approximately 250 nanoseconds, while for a fast plastic scintillator the dominant decay time constant is in the 1 to 4 nanosecond range.

The decay time of a scintillator involves the time required for all the light-emitting luminescence centers to return excited electrons to the valence band. In some of the better scintillators the decay is essentially exponential, with one dominant decay time constant. Unfortunately, most scintillators have a number of components each with different decay time.

Collection Considerations. Because scintillations can occur anywhere in the bulk of the scintillator material and emit photons in all directions, there exists the problem of collecting as many of these photons as possible

on the faceplate of the photomultiplier. If it is assumed that the fluctuation in the number of photons resulting from a single ionizing event follows simple Poisson statistics*, the relative standard deviation in the number arriving at the face plate is given by

$$(N_p)^{1/2}/N_p \qquad (32)$$

where N_p is the average number of photons arriving at the faceplate of the photomultiplier per incident ionizing event. N_p is equal to c E ξ, where c is the average number of photons per unit energy for the scintillation, E is the energy of the incident radiation, and ξ is the fraction of the total number of photons produced which arrive at the faceplate of the photomultiplier.

Eq. (32) implies that it is highly desirable that all emitted photons be collected at the photomultiplier faceplate. This collection problem can be simplified by careful selection of the shape and dimensions of the scintillator to match the photomultiplier photocathode dimensions. The coating of all sides of the scintillator except that which is to be exposed to the photomultiplier faceplate with a material that is highly reflective for the wavelengths of the photons emitted by the scintillator also proves helpful. Because NaI:Tl is damaged by exposure to moist air, it is usually packaged in an aluminum case lined with highly reflective MgO or Al_2O_3 powder; the NaI:Tl scintillator is provided with an exit window of glass or quartz. To avoid total internal reflection, it is important that the indices of refraction of the scintillator material, its window, any light guide, and the photomultiplier faceplate match as closely as possible.

If it is not convenient for the photomultiplier to be directly coupled to the scintillator, as when the photomultiplier entrance window is not flat, light guides can be used. Again, care should be taken in the design of the light guide to assure maximum light transmission. The outer side or surface of the light guide should be polished and coated with a highly reflective material. In some cases, a flexible fiber-optics bundle can be used. An optically transparent silicone-oil coupling fluid should be applied at the scintillator (-light guide, if used)-photomultiplier interface regardless of the light-conduction method used.

The next important consideration in scintillation counting is the conversion of the photons to photoelectrons from the photocathode. The photocathode should have the greatest quantum efficiency possible over the spectral range defined by the spectral emissivity curve of the scintillator. The method of determining the quantum efficiency of a photocathode as a function of wavelength is explained in Appendix E. Of the various photocathodes available, bialkali types, K_2CsSb and Rb_2CsSb, having peak quantum efficiencies in excess of 25%, provide the best spectral match to the emission from most scintillators.

The uniformity of the photocathode, i.e., the variation in quantum efficiency at a given wavelength as a function of position on the photocathode, is also important. Because the number of photoelectrons emitted for a constant number of photons incident on the photocathode is proportional to the quantum efficiency any variation in quantum efficiency as a function of position results in an undesirable variation in the number of photoelectrons emitted as a function of position.

When the scintillation is fairly bright, i.e., when a large number of photons are produced per scintillation, and when the scintillator is thick in comparison to its diameter, as shown in Fig. 105(a), the photocathode is approximately uniformly illuminated during each scintillation. However, if the scintillator is thin in comparison to its diameter, as shown in Fig. 105(b), or if the scintillation is very weak, the illumination of the photocathode as a function of position is closely related to the position of origin of the scintillation; therefore, photocathode uniformity is much more important when a thin scintillator is used. In this case, the use of a light guide may be advantageous. Photocathode uniformity also becomes more important as the energy of the incident radiation becomes less and the number of photons per disintegration is reduced.

*Actually, the variance in the number of photons exiting from the crystal per event is much higher than expected from the simple expression of Eq. (32). See the discussion in Chapter 4 on "Scintillation Counting" related to Eq. G-l 11.

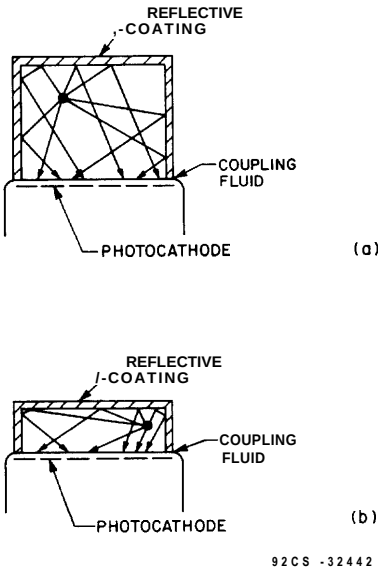

Fig. 105 - Scintillator geometries: (a) thick in comparison to diameter; (b) thin in comparison to diameter.

In some photomultipliers, the collection efficiency for photoelectrons decreases near the outer edges of the photocathode; therefore, best results are obtained when the scintillator is slightly smaller in diameter than the photocathode.

Significant Photomultiplier Characteristics. In scintillation-counting applications (See also the section on "Pulse Counting" in Chapter **4, Photomultiplier Characteristics),** a photomultiplier should be selected to provide a photocathode diameter matching that of the crystal to be used. The most important characteristic of the tube to be used in scintillation counting is then the effective photocathode sensitivity to blue and near-ultraviolet wavelengths. The effective photocathode sensitivity includes the basic quantum efficiency and the collection efficiency of the electron-optical system. Tubes having Venetian-blind dynodes provide a fairly large opening to the first dynode area and thus frequently have better collection efficiency than tubes having a focused-dynode structure, although the focused structure is much better for time resolution. Photomultipliers having the recent "tea-cup" type of first dynode generally have very good collection efficiency and, in addition, are designed to provide increased photocathode emission either by reflected light or by excitation of photoelectrons from photocathode deposited on the side walls of the envelope.

At high count rates, tubes having copper-beryllium dynodes generally provide greater stability than tubes having cesium-antimony dynodes, although for low count rates the latter prove to be satisfactory. A tube having good stability may be expected to shift in gain by no more than 7% in several months of continuous operation at a count rate of 10,000 per second. Variation of pulse height or gain with count rate is also of importance. Well-designed tubes should show a variation in pulse height of less than 1% between count rates of 1000 per second and of 10,000 per second, related to the photopeak, using ^{137}Cs and a NaI:Tl crystal.

Photomultiplier dark noise is of particular importance in scintillation-counting applications when the energy of the ionizing radiation is small, or when very little energy is transferred to the scintillation medium; in short, when the flash per event represents only a few photons. If a photomultiplier is coupled to a scintillator and voltage is applied, the composite of all noise pulses coming from the photomultiplier is referred to as the background of the system. The plot of a frequency distribution of these pulses as a function of energy is shown in Fig. 106.

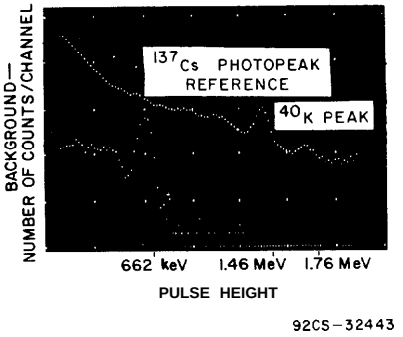

Fig. 106 - Distribution of radiation background pulses as a function of energy. A calibration spectrum showing the ^{137}Cs photopeak is included for reference.

The well-defined peaks seen in the figure are caused by external radiations and can be reduced by placing the photomultiplier and scintillator in a lead or iron vault to reduce background radiation.

It is desirable that the background count of the scintillation counter be as low as possible. Photomultipliers have been developed in which the background count is kept low by the use of radioactively clean metal cans instead of glass-bulb enclosures and faceplates of either **Lucalox*** or sapphire instead of glass. As an additional aid in reducing background, the scintillation counter can be surrounded by another scintillator, such as a plastic sheet equipped with its own photomultipliers. The output from this scintillation shield is then fed into an **anticoincidence** gate with the output from the scintillation counter. The gating helps to reduce the background contributions from both internal and external radioactive contaminants.

Liquid Scintillation Counting

In liquid scintillation counting, the scintillation medium is a liquid and the ionizing radiations to be detected are usually **low**-energy beta rays. Because low-energy beta rays cannot penetrate a scintillation container, the radioactive material is dissolved in a solution containing the scintillator. The scintillator is generally one or more fluorescent solutes in an organic solvent. The **beta**-ray energy is transferred by ionization and by excitation that in turn results in the emission of photons in the near ultraviolet. In some cases, a wavelength shifter is also used to provide radiation at somewhat longer wavelengths more compatible with the spectral responsivity of the photomultiplier.

Important characteristics of the **photo**multiplier in this application are again high responsivity in the spectral region of the scintillation and low background count rate. A useful figure of merit is the square of the counting efficiency divided by the background coincident count rate in a paired photomultiplier arrangement. Further details of liquid scintillation counting applications are discussed in the section "Pulse Counting" in Chapter **4, Photomultiplier Characteristics.**

Cerenkov Radiation Detection

Cerenkov radiation is generated when a charged particle passes through a dielectric with a velocity greater than the velocity of light in the dielectric (i.e., v greater than c/n, where n is the index of refraction of the dielectric). Polarization of the dielectric by the particle results in the development of an electromagnetic wave as the dielectric relaxes. If the velocity of the particle is greater than the velocity of light, constructive interference occurs and a conical **wave**front develops, as illustrated in Fig. 107.

The angle, θ, of the Cerenkov light wave with respect to the direction of the particle is given by the expression

$$\cos\theta = \frac{1}{\beta n} \qquad (33)$$

where **n** is the index of refraction of the **medium and β is the ratio of the particle** velocity to the velocity of light. The spectral energy distribution of the radiation increases **with decreasing wavelength as $1/\lambda^3$ except as** limited by the absorption of the medium.

Cerenkov radiation is the electromagnetic counterpart of the shock wave produced in a gas by an object traveling faster than sound. It is highly directional and occurs mostly in the near-ultraviolet part of the electromagnetic spectrum. Because the radiation is propagated in the forward direction of motion of the charged particle, as shown in Fig. 107, Cerenkov detectors can be made to detect only those particles that enter the system from a restricted solid angle.

Cerenkov radiation produced in an aqueous solution by beta emitters can be useful in radioassay techniques because it is unaffected by chemical quenching and because it offers the advantages, over **liquid**-scintillation counting techniques, of simplified sample preparation and the ability to accommodate large-volume samples. Because a fast particle is required to produce Cerenkov radiation, rather high-energy beta rays are required; e.g., the threshold for Cerenkov radiation is 261 **keV** for electrons in water. Because the photon yield for Cerenkov light is usually very low, the same considerations concerning photomultiplier selection apply for the Cerenkov detection as for liquid-scintillation counting. The tube selected should also be equipped with a faceplate capable of good ultraviolet transmission. In some experiments it may be **im**-

*Registered Trade Name for General Electric Co. material.

portant to select photomultipliers for their speed of response. Depending upon the dispersion of the medium, the duration of the Cerenkov flash can be very short.

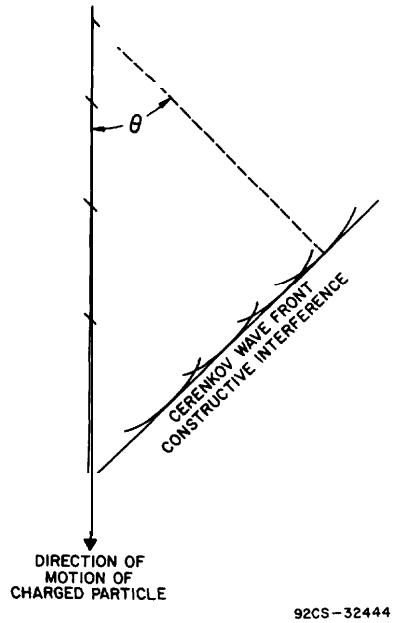

Fig. 107 - Diagram of the Cerenkov radiation mechanism.

Time Spectroscopy

In addition to the energy spectroscopy described above, there are occasions when it is of advantage to measure time differences such as between a pair of gamma rays or a combination of gamma rays and particles in cascade de-exciting some level in a nucleus. In time spectroscopy, some special considerations must be made in selecting the scintillator, photomultipliers, and technique of analyzing the signals from the photomultipliers.

In a photomultiplier, time resolution is proportional to $(n)^{-1/2}$, where n is the average number of photoelectrons per event. It is therefore important to choose a scintillator material that provides a high light yield for a given energy of detected radiation. It is also important that the variation of the time of interaction of the radiation with the scintillator be as small as possible. This minimum variation is assured by attention to scintillator thickness and source-to-detector geometry. The decay time constant of the light-emitting states in the scintillator should be as short as possible, and the geometry and reflective coatings of the scintillator should be selected so that variations in path lengths of photons from the scintillator to the photocathode of the photomultiplier are minimized. The photocathode of the photomultiplier selected should have a high quantum efficiency. In addition, the transit-time dispersion or jitter (variations in the time required for electrons leaving the photocathode to arrive at the anode of the tube) should be small over the entire photocathode area.

The major contribution to transit-time spread occurs in the photocathode-to-first-dynode region and may be a result of the initial kinetic energies of the emitted photoelectrons and their angle of emission. Focusing aberrations, and the single-electron response or rise time, i.e., the output-pulse shape at the anode for a single photoelectron impinging on the first dynode, may also be of some importance. Although the single-electron response theoretically does not have much effect on time resolution, it does change the triggering threshold at which the best time resolution can be obtained.

The most commonly used time-spectroscopy techniques include **leading-edge timing, zero-crossover timing,** and **constant-fraction-of-pulse-height-trigger timing.** The technique used depends on the time resolution and counting efficiency required and the range of the pulse heights encountered. A block diagram of a basic time spectrometer is shown in Fig. 108.

Leading-edge timing makes use of a fixed threshold on the anode-current pulse and provides good time resolution over a narrow range of pulse heights. The fractional pulse height F at which the triggering threshold is set is defined as follows:

$$F = \frac{V_t}{V_a} \qquad (34)$$

where V_t is the discriminator threshold, and V_a is the peak amplitude of the anode-current pulse. The fractional pulse height has a considerable effect on the time resolution obtained; best results are usually obtained with F equal to 0.2.

In fast **zero-crossover timing,** the anode pulse is differentiated. This differentiation produces a bipolar output pulse that triggers

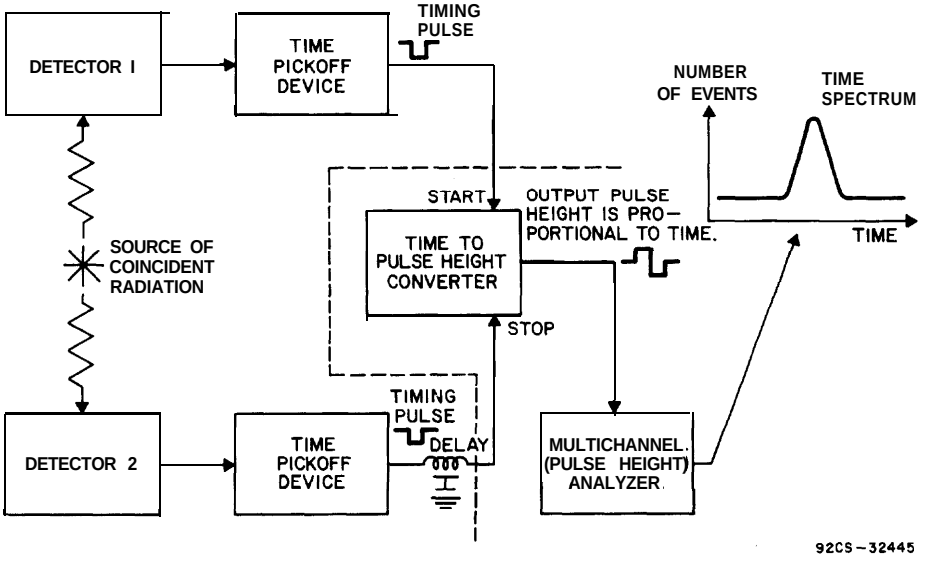

Fig. 108 - Generalized block diagram of a time spectrometer.

the timing discriminator at the zero crossover, the time required to collect approximately 50 per cent of the total charge in the photomultiplier pulse. Zero-crossover timing is second to leadingedge timing for time-resolution work with narrow pulse-height ranges, but is better than the leading-edge method for large pulse-height ranges.

In **constant-fraction triggering,** the point on the leading edge of the anode-current pulse at which leading-edge timing data indicate that the best time resolution can be obtained is used regardless of the pulse height. For this reason, constant-fraction-of-pulse-height timing is the best method for obtaining optimum time resolution no matter what the pulse-height range.

Oil-Well Logging

Logging is the term given to the method of determination of the mineral composition and structure a few miles under the earth's surface. Oil-well logging companies gather data by means of probes, or sondes, that examine the geological media along very deep bore holes. The probes determine various physical and chemical characteristics of the material in their vicinity. Measurements made by the probes comprise the log.

A variety of sondes are used in selected combinations to determine various aspects of the lithology (the character of a rock formation), including density, of the media along the bore hole. The combinations of sondes used depend very much on the borehole media. For example, when a formation-density sonde is used in combination with a neutron sonde in liquid-filled bore holes, both lithology and porosity can be determined. The same pair of sondes allows the measurement of gas and liquid saturation in bore holes drilled through reservoirs of low-pressure gas. The use of the formation-density sonde, along with either an induction or a sonic sonde, permits a similar type of determination. The final result of the logging activity is information concerning the existence of hydrocarbons and other geological media of interest in establishing an oil field.

The formation-density sonde is one of the more sophisticated logging devices. Its operational elements are encased in a rugged cylindrical housing, as shown in Fig. 109. It is designed to withstand the high temperature and shock encountered in probing bore holes miles deep under the earth's surface. The sonde contains a gamma-ray source, such as radioactive cesium 137, a detector consisting of a sodium iodide crystal and a photomultiplier tube, a gamma-ray shield

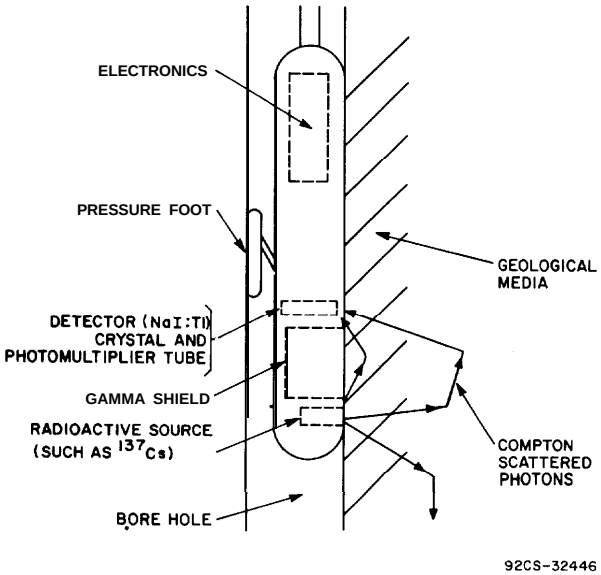

Fig. 109 - Formation-density sonde sends gamma rays into rock formation and then detects returns with ***photomultiplier.***

for the detector, a pressure foot that presses the sonde against the bore-hole wall, and operating electronics. The objective of this sonde is to determine the bulk density of the material in the region of the probe.

Gamma rays from the source interact with the atoms in the geological medium. Compton-scattered gamma rays are detected by the crystal and photomultiplier in the sonde. A knowledge of gamma-ray penetration of bulk media, mass absorption data, and the special effects resulting from the chemical nature of various geological media allows the information imparted by the pulses to be deciphered by the electronics into bulk-density data, which becomes the substance of the geological formation-density log.

Because of the increase in temperature with the depth of the bore hole-to perhaps 150°C at 15,000 feet-a most important characteristic of the photomultiplier is its resistance to high temperature. Of the numerous photocathodes which have been developed, the Na_2KSb "bialkali" photocathode is the most stable at elevated temperatures.[95] (See Fig. 83 and related text.)

As the temperature is increased on a photomultiplier with a Na_2KSb photocathode coupled to a NaI:Tl crystal, the pulse height (^{137}Cs source) gradually decreases, as illustrated in Fig. 110. Most of the decrease is the result of photocathode sensitivity loss, but some is associated with the crystal. Because of the loss in photocathode response and the increase in thermionic emission with temperature, the desired signal is finally lost in the background noise at a temperature near 200°C. Permanent damage to the photocathode may also be expected after many cycles of operation at 200°C.

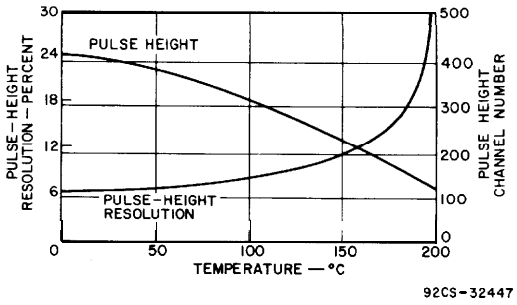

Fig. 110 - Pulse-height resolution and pulse height as a function of temperature for a photomultiplier having a Na_2KSb *photocathode and used with a* NaI:Tl *crystal and a* ^{137}Cs *source.*

Gamma-Ray Camera

The gamma-ray camera originally described by Anger[96] is a more sophisticated

version of the scintillation counter, and is used for locating tumors or other biological abnormalities. The general principle of the gamma camera is illustrated in Fig. 111. A

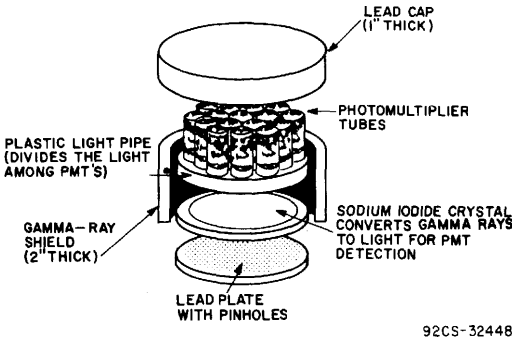

Fig. 111 - Structure of gamma-ray camera.

radioactive isotope combined in a suitable compound is injected into the blood stream of the patient or is ingested orally. Certain compounds or elements are taken up preferentially by tumors or by specific organs of the body, such as iodine in the thyroid gland. As the radioactive isotope disintegrates, gamma rays are ejected from the location of the concentration.

A lead collimator permits gamma rays to pass through it only when they are parallel to the holes in the lead; gamma rays at other angles are absorbed in the lead. In this way, the location of the gamma-ray source may be determined because gamma rays originating on the left side of the organ are caused to impact the left side of the scintillation crystal, etc. The crystal covers an area about 10 inches or more in diameter.

Behind the crystal are, perhaps, 19 photomultiplier tubes in a hexagonal array. The light of the individual scintillation is not collimated but spreads out to all of the 19 tubes. The location of the point of scintillation origin is obtained by an algorithm depending upon the individual signals from each of the photomultipliers. Resolution is obtained in this manner to about 1/4 inch. Each scintillation is then correspondingly located by a single spot on a cathode-ray tube. Counting is continued until several hundred thousand counts are obtained and the organ in question is satisfactorily delineated. Fig. 112 is a reproduction of such a scintigram. The particular advantage of the gamma camera over other techniques such as the CT scanner (described below) is that the gamma camera provides functional information. For example: Tc-99m polyphosphate is used to reveal bone diseases; ^{123}I is used in thyroid studies; ^{127}Xe is inhaled to provide information on lung ventilation.

Of great concern to the designer of gamma cameras and, of course, to the ultimate customer is the inherent resolution capability of the device. Generally, with more photomultiplier tubes sampling the scintillation distribution, the delineation becomes more precise. Most of the original cameras utilized

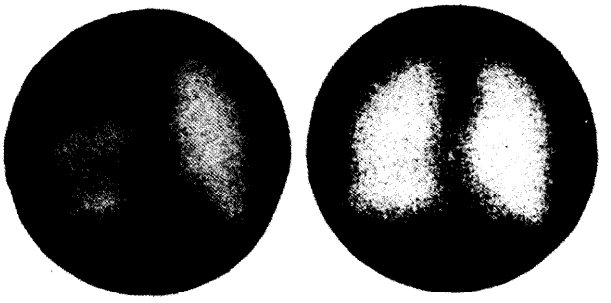

*Fig. 172 - Scintigrams obtained by Lancaster General **Hospital** with a gamma camera. The **scin**tiphoto on the left shows multiple emboli in the right lung; photo on right shows lungs after clearing. The isotope **technitium-99m** was used to tag albumin microspheres-a colloidal form of the albumin protein, with particles ranging in size from 2 to 50 microns. These particles are injected into the bloodstream and are filtered and trapped in the lung capillary bed; the scan can then determine those areas where the capillary bed is intact. Areas of diminished blood flow show as "cold spots."*

a hexagonal array of 19 tubes. By adding another circumferential row, an array of 37 provided better resolution. In the same manner cameras are now available with 61 tubes and even 91. (Note the numerical progression of these hexagonal arrays: 1 + 6 + 12 + 18 + 24 + 30.) Different photomultiplier dimensions also are used to provide instruments with appropriate portability or coverage. Most common has been the 3-inch photomultiplier, but a large number of 2-inch tubes are also used and there is consideration of the use of 1 1/2-inch tubes. Hexagonal 2- and 3-inch tubes have been developed to provide better space utilization, and a photomultiplier with a square faceplate is now available.

Resolution of the gamma-ray camera depends fundamentally upon the pulse-height resolution of the photomultiplier and, hence, the quantum efficiency of the photocathode. The most common photocathode selected for gamma-ray-camera application is the bialkali (K_2CsSb). Also important in the determination of good pulse-height resolution is collection efficiency of the photoelectrons. Large first dynodes are appropriate and the "tea-cup" configuration is used to advantage.

Because each scintillation is sensed by a number of the photomultipliers in the array, the spatial uniformity of the photomultiplier response and its angular response become important especially as related to the algorithm of the gamma-ray-camera design. The camera design may also incorporate modifications in the light pipe such as grooves or etched patterns to provide improved spatial location of the scintillations.

Finally, the stability of the photomultiplier is important in maintaining the resolution and spatial integrity of the display. Although the photomultiplier currents are generally small in this application, changes can occur in the photomultiplier gain which would then result in positional errors in the CRT display. Some gamma-ray-camera designs include a means of recalibrating the array of photomultipliers so that the pulse-height "window" is the same for each tube. This recalibration could be done periodically (once a day) and would contribute significantly to consistent, distortion-free operation.

Computerized Tomographic X-Ray Scanners

The computerized tomographic (CT) scanner produces an X-ray image in an entirely different manner from that of conventional radiography.* The standard X-ray picture is a shadowgraph. Thus, a chest X-ray produces an overlay of shadows from the rib cage and internal body structure. Interpretation is frequently difficult because of the interfering images. The CT scanner, on the other hand, provides a density image that represents a cross section of the patient-a tomograph. Thus, a CT scan of the head would show the outer bone structure, the folds of the brain, and possibly a tumor inside the skull as though a complete thin slice had been taken through the middle of the head. This tomographic image is produced by exposing the head to X-rays at many different angles of entrance. The multiplicity of shadow-type images thus formed are analyzed by a computer, which produces a reconstructed cross-section density image.

A diagram of a typical CT scanner is shown in Fig. 113. An X-ray source producing a fan beam rotates around the patient in a few seconds. (Short periods are desirable to minimize artifacts in the final reconstructed image of the patient's cross section caused by unavoidable motions.) An array of several hundred detectors in an outer circle surrounding the patient provides the data from which a computer derives a tomographic view of the patient's body or head. A typical tomograph is shown in Fig. 114.

Three different X-ray detector systems have been developed for use in CT scanners. All are in use at present by the various CT-scanner manufacturers. Each detector system has its problems, but all seem comparable in ultimate performance.

The original CT-scanner development utilized a crystal and photomultiplier. A subsequent development used a tube containing xenon gas at several atmospheres. The density of the gas and the high atomic weight of xenon provide sufficient absorption so that a large fraction of the X-rays are detected by the resulting ion current. More

*For a more detailed discussion, see the article in Scientific American, October, 1975, p 56, "Image Reconstruction from Projections," R. Gordon, G.T. Herman, and S.A. Johnson.

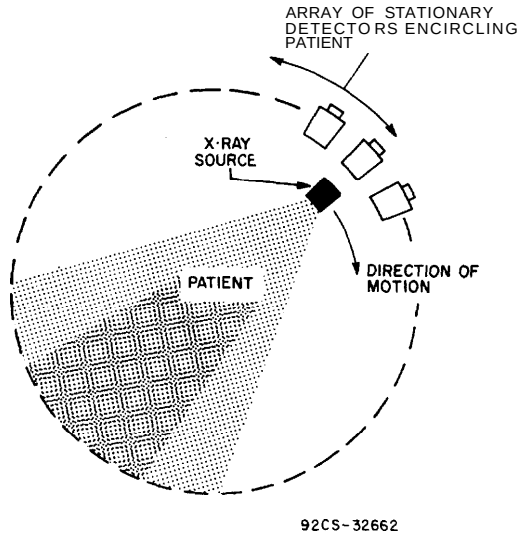

Fig- 113 - Diagram of a typical CT scanner. **X-ray source** *producing a fan beam rotates around the patient. Array of several hundred detectors in outer circle provides the data from which a computer derives a tomographic (cross-section) view of the patient's body or head.*

recently, detector packages have been developed using silicon photocells and a $CdWO_4$ crystal. This latter detector package appears to have cost advantages. Detection with the silicon photocell was not feasible in the early development of CT scanners, but a combination of higher-speed machines and the improved light output of the $CdWO_4$ crystal, relative to the $Bi_3Ge_4O_{12}$ (BGO) crystal, has made this combination an economic possibility.

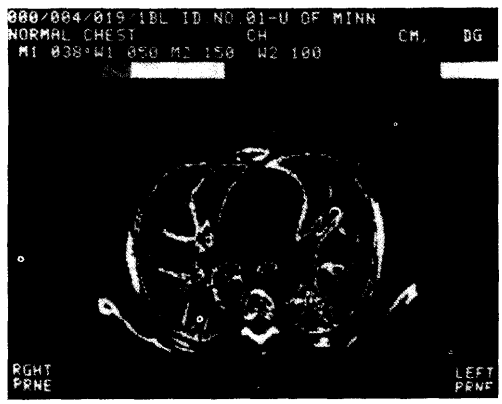

Fig. 114 - Tomograph showing a "slice" of the thoracic cavity. Lung tissue, blood vessels, air passages, ribs, and spine may be observed. (Courtesy Pfizer Medical Systems, Inc.).

The photomultiplier system uses a BGO (bismuth germanate) crystal usually coupled to the photomultiplier by means of a light pipe. Spectral emission from the crystal is illustrated in Fig. 115. It is rich in the **blue-**

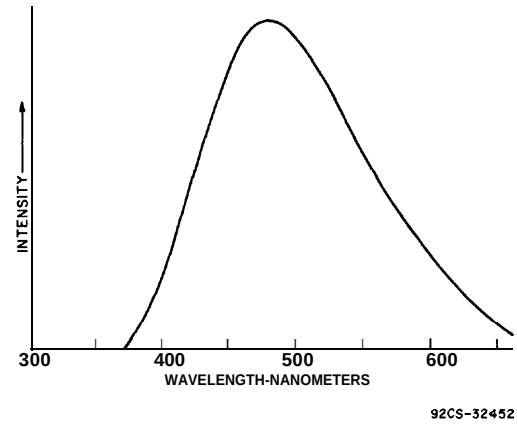

Fig. 115 - Fluorescence spectrum of $Bi_4Ge_3O_{12}$ (Data from Weber and Monchamp[97]).

green region and thus is a good match for bialkali photocathodes. Recently, it has been found that the Rb_2CsSb photocathode is more suitable for use with the BGO crystal than the K_2CsSb photocathode because of

the somewhat higher response and better spectral match. See Fig. 10. The Rb_2CsSb photocathode is also more suitable because it has a lower surface resistance than the K_2CsSb photocathode. See Fig. 36.

In the CT-scanner systems, pulse-height discrimination is not used nor are individual scintillations counted. The photomultiplier is used as an integrator of the light flux in each density measurement. It is important that the photomultiplier provide a linear translation of the light flux into output current and also that there be no overshoot or undershoot in photocurrents as the X-ray beam path changes from outside to through the patient resulting in a signal variation of 1000:1 or more. Typical maximum photocathode current (X-ray path through air only) is of the order of 2 nanoamperes depending on operation conditions. The photomultiplier is usually operated at a modest gain figure of the order of 60,000. High photocathode sensitivity is important in providing minimum noise in the signal so that the inherent signal-to-noise ratio in the transmitted X-ray beam is retained and the X-ray dose to the patient in minimized. The photomultiplier tubes used are either 1/2 inch or 3/4 inch in diameter, depending upon the configuration of the particular CT scanner.

Positron Camera

The positron camera[98,99,100,101,102] provides tomographic presentations based on coincident gamma-ray emission accompanying annihilation of a positron and an electron. Tracer radionuclides such as ^{11}C, ^{13}N, or ^{15}O emit a positron upon disintegration. In the presence of matter such as the brain, the positron interacts almost instantly with an electron resulting in the simultaneous emission of two gamma rays each having an energy of 511 keV, but moving in nearly opposite directions. When a pair of detectors, one on either side of the patient, observes coincident events, the point of radionuclide disintegration lies on a line joining the two detectors. See Fig. 116.

A number of positron cameras have been designed and built, some commercially. Various geometries and reconstruction techniques have been utilized. Complications in design arise when each detector can be in coincidence with any of several detectors on the opposite side of the patient. More than one plane may be utilized to provide three-dimensional data.

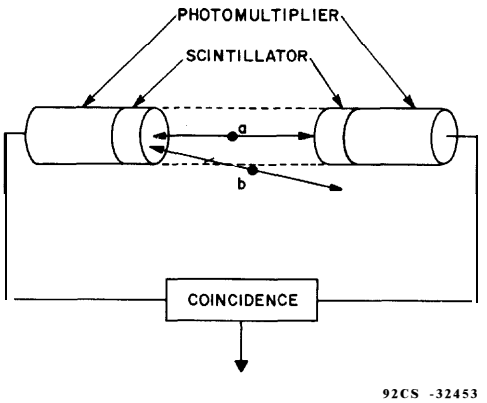

fig. 116 - Principle of positron coincidence detection. A disintegration at "a" results in oppositely directed gamma rays which are detected in coincidence by the pair of scintillator-photomultiplier detectors. An event at "b" results in a count in only one of the detectors. (From G.L. Brownell and C.A. Burnham[98])

Reponse time of the photomultiplier is of particular importance in positron cameras because the discrimination against spurious coincidences improves as the resolution time of the system decreases. Photomultiplier transit time spreads of the order of 2 nanoseconds or less are advantageous in these systems although other time- factors, related to the crystal scintillator (CsF has a time constant of 5 nanoseconds) and circuitry may limit the system discrimination time to perhaps 10-20 nanoseconds. Photomultiplier tubes of ¾-inch and 1 1/2-inch diameter have been the sizes preferred. Of course, high quantum efficiency matching the spectral emission of the scintillators (NaI:Tl, CsF, $Bi_4Ge_3O_{12}$) is also important.

Photometric and Spectrometric Applications

The side-on photomultiplier has in general, been the most widely used tube in photometric and spectrometric applications. The side-on tube is relatively small and has a rectangularly shaped photocathode that matches the shape of the light beam from an exit slit. Spectrometric applications require tubes with good stability, high anode sensitivity, low dark current, and broad spectral sensitivity. A high signal-to-noise ratio is important because of the generally small signal levels.

Before the development of the new negative-electron-affinity type photoemitters, such as gallium arsenide, it was necessary to use more than one detector in the measurement of radiant energy from the near-ultraviolet to the near-infrared part of the spectrum. A photomultiplier having a gallium arsenide photoemitter can now be used to detect radiant energy from the cutoff point of the photomultiplier window in the near-ultraviolet to 910 nanometers.

Spectrophotometry. Spectrophotometers measure the optical density of materials as a function of wavelength and require photomultipliers having a broad spectral range. The results of measurements of the absorption characteristics of substances are frequently expressed in terms of optical density. This logarithmic method correlates with the way the human eye discriminates differences in brightness.

The transmission density D is defined by

$$D = \log_{10} \frac{P_o}{P_t} = \log_{10} \frac{1}{T} \qquad (35)$$

where P_o is the radiant flux incident upon a sample, P_t is the radiant flux transmitted by a sample, and T is the transmission figure equal to P_t/P_o. Density measurements are useful in various applications to films and other transparencies in addition to chemical analysis where concentration of a solution is studied as a function of wavelength.

Color-Balancing Photometry. A color-balancing photometer is used to determine color balance and exposure times necessary to produce photographic color prints from color negatives. Such a device is shown in block diagram form in Fig. 117. It allows the matching of the relative proportions of red, blue, and green light transmitted by a production negative to those of a master color negative. **As** the first step in the matching process, the master negative is used to make an acceptable print. This first print is produced through trial and error by measurement of the relative proportions of red, blue, and green light transmitted through a key area of the master negative; the key area usually consists of a flesh tone or a gray area. The amount of light transmitted is a measure of the density. The exposure time using white light and the lens opening used to obtain the satisfactory print are noted.

Next, an area of the production negative similar to that on the master negative is chosen and the relative proportions of the red, blue, and green light transmitted are measured again. By use of magenta and yellow correcting filters, the color transmitted by the production negative can be balanced with that of the master negative. When the production negative is used, the lens opening is adjusted so that the exposure time with white light is the same as it was for exposure of the master negative. When the values of color-correcting filters and exposure times thus determined are used, prints from the production negative can be obtained which are very nearly as good as those obtained with the master color negative.

Most color-balancing photometers employ steady light sources and handle small-amplitude signals. Consequently, the photomultiplier used must have low values of dark current and good stability. The life expectancy of tubes used in this application is long because the small signal levels reduce the effects of fatigue which might otherwise adversely affect measurement accuracy and repeatability. Low-current operation also provides for linear operation where the anode current is proportional to the input flux over the range of transmission values measured. The intensity range of a color-balancing photometer, given in terms of the ratio of the radiant flux incident upon a sample to the radiant flux transmitted by a sample, is usually of the order of 1000 to 1 or more. It must be remembered that as in most photomultiplier applications, the power supplies used must be capable of providing voltages sufficiently regulated and free from ripple to assure minimum variation in sensitivity with possible line-voltage variation.

Densitometry. Although techniques such as those employed in the color-balancing photometer may be used successfully to measure density over an intensity range of 10 or 100 to 1 (density 1 to density 2), their use becomes increasingly difficult as the range is increased to 1000 to 10,000 to 1 (density 3 to density 4) or more. The large dynamic ranges encountered in color-film processing place

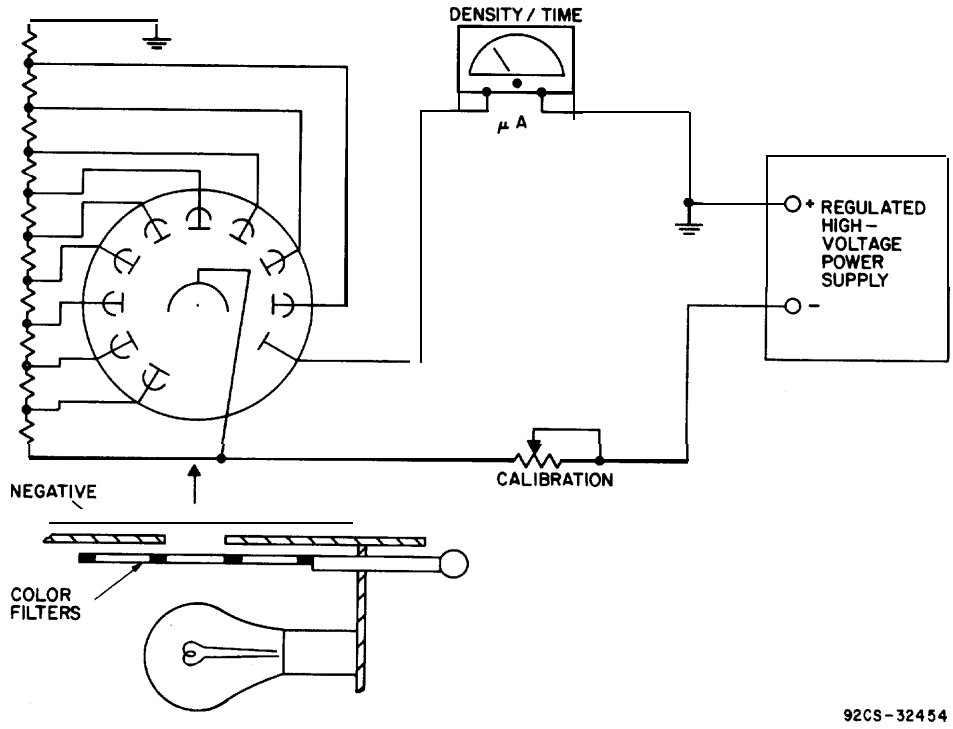

Fig. 117 - Block diagram of a color-balancing photometer.

severe requirements upon the photomultiplier because it must be operated in a constant-voltage mode. Problems develop in this mode at high-density values at which the dark current may become a significant proportion of the signal current. The random nature of this dark current, which precludes its being "zeroed out", may lead to output-signal instability. As a result of the type of operation needed to produce the dynamic range required in density measurements, the photomultiplier anode current is high at low density values. These high currents may result in excessive fatigue, and, depending upon the operating point, perhaps nonlinear operation. As with the color-balancing photometer, a well regulated low-ripple power supply is needed to assure accurate measurements.

Logarithmic Photometry. In the measurement of absorption characteristics, the changes in brightness levels vary over such a large range that it is advantageous to use a photometer whose response is approximately logarithmic. This response enables the photometer to be equipped with a meter or readout scale that is linear and provides precise readings even at high optical densities.

A simplified circuit of a logarithmic photometer capable of measuring film density with high sensitivity and stability and of providing an appropriate logarithmic electrical response and linear meter indication of density over three or four density ranges is shown in Fig. 118.

The circuit of Fig. 118, in which the photomultiplier operates at a constant current, minimizes photomultiplier fatigue and eliminates the need for a regulated high-voltage supply. The feedback circuit illustrated develops a signal across R1 proportional to the anode current. This signal controls the bias applied to the control device and automatically adjusts the current in the voltage-divider network. By this means, the dynode voltage is maintained at a level such that the anode current is held constant at a value selected to minimize the effects of fatigue. At optical densities of 3, the dynode supply voltage may be 1000 volts; at optical densities of less than 1, the dynode voltage

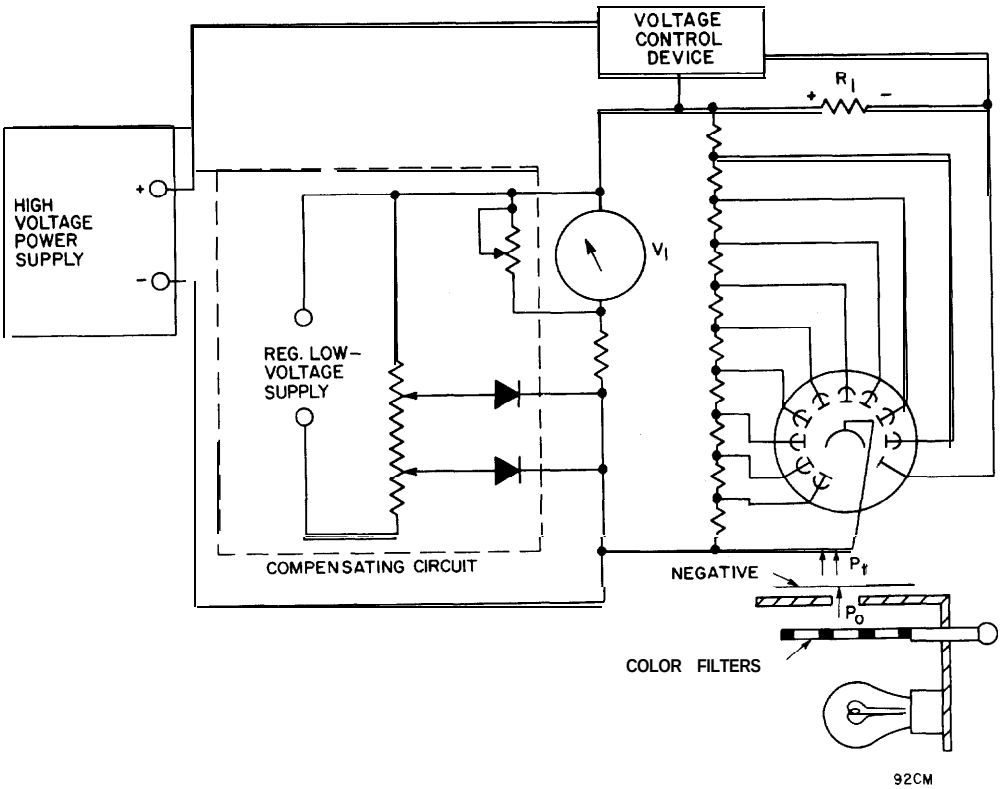

*Fig. **118** - Block diagram of a logarithmic photometer.*

may be as low as 300 volts. Dynode voltage is translated into density by means of the scale on voltmeter V1 .

Because there is an approximately exponential variation of sensitivity of a photomultiplier with applied voltage (see Fig, **48),** in a constant-current mode, the voltage varies almost linearly with the logarithm of the input light flux. The voltage is thus close to a linear measure of the density. A compensating circuit for the lack of linearity is indicated in Fig. 118 in the form of a variable and automatic shunt across the voltmeter V1 . As the density values increase, the effective value of the shunt resistance is reduced. This circuit not only compensates for photomultiplier non-linearity, but also for the non-linearity of the optical system employed.

Spectrometry

Spectrometry, the science of spectrum analysis, applies the methods of physics and physical chemistry to chemical analysis. Spectrometric applications include absorption, emission, **Raman,** solar, and vacuum spectrometry, and fluorometry.

Absorption Spectrometry. Absorption spectrometry, used to detect radiant energy in the visible, ultraviolet, and infrared ranges, is one of the most important of the instrumental methods of chemical analysis. It has gained this importance largely as a result of the development of equipment employing photomultipliers as detectors. The principle underlying absorption spectrometry is the spectrally selective absorption of radiant energy by a substance. The measurement of the amount of absorption aids the scientist in determining the amount of various substances contained in a sample.

The essential components of an absorption spectrometer are a source of radiant energy, a monochromator for isolating the desired spectral band, a sample chamber, a detector for converting the radiant energy to electrical energy, and a meter to measure the electrical energy. The spectral ranges of the

source and detector must be appropriate to the range in which measurements are to be made. In some cases this range may include one wavelength. In others, it may scan all wavelengths between the near-ultraviolet and the near-infrared.

Raman Spectroscopy. There are two types of molecular scattering of light, **Rayleigh** and **Raman. Rayleigh** scattering is the elastic collision of photons with the molecules of a homogeneous medium. Because the scattered photons do not gain energy from or lose energy to the molecule, they have the same energy $h\nu_0$ as the incident photons. A classic example of **Rayleigh** scattering of light from gas molecules is the scattering of the sun's light rays as they pass through the earth's atmosphere. This scattering accounts for the brightness and blueness of the sky.

Raman scattering is the inelastic collision of photons with molecules that produces scattered photons of higher or lower energy than the initial photons. During the collision there is a quantized exchange of energy that, depending on the state of the molecules, determines whether the initial photon gains or loses energy. The differences in energy levels are characteristic of the molecule. If the excitation frequency is ν_1 and the photon emitted after the interaction has a frequency of ν_2, the interaction results in a change in the energy of an initial photon by $h\nu_0$, where $h\nu_0 = |h\nu_2 - h\nu_1|$. When $h\nu_2$ is greater than $h\nu_1$, the initial photon has gained energy from the molecule that was in the excited state. In the reverse case, the initial photon has given up energy to the molecule in the unexcited state.

Early **Raman** instruments had a number of disadvantages and were difficult to use. It was difficult to find a stable high-intensity light source and to discriminate against **Rayleigh** scattering of the exciting line. With the recent development of high-quality monochromators and the advent of the laser light source, a renewed interest in the **Raman** effect as an analytical method of chemical analysis has taken place. **Raman** spectrophotometers are generally used to investigate the structure of molecules and to supplement other methods of chemical analysis, particularly infrared-absorption spectrometry.

The scattered photons from a **Raman interaction** are so few in number that only the highest-quality photomultipliers can be used as detectors. The tube should have high collection efficiency, high gain, good multiplication statistics, low noise, and high quantum efficiency over the spectral range of interest. Fig. 119 shows a **Raman** spectrum. To reduce the effects of **Rayleigh** scattering, a source of noise in **Raman** spectroscopy, the photomultiplier is placed at right angles to the light beam, whose wavelength has been chosen as long as possible within the range of interest.

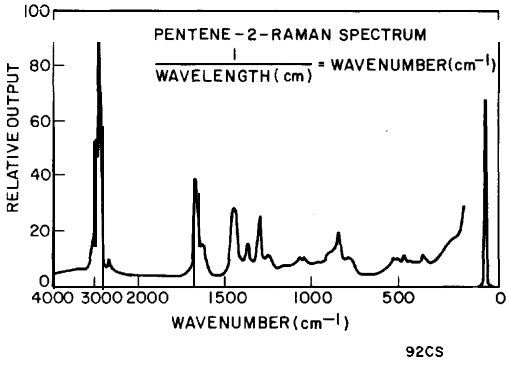

*Fig. 119 - Typical **Raman** spectrum.*

Fluorometry. The fluorometer is another instrument which utilizes the **photomultiplier's** capability for low-light-level detection, its high gain, and its good **signal-to-noise** ratio. There are numerous applications of this instrument in the fields of biochemistry, medical research, and industrial toxicology. Typical applications include the detection and measurement of minute quantities of air pollutants and of components of the blood or urine. Some materials are detected by their own fluorescence; others by their quenching effects on the fluorescence of other materials.

Illustrative of fluorometer operation is the optical design of a model designed by G. K. Turner **associates**[103] shown in Fig. 120. The sample is irradiated by an ultraviolet source filtered to eliminate longer wavelength components of the lamp irradiation. Fluorescent spectra at a longer wavelength pass through a second filter which eliminates scattered ultraviolet radiation.

A second beam from the ultraviolet source provides a calibrated reference flux. Both the fluorescent beam and the reference beam

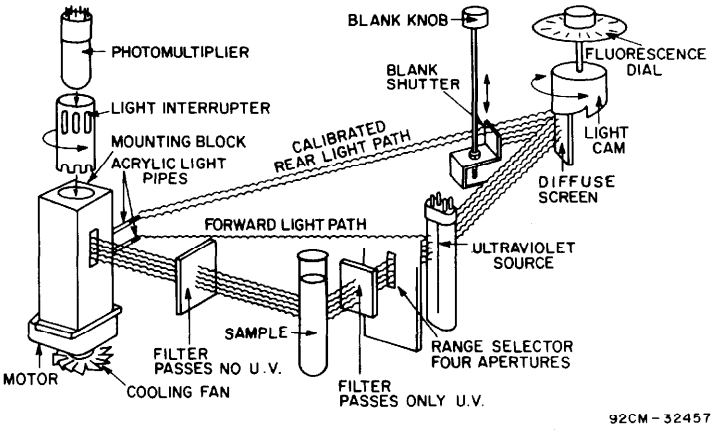

Fig. 120 - Optical arrangement of the Turner fluorometer.[104]

are directed to the photomultiplier and alternately sampled by means of the light interrupter. The output ac signal from the photomultiplier is processed to provide a null signal by means of the light cam and the attached dial records the fluorescence level. The null feature of the device eliminates errors from changes in the photomultiplier or from the ultraviolet source. A third flux indicated by the FORWARD LIGHT PATH is provided so that even for an absence of fluorescence a balance is always possible. The BLANK KNOB provides an adjustment so that the calibration can be adjusted to the zero fluorescence point.

Low-Light-Level Detection

Systems for the detection of low light levels make use of two basic techniques: charge integration, in which the output photocurrent is considered as an integration of the anode pulses which originate from the individual photoelectrons, and the digital technique in which individual pulses are counted.

Charge-Integration Method. In the charge-integration method, either the transit-time spread of the photomultiplier or the time characteristics of the anode circuit cause the anode pulses to overlap and produce a continuous, though perhaps noisy, anode current. The current is modulated by turning the light off and on by means of some mechanical device such as a shutter or light "chopper". The signal becomes the difference between the current in the light-on and light-off conditions.

Detection is limited by noise in the anode current. At low light levels the noise is caused primarily by the fluctuations in dark current of the photomultiplier (as discussed in the section, "Dark Current and Noise" in Chapter **4 Photomultiplier Characteristics** and in Appendix G, "Statistical Theory of Noise in Photomultiplier Tubes. ") The noise may be minimized by reducing the bandwidth of the measuring system. For example, a dc system may be used with a bandwidth of only a few hertz if an appropriate low-level current meter is selected. Bandwidth can also be reduced by some technique of averaging the current fluctuations over a period of time.

Another technique of charge integration is to chop the light signal with a motor-driven chopper disk having uniformly spaced holes or slots. The output current is then fed through an amplifier having a narrow bandwidth tuned to the frequency of chop. Bandwidths of the order of 1 Hz are typical.

Digital Method. In the digital method for the detection of low light levels a series of output pulses, each corresponding to a photoelectron leaving the photocathode of a photomultiplier, appears at the anode. All of the output pulses from the tube are shaped by a preamplifier before they enter a **pulse**-amplitude discrimination circuit. Only those pulses having amplitudes greater than some predetermined value and having the proper rise-time characteristics pass through to the signal-processing circuits. The digital technique is superior to charge integration at

very low light levels because it eliminates the dc leakage component of the dark current as well as dark-current components originating at places other than the photocathode. Fig. 121 shows a digital system in block form.

In the special case in which the digital technique is used to count single photons incident upon the photocathode of a photomultiplier, signal pulses appear at the anode with an average pulse amplitude PH equal to em, where e is the electron charge and $\bar{m}$ is the photomultiplier gain. The number of signal pulses N_a arriving at the anode is given by

$$N_a = N_p \eta_\lambda \qquad (36)$$

where N is the number of photons incident on the photocathode window, and η_λ is the quantum efficiency of the photocathode at the photon wavelength including a factor for the loss of light by reflection and absorption, and a factor for the loss resulting from imperfect electron-collection efficiency of the front end of the photomultiplier.

The dark-noise pulses present in addition to the signal pulses originate mainly from single electrons and have a pulse-height distribution as shown in the simplified dark-noise pulse-height-distribution spectrum of Fig. 122. Region A of Fig. 122 includes circuit-originated noise, some single-electron pulses, and pulses caused by electrons originating at the dynodes in the multiplier section. Pulses originating at the dynodes exhibit less gain than the single-electron pulses from the cathode. Region B represents the single-electron pulse-height distribution and is the region in which the single-photon signal pulses appear. Region C is caused by cosmic-ray muons, after-pulsing, and radioactive contaminants in the tube materials and in the vicinity of the tube. To maximize the ratio of signal pulses to noise pulses in single-photon counting, lower- and upper-level discriminators should be located as shown in the figure. For a discussion of signal-to-noise ratio and the statistics related to pulse counting, see "Pulse Counting Statistics" in Appendix G.

The signal-to-noise ratio may be improved by the square root of the total count time. Increasing the time of count is analogous to decreasing the bandwidth in the charge-integration method. The signal-to-noise ratio can also be improved by decreasing the number of dark-noise pulses. Because these pulses originate at the photocathode surface, the number can be reduced by reducing the area of the photocathode or by reducing the effective photocathode area by using electron optics to image only a small part of the photocathode on the first dynode. It may also be desirable to cool the photomultiplier and thereby reduce the thermionic emission from the photocathode.

In some applications not requiring the use of the full area of the semitransparent photocathode, it may be useful to restrict the active area of the photocathode by specially arranged magnetic fields[104] and thus reduce the collection of thermally emitted electrons from non-utilized areas of the photocathode. Fig. 123 illustrates the design of such a magnetic defocusing system type PF-1011 which includes an 8852 photomultiplier (2-inch diameter, ERMA photocathode, and GaP first dynode). The basic element is a permanent magnet in the form of an annular ring (1) polarized so that the S-pole or N-pole is toward the photocathode. Pole pieces, spacers, and a magnetic-shield cylinder complete the arrangement. The resulting magnetic field is such that only electrons emitted from the central portion of the photocathode arrive at the first dynode. Typical variation of photocathode response as a function of the position of the incident light is shown in Fig. 124. Note that the effective diameter of the photocathode has been reduced to about one eighth of an inch. Total dark emission at room temperature from the magnetically controlled photocathode is reduced by approximately 80:1. If the tube is then cooled to −20 °C, the dark count is still further reduced to about two electrons per second.

Very-Low-Light-Level Photon-Counting Technique. Before beginning very-low-light-level photon counting, the following special precautions must be taken:

1. The power supply and interconnecting circuits must have low-noise characteristics.

2. The optical system must be carefully designed to minimize photon loss and to prevent movement of the image of the object on the photocathode, a possible cause of error if the cathode is non-uniform. It is generally good practice to defocus the image on the

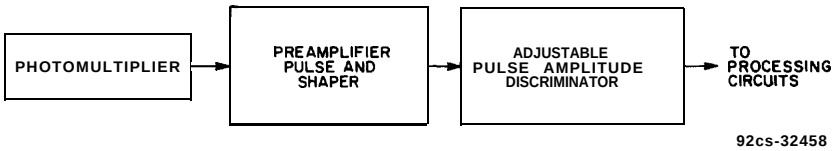

Fig. 121 - Block diagram illustrating a digital system for detection of low light levels.

photocathode, especially in the case of a point source, to minimize problems which may result from a non-uniform photocathode.

3. The photomultiplier must be allowed to stabilize before photon counting is begun. The tube should not be exposed to ultraviolet radiation before use and should, if possible, be operated for 24 hours at the desired voltage before the data are taken.

4. The photomultiplier should be operated with the cathode at ground potential if possible. If the tube is operated with the photocathode at negative high voltage, care must be taken to prevent the glass envelope of the tube from coming into contact with conductors at ground potential or noisy insulators such as bakelite or felt. Without this precaution, a very high dark noise may result as well as permanent damage to the photocathode.

5. Large thermal gradients must not be permitted across the tube as it is cooling. In addition, care must be taken to avoid excessive condensation across the leads of the tube or on the faceplate.

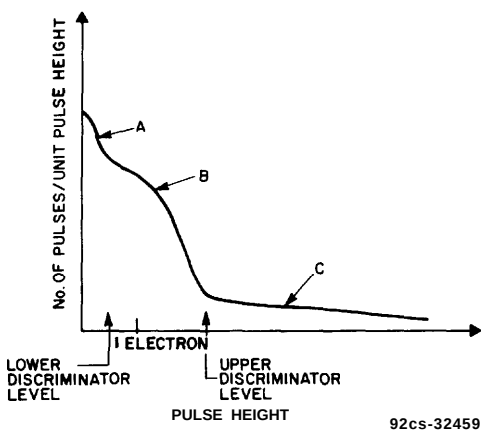

Fig. 122 - Dark-noise pulse-height-distribution spectrum.

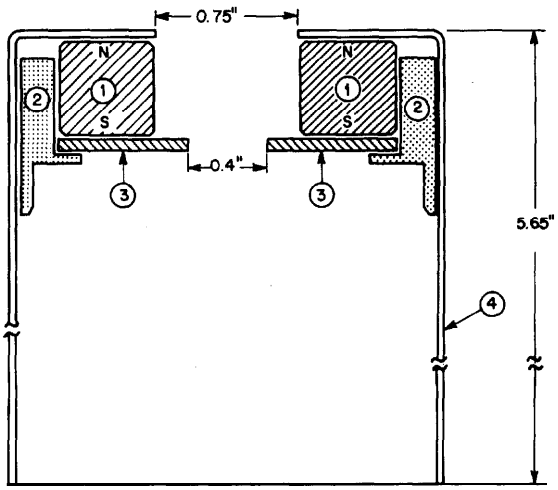

Fig. 123 - Magnetic defocusing system (PF1011) which includes type 8852 photomultiplier. This system permits collection of electrons only from the central part of the photocathode and thus substantially reduces dark emission. Shown are (7) ceramic magnet, (2) spacer-insulator, (3) magnet pole piece of black iron, and (4) magnetic shield cylinder. The assembly is designed to fit over the 8852 envelope.

Photomultiplier Selection for Photon Counting. In the selection of a photomultiplier for use in photon counting, several important parameters must be considered. First, and most important, the quantum efficiency of the photocathode should be as high as possible at the desired wavelength. To minimize the thermionic dark-noise emission, the photocathode area should be no larger than necessary for signal collection; the multiplier structure should utilize as large a fraction as possible of the electrons from the photocathode. The over-all tube should have as low a dark noise as possible. In some applications, the rise time and time-resolution capabilities of the tube may also be important.

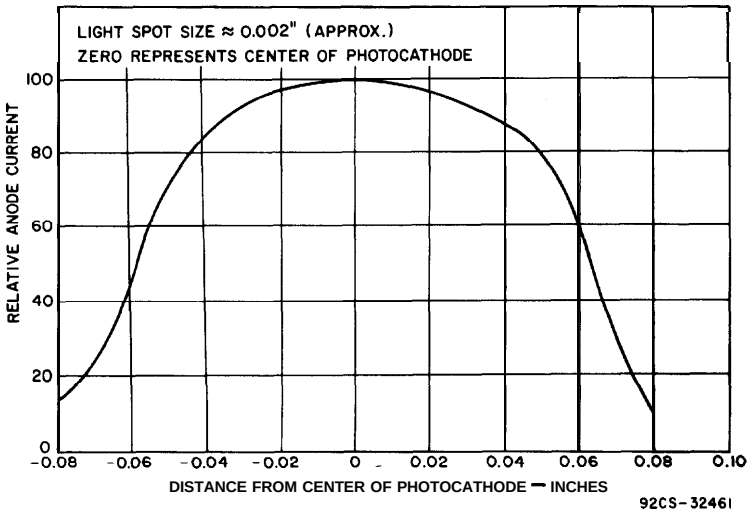

Fig. 124 - Typical variation of photocathode sensitivity as a function of incident-light spot position for an 8852 photomultiplier with the magnetic defocusing system of Fig. 123 affixed to the tube.

A number of more recent developments in photomultiplier design are of considerable significance in photon counting. These developments fall into two major categories, secondary-emission materials and **photo**cathodes. Because of the superior statistics of gallium phosphide (one of the more recently developed secondary-emission materials discussed in the section "Secondary Emission" in Chapter **2 Photomulti**plier **Design),** a tight single-electron distribution curve can be obtained, as shown in Fig. 79. The tight distribution permits easy location of the pulse-height discriminator, as is particularly evident when some of the signal pulses are originated by two or more photoelectrons leaving the cathode simultaneously. If the average number of photoelectrons leaving the photocathode per pulse were three, a pulse-height distribution similar to that shown in Fig. 125 would be obtained. Gallium phosphide provides a higher signal-to-noise ratio than would conventional secondary-emitting materials such as Be0 or Cs_3Sb when used in the same tube.

Photocathode developments include ERMA (Extended Red Multi-Alkali), a semitransparent photocathode having a response to 940 nanometers, and several negative-electron-affinity materials. Perhaps the most significant of these materials is indium gallium arsenide, whose threshold wavelength increases with increasing indium content. Spectral-response curves for some of the more recent photocathodes are shown in the section "Photoemission" in Chapter 2 **Photomultiplier Design.**

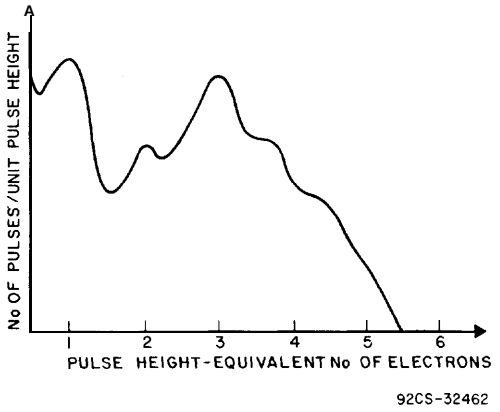

Fig. 125 - Pulse-height distribution obtained with a photomultiplier having a gallium phosphide first dynode. Light level is such that three photoelectrons per pulse time is the most probable number.

Astronomy[105]. Astronomers were among the first users of photomultiplier tubes. The high quantum efficiency, low background noise, and high gain recommend the use of photomultipliers in various astronomical applications. Requirements are often similar to

those for low-level photometry or spectrometry as discussed above. Applications include the guidance of telescopes, intensity measurements, stellar spectrophotometry, Doppler measurement of radial velocities, and the measurement of stellar magnetic fields by measuring Zeeman displacements.

Side-on photomultipliers such as the 1P21 are frequently used in these applications. Refrigeration may be utilized to reduce background. Photon counting may be adopted for very low signal measurement. For applications requiring a wide spectral range, tubes with the GaAs:Cs photocathode are very useful.

Pulsed Photomultipliers

Some years ago, Post[106] demonstrated improved characteristics of photomultiplier tubes by operating them with a pulsed voltage supply. He used side-on photomultipliers types 931A and 1P21 with an applied voltage of between 4 and 5 kilovolts pulsed for 2.5 microseconds or less. At these voltages, 400 to 500 volts per stage, the secondary emission for Cs-Sb dynodes is at a maximum (see Fig. 19) so that the gain becomes relatively insensitive to the variation of the maximum voltage applied. Normally, these tubes could not be operated at such high voltages without incurring destructive run-away dark currents. But, by pulsing the applied voltage, regenerative effects that depend upon transit time of ions are eliminated. Post's circuit is shown in Fig. 126. Not all tubes he tried could tolerate this high voltage without field emission and break-down effects, but on those tubes which were satisfactory initially or which he was able to stabilize by application of repeated high-voltage pulses, he found some very interesting advantages. Peak pulse amplitudes of 0.7 ampere were possible and provided a 70-volt pulse to drive an oscilloscope directly. Thus, a single photoelectron resulted in a 10-to-15-volt output pulse; the tubes were operated at gains in the neighborhood of 10^9 The measured rise time he found to be slightly more than one nanosecond. Refer to Fig. 71. Note in Fig. 126 the termination of the coaxial output line at the photomultiplier end which reduced the output RC time constant. It is pointed out by Post "the loss of a factor of two in voltage by terminating at the multiplier is compensated by voltage doubling at the unterminated end."

Laser Range Finding

A simplified block diagram of a laser range finder is shown in Fig. 127. Such a device may be utilized by the military for

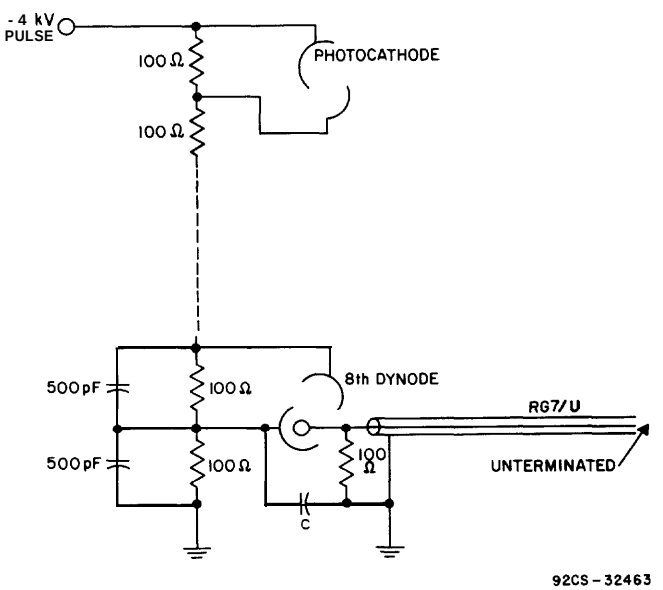

Fig. 126 - Post's voltage divider and bypass capacitor connections of photomultiplier to output coaxial line for pulsed high-voltage operation.[105]

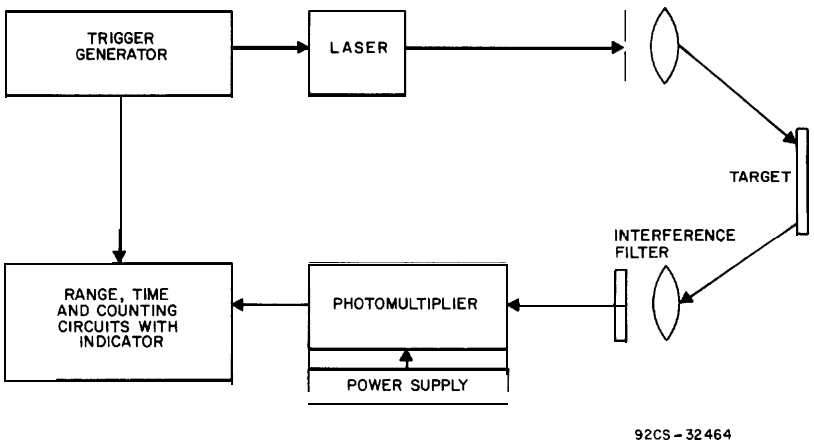

Fig. 127 - Simplified block diagram of a laser range finder.

tank fire control or in various industrial surveying type applications. Typically, a laser is pulsed in a time range of 25 nanoseconds. Measurements are made of beam travel time with a photomultiplier pick up. For example, a ruby laser (0.694 μm) may be used with a 3/4-inch diameter photomultiplier having an S-20 spectral response. Other lasers such as the Nd:YAG (1.06 μm) and solid-state junction lasers such as AlGaAs (0.86 μm) are also used, but because of the longer wavelengths, the detectors are more often silicon avalanche diodes. An interference filter is used to pass the wavelength of radiant energy of the laser with a minimum of background radiation. Photomultipliers used in laser range finding may have a relatively small photocathode, but they must exhibit high quantum efficiency, low dark noise, and fast rise time or an equivalent large bandwidth. Most photomultipliers can provide bandwidths exceeding 100 MHz and at the same time maintain relatively large output signals. The bandwidth of a photomultiplier can be limited by the RC time constant of the anode circuit.

The range of a laser-range-finding system depends on system parameters and operational environment. The maximum range of a given system may be signal-photon limited or background limited. The photon-limited case exists when the background and detector noise can be considered negligible. The maximum range in this case is determined by the signal-to-noise ratio in the photoelectron pulse corresponding to the scattered laser return beam. The signal-to-noise ratio of such a pulse is proportional to the square root of the product of the number of incident photons on the photomultiplier and the quantum efficiency of the photoelectric conversion. If the atmospheric attenuation is neglected and it is assumed that the laser spot falls entirely within the target, the maximum range in this case would be increased as the square root of the quantum efficiency of the photocathode. This increase follows because the number of photons collected by the aperture of the receiving system varies inversely as the square of the distance from the target.

In cases where the laser pulse must be detected against the background of a daylight scene, it is said to be background limited. If atmospheric attenuation again is neglected, the signal is proportional to the number of incident photons times the quantum efficiency of the photocathode. The number of incident photons from the return beam is inversely proportional to the square of the range, again assuming that the target is larger than the laser spot. The noise, however, is independent of the range and is determined by the square root of the product of the incident background radiation and the quantum efficiency. Thus, to a first approximation the range is increased in the background-limited case only by the fourth root of the quantum efficiency. Because the photomultiplier current caused by the background radiation is proportional to the solid angle of the scene from which the

photomultiplier collects radiation, the background current in the photomultiplier may be minimized by the use of a photocathode having a small area or by the use of a limiting aperture on the faceplate of the photomultiplier. No loss in collected laser light need result because the return beam may generally be considered as originating from a point source. The system aperture, of course, must be large enough to avoid optical alignment problems.

Scanning Applications

A number of photoelectrically sensed scanning systems have been devised such as facsimile scanners in which the material to be transmitted-a photograph or printed message-is mounted on a drum that is rotated to provide scan in one dimension. A scanning head moves parallel to the drum axis to provide the other dimension. The picture element is illuminated with a focused light spot and the scattered light is picked up by a photomultiplier, providing high-speed transmission utilizing the modulated output electrical signal.

Two more recently developed scanning systems are the flying-spot scanner for the development of television signals and the supermarket checkout system which recognizes a coded symbol on each product.

Flying-Spot Scanning. The elements of a flying-spot scanning system are shown in Fig. 128. A cathode-ray tube, in conjunction with its power supplies and deflection circuits, provides a small rapidly moving light source which forms a raster on its face. This raster is focused by the objective lens in the optical system onto the object being scanned, a slide transparency or a motion-picture film. The amount of light passing through the film varies with the film density. This modulated light signal is focused upon the photomultiplier by means of the condensing-lens system. The photomultiplier converts the radiant-energy signal into an electrical video signal. The amplifier and its associated equalization circuits increase the amplitude of the video signal as required.

The flying-spot scanning system is capable of providing high-resolution monochromatic performance. With the addition of (a) appropriate dichroic mirrors which selectively reflect and transmit the red, blue, and green wavelengths, (b) two additional photomultipliers with video amplifiers, and (c) appropriate filters, color operation is possible. In color operation, the primary wavelengths are filtered after separation by the light-absorbing filters before being focused upon each of three photomultipliers, one for each color channel. The output of each photomultiplier is then fed to a separate video amplifier.

Flying-spot video-signal generators are used in the television industry primarily for viewing slides, test patterns, motion-picture film, and other fixed images. Systems have been developed for the home-entertainment industry that allow slides and motion-picture film to be shown on the picture tube of any type of commercial television receiver.

A similar system is utilized by the photographic industry to provide accurate exposure control for film copying. By means of the three color controls, the operator may produce a color television display representing the film and can adjust and measure each color component to produce a visually satisfying balance.

Several important considerations must be taken into account if the cathode-ray tube in the system is to produce a light spot capable of providing good resolution. The cathode-ray tube should be operated with as small a light spot as possible. The cathode-ray-tube faceplate should be as blemish-free as possible and the tube should employ a fine-grain phosphor. Blemishes adversely affect signal-to-noise performance and contribute to a loss of resolution.

The spectral output of the cathode-ray-tube phosphor should match the spectral characteristic of the photomultiplier. This match can be rather loose in a monochromatic flying-spot generator. The spectral output of the phosphor of the cathode-ray tube used in a three-color version, however, must include most of the visible spectrum. Phosphors used in monochromatic systems may provide outputs in the ultraviolet region of the spectrum and still perform satisfactorily. Phosphors such as P16 and P15, when used with an appropriate ultraviolet filter, display the necessary short persistence required in a monochromatic system.

The visible portion of the P15 or P24 phosphor is used in color systems. The P15 and P24 phosphors are, however, much

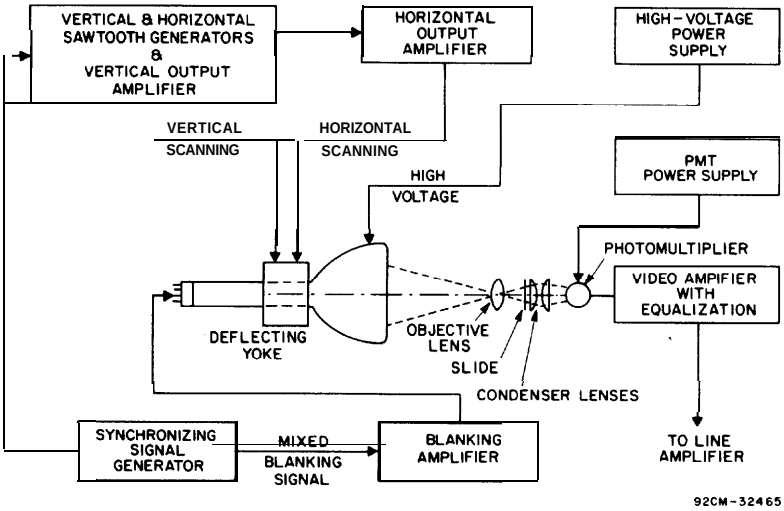

Fig. 128 - Elements of a flying-spot scanning system.

slower than the P16 phosphor and cause a lag in buildup and decay of output from the screen.

The phosphor lag results in trailing, a condition in which the persistence of energy output from the cathode-ray tube causes a continued and spurious input to the photomultiplier as the flying spot moves across the picture being scanned. The result is that a light area may trail into the dark area in the reproduced picture.

Similarly, the lag in buildup of screen output causes a dark area to trail over into the light area. The result of these effects on the reproduced picture is an appearance similar to that produced by a video signal deficient in high frequencies. Consequently, high-frequency equalization is necessary in the video amplifier.

The objective lens used in a flying-spot generator should be of a high-quality enlarger type designed for low magnification and, depending upon the cathode-ray-tube light output, should be corrected for ultraviolet radiation. The diameter of the objective lens should be adequate to cover the slide to be scanned. An enlarging f/4.5 lens with a focal length of 100 millimeters is suitable for use with 35-millimeter slides. The optics should not image the film on the photomultiplier because shading effects would result from non-uniformities of the photomultiplier response. In some cases it may be useful to employ a beam splitter between the cathode-ray tube and the lens and to use a second photomultiplier to sense any non-uniformities in the cathode-ray tube raster display. This sensed signal may then be used to eliminate this source of signal distortion in the primary photomultiplier pickup.

The spectral characteristics of the photomultiplier (or photomultipliers in the case of the three-color system) and the cathode-ray-tube phosphor should match. Usually, a photomultiplier having an S-4 or S-11 (Cs_3Sb) spectral response is suitable for use in a monochromatic system or as the detector for the blue and green channels. An S-20 ($Na_2KSb:Cs$) response is very often utilized for the red channel. The bialkali cathode (K-CS-Sb) is also well suited for the blue channel. The speed of the detector must be sufficient to provide the desired video bandwidth. Most requirements do not exceed 6 to 8 MHz, a figure well within photomultiplier capabilities.

The anode dark current of the photomultiplier should be small compared to the useful signal current. The signal-to-noise ratio will be maximized by operation of the photomultiplier at the highest light levels possible. If necessary, the over-all photomultiplier gain should be reduced to prevent excessive anode current and fatigue.

The amplitude of the light input is usually a compromise between an optimum signal-to-noise ratio and maximum cathode-ray-

tube life. Tube life may be reduced because of loss of phosphor efficiency at high beam-current levels. The signal-to-noise ratio can also be improved by the selection of photomultipliers having the highest photocathode sensitivities possible. However, because the spread of photocathode sensitivities is seldom greater than two or three to one, the improvement afforded by such selection is limited to two or three dB, an improvement difficult to detect during observations of a television display but desirable and necessary in some critical applications.

Photomultiplier gain need only be sufficient to provide a signal of the required level to the succeeding video-amplifier stages. These stages, in addition to providing the necessary amplification and bandwidth to assure good picture quality, incorporate equalization circuits composed of networks having different time constants. The relatively long decay time of these circuits generally results in appreciable reduction of the useful signal-to-noise ratio. Therefore, the use of short-persistence phosphors is recommended to reduce the required amount of equalization.

In addition to the video amplifier, a gamma-correction amplifier is required in each channel. The gammacorrection amplifier assures maximum color fidelity by making the linearity or gamma of the system unity.

Supermarket Checkout Systems. Fig. 129 shows the elements of a supermarket checkout system. The Universal Product Code (UPC), which is to be marked on all products, is scanned by laser beam by means of an oscillating mirror and a rotating mirror system. The pattern of the scan is a network of overlapping sine waves. The reflected pattern contains the modulation of the UPC symbol and is converted by the photomultiplier to an electronic signal that is then analyzed for the content of the code.

The laser used in the supermarket checkout system is usually a low-power He-Ne type with the principal emission line at 633 nanometers. A suitable photomultiplier for this application is a two-inch end-on type having an S-20 ($Na_2KSb:Cs$) spectral response or an extended-red multialkali type. Stability and good signal-to-noise ratio are important characteristics of the photomultiplier tube.

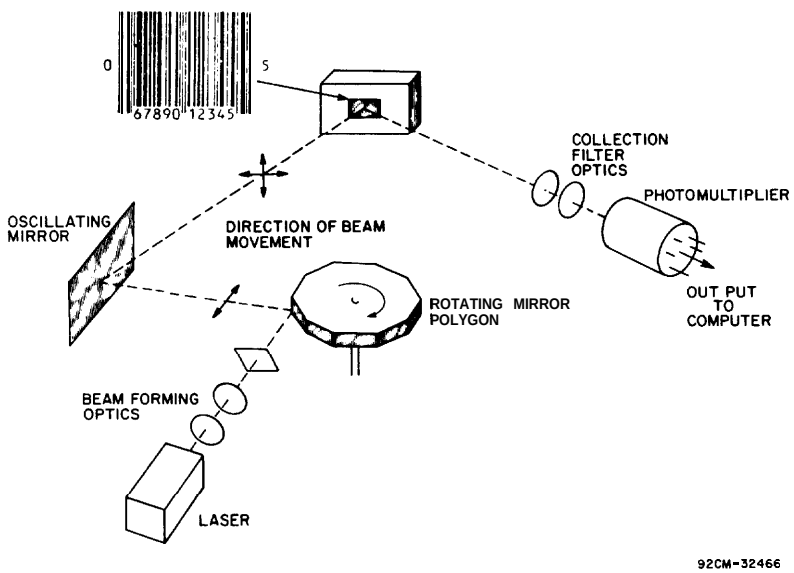

Fig. 129 - Point-of-sale supermarket checkout system. At left is Universal Product Code (UPC) symbol that provides 10-digit product identification. At right is schematic of optical system for scanning the product symbol and detecting the modulation with a photomultiplier.

REFERENCES

91. R.W. Engstrom and E. Fischer, "Effects of voltage-divider characteristics on multiplier phototube response," **Rev. Sci. Instr.,** Vol. 28, pp 525-527, July, 1957.

92. C.R. Kerns, "A high-rate phototube base," **IEEE Trans. Nucl. Sci.,** Vol. NS-24, No. 1, pp 353-355, Feb. 1977.

92a. V.O. Altemose, "Helium diffusion through glass," **J. Appl. Phys.,** Vol. 32, No. 7, pp 1309-1316, 1961.

92b. F.J. Norton, "Permeation of gases through solids," **J. Appl. Phys.,** Vol. 28, No. 1, pp 34-39, 1957.

93. American Institute of Physics Handbook, Third Edition, McGraw-Hill, 1972.

94. R.W. Engstrom, "Luminous Microflux standard," **Rev. Sci. Instrum.** Vol. 26, No. 6, pp 622-623, June, 1955.

95. D.G. Fisher, A.F. McDonie, and A.H. Sommer, "Bandbending effects in Na_2K Sb and K_2Cs Sb photocathodes," **J. Appl. Phys.,** Vol. 45, No. 1, pp 487-8, Jan. 1974.

96. H.O. Anger, "Scintillation camera," **Rev. Sci. Instrum.,** Vol. 29, pp 27-33, 1958.

97. M.J. Weber and R.R. Monchamp, "Luminescence of $Bi_4Ge_3O_{12}$: spectral and decay properties," **J. Appl. Phys.,** Vol. 44, No. 12, pp 5495-99, 1973.

98. G.L. Brownell and C.A. Burnham, "Recent developments in positron scintigraphy," **Instrumentation in Nuclear Medicine,** Vol. 2, Ed: G.J. Hine and J.A. Sorenson, Chapter 4, pp 135-159, Academic Press, 1974.

99. M.E. Phelps, E. J. Hoffman, N.A. Mullani and M.M. Ter-Pogossian, "Application of annihilation coincidence detection to transaxial reconstruction tomography," **J. Nucl. Medicine,** Vol. 16, No. 3, pp 210-224, 1975.

100. S.E. Derenzo, H. Zaklad, and T.F. Budinger , "Analytical study of a high-resolution positron ring detector system for transaxial reconstruction tomography," **J. Nucl. Med.,** Vol. 16, No. 12, pp 1166-73, Dec. 1975.

101. M.E. Phelps, E.J. Hoffman, Sung-Cheng Huang, and D.E. Kuhl, "ECAT: a computerized tomographic imaging system for positron-emitting radiopharmaceuticals," **J. Nucl. Med.,** Vol. 19, No. 6, pp 635-647, June 1978.

102. G.L. Brownell, C. Burnham, B. Ahluwalia, N. Alpert, D. Chester, S. Cahavi, J. Correia, L. Deveau, "Positron imaging instrumentation," **IEEE Trans. Nucl. Sci.,** Vol. 24, No. 2, pp 914-916, Apr. 1977.

103. **Operating and Service Manual, Model 111 Fluorometer,"** G.K. Turner Associates, 2524 Pulgas Ave., Palo Alto, Calif. 94303.

104. G.Y. Farkas and P. Varga, "Reduction of dark current in transparent cathode photomultipliers for use in optical measurements," **J. Sci. Instrum.,** Vol. 41, pp. 704-705, 1964.

105. **Astronomical Techniques,** Edited by W.A. Hiltner, The University of Chicago Press, 1962.

106. R.F. Post, "Performance of Pulsed Photomultipliers," **Nucleonics,** Vol. 10, No. 5, pp 46-50, May 1952.

Appendix A—
Typical Photomultiplier Applications and Selection Guide

The many and varied requirements of equipment designers and experimenters preclude the recommendation of a single photomultiplier as the optimum device for any given application category. In most applications, some trade-offs must be made in electrical characteristics; tube size must be considered; the environment in which the device is to be operated can be an influential factor; and of course, over-all cost is important. Each of these constraints can be best evaluated by the individual designer for the specific application.

This Appendix defines a number of the more common applications of photomultipliers and lists tube types which are suitable or are frequently used for the particular application. The listing is not all-inclusive and is intended to serve only as a general guide for initial type selection. Other photomultipliers may be satisfactory for the specified applications when all system requirements are considered.

CATALOGUE OF PHOTOMULTIPLIER APPLICATION CATEGORIES

Astronomy: The guidance of telescopes, intensity measurements, stellar spectrophotometry, and the like.

Colorimetry: The quantitative color comparison of surfaces (reflectance) and solutions (transmission).

C-T Scanners: A medical X-ray equipment that provides a cross section density map (tomograph) of a patient. A photomultiplier is used to detect and measure the light flux from a scintillating crystal.

Densitometry: The measurement of optical density of photographic negatives, neutral density filters, and similar materials.

Gamma-Ray Cameras: A scintillation counter having a single large crystal and a number of photomultiplier tubes used in medical applications to map the location of isotope disintegrations.

High-Temperature Environments: Applications such as the logging of deep oil wells, or geological exploration, and steel-mill process controls.

Imaging Devices: A cathode-ray tube or moving mirrors can be used as a light source to sequentially illuminate a film positive or negative or a printed page. This system is used in (1) optical character recognition, (2) scanning or printed or written material for transmission by telephone, (3) parts inspection, and (4) reproduction of motion pictures, slides, and educational material on a television receiver (color or black and white).

Inspection, High-Speed: Small objects such as fruits, vegetables, seeds, candy, toys, paper products and even glass, metal, and other industrial parts can be examined for color and defects as they move at high speed past one or more photomultiplier tubes.

Laser Detection: Lasers provide unique light sources; they are spectrally pure and produce very narrow collimated beams. They can be very intense and can be made to produce light pulses of extremely short duration. The photomultiplier provides time resolution in the nanosecond and subnanosecond ranges and is capable of detecting very low light levels such as those received from weak reflected laser light pulses.

Photometry: The measurement of illumination or luminance. Levels of light flux vary over a wide range in photography, astronomy, television, and other applications.

Photon Counting: A method of detecting photons by counting single photoelectrons released from the photocathode.

Pollution Monitoring: The analysis of the level and the nature of contaminants in solutions, gases, and other waste materials.

Positron Camera: A scintillation-counter-type device providing tomographic presentations based on coincident gamma-ray emission accompanying annihilation of a positron and an electron . Medical applications utilize tracer radio nuclides such as ^{11}C, ^{13}N, and ^{15}O.

Process Control: The measurement of transmitted or reflected light in continuous flow processes using solids, liquids, or gases. Detects flaws, improper marking, and changes in color and optical density. By using radioactive sources and scintillators, photomultipliers can be used for the control of the weight and thickness of opaque materials.

Radioimmunoassay (RIA): A technique that enables the measurement of minute quantities of substances in biological fluids as small as 10-12 gram. Compounds are tagged with radioactive isotopes and are measured with a liquid scintillation counter for beta-emitting isotopes or a solid crystal scintillation counter for gamma-emitting isotopes.

Radiometry: The measurement of irradiance or radiance.

Raman Spectrometry: Measurement of the wavelength shift of scattered photons from a highly monochromatic source such as a laser provides information on molecular structure and bonding energy.

Scintillation Counting: The measurement of nuclear radiation by detecting light or single scintillations emitted from a scintillation material receiving nuclear radiation.

Severe Physical Environments: Applications such as oil-well logging, satellites, and military vehicles subject to severe shock and vibration.

Thermoluminescent Dosimetry (TLD): Cer tain phosphors emit light when they are heated after having been exposed to ionizing radiation. Devices using this principle afford personnel protection by determining dosage levels in medical and biological treatments and studies. Energy stored in TLD's is pro portional to dosage over a very wide range.

Time Measurement: In nuclear experiments the "time of flight" of nuclear particles is important. Photomultipliers permit time measurements down to a fraction of a nonosecond.

Spectrophotometry

BURLE Type	Photo-cathode Material	Window Material[1]	No. of Stages	Dia meter[2]
1P21	Cs_3Sb	0080	9	1-1/8"s
1P28	Cs3Sb	8337	9	1-1/8"s
1P28A	Cs3Sb	8337	9	1-1/8"s
1P28B	K_2CsSb	8337	9	1-1/8"s
931A	GaAs	0080	9	1-1/8"s
931B	GaAs	0080	9	1-1/8"s
4526A	Na_2KCsSb	0080	10	1-1/2"d
C31034	GaAs	8337	11	2"e
C31034A	GaAs	8337	11	2"e
S83063E	Na_2KCsSb	7056	10	1-1/8"e
S83068E	Rb_2CsSb	7056	10	1-1/8"e
83089-600	Na_2KCsSb	7056	10	1-1/8"e
83101-600	Rb_2CsSb	B270	10	3/4"e

[1] 0080, B270 – lime glass; 8337 - Schott, 7056 – borosilicate
[2] e – end-window; s – side-window; d – dormer window

TLD

BURLE Type	Photo-cathode Material	Window Material[1]	No. of Stages	Dia meter[2]
8575	K_2CsSb	7740	12	2"e
8850	K_2CsSb	7740	12	2"e
S83062E	Rb_2CsSb	7056	10	1"e
83087-100	Rb_2CsSb	B270	10	3/4"e
83101-600	Rb_2CsSb	B270	10	3/4"e

[1] B270 – lime glass; 7740 – Pyrex ; 7056 - borosilicate
[2] e – end-window

Gamma -Ray Cameras

BURLE Type	Photo-cathode Material	Window Material[1]	No. of Stages	Dia meter[2]
4900	K^2CsSb	B270	10	3" e
6199	Cs_3Sb	0080	10	1-1/2" e
S83010E	Rb_2CsSb	0080	10	1-1/2" e
S83013F	K_2CsSb	0080	10	3-1/2" e
S83019F	K_2CsSb	B270	10	2" e
S83020F	K_2CsSb	B270	10	60mm h,e
S83021E	K_2CsSb	B270	10	3" e
S83022F	K_2CsSb	B270	10	2" h,e
S83025F	K_2CsSb	B270	10	3" h,e
S83049F	K_2CsSb	B270	8	3" e
S83053F	K_2CsSb	B270	8	60mm h,e
S83054F	K_2CsSb	B270	8	2" e
S83056F	K_2CsSb	B270	8	3" h,e
S83069E	K_2CsSb	B270	8	35x46.5mm, mh
S83079E	K_2CsSb	B270	8	3" sq

[1] 0080, B270 – lime glass
[2] e – end-window; h – hexagonal; mh – modified hexagonal; sq - square

High Temperature Environments

BURLE Type	Photo-cathode Material	Window Material[1]	No. of Stages	Dia meter[2]
C31000AP	Na_2KSb	7056	12	2"e
C31016G	Na_2KSb	7056	10	1"e
C83051	Na_2KSb	sa	10	1"e
C83060	Na_2KSb	sa	10	1-1/4"e
C83065	Na_2KSb	7056	10	1"e
83103 100	Na_2KSb	7056	10	3/4"e

[1] sa – sapphire, 7056 – borosilicate
[2] e – end-window

Flying-Spot Scanners

BURLE Type	Photo-cathode Material	Window Material[1]	No. of Stages	Dia meter[2]
4552	K_2CsSb	0080	9	1-1/8"s
1P21	Cs_3Sb	0080	9	1-1/8"s
931A	Cs_3Sb	0080	9	1-1/8"s
931B	K_2CsSb	0080	9	1-1/8"s
6199	Cs_3Sb	0080	10	1-1/2"e
83087-100	Rb_2CsSb	B270	10	3/4"e
83090-600	Rb_2CsSb	B270	9	3/4"e
83101-600	Rb_2CsSb	B270	10	3/4"e
S83010E	Rb_2CsSb	0080	10	1-1/2"e

[1] 0080 – lime glass; 8337 - Schott
[2] e – end-window; s – side-window

Inspection, High Speed

BURLE Type	Photo-cathode Material	Window Material[1]	No. of Stages	Dia meter[2]
1P21	Cs_3Sb	0080	9	1-1/8" s
4552	K_2CsSb	0080	9	1-1/8" s
6199	Cs_3Sb	0080	10	1-1/2" e
931A	Cs_3Sb	0080	9	1-1/8" s
931B	K_2CsSb	0080	9	1-1/8" s
S83062E	Rb_2CsSb	7056	10	1" e
S83010E	Rb_2CsSb	0080	10	1-1/2" e
83087-100	Rb_2CsSb	B270	10	3/4"e
83090-600	Rb_2CsSb	B270	9	3/4" e
83101-600	Rb_2CsSb	B270	10	3/4" e

[1] 0080, B270 – lime glass, 7056 – borosilicate
[2] e – end-window; s – side-window

Raman Spectroscopy

BURLE Type	Photo-cathode Material	Window Material[1]	No. of Stages	Dia meter[2]
8850	K_2CsSb	7740	12	2”e
8852	Na_2KCsSb	7740	12	2”e
C31034	GaAs	8337	11	2”e
C31034A	GaAs	8337	11	2”e

[1] 8337 - Schott; 7740 – Pyrex
[2] e – end-window

Laser Detection

BURLE Type	Photo-cathode Material	Window Material[1]	No. of Stages	Dia meter[2]
4526A	Na_2KCsSb	0080	10	1-1/2"d
8575	K_2CsSb	7740	12	2"e
8850	K_2CsSb	7740	12	2"e
8852	Na_2KCsSb	7740	12	2"e
S83063E	Na_2KCsSb	7056	10	1-1/8"e
83087-100	Rb_2CsSb	B270	9	3/4"e
83101-600	Rb_2CsSb	B270	10	3/4"e
C31034	GaAs	8337	11	2"e
C31034A	GaAs	8337	11	2"e

[1] 0080, B270 – lime glass; 8337 - Schott; 7740 – Pyrex 7056 – borosilicate
[2] e – end-window; d – dormer window

Photometry

BURLE Type	Photo-cathode Material	Window Material[1]	No. of Stages	Dia meter[2]
1P21	Cs_3Sb	0080	9	1-1/8”s
931A	Cs_3Sb	0080	9	1-1/8”s
931B	K_2CsSb	0080	9	1-1/8”s
4552	K_2CsSb	0080	9	1-1/8”s

[1] 0080 – lime glass
[2] s – side-window

Photon Counting

BURLE Type	Photo-cathode Material	Window Material[1]	No. of Stages	Dia meter[2]
8575	K_2CsSb	7740	12	2"e
8850	K_2CsSb	7740	12	2"e
8852	Na_2KCsSb	7740	12	2"e
8854	K_2CsSb	8337	14	5"e
C31034	GaAs	8337	11	2"e
C31034A	GaAs	8337	11	2"e
S83062E	Rb_2CsSb	7056	10	1-1/2"e
83089-600	Na_2KCsSb	7056	10	1-1/8"e
83090-600	Rb_2CsSb	B270	9	3/4"e
83101-600	Rb_2CsSb	B270	10	3/4"e

[1] 0080, B270 – lime glass; 8337 - Schott; 7740 – Pyrex 7056 – borosilicate
[2] e – end-window

Positron Cameras

BURLE Type	Photo-cathode Material	Window Material[1]	No. of Stages	Dia meter[2]
83087-100	Rb_2CsSb	B270	10	3/4"e
83090-600	Rb_2CsSb	B270	9	3/4"e
83101-600	Rb_2CsSb	B270	10	3/4"e
83102 100	Rb_2CsSb	0080	9	1"e
S83062E	Rb_2CsSb	7056	10	1"e

[1] 0080, B270 – lime glass, 7056 – borosilicate
[2] e – end-window

Process Control

BURLE Type	Photo-cathode Material	Window Material[1]	No. of Stages	Dia meter[2]
1P21	Cs_3Sb	0080	9	1-1/8"s
1P28	Cs_3Sb	8337	9	1-1/8"s
1P28A	Cs_3Sb	8337	9	1-1/8"s
1P28B	K_2CsSb	8337	9	1-1/8"s
931A	Cs_3Sb	0080	9	1-1/8"s
931B	K_2CsSb	0080	9	1-1/8"s
2060	Cs_3Sb	0080	10	1-1/2"e
4856	K_2CsSb	0080	10	2"e
4900	K_2CsSb	0080	10	3"e
6199	Cs_3Sb	0080	10	1-1/2"e
S83010E	Rb_2CsSb	0080	10	1-1/2"e
S83019F	K_2CsSb	B270	10	2"e
S83021E	K_2CsSb	B270	10	3"e
S83049F	K_2CsSb	B270	8	3"e
S83054F	K_2CsSb	B270	8	2"e
S83079E	K_2CsSb	B270	8	3"sq,e

[1] 0080, B270 – lime glass; 8337 - Schott
[2] e – end-window; s – side-window

Severe Physical Environments

BURLE Type	Photo-cathode Material	Window Material[1]	No. of Stages	Dia meter[2]
83101 100	Rb_2CsSb	B270	10	3/4"e
C31016G	Na_2KSb	0080	10	1"e
C83051	Na_2KSb	sa	10	1"e
C83060	Na_2KSb	sa	10	1-1/4"e

[1] 0080, B270 – lime glass; sa - sapphire
[2] e – end-window

Radiometry

BURLE Type	Photo-cathode Material	Window Material[1]	No. of Stages	Dia meter[2]
1P21	Cs_3Sb	0080	9	1-1/8"s
1P28	Cs_3Sb	8337	9	1-1/8"s
1P28A	Cs_3Sb	8337	9	1-1/8"s
1P28B	K_2CsSb	8337	9	1-1/8"s
931A	Cs_3Sb	0080	9	1-1/8"s
931B	K_2CsSb	0080	9	1-1/8"s
4526A	Na_2KCsSb	0080	9	1-1.2"d
2060	Cs_3Sb	0080	10	1-1/2"e
6199	Cs_3Sb	0080	10	1-1/2"e
8575	K_2CsSb	7740	12	2"e
8850	K_2CsSb	7740	12	2"e
8852	Na_2KCsSb	7740	12	2"e
S83010E	Rb_2CsSb	0080	10	1-1/2"e
S83062E	Rb_2CsSb	7056	10	1"e
83087-100	Rb_2CsSb	B270	10	3/4"e
83101-600	Rb_2CsSb	B270	10	3/4"e

[1] 0080, B270 – lime glass; 8337 - Schott; 7740 - Pyrex 7056 – borosilicate
[2] e – end-window: s – side-window: d – dormer window

Time Measurement

BURLE Type	Photo-cathode Material	Window Material[1]	No. of Stages	Dia meter[2]
8575	K_2CsSb	7740	12	2"e
8850	K_2CsSb	7740	12	2"e
8852	Na_2KSb	7740	12	2"e
8854	K_2CsSb	8337	14	5"e
S83062E	Rb_2CsSb	7056	10	1"e
S83068E	Rb_2CsSb	7056	10	1-1/8"e
83087-100	Rb_2CsSb	B270	10	3/4"e
83101-600	Rb_2CsSb	B270	10	3/4"e

[1] 0080, B270 – lime glass; 8337 - Schott; 7740 – Pyrex, 7056 – borosilicate
[2] e – end-window

Scintillation Counting

BURLE Type	Photo-cathode Material	Window Material[1]	No. of Stages	Dia meter[2]
2060	Cs_3Sb	0080	10	1-1/2"e
4900	K_2CsSb	0080	10	3"e
6199	Cs_3Sb	0080	10	1-1/2"e
83103 100	Na_2KSb	7056	10	3/4"e
8575	K_2CsSb	7740	12	2"e
8850	K_2CsSb	7740	12	2"e
8852	Na_2KCsSb	7740	12	2"e
8854	K_2CsSb	8337	14	5"e
C31000AP	Na_2KSb	7056	12	2"e
C31016G	Na_2KSb	0080	10	1"e
C31016H	Na_2KSb	0080	10	1"e
C31034	GaAs	8337	11	2"e
C31034A	GaAs	8337	11	2"e
S83006F	K_2CsSb	0080	10	5"e
S83062E	Rb_2CsSb	7056	10	1"e
S83010E	Rb_2CsSb	0080	10	1-1/2"e
83087-100	Rb_2CsSb	B270	10	3/4"e
83092-500	Na_2KSb	0080	10	1"e
83101-600	Rb_2CsSb	B270	10	3/4"e

[1] 0080, B270 – lime glass; 8337 - Schott; 7740 – Pyrex 7056 – borosilicate
[2] e – end-window

Radioimmunoassay

BURLE Type	Photo-cathode Material	Window Material[1]	No. of Stages	Dia meter[2]
4856	K_2CsSb	0080	10	2"e
4900	K_2CsSb	0080	10	3"e
6199	Cs_3Sb	0080	10	1-1/2"e
S83068E	Rb_2CsSb	7056	10	1-1/8"e
S83010E	Rb_2CsSb	0080	10	1-1/2"e
S83019F	K_2CsSb	B270	10	2"e
S83054F	K_2CsSb	B270	8	2"e

[1] 0080, B270 – lime glass; 7056 – borosilicate
[2] e – end-window

Densitometry

BURLE Type	Photo-cathode Material	Window Material[1]	No. of Stages	Dia meter[2]
1P21	Cs_3Sb	0080	9	1-1/8"s
1P28	Cs_3Sb	8337	9	1-1/8"s
931A	GaAs	0080	9	1-1/8"s
931B	GaAs	0080	9	1-1/8"s
4552	K_2CsSb	0080	9	1-1/8"s

[1] 0080 – lime glass; 8337 - Schott
[2] s – side-window

Colorimetry

BURLE Type	Photo-cathode Material	Window Material[1]	No. of Stages	Dia meter[2]
1P21	Cs_3Sb	0080	9	1-1/8"s
1P28	Cs_3Sb	8337	9	1-1/8"s
931A	GaAs	0080	9	1-1/8"s
931B	GaAs	0080	9	1-1/8"s
83089-600	Na_2KCsSb	7056	10	1-1/8”e
4552	K_2CsSb	0080	9	1-1/8"s

[1] 0080 – lime glass; 8337 – Schott; 7056 – borosilicate
[2] s – side-window; e – end-window

Astronomy

BURLE Type	Photo-cathode Material	Window Material[1]	No. of Stages	Dia meter[2]
1P21	Cs_3Sb	0080	9	1-1/8"s
1P28	Cs_3Sb	8337	9	1-1/8"s
1P28B	K_2CsSb	8337	9	1-1/8"s
8575	K_2CsSb	7740	12	2"e
8850	K_2CsSb	7740	12	2"e
8852	Na_2KCsSb	7740	12	2"e
C31034	GaAs	8337	11	2"e
C31034A	GaAs	8337	11	2"e

[1] 0080 – lime glass; 8337 - Schott; 7740 - Pyrex
[2] e – end-window; s – side-window

Pollution Monitoring

BURLE Type	Photo-cathode Material	Window Material[1]	No. of Stages	Dia meter[2]
4526A	Na_2KCsSb	0080	9	1-1/2"d
S83063E	Rb_2CsSb	7056	10	1-1/8"e
8850	K_2CsSb	7740	12	2"e
8852	Na_2KCsSb	7740	12	2"e
83089-600	Na_2KCsSb	7056	10	1-1/8"e

[1] 0080 – lime glass; 7740 – Pyrex, 7056 – borosilicate
[2] e – end-window; d – dormer window

Cerenkov Radiation

BURLE Type	Photo-cathode Material	Window Material[1]	No. of Stages	Dia meter[2]
8850	K_2CsSb	7740	12	2"e
8854	K_2CsSb	8337	14	5"e
S83062E	Rb_2CsSb	7056	10	1"e
83090-600	Rb_2CsSb	B270	9	3/4"e
83101-600	Rb_2CsSb	B270	10	3/4"e

[1] 0080, B270 – lime glass; 7740 – Pyrex, 8337 - Schott
7056 – borosilicate
[2] e – end-window

This page is blank.

Appendix B—
Glossary of Terms Related to Photomultiplier Tubes and Their Applications

This Appendix contains a glossary of terms frequently used in connection with photomultiplier tubes and their applications. Where suitable definitions were available from established standards or other reliable sources, they were used, possibly with minor modifications. For these cases, the sources of the definitions are indicated by the reference number at the end of the definition. In many cases, however, the definitions were prepared by the writers of this Manual. In these latter cases, no source reference is indicated after the definition.

Absorptance: The ratio of the radiant flux absorbed in a body of material to that incident upon it. If the absorptance is a, the reflectance is ϱ, and the transmittance is τ,

$$a + \varrho + \tau = 1.$$

Acceptor: An impurity element in a p-type semiconductor that may become ionized by taking an electron from the valence band and induce conduction by holes. For example, boron with a valence of three is a possible acceptor impurity in silicon (valence, four).

Afterpulse: A spurious pulse induced in a photomultiplier by a previous pulse. (112)

Angle of incidence: The angle between a ray of light striking a surface and the normal to that surface.

Angstrom unit, Å: 10^{-10} meter, or 0.1 nanometer. In the International System of Units (SI units), the nanometer or micrometer is the preferred unit for use in specification of wavelengths of light.

Anode: An electrode through which a principal stream of electrons leaves the interelectrode space. In a photomultiplier, the anode is operated at a voltage positive with respect to that of the last dynode and collects the secondary electrons emitted from the last dynode. (112)

Anticoincidence circuit: A circuit that produces a specified output signal when one (frequently predesignated) of two inputs receives a signal and the other receives no signal within an assigned time interval. (112)

Background counts (in radiation counters): Counts caused by ionizing radiation coming from sources other than that to be measured. (112)

Bandwidth: In electrical measurements, the difference between limiting frequencies in a frequency band, expressed in hertz (cycles per second). The noise equivalent bandwidth is the bandwidth of a rectangular equivalent spectrum and may be defined as

$$B = \frac{1}{A^2} \int_0^\infty |H(j\omega)|^2 df$$

where $H(j\omega)$ is the transfer function of the circuit, A is the maximum absolute value of $H(j\omega)$, and f and ω are frequency and angular frequency. (110)

Bleeder: Resistive voltage divider.

Cage: Part of a photomultiplier including the dynodes, focusing structure, anode, and support members.

Candela, cd: The SI unit of luminous intensity .

Cathode: See Photocathode.

CAT-Scanner or CT-Scanner: Computerized Axial Tomography - scanner; a medical X-ray equipment which provides a cross-sectional density map of a patient. In a typical device, an X-ray fan beam incident

on and rotating around the patient is detected by a large array of scintillation crystals and photomultiplier tubes.

Cerenkov radiation: Radiation generated by a high-energy charged particle moving through a dielectric with a velocity greater than the velocity of light in the dielectric (i.e., greater than c/n where n is the index of refraction of the dielectric).

Channel, channel number: In scintillation counting, a number proportional to pulse height specifying a generally narrow range of pulse heights.

Channel multiplier: A tubular **electron-**multiplier having a continuous interior surface of secondary-electron emissive material. **(107)**

Coincidence circuit: A circuit that produces a specified output signal when and only when a specified number (two or more) or a specified combination of input terminals receives signals within an assigned time interval. (112)

Collection efficiency: The fraction of electrons emitted by the photocathode of a photomultiplier that lands on the first dynode. Or more generally, the fraction of electrons emitted by one electrode that lands on the next electrode (dynode or anode).

Color temperature: The temperature of a black body radiator such that its chromaticity is the same as that of the light under consideration. (109)

Conduction band: A partially filled energy band in which the electrons can move freely, allowing the material to carry an electric current. The term is usually restricted to semiconductors and insulators, where the conduction band is normally empty and is separated by an energy-gap from the full bands below it. **(109)**

Count (in radiation counters): A single response of the counting system. (112)

Counting efficiency (scintillation counters): The ratio of (1) the average number of photons or particles of ionizing radiation that produce counts to (2) the average number incident on the sensitive area. (112)

Crosstalk: As applied to photomultipliers used in liquid scintillation counting, light originating internally in one photomultiplier and transmitted to another, causing coincident background pulses.

Crystal: See Scintillator.

Curie, Ci: A unit of radioactivity defined as the quantity of an radioactive nuclide in which the number of disintegrations per second is 3.7 x 10^{10}. **(B4)**

Current amplification (photomultipliers): The ratio of (1) the output signal current to (2) the photoelectric signal current from the photocathode. (112)

Dark current: That current flowing in the cathode circuit (cathode dark current) or in the anode circuit (anode dark current) in the absence of light or radiation in the spectrum to which the photomultiplier is sensitive.

Delay line: A transmission line for introducing signal time delay. (112)

Delta function (Dirac Delta Function): A function $\delta(u)$ such that $\delta(u) = 0$ for $u \neq 0$, and $\int \delta(u)\, du = 1$, when the integration is carried out over the full range of the variable. Pulsed light sources are sometimes referred to as **delta light sources** when the length of the pulse is short with respect to the response time of the photomultiplier or detecting instrument.

Detectivity, D: Reciprocal noise equivalent power, NEP; it is expressed in W^{-1}. **Detectivity** is a figure of merit providing the same information as NEP but describes the characteristic such that the **lower** the radiation level to which the photodetector can respond, the higher the **detectivity.** See **Noise Equivalent Power. (108)**

Discriminator, constant-fraction pulse-height: A pulse-height discriminator in which the threshold changes with input amplitude in such a way that the triggering point corresponds to a constant fraction of the input pulse height. (112)

Discriminator, pulse-height: A circuit that produces a specified output signal if and only if it receives an input pulse whose amplitude exceeds in one case or is less than an assigned value in another case. (112)

Donor: An impurity element in an n-type semiconductor that may become ionized by losing an electron to the conduction band and induce conduction by electrons. For example, phosphorus with a valence of five is a possible donor impurity in silicon (valence, four).

Dynode: An electrode that performs a useful function, such as current amplification, by means of secondary emission. (107)

EADCI, Equivalent Anode Dark Current Input: The input flux in lumens or watts at a specific wavelength which results in an increase in the anode current of a photomultiplier tube just equal to the anode dark current.

E^2/B: A figure of merit used to evaluate performance of liquid scintillation counters. **E** is the counting efficiency in per cent. **B** is the number of background coincident counts per minute.

Electron affinity, E_A: The energy, usually expressed in electron volts, required to move an electron from the bottom of the conduction band to the vacuum level.

Electron multiplier: That portion of the photomultiplier consisting of dynodes that produce current amplification by secondary electron emission. (112)

Electron resolution: The ability of the electron multiplier section of the photomultiplier to resolve inputs consisting of n and n + 1 electrons. This ability may be expressed as a fractional FWHM of the n^{th} peak, or as the peak-to-valley ratio of the n^{th} peak to the valley between the n^{th} and the $(n+1)^{th}$ peaks. (112)

Electron volt: The energy received by an electron in falling through a potential difference of one volt. (108)

Equivalent Noise Input, ENI: That value of input radiant or luminous flux that produces an rms signal current that is just equal to the rms value of the noise current in a specified bandwidth (Usually 1 Hz). See **Noise Equivalent Power. (108)**

Exitance: The density of radiant flux emitted from a surface. **Radiant exitance** is the integral of radiant flux over all wavelengths with units of watt per square meter. **Luminous exitance** is the total of all luminous flux from a surface with units of lumen per square meter. **Spectral radiant exitance** is the exitance at a particular wavelength for a specified wavelength interval; units are watt per square meter and micrometer. The term **emittance** (now deprecated) is synonomous with exitance. Sometimes the term exitance is used to indicate the density of radiant flux **incident** upon a surface. It is recommended, however, that the use of the term exitance be restricted to emission **from** a surface because terms such **as irradiance, spectral irradiance,** and **illuminance** are commonly used to indicate flux density incident on a surface.

Extended Red Multi-Alkali, ERMA: A designation of a Na_2K Sb:Cs photocathode processed to obtain increased **red-near-infrared** response.

Fall time: The mean time difference of the trailing edge of a pulse between the 90- and 10-per cent amplitude points.

Fatigue: The tendency of a photomultiplier responsivity to decrease during operation. Most commonly, responsivity loss is the result of a lowering of secondary emission, particularly in the latter stages of a photomultiplier. Recovery may or may not occur during a period of idleness.

Fermi level: The value of the electron energy at which the Fermi distribution function has the value one-half. (107)

Focusing electrode: An electrode whose potential is adjusted to control the **cross-sectional** area of the electron beam. (112)

Flying-Spot Scanner: A system for generating video signals for a television display. In a typical conception, the scanned raster of a cathode-ray tube is focused onto a photographic transparency. The modulated transmitted light signal is directed onto the **photocathode** of a photomultiplier tube which provides the electrical video signal.

Footcandle: A unit of illuminance equal to one lumen per square foot. The SI unit of **illuminance,** the lux (lumen per square meter), is preferred. (108)

Footlambert: A unit of luminance equal to π^{-1} **candela per square foot. The SI unit,** the candela per square meter (nit), is preferred. (108)

Forbidden band: In the band theory of solids, a range of energies in which there are no electronic levels. (109)

Full Width at Half Maximum, FWHM: The full width of a distribution measured at half the maximum ordinate. For a normal distribution it is equal to $2(2 \ln 2)^{1/2}$ times the **standard deviation σ. (112)**

Gain (photomultipliers). See Current Amplification.

Gamma-ray camera: A device used in nuclear medicine to image distributions of gamma-ray emitters. In a typical instrument, gamma rays emanating from tracer elements introduced into the patient are collimated and cause scintillations in a single large, thin sodium iodide crystal. An array of photomultiplier tubes views the crystal and provides addressing information with which an output image of dots is constructed on a cathode-ray tube.

Hertz: Hz, the SI unit of frequency equivalent to cycle per second. (108)

Hysteresis: A borrowed term to describe a cyclic gain variation in photomultipliers sometimes observed as a result of insulator charging and discharging.

Illuminance: The density of the luminous flux on a surface; it is the quotient of the flux by the area of the surface when the latter is uniformly illuminated. The SI unit is the lux, lumen per square meter. (109)

Irradiance: The density of radiant flux on a surface; it is the quotient of the flux by the area of the surface when the latter is uniformly irradiated. The SI unit is the watt per square meter.

Lambert's cosine law: A law stating that the flux per solid angle in any direction from a plane surface varies as the cosine of the angle between that direction and the perpendicular to the surface. (107)

Light pipe: An optical transmission element that utilizes unfocused transmission and reflection to reduce photon losses. (112)

Liquid scintillation counter: The combination of a liquid scintillator and one or more (usually two) photomultiplier tubes used to measure or count radioactive disintegrations. The most common application is the counting of beta rays emanating from a sample mixed with the liquid scintillator.

Lumen, lm: The SI unit of luminous flux. It is equal to the flux through a unit solid angle (steradian) from a uniform point source of one candela. (107, 108)

Luminance: The luminous intensity per projected area normal to the line of observation. Formerly called **photometric brightness or brightness. (108)**

Luminous efficacy: The quotient of the total luminous flux by the total radiant flux. It is expressed in lumens per watt. For example, the maximum luminous efficacy of a black body (which occurs at about 6600 K) is 95 lumens per watt. (108)

Luminous efficiency: The ratio of the luminous efficacy of a given source to the maximum spectral luminous efficacy. For example, the maximum luminous efficiency of a black body (which occurs at about 6600 K) is 95 lumens per watt/680 lumens per watt = 0.14.

Luminous intensity: The luminous flux per unit solid angle in the direction in question. It is expressed in **candelas** (lumens per **steradian**). (107)

Lux, **lx:** The SI unit of illuminance equal to the flux of one lumen uniformly distributed over an area of one square meter.

Microchannel plate: An array of small aligned channel multipliers usually used for intensification. (107)

Multichannel Analyzer, MCA: See Pulse-height analyzer.

Negative Electron Affinity, NEA: A term referring to an electron emitter whose surface has been treated with an electropositive material in such a way that the conduction band minimum lies above the vacuum level.

Nit: The name recommended by the International Commission on Illumination for the unit of luminance equal to one candela per square meter. Note: Candela per square meter is the unit of luminance in the International System of Units (SI). (107)

Noise (photomultiplier tubes): The random output that limits the minimum observable signal from the photomultiplier tube. (112)

Noise Equivalent Power, NEP: The radiant flux in watts incident on a detector which gives a signal-to-noise ratio of unity. The bandwidth and the manner in which the radiation is chopped must be specified as well as the spectral content of the radiation. The most common spectral specification is for monochromatic radiation at the peak of the detector response. (Some detector manufacturers rate their detectors in terms of an NEP having units of watts $Hz^{-1/2}$. Assuming that the noise spectrum is flat within the range of the specification and that NEP is normally specified for a bandwidth of one hertz, the two forms of NEP are numerically equal.) (108)

Noise&signal, (photomultiplier tubes): The noise output resulting from the statistical variation in the signal current itself as contrasted with that which may be present when the detector is in the dark.

Opaque photocathode: A photocathode wherein photoelectrons are emitted from the same surface as that on which the photons are incident. **(Also** called **reflective photocathode.)** (112)

Peak-to-valley ratio: In a **pulse-height**-distribution characteristic, the ratio of the counting rate at the maximum to that at the minimum-usually preceding the maximum.

Photocathode: An electrode used for obtaining photoelectric emission when irradiated. (112)

Photocell: A solid-state photosensitive electron device in which use is made of the variation of the current-voltage characteristic as a function of incident radiation. (112)

Photomultiplier, PMT: A phototube with one or more dynodes between its photocathode and output electrode. (112)

Photon counting: The technique, using a photomultiplier, of counting output pulses originating from single photoelectrons.

Photopic vision: Vision mediated essentially or exclusively by the cones. It is generally associated with adaptation to luminance of at least 3 **candelas** per square meter. (107)

Phototube: An electron tube that contains a photocathode and has an output depending at every instant on the total photoelectric emission from the irradiated area of the photocathode. (112)

Plateau: (counter): The portion of the counting-rate-versus-voltage characteristic curve in which the counting rate is substantially independent of the applied voltage. (109)

Pulse-height analyzer, PHA: An instrument capable of indicating the number or rate of occurrence of pulses falling within each of one or more specified amplitude ranges. **(112)**

Pulse-height distribution: A histogram displaying the pulse count versus channel number as obtained with a multichannel analyzer, particularly as applied to scintillation counting.

Pulse-height resolution, PHR: The ratio of the full width at half maximum of the **pulse**-height-distribution curve to the pulse height corresponding to the maximum of the distribution curve. In scintillation spectroscopy, it is customary to state pulse-height resolution as a percentage. (112)

Pulse jitter: A relatively small variation of the pulse spacing in a pulse train. In photomultipliers, pulse jitter is the result of electron transit time variations. (109)

Pulse width: The time interval between the first and last instants at which the instantaneous amplitude reaches a stated fraction of peak pulse amplitude. (109)

Quantum efficiency (photocathodes): The average number of electrons photoelectrically emitted from the photocathode per incident photon of a given wavelength. (107)

Rad: A unit of absorbed radiation equal to 100 ergs per gram-O.01 J/kg in SI units. (109)

Radiance: The radiant flux per unit solid angle per unit of projected area of the source. The SI unit is the watt per steradian and square meter, $Wsr^{-1} m^{-2}$. (109)

Radiant intensity: The radiant flux proceeding from the source per unit solid angle in the direction considered. The SI unit is watt per steradian. (107)

Reflectance: The ratio of the radiant flux reflected from a body of material to that incident upon it. **(See Absorptance.)**

Reflective photocathode: A photocathode wherein photoelectrons are emitted from the same surface as that on which the photons are incident. **(Also** called **opaque photocathode.)**

Rem: Abbreviation for roentgen equivalent man. (1) In older usage, the dose (absorbed) of any ionizing radiation that will produce the same biological effect as that produced by one roentgen of high voltage x-radiation. (2) The unit of the RBE (relative biological effectiveness) dose that is equal to the absorbed dose in rads times the RBE. (109)

Resistance per square: The resistance of a square of a thin conductive coating measured between opposite sides of the square. The value is independent of the size of the square.

Responsivity: The ratio of the output current or voltage to the input flux in watts or lumens. For example, as applied to photomultipliers: radiant responsivity expressed in $mA\ W^{-1}$ at a specific wavelength or luminous responsivity expressed in $\mu A\ lm^{-1}$. (108)

Rise **time:** The mean time difference of the leading edge of a pulse between the 10- and 90-percent amplitude points.

Roentgen: A unit of X- or gamma-radiation exposure such that the associated secondary ionizing particles produce, in air, ions carrying one electrostatic unit of charge of either sign per 0.001293 gram of air. This quantity is the equivalent of 2.58×10^{-4} coulomb per kilogram of air. (109)

Scintillation counter: The combination of scintillator , photomultiplier, and associated circuitry for detection and measurement of ionizing radiation. (112)

Scintillator: The body of scintillator material together with its container. (107)

Scotopic vision: Vision mediated essentially or exclusively by the rods. It is generally associated with adaptation to luminance below about 0.03 candela per square meter. (107)

Secondary emission: Electron emission from solids or liquids due directly to bombardment of their surfaces by electrons or ions. (107)

Secondary emission ratio (electrons): The average number of electrons emitted from a surface per incident primary electron. **Note:** The result of a sufficiently large number of events should be averaged to ensure that statistical fluctuations are negligible. (107)

Semitransparent photocathode: A photocathode in which radiant flux incident on one side produces photoelectric emission from the opposite side. Synonymous with **Transmission-mode photocathode.** (112)

Sensitivity: See Responsivity, the preferred term.

Spectral luminous efficacy (radiant flux): The quotient of the luminous flux at a given wavelength by the radiant flux at that wavelength. It is expressed in lumens per watt. The maximum spectral luminous efficacy, $K(\lambda)_{max}$, is 680 lumens per watt at a wavelength of 555 nm. (107)

Spectral luminous efficiency (radiant flux): The ratio of the spectral luminous efficacy for a given wavelength to the maximum spectral luminous efficacy. Accordingly, the spectral luminous efficiency, V(X), is the ratio $V(X) = K(X)/680$ and is identical to the standard visibility factor of the photopic human eye and to the y-tristimulus value $(\bar{y}_\lambda)$ for the standard observer in the CIE tristimulus system. (107, 111)

Spectral radiant intensity: Radiant intensity per unit wavelength interval; for example, watts per (steradian-nanometer). (107)

Stage: One step of a multiplier, as one dynode stage.

Stem: The portion of a photomultiplier envelope containing the leads to electrodes.

Steradian: The unit of solid angle which subtends an area equal to the square of the radius. (107)

Tea-cup: Descriptive term for an RCA photomultiplier type having a large cup-shaped first dynode.

Time jitter: See Transit-time spread.

Time-to-amplitude converter, TAC: An instrument producing an output pulse whose amplitude is proportional to the time difference between start and stop pulses. (112)

Traceability: Process by which the assigned value of a measurement is compared, directly or indirectly, through a series of calibrations to the value established by the U.S. national standard. (107)

Transit time: For a discussion of the several definitions of this term, refer to the section "Time Effects" in Chapter **4. Photomultiplier Characteristics.**

Transit-time spread: The FWHM (full-width-at-half maximum) of the time distribution of a set of pulses each of which corresponds to the photomultiplier transit time for that individual event. (112)

Transmission-mode photocathode: A photocathode in which radiant flux incident on one side produces photoelectric emission from the opposite side. Synonymous with **Semitransparent photocathode.** (112)

Transmittance: The ratio of the radiant flux transmitted through a body of material to

that incident upon it. **See Absorptance.**

Vacuum level: The minimum potential energy level an electron must reach to escape entirely from the attraction of a solid or an atom.

Valence band: The range of energy states in the spectrum of a solid crystal in which lie the energies of the valence electrons that bind the crystal together. (107)

Venetian-blind dynode: A descriptive term for a photomultiplier dynode structure. The dynode is constructed with a number of parallel slats with space between permitting secondary electrons to be directed to the next stage.

Voltage divider (photomultiplier): A series string of resistors across which a voltage is applied providing an appropriate voltage drop per stage.

Work function: The minimum energy required to remove an electron from the Fermi level of a material into field-free space. (107)

REFERENCES

107. IEEE Standard Dictionary of Electrical and Electronics Terms, Wiley-Interscience.

108. **RCA Electro-Optics Handbook,** EOH-11.

109. **The International Dictionary of Physics and Electronics,** D. Van Nostrand.

110. **Information Transmission, Modulation, and Noise,** Mischa Schwartz, McGraw-Hill, 1959.

111. Leo Levi, **Applied Optics, Vol. 1,** John Wiley and Sons, Inc., 1968.

112. **An American National Standard, IEEE Standard Test Procedures for Photomultipliers for Scintillation Counting and Glossary for Scintillation Counting Field.** ANSI N42.9-1972; IEEE Std 398-1972.

Appendix C—
Spectral Response Designation Systems

The spectral response of a photomultiplier tube depends primarily on the chemical components of the photocathodes. Differences in spectral response, however, can result from variations in the processing of photocathodes even for the same chemicals. Some photocathodes are of the "opaque" or "reflective" type where the photoemission is from the same side as the excitation. Others, having essentially the same chemistry but of the "semitransparent" type where the photoemission is from the side opposite from that of the excitation, may have a somewhat different spectral response. The short-wavelength-cutoff characteristic of the spectral response is the result of the transmission characteristic of the particular glass used for the photocathode window.

S-Designation System

In the early 1940's, the JEDEC (Joint Electron Devices Engineering Council) industry committee on photosensitive devices developed the "W-system of designating spectral responses. The philosophy included the idea that the product user need only be concerned about the response of the device, not by how it might be fabricated. And, in fact, the chemical compositions of some of the photocathodes and dynodes were considered proprietary by various manufacturers. S-numbers were registered from S-l through S-40. See Table C-I. Subsequently, the lack of activity of the industry committee on photosensitive devices resulted in independent assignment of codes for spectral responses. In other cases, the spectral response was described by a curve and an actual description of the photocathode composition and of the window material.

The following material is a brief account of the different designation systems and their relationship and meaning. This information is of value to the photomultiplier user because it will help in the interpretation of the published spectral characteristics data for a specific tube type regardless of which response designation system is used.

Numerical System

In 1971 RCA/BURLE introduced a numerical system of spectral response designations supplementing and overlapping the JEDEC S-designation system. The reason for this extended system was the proliferation of spectral responses resulting from the combinations of different glasses, new photocathode types, and processing variations. Table C-II is a catalogue of this 1971 numbering system providing an identification and description of each number.

Alphanumeric Coded System

In 1976, RCA/BURLE changed its number system for spectral-response characteristics to an alphanumeric combination coded system. The new designations were combinations of alphanumerics based on (1) the photocathode material, (2) the window material, and (3) the photocathode operating mode. Table C-III provides the code for the spectral response designation in four columns. The first two digits in the designation number (Column I) indicate the photocathode material; the following alphabetic character (Column II) indicates the window material; the next alphabetic character (Column III) indicates the photocathode operating mode. Where required, the letter "X" is used as a suffix to the designation to indicate an extended response in the red or near infrared.

As an example of the usage of this system, tube type 931A has a spectral response that was previously designated as 102 (S-4) in Table C-II. This tube type has a Cs_3Sb photocathode, a 0080 lime glass window,

and a reflection-type photocathode. Its designation according to the 1976 code system is 20AR.

Similarly, a tube type having a Cs_3Sb photocathode, a 0080 glass window, and a transmission-type photocathode is designated 20AT. This response was previously designated 107 (S-l 1).

Current Practices

When the coded spectral response designation system was devised in 1976, it was anticipated that all the information provided by the code would be useful to customers in specifying the type of photomultiplier needed. Experience has indicated that very few are sufficiently acquainted with the code to make good use of it. Instead, most knowledgeable customers prefer to be informed directly of the nature of the photocathode and the window. As a result, therefore, BURLE has discontinued the use of coded spectral response designations except for occasional reference to some of the more common JEDEC S-numbers, which have become well established. Instead, reference is made to the photocathode material, the window material, and any special processing information. In addition, typical spectral response and other related data are provided .

Table C-I Spectral Response Designations as Specified by JEDEC

S-Designation	Photocathode Composition	Window*	Notes
S-l	Ag-O-Cs	lime glass	semitransparent or opaque
S-2	(Obsolete; formerly similar to S-l)		
S-3	Ag-O-Rb	lime glass	opaque
S-4	Cs_3Sb	lime glass	opaque
S-5	Cs_3Sb	Corning 9741	opaque
S-6	Na	uv transmitting	opaque
S-7	Ag-O-Rb-Cs	borosilicate	opaque
S-8	Cs_3Bi	lime glass	opaque
S-9	(Obsolete; formerly similar to S-l1)		
S-10	Ag-Bi-O-Cs	lime glass	semitransparent
S-11	Cs_3Sb	lime glass	semitransparent
S-12	(CdS - a photoconductive crystal)		
S-13	Cs_3Sb	fused silica	semitransparent
S-14	(Ge - photovoltaic)		
S-15	(CdS-CdSe - a photoconductor)		
S-16	(CdSe - a photoconductor)		
S-17	Cs_3Sb	lime glass	opaque with reflecting substrate
S-18	(Sb-S - photoconductor, camera tubes)		
S-19	Cs_3Sb	fused silica	opaque
S-20	$Na_2KSb:Cs$	lime glass	semitransparent
S-21	Cs_3Sb	Corning 9741	semitransparent
S-22	(Not used)		
S-23	Rb-Te	fused silica	semitransparent
S-24	(Not used)		
S-25	$Na_2KSb:Cs$	lime glass	semitransparent, processed for extended red response
S-26	(InSb - photovoltaic)		
S-27	(Ge:Au - photoconductive)		
S-28	(InAs - photovoltaic)		
S-29	(PbSe - photoconductive)		
S-30	(Ge:Cu - photoconductive)		
S-31	(PbS - photoconductive)		
S-32	(PbS - photoconductive)		
S-33	(PbS - photoconductive)		
S-34	(InAs - photovoltaic)		
S-35	(InSb - photoconductive)		
S-36	(GaAs - photovoltaic)		
S-37	(Si - photovoltaic)		
S-38	(PbSe - photoconductive)		
S-39	(PbSe - photoconductive)		
S-40	(Ge:Hg - photoconductive)		

***Window may be of material other than that specified, but it will have equivalent spectral characteristics.**

References: 113, 114

Table C-II RCA/BURLE 1971 Spectral Response Numbering Code

Number	JEDEC S-Designation	Photocathode Composition	Window	Notes
101	S-l	**Ag-o-cs**	lime glass	
102	S-4	Cs_3Sb	lime glass	
103		**Cs_3Sb**	Corning 9741 glass	**uv** transmitting
104	S-5	Cs_3Sb	Corning 9741 glass	**uv** transmitting
105	S-8	Cs-Bi	lime glass	
106	S-10	Ag-Bi-O-Cs	lime glass	
107	S-l 1	Cs_3Sb	lime glass	
108	S-13	Cs_3Sb	**SiO_2**	
109	S-19	Cs_3Sb	**SiO_2**	
110	S-20	**$Na_2KSb:Cs$**	Borosilicate glass	
111		**$Na_2KSb:Cs$**	lime glass	
112		**$Na_2KSb:Cs$**	Corning 9823 glass	uv transmitting
113		**$Na_2KSb:Cs$**	Pyrex	
114		**$Na_2KSb:Cs$**	**SiO_2**	
115		K_2CsSb	Lime or **boro-** silicate glass	
116		K_2CsSb	Pyrex	
117		**K_2CsSb**	Corning 9823 glass	uv transmitting
118		K_2CsSb	Corning 9741 glass	uv transmitting
119		**$Na_2KSb:Cs$**	Pyrex	extended red: ERMA III
120		K_2CsSb	Sapphire, uv grade	
121		Cs-Te	**SiO_2**	
122		**K_2CsSb**	Al_20_3	
123		Cs_3Sb	Sapphire, uv grade	
124		**Cs_3Sb**	Corning 9741 glass	
125		Cs-Te	**LiF**	
126		**K_2CsSb**	Borosilicate or lime glass	
127		Ag-Bi-O-Cs	Corning 9741 glass	
128		Ga-As	Corning 9741 glass	
129		Ga-As-P	Corning 9741 glass	
130		**$Na_2KSb:Cs$**	Borosilicate or lime glass	
131		**$Na_2KSb:Cs$**	Borosilicate glass	extended red: ERMA III
132		**$Na_2KSb:Cs$**	Lime or borosilicate glass	extended red: ERMA II
133		K_2CsSb	**SiO_2**	
134		Ga-As	Sapphire, uv grade	
135		Ga-As-P	Sapphire, uv grade	
136		K_2CsSb	Lime glass	

Table C-II RCA/BURLE 1971 Spectral Response Numbering Code (cont'd)

Number	JEDEC S-Designation	Photocathode Composition	Window	Notes
137		$Na_2KSb:Cs$	Corning 9741 glass	extended red: ERMA II
138		$Na_2KSb:Cs$	Corning 9741 glass	extended red: ERMA I
139		Na_2KSb	Borosilicate glass	high temperature
140		$In_{.06}$-$Ga_{.94}$-As	Corning 9741 glass	Type I
141		$In_{.12}$-Ga-$_{.88}$-As	Corning 9741 glass	Type II
142		$In_{.18}$-$Ga_{.82}$-As	Corning 9741 glass	Type III

Table C-III RCA/BURLE 1976 Coded System for Spectral Response Designation

Column I

10 = AgOCs
15 = AgBiOCs
20 = CsSb
25 = CsBi
30 = CsTe
35 = KCsSb (Bialkali)
40 = NaKSb (High temperature bialkali)
45 = RbCsSb
50 = NaKCsSb (Multialkali)
51 = NaKCsSb (ERMA I)
52 = NaKCsSb (ERMA II)
53 = NaKCsSb (ERMA III)
60 = GaAs
71 = InGaAs (Type I)
72 = InGaAs (Type II)
73 = InGaAs (Type III)

Column II

A = 0080 (lime glass) or 7056 (Borosilicate glass)
C = 7740 (Pyrex)
E = 9741 (UV transmitting glass)
G = 9823 (UV transmitting glass)
J = SiO_2 (Fused silica)
M = UV-grade Sapphire
P = LiF

Column III

D = Dormer-window type
R = Reflection Type
T = Transmission Type

Column IV

X = Extended Response

REFERENCES

113. "Relative spectral response data for photosensitive devices ("S" curves)", JEDEC Publication No. 50, Electronic Industries Association, Engineering Department, 2001 Eye Street, N.W., Washington, D.C. 20006 (1964)

114. "Typical characteristics of photosensitive surfaces," JEDEC Publication No. 61, Electronic Industries Association, Engineering Department, 2001 Eye Street, N. W., Washington, D.C. 20006. (1966)

Appendix D—
Photometric Units and Photometric-to-Radiometric Conversion

Photometry is concerned with the measurement of light. Because the origins of the photoelectric industry were associated with the visible spectrum, the units first used for evaluating photosensitive devices were photometric. Today, however, even though many of the applications of photosensitive devices are for radiation outside the visible spectrum, the photometric units are still retained for many purposes. Because these units are based on the characteristics of the eye, this discussion begins with a consideration of some of these characteristics.

CHARACTERISTICS OF THE EYE

The sensors in the retina of the human eye are of two kinds: "cones" which predominate the central (or foveal) vision and "rods" which provide peripheral vision. The cones are responsible for our color vision; rods provide no color information but in the dark-adapted state are more sensitive than the cones and thus provide the basis of dark-adapted vision. Because there are no rods in the fovea1 region, faint objects can more readily be observed at night when the eye is not exactly directed toward the faint object. The response of the light-adapted eye (cone vision) is referred to as the Photopic eye response; the response of the dark-adapted eye (rod vision) is referred to as Scotopic eye response.

Although characteristics of the human eye vary from person to person, standard luminosity coefficients for the eye were defined by the Commission Internationale d'Eclairage (International Commission on Illumination) in 193 1. These standard C . I. E. luminosity coefficients for photopic vision are given in Table D-I. They represent the relative luminous equivalents of an equal-energy spectrum for each wavelength in the visible range, assuming foveal vision. An absolute "sensitivity" figure established for the standard eye relates photometric units and radiant power units. At 555 nanometers, the wavelength of maximum sensitivity of the eye, one watt of radiant power corresponds to approximately 680 lumens. The quotient of the luminous flux at a given wavelength by the radiant flux at that wavelength is referred to as the **Spectral Luminous Efficacy ,**

$$K(\lambda) = \Phi v_\lambda / \Phi e_\lambda (\mathrm{lm\,W^{-1}}) \qquad \text{D-l}$$

Various determinations of the maximum value, K (555 nanometers), have varied somewhat from the nominal value of 680 lumens per watt.

For the dark-adapted eye, the peak sensitivity increases and is shifted toward the violet end of the spectrum. A tabulation of the relative scotopic vision is also given in Table D-I. The peak luminosity for scotopic vision occurs at 511 nanometers and is the equivalent of 1746 lumens/watt. Fig. D-l shows the comparison of the absolute luminosity curves for scotopic and photopic vision as a function of wavelength.

The sensitivity of the eye outside the wavelength limits shown in Table D-I is very low, but not actually zero. Studies with intense infrared sources have shown that the eye is sensitive to radiation of wavelength at least as long as 1050 nanometers. Fig. D-2 shows a composite curve given by Griffin, Hubbard, and Wald[115] for the sensitivity of the eye for both foveal and peripheral vision from 360 to 1050 nanometers. According to Goodeve[116] the ultraviolet sensitivity of the eye extends to between 302.3 and 312.5 nanometers. Below this level the absorption

Table D-I
Relative Luminosity Values for Photopic and Scotopic Vision

Wavelength (nm)	Photopic Vλ ($B>3$ cd m^{-2})	Scotopic Vλ ($B < 3 \times 10^{-5}$ c d m^{-2})
350	—	0.0003
360	—	0.0008
370	—	0.0022
380	0.00004	0.0055
390	0.00012	0.0127
400	0.0004	0.0270
410	0.0012	0.0530
420	0.0040	0.0950
430	0.0116	0.157
440	0.023	0.239
450	0.038	0.339
460	0.060	0.456
470	0.091	0.576
480	0.139	0.713
490	0.208	0.842
500	0.323	0.948
510	0.503	0.999
520	0.710	0.953
530	0.862	0.849
540	0.954	0.697
550	0.995	0.531
560	0.995	0.365
570	0.952	0.243
580	0.870	0.155
590	0.757	0.0942
600	0.631	0.0561
610	0.503	0.0324
620	0.381	0.0188
630	0.265	0.0105
640	0.175	0.0058
650	0.107	0.0032
660	0.061	0.0017
670	0.032	0.0009
680	0.017	0.0005
690	0.0082	0.0002
700	0.0041	0.0001
710	0.0021	—
720	0.00105	—
730	0.00052	—
740	0.00025	—
750	0.00012	—
760	0.00006	—
770	0.00003	—

of radiation by the proteins of the eye lens apparently limits further extension of vision into the ultraviolet. Light having a wavelength of 302 nanometers is detected by its fluorescent effect in the front part of the eye.

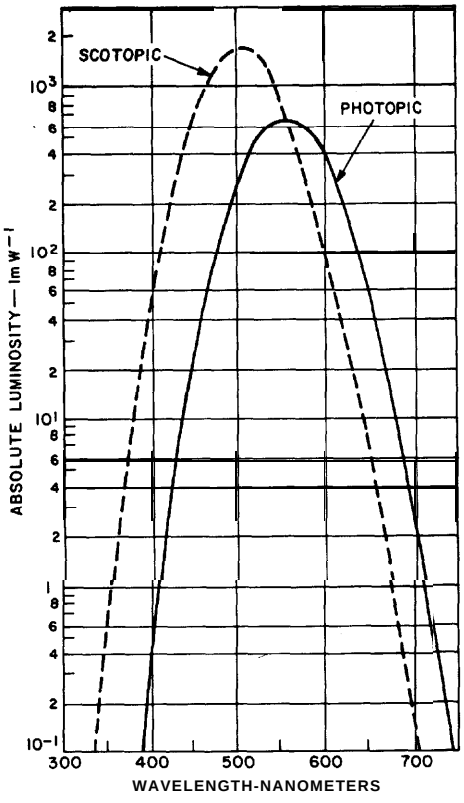

Fig. D-7 - Absolute luminosity curves for scotopic and photopic eye response.

PHOTOMETRIC UNITS

Luminous intensity (or candlepower) describes luminous flux per unit solid angle in a particular direction from a light source. The measure of luminous intensity is the fundamental standard from which all other photometric units are derived. The standard of luminous intensity is the **candela;** the older term candle is sometimes still used, but refers to the new candle or candela.

The candela is defined by the radiation from a black body at the temperature of solidification of platinum. **A** candela is **one**-sixtieth of the luminous intensity of one square centimeter of such a radiator.

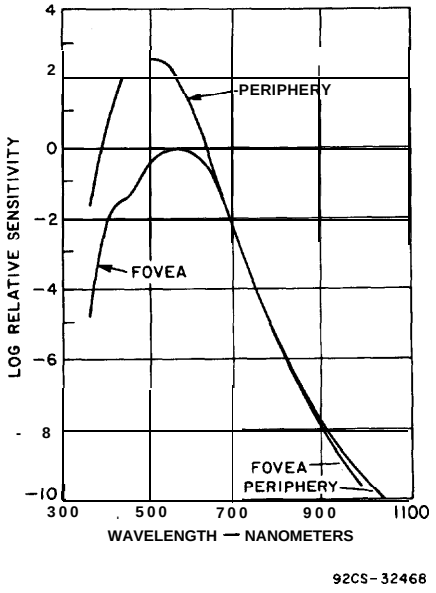

Fig. D-2 - Relative spectral sensitivity of the dark-adapted foveal and peripheral retina.

A suitable standard for practical photoelectric measurements is the AJ2239 calibrated lamp, which operates at a current of about 4.5 amperes and a voltage of 7 to 10 volts. A typical lamp calibrated at a color temperature of 2856 **K** provides a luminous intensity of 55 candelas. The luminous intensity of a tungsten lamp measured in candelas is usually numerically somewhat greater than the power delivered to the lamp in watts.

A color temperature of 2870 K served as the basic test standard in this country for about 30 years. A change had been made to agree with C.I.E. illuminant A, a more widespread standard that at first required a color temperature of 2854 K, but has more recently been adjusted to 2856 **K** to accommodate to the international practical temperature scale of **1968.** See also Appendix F. The difference between the old lamp standard at 2870 **K** and at the new temperature is generally negligible. [117]

Luminous flux is the rate of flow of light energy, the characteristic of radiant energy that produces visual sensation. The unit of luminous flux is the **lumen,** which is the flux emitted per unit solid angle by a uniform point source of one candela. Such a source **produces a total luminous flux of 4π lumens.**

A radiant source may be evaluated in terms of luminous flux if the radiant-energy

distribution of the source is known. If W(λ) is the total radiant power in watts per unit wavelength, total radiant power over all wavelengths is $\int_0^\infty W(\lambda)\, d\lambda$, and the total luminous flux Φ in lumens can be expressed as follows:

$$\Phi = 680 \int_0^\infty W(\lambda)\, V(\lambda)\, d\lambda \qquad \text{D-2}$$

where V(λ) represents the spectral luminous efficiency. The lumen is the most widely used unit in the rating of photoemissive devices. For photomultipliers, the typical test levels of luminous flux range from 10^{-7} to 10^{-5} lumen (0.1 to 10 microlumens).

Illuminance (or **illumination)** is the density of luminous flux incident on a surface. A common unit of illuminance is the **footcandle,** the illumination produced by one lumen uniformly distributed over an area of one square foot. It follows that one candela produces an illuminance of one footcandle at a distance of one foot. The preferred SI unit (International System of Units) of **illuminance** is the lux, which is the illumination produced by one lumen uniformly distributed over an area of one square meter. (1 lx = 1 lm m^{-2}) It also follows that one candela produces an illuminance of one lux at a distance of one meter.

1 lux = 0.0929 footcandle

Table D-II lists some common values of illuminance. Further information concerning natural radiation is shown in Fig. D-3 which indicates the change in natural illumination at ground level during, before, and after sunset for a condition of clear sky and no moon.[118]

Photometric luminance (or brightness) is a measure of the luminous flux per unit solid angle leaving a surface at a given point in a given direction, per unit of projected area. The term photometric luminance is used to distinguish a physically measured luminance from a subjective brightness. The latter varies with illuminance because of the shift in spectral response of the eye toward the blue region at lower levels of illuminance. The term luminance describes the light emission from a surface, whether the surface is self-luminous or receives its light from some external luminous body.

Table D-II
Typical Values of Natural Scene Illuminance

Sky Condition	Approx. Levels of Illuminance-lux (lm m-2)
Direct sunlight	1-1.3 x 10^5
Full daylight (not direct sunlight)	1-2 x 10^4
Overcast day	10^3
Very dark day	10^2
Twilight	10
Deep twilight	1
Full moon	10^{-1}
Quarter moon	10^{-2}
Moonless, clear night sky	10^{-3}
Moonless, overcast night sky	10^{-4}

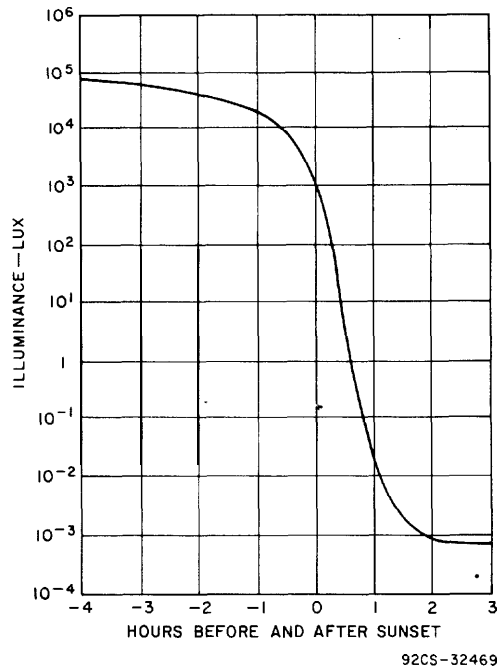

Fig. D-3 - Natural illuminance on the earth for the hours immediately before and after sunset with a clear sky and no moon.

For a surface that is uniformly diffusing, luminance is the same regardless of the angle from which the surface is viewed. This condition results from the fact that a uniformly diffusing surface obeys Lambert's Law (the cosine law) of emission. Thus, both the emission per unit solid angle and the projected area are proportional to the cosine of the angle between the direction of observation and the surface normal.

The SI unit of luminance is the **candela per square meter** or a lumen per steradian and square meter. This unit is called the nit. A commonly used unit of luminance is the **footlambert, which is equal to $1/\pi$ candela** per square foot.

1 nit = 0.2919 footlambert

The relationship between luminance and total luminous flux from a uniform diffuser is illustrated by the use of Fig. D-4.

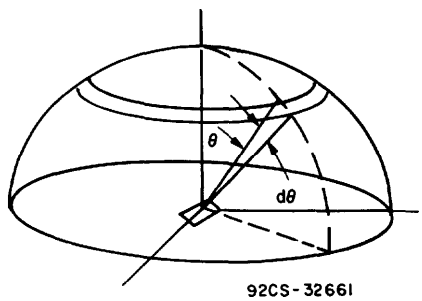

Fig. D-4 - Diagram illustrating Lambert's law and the calculation of total luminous flux from a diffuse radiator.

Consider an elementary portion of the diffusing surface having an area, **A,** and a luminance of L. The projected area at the **angle, θ, is A cos θ. The solid angle represented by the differential area on the surface of the hemisphere is 2π sin θ dθ. The** luminance, L, represents the luminous flux per unit solid angle leaving the surface per unit of projected area. Therefore, the flux **into the differential area defined by dθ, is**

$$2\pi \, AL \sin\theta \cos\theta \, d\theta,$$

and the total flux from the area, A, is given by

$$\phi = \int_0^{\pi/2} 2\pi \, AL \sin\theta \cos\theta \, d\theta$$
$$= \pi \, AL \qquad \text{D-3}$$

Note that for a unit area of 1 meter^2, and a luminance of 1 nit, the total flux emitted is π lumens. When the unit is a footlambert ($1/\pi$ lumen per square foot and steradian), L/π must be substituted for L in Eq. D-3 and, in this case, the total flux emanating from one square foot is one lumen for a luminance of one footlambert. The use of the English system of units thus has the peculiar advantage that if an illuminance of 1 footcandle falls on a perfectly diffusing and reflecting surface, its luminance is 1 footlambert. As a result, an instrument reading illuminance in footcandles indicates photometric luminance in footlamberts if the instrument is illuminated essentially from the entire hemisphere. (This statement neglects the possible perturbation caused by the measurement instrument.)

On the other hand if a perfectly diffusing and reflecting surface is illuminated with 1 **lux, its luminance would be $1/\pi$ candelas per** square meter (nits).

Table D-III provides data on luminance values of various sources. Table D-IV is a conversion table for various photometric units.

Table D-III
Luminance Values for Various Sources

Source	Luminance (Footlamberts)	Luminance (Candelas m^{-2})
Sun, as observed from Earth's surface at meridian	4.7×10^8	1.6×10^9
Moon, bright spot, as observed from Earth's surface	730	2500
Clear blue sky	2300	7900
Lightning flash	2×10^{10}	7×10^{10}
Atomic fission bomb, 0.1 millisecond after firing, 90-feet diameter ball	6×10^{11}	2×10^{12}
Tungsten filament lamp, gas-filled, 16 lumen/watt	6×10^6	9×10^6
Plain carbon arc, positive crater	4.7×10^6	1.6×10^7
Fluorescent lamp, T-12 bulb, cool white, 430 mA, medium loading	2000	7000
Color television screen, average brightness	50	170

CALCULATION OF RADIANT RESPONSIVITY FROM LUMINOUS RESPONSITIVITY

Specification of photocathode responsivity is most frequently given in terms of lumens from a tungsten source at a color temperature of 2856 K. If a relative spectral response is known, it is possible to calculate the absolute radiant responsivity of the photocathode as follows.

Let the relative spectral response (with a maximum value of unity) of the photocathode be represented by $R(\lambda)$. Designate the absolute radiant response at the peak of the response curve by σ. The complete radiant response characteristic is then given by $\sigma R(\lambda)$. Let the spectral distribution of the lamp radiation striking the photocathode be given by $W(\lambda)$ in watts per unit wavelength. The response of the photocathode (in amperes) to the total radiation is then given by

$$\int \sigma R(\lambda)\, W(\lambda)\, d\lambda \qquad \text{D-4}$$

The integration is done over the complete range of wavelengths either as limited by $R(\lambda)$ or $W(\lambda)$.

The light flux (in lumens) represented by the total radiant flux is given by

$$680 \int V(\lambda)\, W(\lambda)\, d\lambda \qquad \text{D-5}$$

where $V(\lambda)$ is the spectral luminous efficiency as given in Table D-I and 680 lumens per watt is taken as the maximum spectral luminous efficacy.

The luminous responsivity of the photocathode in amperes per lumen is then given by the ratio of expressions D-4 and D-5:

$$S = \frac{\sigma \int R(\lambda)\, W(\lambda)\, d\lambda}{680 \int V(\lambda)\, W(\lambda)\, d\lambda} \qquad \text{D-6}$$

From Eq. D-6, the maximum radiant responsivity, σ, may be obtained in units of amperes per watt:

$$\sigma = \frac{680\, S \int V(\lambda)\, W(\lambda)\, d\lambda}{\int R(\lambda)\, W(\lambda)\, d\lambda} \qquad \text{D-7}$$

Note that the absolute magnitude of the function $W(\lambda)$ need not be known. For a test lamp operated at a color temperature of 2856 K, a tabulation of $W(\lambda)$ is given in Table F-I in Appendix F. The integrations indicated in Eq. D-7 have been performed for most photocathode spectral responses. A tabulation of the value σ/S, in lumens per watt, is provided in Table I. This factor represents the ratio of the peak radiant responsitivity in amperes per watt to the luminous responsivity in amperes per lumen.

Table D-IV
Conversion Table for Various Photometric Units

SI Units	Other Units
Luminous Intensity (I)	
1 candela (cd) = 1 lumen/steradian (lm sr^{-1})	
Luminous flux (Φ)	
lumen (lm); 4π lumens = total flux from uniform point source of 1 candela	
Illuminance (E)	
1 lux (lx) = 1 lumen/meter^2 (lm m^{-2})	1 footcandle (fc) = 1 lumen/foot^2
1 lux = 0.0929 footcandle	
Luminance (L)	
1 nit (nt) = 1 candela/meter^2 = 1 lm sr^{-1} m^{-2} (nit)	1 footlambert (fL) = $1/\pi$ candela/foot^2
1 nit = 0.2919 footlambert	

REFERENCES

115. D.R. Griffin, R. Hubbard, and G. Wald, "The sensitivity of the human eye to infrared radiation," **JOSA,** Vol. 37, No. 7, pp 546, (1947).

116. C.F. Goodeve, "Vision in the ultraviolet," **Nature** (1934)

117. R.W. Engstrom and A.L. Morehead, "Standard test lamp temperature for photosensitive devices-relationship of absolute and luminous sensitivities," **RCA Review,** Vol. 28, pp 419-423 (1967)

118. **I.E.S. Lighting Handbook,** Illuminating Engineering Society, New York, New York (1959).

Appendix E—
Spectral Response and Source-Detector Matching

This appendix covers the significance of the spectral response of photomultiplier tubes; describes some of the methods used for measuring this response; and discusses in some detail the calculations and other considerations useful for matching the radiation source and the photomultiplier tube type for a specific application.

SPECTRAL-RESPONSE CHARACTERISTICS

A spectral-response characteristic is a display of the response of a photosensitive device as a function of the wavelength of the exciting radiation. Such curves may be on an absolute or a relative basis. In the latter case the curves are usually normalized to unity at the peak of the spectral-response curve. For a photocathode the absolute radiant sensitivity is expressed in amperes per watt. Curves of absolute spectral response may also be expressed in terms of the quantum efficiency at the particular wavelength. If the curve is presented in terms of amperes per watt, lines of equal quantum efficiency may be indicated for convenient reference. Typical curves are usually included in the published tube data. It should be understood that because of variations in processing, deviations from these typical curves may be expected. It would not be unusual for the wavelength for peak response to vary by 30 nanometers from the typical value. The same variation may be expected in the long-wavelength cutoff as judged by the wavelength for which the response is 10% of the maximum. On the other hand, the short-wavelength cutoff is more closely held by the glass transmission characteristic of the envelope.

The relationship between the spectral responsivity, σ, and the quantum efficiency, η, may be established as follows: The energy of a photon is

$$E_p = h\nu = hc/\lambda \qquad \text{E-1}$$

where h is Planck's constant, ν is the frequency of the incident radiation, c is the velocity of light, and λ is the wavelength of the incident radiation. If the quantum efficiency is given by η (the ratio of the number of emitted photoelectrons to the number of incident photons), the responsivity is given by

$$\sigma = [\eta e]/[hc/\lambda] = \frac{\eta e \lambda}{h c} \qquad \text{E-2}$$

in units of coulombs per joule or amperes per watt where e is the charge on the electron. Solving for the quantum efficiency:

$$\eta = \frac{hc}{e} \quad \frac{\sigma}{\lambda}$$

$$= 1.240 \times 10^{-6}\, \sigma/\lambda$$

where the wavelength is given in meters. If λ is given in nanometers, σ is given in milliamperes per watt, and η is given in per cent:

$$\eta = 124.0\, \sigma/\lambda \qquad \text{E-3}$$

MEASUREMENT TECHNIQUES

In order to determine a spectral-response characteristic, (1) a source of essentially monochromatic radiation, (2) a current-sensitive instrument to measure the output of the photocathode, and (3) a method of calibrating the monochromatic radiation for its magnitude in units of power are required.

Monochromatic radiation is often provided by a prism or a grating type of monochromator. Interference filters may also be used to isolate narrow spectral bands.

Although interference filters do not provide the flexibility of a monochromator, they may be indicated in situations in which repeated measurements are required in a particular region of the spectrum.

The width of the spectral transmission band in these measurements must be narrow enough to delineate the spectral-response characteristic in the required detail. However, for the most part, spectral-response characteristics do not require fine detail and generally have broad peaks with exponential cutoff characteristics at the long-wavelength limit and rather sharp cutoffs at the short-wavelength end. For spectral measurements, therefore, a reasonably wide band is used. Such a band has the following important advantages: (1) because the level of radiation is higher, measurements are easier and more precise; and (2) spectral leakage in other parts of the spectrum is relatively less important. Spectral leakage is a problem in any monochromator because of scattered radiation, and in any filter because there is some transmission outside the desired pass band. A double monochromator may be used and will greatly reduce the spectral leakage outside the pass band. The double monochromator is at a disadvantage in cost and complexity. If a pass band of 10 nanometers is used, spectral leakage can be insignificant for most of the spectral measurements. At the same time, this pass band is narrow enough to avoid distortion in the measured spectral-response characteristic. It is often advisable to vary the pass band depending upon what part of the curve is being measured. For example, at the long-wavelength cutoff where the response of the photocathode may be very small, the leakage spectrum may play an important part; thus it is advisable to increase the spectral bandpass of the measurement. Wide pass-band color filters that exclude the wavelength of the measurement and include the suspected spectral leakage region, or vice versa, are used in checking the magnitude of the possible leakage spectrum.

ENERGY SOURCES

Various radiant-energy sources are used to advantage in spectral-response measurements. A tungsten halogen lamp is useful from 350 nanometers to wavelengths much greater than 1000 nanometers because of its uniform and stable spectral-emission characteristic. A mercury vapor discharge lamp provides a high concentration in specific radiation lines and thus minimizes the background scattered-radiation problem. The mercury lamp is particularly useful in the ultraviolet end of the spectrum where the tungsten lamp fails. Another useful source for the ultraviolet is the deuterium lamp. (See the discussion on radiant energy sources in Appendix F.)

MEASUREMENT OF RADIANT POWER OUTPUT

A radiation thermocouple or thermopile having a black absorbing surface is commonly used to measure the radiation power output at a specific wavelength. Although these devices are relatively low in sensitivity, they do provide a reasonably reliable means of measuring radiation independent of the wavelength. The limitation to their accuracy is the flatness of the spectral absorption characteristic of the black coating on the detector. Throughout the visible and near-infrared regions there is usually no problem. There is some question, however, as to the flatness of the response in the ultraviolet part of the spectrum.

The output of the thermocouple or thermopile is a voltage proportional to the input radiation power. This voltage is converted by means of a suitable sensitive voltmeter to a calibrated measure of power in watts. The calibration may be accomplished by means of standard radiation lamps obtained from the National Bureau of Standards. It is theoretically possible to calculate the monochromatic power from a knowledge of the emission characteristic of the source, the dispersion characteristic of the monochromator or the transmission characteristic of the filter, and from the transmission characteristic of the various lenses. This procedure is difficult, subject to error, and is not recommended except perhaps in the case of a tungsten lamp source combined with a narrow-band filter system.

Another useful reference standard is the pyroelectric detector. In this case, the radiation to be measured must be interrupted by means of a light chopper at about 15 hertz. Absolute calibration might proceed in a

manner similar to that of the thermopile. Special pyroelectric detectors have been fabricated that can be self-calibrated by means of electric power input. [119]

MEASUREMENT OF PHOTOCATHODE OUTPUT

For measuring the spectral characteristic of a photocathode, a very sensitive ammeter is required. When the output of the photocathode of a photomultiplier is measured, the tube is usually operated as a photodiode by connecting all elements other than the photocathode together to serve as the anode. When the photomultiplier is operated as a conventional photomultiplier, the output is very easy to measure. It is necessary, however, to be careful to avoid fatigue effects which could distort the spectral-response measurement. It should be noted that the spectral response of a photomultiplier may be somewhat different from that of the photocathode alone because of the effect of initial velocities on collection efficiency at the first dynode and because of the possibility of a photoeffect on the first dynode by light transmitted through the photocathode, especially if the first dynode is a photosensitive material such as cesium-antimony.

SOURCE AND DETECTOR MATCHING

One of the most important parameters to be considered in the selection of a photomultiplier type for a specific application is the photocathode spectral response. The spectral response of BURLE photomultiplier tubes covers the spectrum from the ultraviolet to the near-infrared region. In this range there are a large variety of spectral responses to choose from. Some cover narrow ranges of the spectrum while others cover a very broad range. The published data for each photomultiplier type show the relative and absolute spectral-response curves for a typical tube of that particular type. The relative typical spectral-response curves published may be used for matching the detector to a light source for all but the most exacting applications. The matching of detector to source consists of choosing the photomultiplier tube type that has a spectral response providing maximum overlap of the spectral distributions of detector and light source.

MATCHING CALCULATIONS

The average power radiating from a light source may be expressed as follows:

$$P = P_0 \int_0^\infty W(\lambda)\, d\lambda \qquad \text{E-4}$$

where P_0 is the incident power in watts per unit wavelength at the peak of the relative spectral radiation characteristic, $W(\lambda)$, which is normalized to unity.

If the absolute spectral distribution for the light source and the absolute spectral response of the photomultiplier tube are known, the resulting photocathode current I_k when the light is incident on the detector can be expressed as follows:

$$I_k = \sigma P_0 \int_0^\infty W(\lambda)\, R(\lambda)\, d\lambda \qquad \text{E-5}$$

Where σ is the radiant sensitivity of the photocathode in amperes per watt at the peak of the relative curve, and $R(\lambda)$ represents the relative photocathode spectral response as a function of wavelength normalized to unity at the peak. When Eq. E-4 is solved for the peak power per unit wavelength, P_0, and this solution is substituted into Eq. E-5, the cathode current is expressed as follows:

$$I_k = \sigma P \frac{\int_0^\infty W(\lambda)\, R(\lambda)\, d\lambda}{\int_0^\infty W(\lambda)\, d\lambda} \qquad \text{E-6}$$

The ratio of the dimensionless integrals can be defined as the **matching factor,** M. The matching factor is the ratio of the area under the curve defined by the product of the relative source and detector spectral curves to the area under the relative spectral source curve.

$$M = \frac{\int_0^\infty W(\lambda)\, R(\lambda)\, d\lambda}{\int_0^\infty W(\lambda)\, d\lambda} \qquad \text{E-7}$$

Fig. E-l shows an example of the data involved in the evaluation of the matching factor, M, as given in Eq. E-7.

If the input light distribution incident on the detector is modified with a filter or any other optical device, the matching-factor formulas must be changed accordingly. If the transmission of the filter or optical device is $f(\lambda)$, the matching factor will be

$$M = \frac{\int_0^\infty W(\lambda)\, R(\lambda)\, f(\lambda)\, d\lambda}{\int_0^\infty W(\lambda)\, f(\lambda)\, d\lambda} \qquad \text{E-8}$$

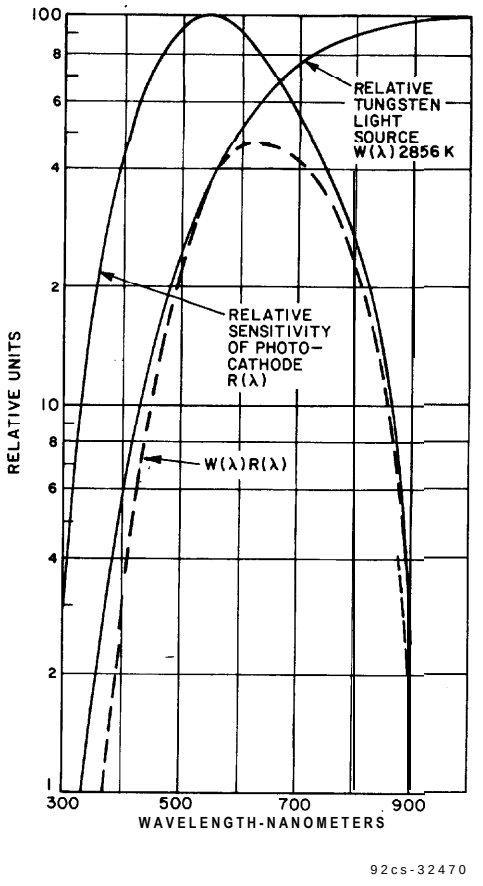

Fig. E-1 - Graphic example of factors used in evaluation of matching factor, M.

Table E-I shows a number of matching factors calculated for various light sources and spectral response characteristics. When the spectral range of a source exceeded 1200 nanometers, the integration was terminated at this wavelength. Because none of the photoresponses exceed 1200 nanometers, conclusions as to the relative merit of various combinations are still valid.

It should also be noted that since these data were originally published there has been a proliferation of photocathode development. Many of the new photocathodes, however, have spectral responses similar to those listed in Table E-l. As a result, the spectral matching factors given could also be used for many of the new photocathodes. For example, the data on S-l 1 could well be substituted for photocathodes such as Rb_2CsSb, K_2CsSb or Na_2KSb, with only moderate error.

When M is substituted for the integral ratio in Eq. E-6, the photocathode current becomes

$$I_k = \sigma PM \qquad \text{E-9}$$

except that it must be noted that P in Eq. E-9 is now given by

$$P = P_o \int_0^{1200} W(\lambda)\, d\lambda \qquad \text{E-10}$$

In any photomultiplier application it is desirable to choose a detector having a photocathode spectral response that will maximize the photocathode current, I_k, for a given light source. Maximizing the cathode current is important to maximize the signal-to-noise ratio. From Eq. E-9, it can be seen that the product of the matching factor M and the peak absolute photocathode sensitivity σ **must be maximized to maximize the** cathode current.

The importance of taking into account the absolute photocathode sensitivity, as well as the matching factor, is illustrated by a comparison of the S-l and S-20 photocathodes with a tungsten light source operating at a color temperature of 2856 K. The S-l and the S-20 matching factors are 0.516 and 0.112, respectively. From the matching factors alone it appears that the S-l is the best choice of photocathode spectral response. The S-l has a peak absolute sensitivity of 2.3 milliamperes per watt and the S-20 has a peak absolute sensitivity of 64 milliamperes per watt. Then, from Eq. E-9 the expected photocathode currents are

I_k(S-1)=0.0023 x 0.516 P=0.00119 P

I_k(S-20)=0.064 x 0.112 P=0.00717 P

These calculations show that the S-20 photocathode will provide a response to the tungsten lamp six times that of the S-l photocathode.

REFERENCES

119. W.M. Doyle and B.C. McIntosh (Laser Precision Corp., Irvine, California) and Jon Geist (National Bureau of Standards, Washington, D.C.), "Implementation of a system of optical calibration based on pyroelectric radiometry," **Optical Engineering,** Vol. 15, No. 6, pp 541-548, (Nov.-Dec. 1976)

120. E.H. Eberhardt, "Source-detector spectral matching factors," **Applied Optics,** Vol. 7, p 2037 (1968)

Table E-1
Spectral Matching Factors**

Light Source	Notes	Photocathodes S1 k	S4 k	S10 k	S11 k	S17 k	S20 k	S25 k	Other Detectors Photopic eye l	Scotopic eye m
Phosphors										
P1	a	0.278	0.498	0.807	0.687	0.892	0.700	0.853	0.768	0.743
P4	a,b	0.310	0.549	0.767	0.661	0.734	0.724	0.861	0.402	0.452
P7	a	0.312	0.611	0.805	0.709	0.773	0.771	0.882	0.411	0.388
P11	a	0.217	0.816	0.949	0.914	0.954	0.877	0.953	0.201	0.601
P15	a	0.385	0.701	0.855	0.787	0.871	0.802	0.904	0.376	0.495
P16	a	0.830	0.970	0.853	0.880	0.855	0.902	0.922	0.003	0.042
P20	a	0.395	0.284	0.612	0.427	0.563	0.583	0.782	0.707	0.354
P22B	c	0.217	0.893	0.974	0.960	0.948	0.927	0.979	0.808	0.477
P22G	c	0.278	0.495	0.807	0.686	0.896	0.699	0.855	0.784	0.747
P22R	c	0.632	0.036	0.264	0.055	0.077	0.368	0.623	0.225	0.008
P24	a	0.279	0.545	0.806	0.696	0.827	0.725	0.869	0.540	0.621
P31	a,d	0.276	0.533	0.811	0.698	0.853	0.722	0.868	0.626	0.65 1
NaI	e	0.534	0.923	0.885	0.889	0.889	0.900	0.933	0.046	0.224
Lamps										
2870/2856 std	f	0.516*	0.046*	0.095*	0.060*	0.072*	0.112*	0.227*	0.071†*	0.040*
Fluorescent	g	0.395	0.390	0.650	0.496	0.575	0.635	0.805	0.502	0.314
Sun										
In space	h	0.535*	0.308*	0.388*	0.328*	0.380*	0.406*	0.547*	0.179*	0.172*
+2 air masses	h,i	0.536*	0.236*	0.348*	0.277*	0.315*	0.360*	0.513*	0.197*	0.175*
Day sky	j	0.537*	0.520*	0.556*	0.508*	0.589*	0.581*	0.700*	0.170*	0.218*
Blackbodies										
6000K	-	0.533*	0.308*	0.376*	0.320*	0.375*	0.397*	0.521*	0.167*	0.159*
3000K	-	0.512*	0.053*	0.102*	0.067*	0.080*	0.120*	0.232*	0.075*	0.044*
2870 K	-	0.504*	0.044*	0.090*	0.057*	0.069*	0.106*	0.216*	0.067*	0.038*
2856 K	-	0.500*	0.042*	0.088*	0.055*	0.068*	0.103*	0.211*	0.065*	0.037*
2810 K	-	0.493*	0.039*	0.081*	0.051*	0.062*	0.097*	0.150*	0.061*	0.034*
2042 K	-	0.401*	0.008*	0.023*	0.011*	0.014*	0.033*	0.090*	0.018*	0.007*

*Entry valid only for 300-1200-nm wavelength interval.

†For the total wavelength spectrum this entry would be 0.0294.

Notes: a Registered spectral distribution. Data extrapolated as required.
b Sulfide type.
c BURLE data.
d Low brightness type.
e Harshaw Chemical Co. data.
f Standard test lamp distribution.
g General Electric Co. data.
h From **Handbook of Geophysics.**
i Approximately noon sea level flux at 60° latitude.
j From Gates ***(Science, Vol.*** 151, p 523 (1966)) between 300 nm and 530 nm. between 300 nm and 530 nm. **A** 12,000 K blackbody spectra) distribution was assumed between 530 nm and 1200 nm.
k Registered spectral distribution. Data extrapolated as required.
l Standard tabulated photopic visibility distribution.
m Standard tabulated scotopic visibility distribution.

** Data from E.H. Eberhardt, 120.

Appendix F - Radiant Energy and Sources

Radiant energy is energy traveling in the form of electromagnetic waves. It is measured in joules, ergs, or calories. The rate of flow of radiant energy is called radiant flux, and it is expressed in watts (joules per second).

Planck's equation for the spectral radiant exitance of a black body in a vacuum is

$$M_\lambda = \frac{2\pi c^2 h}{\lambda^5 (e^{hc/\lambda kT} - 1)} \quad \text{F-1}$$

(in W $m^{-2} m^{-1}$),

where

λ = wavelength (m)
h = Planck's constant (J s)
c = velocity of light (m s^{-1})
k = Boltzmann's constant (J K^{-1})
T = absolute temperature (K)

BLACK-BODY RADIATION

As a body is raised in temperature, it first emits radiation primarily in the invisible infrared region. Then, as the temperature is increased, the radiation shifts toward the shorter wavelengths. A certain type of radiation called black-body radiation is used as a standard for the infrared region. Other sources may be described in terms of the black body.

A black body is one which absorbs all incident radiation; none is transmitted and none is reflected. Because, in thermal equilibrium, thermal radiation balances absorption, it follows that a black body is the most efficient thermal radiator possible. A black body radiates more total power and more power at a particular wavelength than any other thermally radiating source at the same temperature. Although no material is ideally black, the equivalent of a theoretical black body can be achieved in the laboratory by providing a hollow radiator with a small exit hole. The radiation from the hole approaches that from a theoretical black radiator if the cross-sectional area of the cavity is large compared with the area of the exit hole. The characteristic of 100-per-cent absorption is achieved because any radiation entering the hole is reflected many times inside the cavity.

The radiation distribution for a source which is not black may be calculated from the black-body radiation laws provided the emissivity as a function of wavelength is known. Spectral emissivity is defined as the ratio of the output of a radiator at a specific wavelength to that of a black body at the same temperature. Tungsten sources, for which tables of emissivity data are available,[121] are widely used as practical standards, particularly for the visible range. Tungsten radiation standards for the visible range are frequently given in terms of color temperature, instead of true temperature. The color temperature of a selective radiator is determined by comparison with a black body. When the outputs of the selective radiator and a black body are the closest possible approximation to a perfect color match in the range of visual sensitivity, the color temperature of the selective radiator is numerically the same as the black-body true temperature. For a tungsten source, the relative distribution of radiant energy in the visible spectral range is very close to that of a black body, although the absolute temperatures differ. However, the match of energy distribution becomes progressively worse in the ultraviolet and infrared spectral regions.

TUNGSTEN SOURCES

Tungsten Lamps

Tungsten lamps are probably the most important type of radiation source because of

their availability, reliability, and constancy of operating characteristics. Commercial photomultiplier design has been considerably influenced by the characteristics of the tungsten lamp. A relative spectral-emission characteristic for a tungsten lamp at 2856 K color temperature is shown in Fig. F-l.

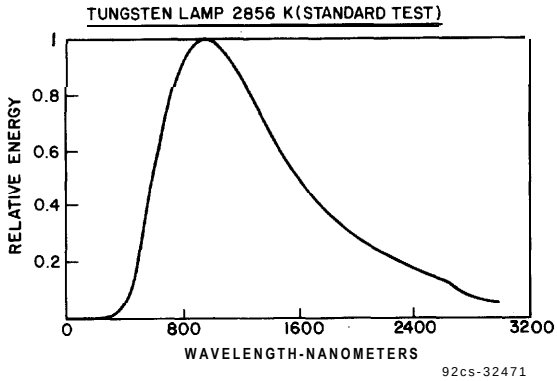

Fig. F-1 - Relative spectral-emission characteristic for a *tungsten lamp at a color temperature of 2856 K.*

As a result of the work of industry committees, virtually the entire photosensitive-device industry in the United States uses the tungsten lamp at 2856 K color temperature* as a general test source. The lamp is calibrated in lumens and is utilized in the infrared spectrum as well as the visible. Typical as well as maximum and minimum photosensitivities are quoted in microamperes per lumen.

The principal disadvantages of using the tungsten lamp as an industry standard test are that it does not provide a direct measure of radiant sensitivity as a function of wavelength and that it is a somewhat misleading term when the response of the photomultiplier lies outside the visible range. To assist the scientist in using photomultipliers, technical specifications for BURLE photomultiplier types include photocathode spectral-response curves which give the sensitivity in absolute terms such as amperes per watt and quantum efficiency as a function of wavelength. Methods of computing the response of a given photodetector to a particular radiation source are outlined in **Appendix E, Spectral Response and Source-Detector Matching.**

The relative spectral irradiance from a standard tungsten test lamp operated at 2870 K or 2854 K color temperature has been calculated by Engstrom and Morehead.[123] Their data utilized the black body characteristic, the tungsten spectral emissivity, and the transmission of the lamp envelope. Tabulated data (ST-3340) are available from BURLE Application Engineering. Their data in the wavelength range 300 to 1200 nanometers has been adjusted to a temperature of 2856 K color temperature and are shown in Table F-I. The data are normalized to unity at the maximum. The conversion was made by multiplying by the appropriate Planckian functions with a value for the second radiation constant, C_2 = 14,387.86 μm K.[124]

Tungsten-Halogen Lamps

A variation of the tungsten lamp is the tungsten-halogen lamp which is remarkable in that it can be operated at relatively high temperatures with increased life and with practically constant light output until the end of life.[125] Darkening of the envelope is virtually prevented in these lamps by a reaction of the halogen gas and the evaporated tungsten. In a typical application the lamp may contain between 0.2 and 0.3 micromoles/per cubic centimeter of I_2 which is broken down to atomic iodine by the heat of the filament. The atomic iodine reacts with the evaporated tungsten on the envelope wall to form WI,. The volatile WI_2 diffuses to the filament where it is decomposed, depositing W on the filament and freeing I to repeat the cycle.

The temperature of the envelope wall must be in the range 250 to 1200°C for the iodine cycle to operate successfully. It is common, therefore, for the envelopes to be made of quartz. Because the envelopes are small, even for high power lamps, the wall attains the proper temperature. If the envelope wall is at too low a temperature, the WI_2 will not be desorbed and a brown deposit of WI_2 will be formed. At too high a wall temperature, the reaction, WI_2 - W + 2I will occur and

*Formerly 2870 **K**, but changed to agree with C.I.E. designated Illuminant A at 2854 K, and again more recently to 2856 **K** because of the adoption of the international practical temperature scale of 1968.[122]

Table F-I
Relative Spectral Irradiance from a Tungsten Test Lamp Operated at a Color Temperature of 2856 K

Wavelength, nm	Relative spectral Irradiance	Wavelength, nm	Relative spectral Irradiance	Wavelength, nm	Relative spectral Irradiance
300	.0004	610	.5179	910	.9916
310	.0017	620	.5449	920	.9945
320	.0044	630	.5717	930	.9965
330	.0078	640	.5984	940	.9977
340	.0117	650	.6249	950	.9990
350	.0164	660	.6500	960	1.0000
360	.0221	670	.6747	970	.9985
370	.0285	680	.6988	980	.9963
380	.0361	690	.7219	990	.9961
390	.0450	700	.7438	1000	.9934
400	.0551	710	.7649	1010	.9909
410	.0663	720	.7860	1020	.9865
420	.0789	730	.8054	1030	.9823
430	.0928	740	.8233	1040	.9787
440	.1082	750	.8402	1050	.9747
450	.1249	760	.8557	1060	.9692
460	.1428	770	.8719	1070	.9647
470	.1623	780	.8861	1080	.9582
480	.1830	790	.8993	1090	.9529
490	.2048	800	.9114	1100	9457
500	.2278	810	.9228	1110	.9412
510	.2517	820	.9346	1120	.9321
520	.2766	830	.9444	1130	.9257
530	.3025	840	.9545	1140	.9174
540	.3286	850	.9624	1150	.9111
550			.9692	1160	.9037
560	.3826	870	.9751	1170	.8948
570	.4097	880	.9809	1180	.8868
580	.4368	890	.9862	1190	.8796
590	.4636	900	.9893	1200	.8704
600	.4906				

If these normalized data, $W_{2856}(\lambda)$, are taken to represent watts per 10-nanometer interval, the sum, $\Sigma\, W_{2856}(\lambda) \cdot V(\lambda) = 4.113$, where $V(\lambda)$ represents the relative spectral luminous efficiency values. If the maximum luminous efficacy at 555 nanometers is $K(\lambda)_{max}$ = 680 lumens per watt, the luminous flux represented by the tabular values is 2797 lumens. (There is some uncertainty about the value 680 lumens per watt; various slightly differing values have been reported in recent years.)

the W will not be removed from the wall.

Because of the higher operating temperatures and the long life with minimum envelope darkening, the tungsten-halogen lamps are useful as standard test lamps.[126]

Robert Saunders, Jr., of the Optical Radiation Section of the National Bureau of Standards has developed an empirical formula* representing the spectral irradiance of 1000-watt quartz-halogen type DXW lamps. Saunders formula is

$$E = \frac{(A + B\lambda + C\lambda^2 + D\lambda^3)\, e^{a} e^{-C_2 T_s \lambda}}{\lambda^5} \quad \text{F-2}$$

The fit of this formula to the actual data is of the order of 0.1% at each wavelength in the range of 350 to 900 nanometers for each of four lamps tested. Rounded-off averages of the constants in Eq. F-2 are A=0.867; $B = 9.33 \times 10^{-4}$; $C = -1.42 \times 10^{-6}$; $D = 6.08 \times 10^{-10}$. The wavelength, λ, is expressed in nanometers. T_s is the apparent black-body temperature. The term e^a represents a magnitude. Saunder's data were taken at a temperature, T_s, of approximately 3025 K.

For various purposes it is useful to have a tabulation of the relative radiant spectral flux from a tungsten-halogen lamp operating at 3200 **K** color temperature. Saunder's data were used to extrapolate to this temperature. A value of T_s = 3184 K was found to provide a spectral distribution most closely fitting a black body at 3200 K and thus providing a color temperature of 3200 K. Using a value of 1.4388 x 10^7 nm K for the second radiation constant, C_2, the relative spectral radiant flux values from such a lamp were determined from Eq. F-2 and are tabulated in Table F-II.

ARC AND GAS-DISCHARGE SOURCES.

Mercury Lamps

Of the various types of electrical discharge that have been used as radiation sources, the mercury arc is one of the most useful. The character of the light emitted from a mercury arc varies with pressure and operation conditions. At low pressure, the spectral output consists of sharp lines, which are very useful as reference spectra. Table F-III provides a list of some of the mercury lines in the visible and near-visible spectral range. In the case of germicidal lamps, most of the energy radiated is in one spectral line, 253.7 nanometers.

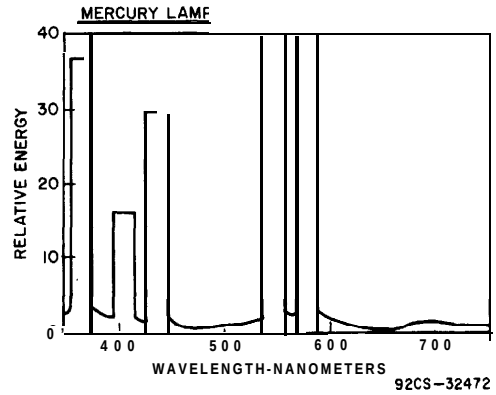

Fig. F-2 - Typical spectral-emission curve for a water-cooled mercury-arc lamp at a pressure of 130 atmospheres.

At increasing pressures, the spectral-energy distribution from the arc changes from the typical mercury-line spectral characteristic to an almost continuous spectrum of high intensity in the near-infrared, visible, and ultraviolet regions. Fig. F-2 shows the spectral-energy distribution from a water-cooled mercury arc at a pressure of 130 atmospheres.

Deuterium Lamps

These lamps provide a continuous, line-free spectrum in the ultraviolet range. The lamps are useful in spectrophotometry and related applications. A typical relative spectral energy distribution from a deuterium lamp is shown in Fig. F-3. Deuterium lamps may also be obtained with calibrated spectral irradiance over the wavelength range of 180 to 400 nanometers.

Zirconium Concentrated-Arc Lamps

A very useful point source■ is the **zirconium concentrated-arc lamp.** Concentrated-arc lamps are available with ratings

*Private Communication

@More detailed information on arc and gas-discharge sources may be found in **Handbook of Optics,** sponsored by the Optical Society of America, W. G. Driscoll and W. Vaughan, editors, McGraw-Hill, 1978.

■These lamps may be obtained from Cenco Company.

Table F-II
Relative Spectral Irradiance from a Tungsten-Halogen Lamp in a Quartz Envelope Operated at a Color Temperature of 3200 K

Wavelength, nm	Relative Spectral Irradiance	Wavelength, nm	Relative Spectral Irradiance	Wavelength, nm	Relative Spectral Irradiance
300	.0109	610	.6714	910	.9969
310	.0151	620	.6966	920	.9950
320	.0204	630	.7211	930	.9924
330	.0269	640	.7444	940	.9893
	.0347	650	.7669	950	.9859
350	.0440	660	.7883	960	.9820
360	.0548	670	.8086	970	.9778
370	.O671	680	.8280	980	.9733
380	.0811	690	.8464	990	.9683
390	.0967	700	.8636	1000	.9629
400	.1139	710	.8796	1010	.9572
410	.1327	720	.8945	1020	.9515
420	.1531	730	.9083	1030	.9454
430	.1749	740	.9213	1040	.9392
440	.1981	750	.9327	1050	.9327
450	.2224	760	.9434	1060	.9259
460	.2480	770	.9530	1070	.9194
470	.2745	780	.9618	1080	.9125
480	.3018	790	.9694	1090	.9052
490	.3299	800	.9763	1100	.8984
500	.3585	810	.9820	1110	.8911
510	.3875	820	.9870	1120	.8838
520	.4169	830	.9912	1130	.8766
530	.4463	840	.9943	1140	.8693
540	.4757	850	.9969	1150	.8621
550	.5048	860	.9985	1160	.8544
	.5338	870	.9996	1170	.8472
570	.5625	880	1.0000	1180	.8399
580	.5908	890	.9996	1190	8326
590	.6183	900	.9985	1200	.8254
600	.6450				

If these normalized data, $W_{3200}(\lambda)$, are taken to represent watts per 10-nanometer interval, the sum, $\Sigma W_{3200}(\lambda) \cdot V(\lambda) = 5.678$, where $V(\lambda)$ represents the relative spectral luminous efficiency values. If the maximum luminous efficacy at 555 nanometers is $K(\lambda)_{max}$ =680 lumens per watt, the luminous flux represented by the tabular values is 3861 lumens. (There is some uncertainty about the value 680 lumens per watt; various slightly differing values have been reported in recent years.)

Table F-III
Some of the Principal Spectral Lines Characteristic of a Low-Pressure Mercury Discharge (in nanometers)

237.8	365.0
253.7	404.7
265.3	435.8
296.7	546.1
302.1	577.0
313.2	579.0
334.1	

(A more complete table may be found in **American Institute of Physics Handbook,** Third edition, 1972, McGraw-Hill, pp 7-92 -7-96.)

from 2 to 300 watts, and in point diameters from 0.08 mm to 2.9 mm. These lamps require one special circuit to provide a high starting voltage and another well-filtered and ballasted circuit for operation.

Arc Lamps

The **carbon** arc is a source of great intensity and high color temperature. A typical energy-distribution spectrum of a dc **high-**intensity arc is shown in Fig. F-4. Figs. F-5 and F-6 show relative spectral-emission characteristic curves for xenon and argon **arcs.**

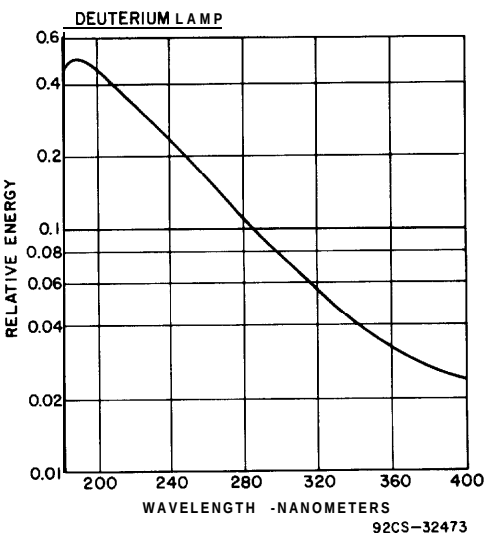

Fig. F-3 - Typical relative spectral energy distribution from a deuterium lamp. (From Optronic Laboratories, Inc., Silver Spring, Md.)

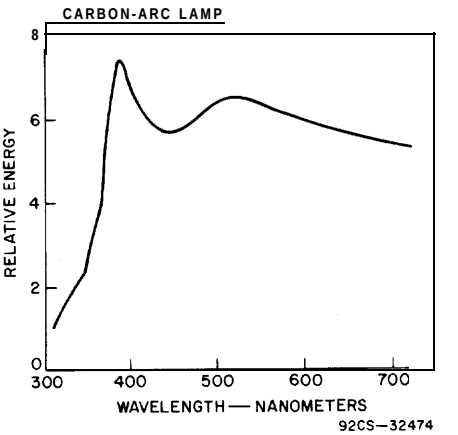

Fig. F-4 - Typical spectral-emission curve for a dc high-intensity carbon-arc lamp.

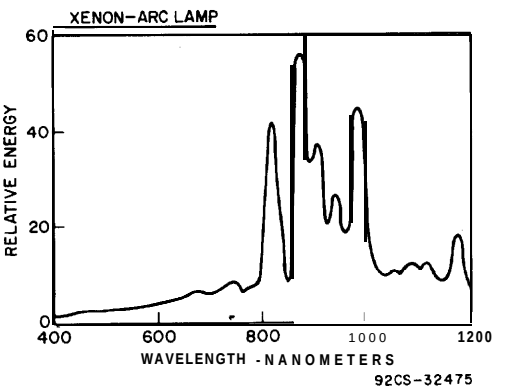

Fig. F-5 - Typical spectral-emission curve for a xenon-arc lamp.

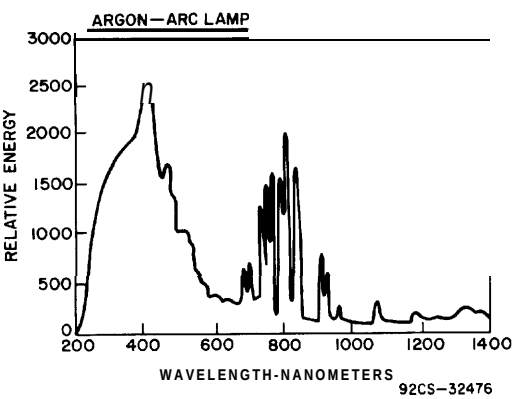

Fig. F-6 - Typical spectral-emission curve for an argon-arc lamp.

Fluorescent Lamps

The common **fluorescent lamp,** a very efficient light source, consists of an argon-mercury glow discharge in a glass envelope internally coated with a phosphor that converts ultraviolet radiation from the discharge into useful light output. There are numerous types of fluorescent lamps, each with a different output spectral distribution depending upon the phosphor and gas filling. The spectral response shown in Fig. F-7 is a typical curve for a fluorescent lamp of the daylight type.

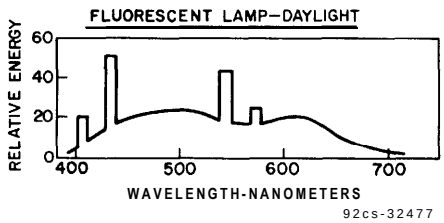

Fig. F-7 - Typical spectral-emission curve for a daylight-type fluorescent lamp.

SUMMARY OF TYPICAL SOURCES

Table F-IV provides typical parameters for the most commonly used radiant energy sources.

LASERS AND LIGHT-EMITTING DIODES

In recent years the development of various types of lasers and **p-n light-emitting diodes** with very high modulation frequencies and short rise times has increased the types of sources that photomultipliers are called upon to detect. Although many of these interesting devices have their principal wavelengths of emission in the infrared beyond the sensitivity range of photomultiplier tubes, some do not. Because of the growing importance of laser applications and the use of photomultipliers for detecting their radiation, Tables F-V through F-IX are provided as reference data on crystalline, gas, and liquid lasers, and on p-n junction light-emitting diodes.

Table F-IV
Summary of Typical Sources/Parameters for the Most Commonly Used Radiant Energy Sources

Lamp Type	DC Input Power (watts)	Arc Dimensions (mm)	Luminous Flux (lm)	Luminous Efficiency (lm W^{-1})	Average Luminance (cd mm^{-2})
Mercury Short Arc (high pressure)	200	2.5 x 1.8	9500	47.5	250
Xenon Short Arc	150	1.3 x 1.0	3200	21	300
Xenon Short Arc	20,000	12.5 x6	1,150,000	57	3000 (in 3 mmx6mm)
Zirconium Arc	100	1.5 (diam.)	250	2.5	100
Vortex-Stabilized Argon Arc	24,800	3x10	422,000	17	1400
Tungsten Light Bulbs	10	-	79	7.9	10
	100	-	1630	16.3	
	1,000	-	21,500	21.5	25
Fluorescent Lamp Standard Warm White	40	-	2,560	64	-
Carbon Arc Non-Rotating	2,000	=5x5	36,800	18.4	175
Rotating	15,800	= 8 x 8	350,000	22.2	800
Deuterium Lamp	40	1.0 (diam.)	(Nominal irradiance at 250 nm at 30 cm = 0.2 $\mu W\ cm^{-2}\ nm^{-1}$)		

Table F-V
Typical Characteristics of a Number of Useful Crystal Laser Systems

Host	Dopant	Wavelength of Laser (μm)	Mode and Highest Temperature of Operation (K)
Al_2O_3	0.05% Cr^{3+}	0.6934 0.6929	CW,P 350 P 300
Al_2O_3	0.5% Cr^{3+}	0.7009 0.7041 0.7670	P 77 P 77 P 300
MgF_2	1% Ni^{2+}	1.6220	P 77
MgF_2	1% Co^{2+}	1.7500 1.8030	P 77 P 77
ZnF_2	1% Co^{2+}	2.6113	P 77
$CaWO_4$	1% Nd^{3+}	1.0580 0.9145 1.3392	CW 300 P 77 P 300
CaF_2	1% Nd^{3+}	1.0460	P 77
$CaMoO_4$	1.8% Nd^{3+}	1.0610	CW 300
$Y_3Al_5O_{12}$	Nd^{3+}	1.0648	CW 360 P 440
LaF_3	1% Nd^{3+}	1.0633	P 300
LaF_3	1% Pr^{3+}	0.5985	P 77
$CaWO_4$	0.5% Pr^{3+}	1.0468	P 77
$Y20_3$	5% Eu^{3+}	0.6113	P 220
CaF_2	Ho^{3+}	0.5512	P 77
$CaWO_4$	0.5% Ho^{3+}	2.0460	P 77
$Y_3Al_5O_{12}$	Ho^{3+}	2.0975	CW 77 P 300
$CaWO_4$	1% Er^{3+}	1.6120	P 77
$Ca(NbO_3)_2$	Er^{3+}	1.6100	P 77
$Y_3Al_5O_{12}$	Er^{3+}	1.6602	P 77
$CaWO_4$	Tm^{3+}	1.9110	P 77
$Y_3Al_5O_{12}$	Tm^{3+}	2.0132	CW 77 P 300
Er_2O_3	Tm^{3+}	1.9340	CW 77
$Y_3Al_5O_{12}$	Yb^{3+}	1.0296	P 77

CW = Continuous P = Pulse

Table F-V
Typical Characteristics of a Number of Useful Crystal Laser Systems (Cont'd)

Host	Dopant	Wavelength of Laser (μm)	Mode and Highest Temperature of Operation (K)
CaF_2	0.05 % U^{3+}	2.6130	P 300 CW 77
SrF_2	U^{3+}	2.4070	P 90
CaF_2	0.01 % Sm^{2+}	0.7083	P 20
SrF_2	0.01% Sm^{2+}	0.6969	P 4.2
CaF_2	0.01% Dy^{2+}	2.3588	CW 77 P 145
CaF_2	0.01% Tm^{2+}	1.1160	P 27 CW 4.2

CW = Continuous P = Pulse

Table F-VI
Comparison of Characteristics of Continuous Crystalline Lasers

Material Active System	Sensitizer	Optical Pump	Wave-Length (μm)	Eff.(%)	Power (Watts)	Operating Temp.(K)
$Dy^{2+}CaF_2$	-	W	2.36	0.06	1.2	77
$Cr^{3+}Al_2O_3$	-	Hg	0.69	0.1	1.0	300
$Nd^{3+}Y_3Al_5O_{12}$	-	W	1.06	0.2	2	300
			1.06	0.6	15	300
$Nd^{3+}Y_3Al_5O_{12}$	-	Plasma Arc	1.06	0.2	200	300
$Nd^{3+}Y_3Al_5O_{12}$	Cr^{3+}	Na Doped Hg	1.06	0.4	0.5	300
$Nd^{3+}Y_3Al_5O_{12}$		Hg			10	300
$Ho^{3+}Y_3Al_5O_{12}$	[Er^{3+}, Yb^{3+}, Tm^{3+}]	W	1.12	5.0	15	77

Table F-VII
Typical Characteristics for Two Liquid Lasers

Liquid	Principal Wavelength (μm)	Pulse Energy(J) (Pulse Width)
Eu(O-ClBTFA)$_4$DMA*	0.61175	0.1 J
Nd + ^{3}SeOCl$_2$**	1.056	10 J (150 μs)

+dimethylammonium salt of tetrakis europium-ortho-chloro-benzoyltrifluoracetonate.
**trivalent neodymium in selenium oxychloride.

Table F-VIII
Typical Characteristics of a Number of Useful Gas Lasers

Gas	Principal Wavelengths (μm)	Output Power		
		Typical	Maximum	Pulsed or Continuous
Ne (ionized)	0.3324	-	10 mW	Pulsed
			10 mW	CW
Ne (unionized)	0.5401	-	1 kW	Pulsed
He-Ne (unionized)	0.5944-0.6143	10 μW	-	Pulsed
	0.6328	1 mW	150 mW	
	1.1523	l-5 mW	25 mW	CW
	3.3913	<1 mW	10 mW	CW
Xe (ionized)	0.4603-0.6271	5 mW	-	Pulsed
	0.5419-0.6271	10 mW	1 W	CW
	0.4965 - 0.5971	1 mW	1 W	Pulsed
Xe (unionized)	2.026	1 mW	10 mW	CW
	3.507	-	1 mW	CW
	5.575	0.5 mW	5 mW	CW
	9.007	0.5 mW	5 mW	CW
A (ionized)	0.4880	0.5 W	5W	CW
	0.5145	0.5 W	5 W	CW
	0.4545 to 0.5287	1.5 W	40 W	CW
N_2 (ionized	0.33	-	200 kW	Pulsed
		-	100 mW	CW
Kr (ionized)	0.3507	-	300 mW	CW
	0.5208-0.6871	-	3 W	CW
	0.5682	-	100 mW	CW
CO_2 (molecular excitation)	10.552 10.572 10.592	50 W	3.2 kW	CW
CF_3I	1.315	-	10 kW	Pulsed
H_2O (molecular excitation)	27.9	-	1.2 W	Pulsed
	118	-	1 mW	Pulsed
	118	-	10 μW	CW
CN (molecular excitation)	337	-	50 mW	Pulsed

Table F-IX
Typical Characteristics of p-n Junction Light-Emitting Diodes

crystal	Wavelength (μm)	Laser Action
PbSe	8.5	Yes
PbTe	6.5	Yes
InSb	5.2	Yes
PbS	4.3	Yes
	3.15	Yes
$(In_xGa_{1-x})As$	0.85-3.15	Yes
In P_xAs_{1-x})	0.91-3.15	Yes
GaSb	1.6	No
InP	0.91	Yes
GaAs	0.90	Yes
$Ga_xAl_{1-x}As$	0.80-0.90	Yes
$Ga(As_{1-x}P_x)$	0.55-0.90	Yes
CdTe	0.855	No
$(Zn_xCd_1$-x)Te	0.59-0.83	No
CdTe-ZnTe	0.56-0.66	No
BP	0.64	No
Cu_2Se-ZnSe	0.40-0.63	No
$Zn(Se_xTe_{1-x})$	0.627	No
ZnTe	0.62	No
GaP	0.565	No
GaP	0.68	No
SiC	0.456	?

LIGHT SOURCES FOR TESTING

Monochromatic sources of many wavelengths may be produced by narrow-band filters or monochromators. Narrow-band filters are more practical for production testing, but, at best, such tests are time-consuming and subject to error. Monochromatic sources are not used in general-purpose testing because most applications involve broader-band light sources; a monochromatic test might grossly misrepresent the situation because of spectral-response variations.

A broad-band source is probably more useful as a single test because it tends to integrate out irregularities in the spectral-response characteristic and more nearly represents the typical application. The tungsten lamp has been used for many years because it is relatively simple, stable, and inexpensive, and maintains its calibration. The tungsten lamp emits a broad band of energy with relatively smooth transitions from one end of the spectrum to the other. Its principal disadvantage as a general source is its lack of ultraviolet output and relatively low blue output.

Sources such as arcs and glow discharges are difficult to calibrate and show serious time variations.

Filters are frequently used to narrow the spectral range for specific purposes; however, they sometimes contribute to errors because of significant transmission outside the band of interest. Filters are also subject to change in transmission with time and are very difficult to reproduce with identical characteristics.

In many applications it is appropriate to test photomultipliers in the same manner in which they are to be utilized in the final application. For example, photomultipliers to be used in scintillation counting may be tested by means of an NaI:Tl crystal and a ^{137}Cs source or a simulated NaI light source utilizing a tungsten lamp whose light passes through a one-half stock-thickness Corning CS5-58 filter (5113 glass). Interference-type filters are becoming increasingly important in isolating specific wavelengths for testing photomultiplier tubes for laser applications.

When a photomultiplier is manufactured for a variety of purposes, including scientific applications, it would be highly desirable if sensitivity were specified by a complete spectral response in terms of quantum efficiency or radiant sensitivity. This information could then be utilized with the known spectral emission of any source to compute the response of the photomultiplier to that source. Complete spectral sensitivity data, however, are rarely provided because it is unnecessary for most practical situations and would considerably increase device costs.

REFERENCES

121. J.C. DeVos, "A new determination of the emissivity of tungsten ribbon," Physica, Vol. 20, pp 107-131, (1954).

122. "Color temperature, luminous efficacy and the international practical temperature scale of 1968," **National Bureau of Standards Technical News Bulletin,** Vol. 54, No. **9,** pp 206-7, Sept. 1970.

123. R.W. Engstrom and A.L. Morehead, "Standard test-lamp temperature for photosensitive devices-relationship of absolute and luminous sensitivities," **RCA Rev.,** Vol. 28, pp 419-423 (1967).

124. E.R. Cohen, CODATA Bulletin 11, Dec. 1973. See also D.G. Fink and H.W. Beaty, **Standard Handbook for Electrical Engineers,** 11th Edition, McGraw-Hill, 1978.

125. E.G. Zubler and F.A. Mosby, "An iodine incandescent lamp with virtually 100 per cent lumen maintenance," **Illuminating Engineering,** Vol. 54, No. 12, pp 734-740, Dec. 1959.

126. R. Stair, W.E. Schneider and J.K. Jackson, "A new standard of spectral irradiance," **Appl. Opt.,** Vol. 2, p 1151, (1963).

Appendix G - Statistical Theory of Noise in Photomultiplier Tubes

Generating Functions

In this treatment of noise and signal-to-noise ratio in photomultiplier operation, generating functions[127] will be used to develop the statistics of the different processes and their combinations. This approach has been selected because it provides a general, straightforward, and relatively simple method of solving problems of this nature. Those not acquainted with the use of generating functions may find it worthwhile to investigate some of the sources in reference[127]. A short summary of generating functions and their use is provided in this section. Others may use this Appendix for the summarized expressions relating to photomultiplier statistics.

A generating function may be defined as

$$Q(s) = \sum_{n=0}^{N} s^n P_n \qquad \text{G-1}$$

where the various values, P_n, represent the probabilities of a score of **n** in a given event. Thus, P_o is the probability of a score of 0; P_1, the probability of a score of 1, etc. Note that

$$Q(1) = 1 \qquad \text{G-2}$$

because the sum of all the probabilities of the various scores must total unity.

The **average score** is determined by taking the first derivative of the generating function at the value of $s = 1$:

$$\frac{\partial Q(s)}{\partial s} = Q'(s) = \sum_{n=0}^{N} n s^{n-1} P_n$$

and

$$Q'(1) = \sum_{n=1}^{N} n\, P_n = \bar{n} \qquad \text{G-3}$$

The value of P_n may be retrieved from the generating function by the following expression:

$$P_n = \frac{1}{n!} \cdot \frac{\partial^n Q(s)}{\partial s^n}\bigg|_{s=0} \qquad \text{G-4}$$

The **variance** is defined as

$$\sigma^2 = \sum_{n=0}^{N} (n - \bar{n})^2 \cdot P_n \qquad \text{G-5}$$

Variance may be found from the generating function by the following relationship:

$$\sigma^2 = Q''(1) + Q'(1) - [Q'(1)]^2 \qquad \text{G-6}$$

The equivalence of Eqs. G-5 and G-6 is readily demonstrated.

Expanding Eq. G-5 as follows:

$$\sigma^2 = \Sigma n^2 P_n - 2\bar{n}\Sigma n P_n + \bar{n}^2 \Sigma P_n$$
$$= \Sigma n^2 P_n - \bar{n}^2 \qquad \text{G-7}$$

because of the G-2 and G-3 relationships. In evaluating G-6, note that

$$Q''(1) = \Sigma n(n-1) P_n = \Sigma n^2 P_n - \bar{n} \qquad \text{G-8}$$

Substituting G-3 and G-8 in G-6 establishes the identity of G-6 and G-7, and thus of G-6 and G-5.

Additive Events

Now, suppose there are two independent events whose scores are to be added. An example is the roll of two dice, or in the case of a photomultiplier, the photocathode current generated thermally and photoelectrically. Assume two corresponding generating functions: $Q_A(s)$ and $Q_B(s)$. It may be shown that the generating function for the sum is

$$Q_{A+B}(s) = Q_A(s) \cdot Q_B(s) \qquad \text{G-9}$$

and that the averages and variances add as follows:

$$\bar{n}_{A+B} = \bar{n}_A + \bar{n}_B \qquad \text{G-10}$$

and

$$\sigma^2_{A+B} = \sigma^2_A + \sigma^2_B \qquad \text{G-11}$$

In the case of additive events that are not independent, the variance for the sum must also contain a term for the effect of the correlation between the two prime events. Thus

$$\sigma^2_{A+B} = \sigma^2_A + \sigma^2_B + 2\,\mathrm{COV}(X_A, X_B) \quad \text{G-12}$$

where $\mathrm{COV}(X_A,X_B)$ is the covariance of the two variables, X_A and X_B, each of which take on the integral values, n_A and n_B. The covariance is the mathematical expectation of the product of the variables less the product of the means.

The case of **subtraction** is just a modification of the addition. In this case

$$\bar{n}_{A-B} = \bar{n}_A - \bar{n}_B \quad \text{G-13}$$

and, as before,

$$\sigma^2_{A-B} = \sigma^2_A + \sigma^2_B \quad \text{G-13a}$$

Cascade Events

Consider a pair of independent sequential events such as the emission of photoelectrons and the multiplication that occurs at the first dynode of a photomultiplier. Each photoelectron is multiplied by a secondary emission factor that has an average value and a variance. Assume two generating functions: A(s) for the primary event, and B(s) for the secondary or multiplying event. It may then be shown that the generating function for the cascaded event is

$$Q_{AB}(s) = A[B(s)] \quad \text{G-14}$$

and that the average product and variance of the product are:

$$\bar{n}_{AB} = \bar{n}_A \cdot \bar{n}_B \quad \text{G-15}$$

$$\sigma^2_{AB} = \bar{n}^2_B \sigma^2_A + \bar{n}_a \sigma^2_B \quad \text{G-16}$$

Multiplication

In the case of the cascaded event relating to the photomultiplier, each electron from the preceding stage is acted on independently by the secondary emission gain. In contrast, consider the case of multiplication of two independent scores: i.e., a die is rolled and the score noted, then rolled again and scores multiplied. The order of the events is not significant. The generating function for one event may be

$$A(s) = \sum_n s^n A_n \quad \text{G-17}$$

and for the other

$$B(s) = \sum_r s^r B_r \quad \text{G-18}$$

For the product, the generating function is

$$Q_{A\cdot B} = \sum_n A_n \sum_r s^{n\cdot r} B_r \quad \text{G-19}$$

Using Eqs. G-3 and G-6, the average product score and its variance are

$$\bar{n}_{A\cdot B} = \bar{n}_A \cdot \bar{n}_B \quad \text{G-20}$$

$$\sigma^2_{A\cdot B} = \sigma^2_A \sigma^2_B + \sigma^2_A \bar{n}^2_B + \sigma^2_B \bar{n}^2_A \quad \text{G-21}$$

PHOTON NOISE

If the photon flux impinging upon the photocathode originates from a thermal broad-band source, the photons can be assumed to be emitted at random time intervals. Under such conditions, the probability that n photons will strike the photocathode in a time interval τ is given by a Poisson distribution, as follows:

$$P(n,\tau) = \frac{(I_p\tau)^n}{n!} \exp(-I_p\tau) \quad \text{G-22}$$

where I_p is the average photon-arrival rate. The average value for n and the variance in n, σ_p^2, can be obtained directly from $P(n, \tau)$:

$$\bar{n} = I_p\tau \quad \text{G-23}$$

$$\sigma^2_p = I_p\tau = \bar{n} \quad \text{G-24}$$

The signal-to-noise ratio $\bar{n}/\sigma_p$ is given by

$$\mathrm{SNR} = (I_p\tau)^{1/2} \quad \text{G-25}$$

Thus;the signal-to-noise ratio of the photon flux increases as $\sqrt{I_p\tau}$.

There are a few cases in which the fluctuation in the photon flux has an additional term. [128] In broad-band thermal sources, however, Eq. G-24 yields the proper expression for the noise in the input photon flux.

PHOTOEMISSION NOISE

The physics of photoemission and photocathodes is discussed in Chapter 2 on **Photomultiplier Design.** In the following discussion it is assumed that the time between the absorption of a photon and the subsequent emission of an electron, when emission occurs, is short (about 10^{-12} second). In addition, it is assumed that all the statistical processes of absorption, electron transport within the photocathode, and photoemission can be described and characterized by one number, the quantum efficiency η. For a given photocathode, η is a function of the photon wavelength.

A simple model of photoemission will aid in understanding the noise contributions of the photocathode. For each photon that strikes the photocathode, an electron is emitted with probability η. Optical-reflection effects at the various cathode interfaces are accounted for in the value of η. The chance that no electron is emitted is $1-\eta$.

The statistics for this process can be found through the use of the generating function $Q_{p.c.}(s)$ such as Eq. G-1. In the simplified model of the photocathode this function is given by

$$Q_{p.c.}(s) = (1-\eta) + s\eta \qquad \text{G-26}$$

From Eq. G-3, it can be seen that the average output is given by

$$\bar{n} = \eta \qquad \text{G-27}$$

and from Eq. G-6, the variance is given by

$$\sigma^2 = \eta - \eta^2 \qquad \text{G-28}$$

For the purpose of discussion, it is assumed that the variance of the photon arrival rate is zero; that is, there is a steady stream of photons impinging upon the photocathode. The photons are equally spaced in time and arrive at a rate of I_p photons per second. In an interval τ (where τ is much larger than $1/I_p$), the number of photons N striking the photocathode is equal to $I_p\tau$. Because by hypothesis I_p is constant, the number N does not fluctuate. In a time τ, the average number of photoelectrons n emitted from the photocathode is equal to ηN. The fluctuations in photoelectron number can be computed by use of Eq. G-16 for the total variance for two cascaded statistical processes. Because the photon flux does not fluctuate, the variance, $\sigma_A^2 = 0$. The average value $\bar{n}_A = N$. Substituting these values and the average and variance values for the photoemission process given by G-26 and G-27 in G-16, the total variance in the photoelectron number is given by

$$\sigma_{p.e.}^2 = N(1-\eta)\eta \qquad \text{G-29}$$

The average value of the photoemission is given by ηN. In this case the signal-to-noise ratio of the photon flux is infinite because it does not fluctuate; however, the photoelectron number has a signal-to-noise ratio given by the ratio of the average to the square root of the variance:

$$\text{SNR}_{p.e.} = \left[\frac{\eta N}{1-\eta}\right]^{1/2} \qquad \text{G-30}$$

Thus, for quantum efficiencies less than unity, the statistics of the photoemission process result in a finite signal-to-noise ratio for the photoelectron number even though there is no assumed noise in the photon stream.

In practice, the signal-to-noise ratio of the input photon flux is never infinite; the flux always contains some noise. In most sources, the signal-to-noise ratio of the photon flux is given by Eq. G-25.

Again, by the use of Eqs. G-15 and G-16 for cascaded events, expressions are obtained for the average and variance of the photoemission, this time assuming $\bar{n}_p$ is the average number of photons arriving in a time interval τ and $\sigma_p^2 = \bar{n}_p$.

The average number of photoelectrons and the variance in the photoelectron number are stated, respectively, as

$$\bar{n}_{p.e.} = \eta\bar{n}_p \qquad \text{G-31}$$

and $\sigma_{p.e.}^2 = \bar{n}_p\eta(1-\eta) + \eta^2\bar{n}_p$

or $$\sigma_{p.e.}^2 = \eta\bar{n}_p \qquad \text{G-32}$$

It should be noted that the statistical conversion process within the photocathode has not altered the functional form of the variance; it is still proportional to the average number of particles. The photoelectrons appear to emanate from a random source of electrons with average value $\eta\bar{n}_p$. It is as though the average photon number were reduced by a factor η in the conversion process, a result that depends on the variance of the photon flux being equal to $\bar{n}_p$.

The photoelectron signal-to-noise ratio is

$$\text{SNR}_{p.e.} = [\eta\bar{n}_p]^{1/2} \qquad \text{G-33}$$

A quantum efficiency of 40 per cent reduces the signal-to-noise ratio of the photoelectron flux to about 63 per cent of that of the photon flux.

It is important to realize that the degradation in signal-to-noise ratio as a result of η being less than unity is irreversible in that no amount of noise-free amplification can improve the photoelectron signal-to-noise ratio.

In some applications, multiphoton pulses form the input signal. In these applications, integral numbers of photoelectrons are emitted from the photocathode within a time

that is short with respect to the resolution time of the photomultiplier. Examples of this type of input can be found in radioactive tracer scintillations, such as those observed in tritium and carbon spectroscopy.

If, with η equal to 1, the input signal consists of a steady train of photon pulses widely spaced in time, each pulse consisting of m photons, a steady train of photoelectron pulses would result, each consisting of m electrons. For values of η less than 1, the number of electrons in each pulse, r, can vary from 0 to m ($0 \leqslant r \leqslant m$).

For single photon input, it was found (Eqs. G-27 and G-28) that $\bar{n} = \eta$ and $\sigma^2 = \eta - \eta^2$. For a two photon input, the statistics for additive independent events (Eqs. G-10 and G-11) may be used. Therefore,

$$\bar{n}_2 = 2\eta$$

and $\sigma_2^2 = 2\eta(1 - \eta)$.

Obviously, this addition may be continued to a total of m photons input. Then

$$\bar{n}_m = m\eta \qquad \text{G-34}$$

$$\sigma_m^2 = m\eta(1 - \eta). \qquad \text{G-35}$$

It is useful to examine the distribution of photoelectrons per pulse of m photons. By an extension of Eq. G-9, the generating function is given by

$$Q_m(s) = [Q_1(s)]^m \qquad \text{G-36}$$

But $Q_1(s)$ is given by Eq. G-26. Therefore,

$$Q_m(s) = [(1 - \eta) + s\eta]^m \qquad \text{G-37}$$

The probability that r photoelectrons will be emitted is given by use of Eq. G-4,

$$P_r(\eta) = \frac{1}{(r)!} \left. \frac{\partial^r Q_m(s)}{\partial s^r} \right|_{s=0} \qquad \text{G-38}$$

or

$$P_r(\eta) = \eta^r (1 - \eta)^{m-r} \left[\frac{m!}{r!(m-r)!} \right] \qquad \text{G-39}$$

Eq. G-39 is just the coefficient of s_r in the expression for $Q_m(s)$. $P_r(\eta)$ is composed of the chance of r successful photoemissions (η^r), the chance of (m-r) failures to photoemit $[(1 - \eta)^{m-r}]$, and the binomial coefficient $\left[\frac{m!}{r!(m-r)!} \right]$ which describes the number of ways such an output can occur among the m-photon inputs.

Figs. G-1 and G-2 show the probability distribution for photoemission from the photocathode for a train of 4-photon input pulses and for two different values of η. The spectrum in Fig. G-1 is computed with $\eta = 0.4$ and that of Fig. G-2 with $\eta = 0.01$.

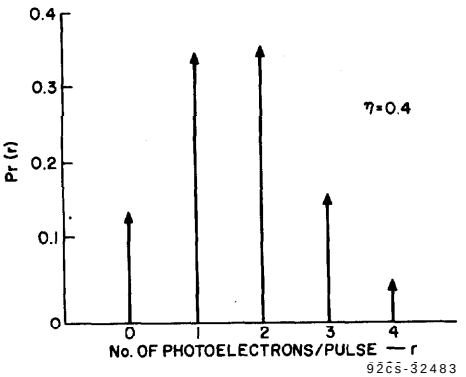

Fig. G-1 - Photoelectron output pulse spectrum resulting from a flux of 4-photon input pulses computed with $\eta = 0.4$.

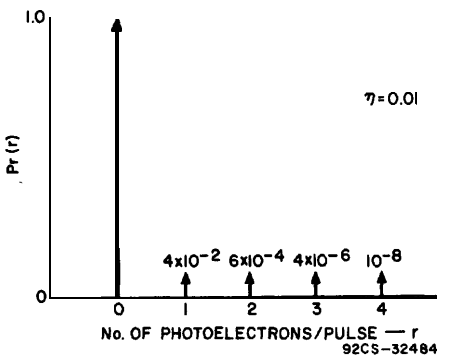

Fig. G-2 - Photoelectron output pulses resulting from a flux of 4-photon input pulses computed with $\eta = 0.01$.

The difference is striking. With $\eta = 0.4$, there is no photoemission only 13 per cent of the time; most of the photoemission is divided between 1- and (2-, 3-, of 4-) photoelectron pulses in the ratio of 13 to 20. In sharp contrast, when $\eta = 0.01$, photoemission does not occur 96 per cent of the time. Of the times when photoelectrons are emitted, single-electron pulses occur 70 times more often than any others; 3- and 4-photoelectron pulses almost never occur. It should be clear that in multiphoton-pulse spectroscopy it is important that η be as high as possible.

The signal-to-noise ratio expected in the photoelectron pulse distribution generated from an m-photon input depends upon the quantum efficiency. From Eqs. G-34 and G-35, the relation

$$SNR_{p.e.} = \left[\frac{m\eta}{1-\eta}\right]^{1/2} \qquad \text{G-40}$$

is obtained.

THERMAL EMISSION ADDED TO PHOTOEMISSION NOISE

Another source of photocathode noise is the thermionic emission of single electrons. The strength of the emission varies with photocathode type. In the bialkali cathode, for example, thermionic emission is virtually absent; on the other hand, Ag-O-Cs photocathodes exhibit relatively large dark currents as a result of thermionic emission. These currents can be eliminated to some extent by cooling the tube.

Randomly emitted thermionic electrons add a term to the fluctuation in the photoelectron current proportional to their number. Because of their independence with respect to any usual signal current, the term adds to that of the signal noise in quadrature. (See Eq. G-l1.) That is,

$$\sigma^2_{p.e.} = \eta\bar{n}_p + \bar{n}_{th} \qquad \text{G-41}$$

where $\bar{n}_{th}$ is the average number of thermionic electrons emitted in a time τ, and $\eta\bar{n}_p$ is the average number of photoelectrons emitted in the same time.

STATISTICS RELATED TO SECONDARY EMISSION

Although the amplification (multiplication) of the photoelectron current in the dynode chain of a photomultiplier is often referred to as noise-free, careful examination of the statistics of the gain mechanisms involved shows that this statement is not entirely correct. Approximate noise-free operation can be attained, however, with the use of proper electron optics and newly developed dynode materials. In the following discussion the statistical gain processes in the individual dynodes are examined and then combined to yield the statistical properties of the entire multiplier chain. Much of the work presented was accomplished at a very early stage in photomultiplier history.[129]

For a given primary energy, it is possible to obtain any number of secondaries n_s from zero to a maximum $n_{s(max)}$. The maximum number is given by the quotient of the primary energy E_p and the energy required to produce a hole-electron pair within the dynode ε_p, as follows:

$$n_{s(max)} = E_p/\varepsilon_p \qquad \text{G-42}$$

Over many repeated measurements using primary electrons of the same energy, a truncated distribution is obtained for n_S. A model that describes the observed distributions from most practical dynodes follows.

The observed number distributions for secondary electrons vary among the different types of dynodes used commercially. Nearly all the distributions fall within the class limited by a Poisson distribution[130] at one extreme and an exponential distribution at the other.[131] To describe this wide variety of distributions the Polya, or compound Poisson, distribution is employed.[132] Through the adjustment of one parameter, the distribution runs from purely Poisson to exponential. Therefore, this one distribution can be used to describe and to interpret the bulk of the observed secondary-emission statistics.

The distribution has the following form:

$$P(n, b) = \frac{\mu^n}{n!}(1 + b\mu)^{-n-1/b} \cdot \prod_{j=1}^{n-1}(1 + jb) \qquad \text{G-43}$$

where P(n,b) is the probability of observing n secondaries, μ is the mean value of the distribution, and b is the parameter controlling the shape of the distribution. With b = 0, the distribution is Poisson, as follows:

$$P(n,o) = \frac{\mu^n}{n!}\, e^{-\mu} \qquad \text{G-44}$$

With b = 1, an exponential distribution results, as given by:

$$P(n, 1) = \mu^n(1 + \mu)^{-(n+1)} \qquad \text{G-45}$$

Fig. G.3 shows a family of distributions for various values of b.

The generating function for P(n,b) is given by

$$Q(s) = [1 + b\mu(1 - s)]^{-1/b} \qquad \text{G-46}$$

From Eqs. G-3 and G-6

$$\bar{n} = \mu \qquad \text{G-47}$$

and

$$\sigma^2 = b\mu^2 + \mu \qquad \text{G-48}$$

The fluctuations increase as μ^2 for an exponential distribution (b = 1), but increase only as μ for the Poisson distribution. The signal-to-noise ratio is given by

$$\frac{\bar{n}}{\sigma} = \mu/(b\mu^2 + \mu)^{1/2} \qquad \text{G-49}$$

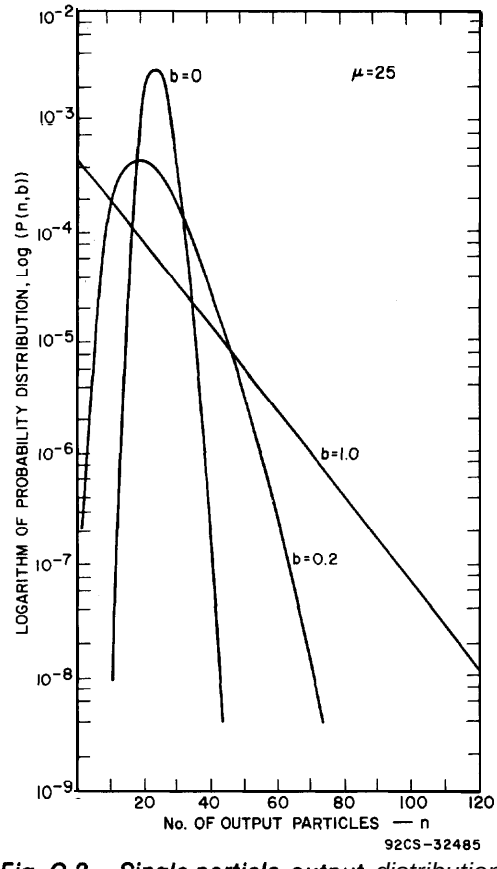

Fig. G-3 - Single-particle output distribution for a dynode displaying Polya statistics. *A value of b = gives an exponential distribution; b = 0 gives a Poisson distribution; b = 0.2 is intermediate between the two extreme values.*

Fig. G-4 shows a log-log plot of the signal-to-noise ratio as a function of μ with b as a parameter. The signal-to-noise ratio improves with increasing μ for the Poisson distribution, but approaches unity with large μ in the exponential distribution. In fact, for any non-zero value of b, the signal-to-noise ratio approaches $b^{-1/2}$ for large μ. As shown in Fig. G-4, even small departures from

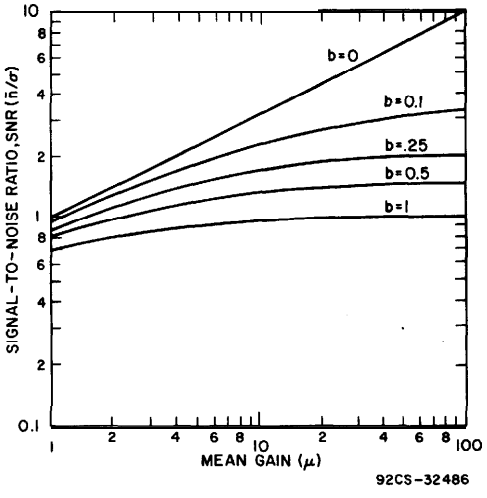

Fig. G-4 - A comparison of the SNR as a function of the mean value μ for a number of Polya distributions. For Poisson statistics (b = 0), the SNR increases as the square root of μ. With 0 < b ≤ 1, the SNR approaches the square root of b - for large mean gains.

Poisson statistics significantly reduce the signal-to-noise ratio at moderately high gains of 10 to 20. It can be anticipated that departures from Poisson statistics degrade the single-electron pulse-height resolution.

The Polya distribution has an interesting interpretation with respect to secondary-emission statistics. [132] For non-zero values of b, the distributions described by Eq. G-43 can be shown to be composed of a number of different Poisson processes, each with a different mean value. The mean values are, in turn, distributed according to the Laplace distribution. When b equals 0, the distribution of the mean values collapses to a delta function at the value μ, leading to a purely Poisson distribution. For b equals 1, the distribution of the mean values is exponential. The physical interpretation for a dynode displaying non-Poisson statistics is that physical non-uniformities on the dynode surface cause each element of the surface to have a different mean value for emission. Although each small element exhibits Poisson statistics with respect to emission, the total emission from the entire dynode is non-Poisson because it comprises a distribution of Poisson distributions. It is possible that the basic emission process from a given dynode is not a Poisson process. However,

high-gain GaP dynodes exhibit nearly Poisson statistics[130] and at present it is believed that departures from this norm are caused, to a large extent, by dynode nonuniformities.

The departure from Poisson statistics affects the single-particle pulse-height resolution. Fig. G-5 shows the output-pulse distribution from a single dynode for a number of multiple-particle inputs. The resolution is clearly degraded in passing from a Poisson distribution to an exponential one. With the exponential distribution shown in Fig. G-5, it would be difficult to distinguish among one-, three-, and five-particle input pulses, whereas the problem virtually disappears for a Poisson distribution.

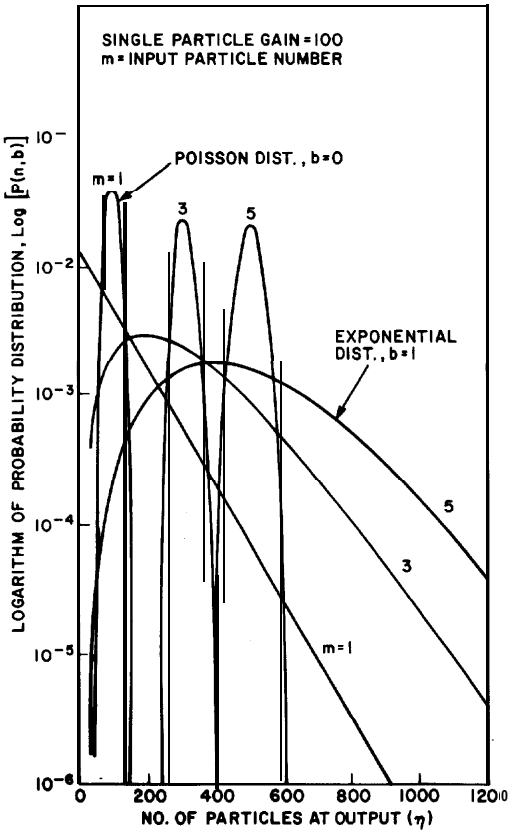

Fig. G-5 - A comparison of multiple-particle distributions from a single dynode having Poisson and exponential distribution. Clearly, the particle resolution characteristics of the exponential distribution are much poorer.

Statistics for a Series of Dynodes

Assume that one primary electron impinging on the first dynode releases, on the average, δ_1 secondaries with variance σ_1^2. The output of the first dynode striking the second dynode produces an average gain at the second stage of $\bar{m}_2$ and a variance of σ_{m2}^2. From Eqs. G-15 and G-16 for cascade events, the average gain and its variance may be related to the individual dynode statistics as follows:

$$\bar{m}_2 = \delta_1 \cdot \delta_2 \qquad \text{G-50}$$

and

$$\sigma_{m2}^2 = \delta_2^2\sigma_1^2 + \delta_1\sigma_2^2 \qquad \text{G-51}$$

where δ_2 and σ_2^2 are the average secondary emission and variance for the second dynode for a single-input electron. Continuing in this manner, the gain and fluctuation from the third stage are given by

$$\bar{m}_3 = \delta_1 \cdot \delta_2 \cdot \delta_3 \qquad \text{G-52}$$

and

$$\sigma_{m3}^2 = \delta_3^2[\delta_2^2\sigma_1^2 + \delta_1\sigma_2^2] + \delta_1\delta_2\sigma_3^2 \qquad \text{G-53}$$

Eq. G-53 can be rearranged to read

$$\sigma_{m3}^2 = [\delta_1\delta_2\delta_3]^2 \cdot \left\{\frac{\sigma_1^2}{\delta_1^2} + \frac{\sigma_2^2}{\delta_1\delta_2^2} + \frac{\sigma_3^2}{\delta_1\delta_2\delta_3^2}\right\} \qquad \text{G-54}$$

The extension of Eqs. G-53 and G-54 to k stages is accomplished by adding terms to Eqs. G-50 and G-51 as follows:

$$\bar{m}_k = \delta_1 \cdot \delta_2 \cdot \cdots \delta_k \qquad \text{G-55}$$

$$\sigma_{mk}^2 = (\bar{m}_k)^2\left[\frac{\sigma_1^2}{\delta_1^2} + \frac{\sigma_2^2}{\delta_1 \cdot \delta_2^2} + \cdots \frac{\sigma_k^2}{(\delta_1 \cdot \delta_2 \cdots \delta_{k-1})\delta_k^2}\right] \qquad \text{G-56}$$

Eq. G-55 states the expected results: that the total average gain for a series of k dynodes is the product of the secondary-emission yields of the individual dynodes in the series. Eq. G-56 shows that the relative contribution of any state to the total fluctuation decreases with the proximity of the dynodes to the output end of the chain. The first stage contributes most to the total variance. The higher the first-stage gain, the less each subsequent stage contributes to the total variance. This property is an important feature of the high-gain GaP first-dynode photomultipliers.

The signal-to-noise ratio for the multiplier chain is given by

$$\frac{\bar{m}_k}{\sigma_{mk}} = \left[\frac{\sigma_1^2}{\delta_1^2} + \frac{\sigma_2^2}{\delta_1\delta_2^2} + \cdots \frac{\sigma_k^2}{(\delta_1 \cdot \delta_2 \cdots \delta_{k-1})\delta_k^2}\right]^{-1/2} \quad \text{G-57}$$

For large first-stage gains, the multiplier signal-to-noise ratio is high. Most of the noise contribution is from the first stage. If, in addition to a large gain, the first stage exhibits Poisson statistics, as explained above, the signal-to-noise ratio becomes

$$SNR_k = \frac{\bar{m}_k}{\sigma_{mk}} \approx \sqrt{\delta_1} \quad \text{G-58}$$

The noise added to the input signal is very small. It is in this sense that the multiplication chain is said to provide noise-free gain.

Multiple-Particle Inputs

The output-pulse distribution for multiple-particle inputs is obtained from the generating function for the multiplier chain.

By an extension of Eq. G-14 for the generating function for a cascaded event, the generating functions for a chain of k dynodes may be obtained:

$$Q_k(s) = Q_1\{Q_2[\cdots Q_k(s)]\}$$

The probability $P_k(n)$ of observing n electrons (for a one-electron input) at the output of a k-stage chain is derived from Eq. G-4 as follows:

$$P_k(n) = \frac{1}{n!}\left.\frac{\partial^n Q_k(s)}{\partial s^n}\right|_{s=0} \quad \text{G-60}$$

The generating function for a k-stage multiplier chain for multiple-particle inputs is given by extension of Eq. G-9 as follows:

$$Q_k(s,m) = [Q_k(s)]^m \quad \text{G-61}$$

The probability of observing n output electrons from m input particles is therefore given by

$$P_k(n,m) = \frac{1}{n!}\left.\frac{\partial_n[Q_k(s)]^m}{\partial s^n}\right|_{s=0} \quad \text{G-62}$$

When identical dynodes are used, the output distribution for single-electron input pulses evolves toward a steady-state distribution after four or five stages, and exhibits little change thereafter. Fig. G-6 shows some single-electron distribution[132] computed by use of the Polya statistics for each stage in the chain as explained above. As b approaches 1, the distribution becomes more sharply peaked.

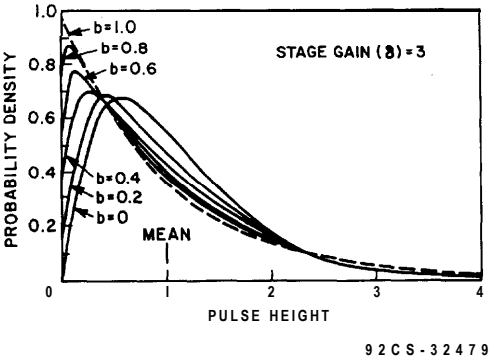

Fig. G-6 - Computed single-electron distribution for a range of values of parameter b. Parameter b is defined in Appendix B.

Computer values of multiple-particle outputs for a two-stage structure are shown in Fig. G-7.[131] The two curves relate to two different structures that have the same dynode as a first stage. The solid-line curve shows the output when the first stage is followed by **a high-gain ($\delta = 500$) second stage having** nearly pure Poisson statistics (b = 0.01). The output peaks are sharply defined, and pulses up to a ten-electron input pulse are clearly resolvable. The dashed line describes the final output distribution when the first stage

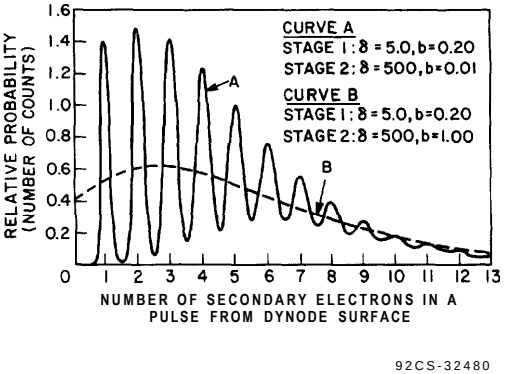

Fig. G-7 - Theoretical pulse-height distribution.

is followed by a high-gain ($\delta = 500$) dynode having an exponential output distribution. Individual peaks are no longer discernible; the large variance associated with the exponential statistics of the second stage eliminates all the structure in the output of the first stage.

BURLE has developed a high-gain gallium phosphide dynode which, when used as the first stage in a conventional copper beryllium multiplier chain, greatly increases the pulse-height resolution of the photomultiplier. The high-gain first stage in a photomultiplier having multiple photoelectron events originating from the photocathode is similar to the case illustrated in Fig. G-7 for a multiplier where the high-gain second dynode amplifies the multiple pulses originating from the first dynode which in turn are initiated by single electrons. Typical gains for the gallium phosphide dynodes are 30 to 45, and their statistics are nearly Poisson. Fig. G-8 shows the multiple-particle pulse-height distribution for the tube, and Fig. G-9 shows the pulse-height curves for a tritium scintillation input for a conventional tube using the standard copper-beryllium first dynode along with that for a tube with a gallium phosphide first dynode. The increased resolution of the gallium phosphide dynode is clearly shown.

Note: The first photoelectron peak of the 8850 spectra includes dark noise from the photomultiplier, chemiluminescence and phosphorescence from the vial and cocktail, as well as H^3 disintegration.

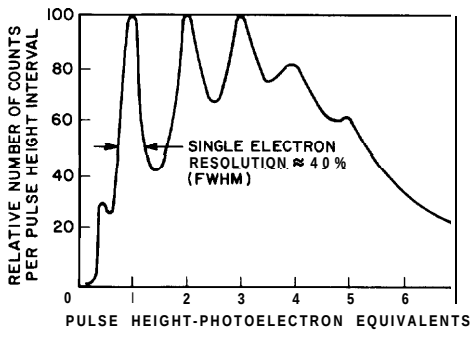

Fig. G-8 - Typical photoelectron pulse-height spectrum for a photomultiplier having a GaP first dynode.

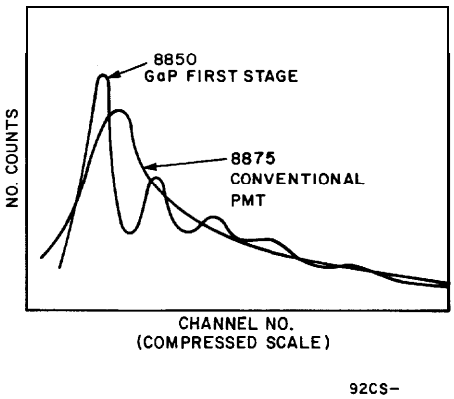

Fig. G-9 - A comparison of the tritium scintilla pulse-height spectra obtained using a conventional photomultiplier having all CuBe dynodes and a photomultiplier having a Ga first stage. Note: The first photoelectron peak of the 8850 spectra includes dark noise from the photomultiplier, chemiluminescence and phosphorescence from the vial and cocktail, as well as ^3H disintegration.

FLUCTUATIONS IN THE TUBE AS A WHOLE

In the previous sections the noise contributions from the photocathode and the multiplier chain were considered. These results can be combined to obtain the signal-to-noise ratio for the photomultiplier as a whole.

The average number of photoelectrons from the photocathode in a time τ is given by

$$\bar{n}_{p.e.} = \eta \cdot \bar{n}_p \qquad \text{G-63}$$

The variance is given by

$$\sigma^2_{p.e.} = \eta \cdot \bar{n}_p \qquad \text{G-64}$$

It is assumed that $\sigma_p^2 = \bar{n}_p$ or that the input flux of photons displays Poisson statistics. If the form for σ_p^2 is not the result of a Poisson process, Eq. G-16 must be used to obtain $\sigma^2_{p.e.}$.

Using these expressions to describe the input to the photomultiplier chain, the average number of electrons collected at the anode can be stated as follows:

$$\bar{n}_a = \eta \cdot \bar{n}_p \cdot \bar{m}_k \qquad \text{G-65}$$

where $\bar{m}_k$ is given in Eq. G-55 and is the average gain of a k-stage multiplier. The variance for the output electron stream is given by

$$\sigma_a^2 = \bar{m}_k^2 \cdot \eta \cdot \bar{n}_p + \eta \cdot \bar{n}_p \cdot \sigma^2_{mk} \qquad \text{G-66}$$

where σ_{mk}^2 is given by Eq. G-56 and is the variance in the average gain of a k-stage multiplier chain.

Eq. G-66 can be rearranged as follows:

$$\sigma_a^2 = \eta\bar{n}_p(\bar{m}_k^2 + \sigma_{mk}^2) \qquad \text{G-67}$$

For equal-gain stages described by Poisson statistics in the multiplier chain, Eq. G-56 becomes

$$\sigma_{mk}^2 = \frac{\bar{m}_k^2}{(\delta - 1)}\left(1 - \frac{1}{\delta^k}\right) \qquad \text{G-68}$$

Neglecting the $1/\delta^k$ term and substituting the result and δ^k for m_k in Eq. G-67,

$$\sigma_a^2 = \eta\bar{n}_p\left[\delta^{2k}\left(1 + \frac{1}{\delta - 1}\right)\right] \qquad \text{G-69}$$

In this case

$$\text{SNR}_a = \sqrt{\eta\bar{n}_p \Big/ \left(\frac{\delta}{\delta - 1}\right)}. \qquad \text{G-70}$$

High dynode gains imply that $1/(\delta - 1)$ is much less than 1 and hence that

$$\sigma_a^2 = \eta\bar{n}_p(\delta^{2k}). \qquad \text{G-71}$$

The signal-to-noise ratio at the anode is given by

$$\text{SNR}_a = \frac{\bar{n}_a}{\sigma_a} = (\eta\bar{n}_p)^{1/2} \qquad \text{G-72}$$

For high-gain dynodes exhibiting Poisson statistics, therefore, SNR_a is essentially that of the photoelectrons, $\text{SNR}_{p.e.}$, as given in Eq. G-33.

In a photomultiplier in which the dynode gain is not high but still exhibits Poisson statistics, SNR_a is given by

$$\text{SNR}_a = \frac{(\eta\bar{n}_p)^{1/2}}{\left[\frac{\delta}{\delta - 1}\right]^{1/2}} \qquad \text{G-73}$$

As an example, with $\delta = 4$ the SNR_a is decreased by a factor of 0.87 from its value for very large δ. Doubling δ to a value of 8 changes the degradation factor to 0.94. Further increases in δ do not improve the SNR_a very much.

In the case of fully exponential dynode statistics, the variance for each dynode in a chain of identical dynodes is given by Eq. G-48; i.e.,

$$\sigma_s^2 = \delta^2 + \delta \qquad \text{G-74}$$

where δ is the average gain per stage. The total anode fluctuation then becomes

$$\sigma_a^2 = (\eta\bar{n}_p)\left[\delta^{2k}\left(1 + \frac{(\delta + 1)}{(\delta - 1)}\right)\right] \qquad \text{G-75}$$

For large dynode gains,

$$\sigma_a^2 \approx 2(\eta\bar{n}_p)\delta^{2k} \qquad \text{G-76}$$

Even for large dynode gains, exponential statistics increase σ_a^2 by a factor of 2, with the result that SNR_a decreases by $1/\sqrt{2}$. This drop in SNR, is accompanied by a severe loss in single- and multiple-electron pulse-height resolution, as shown in Fig. G-7. To resolve single-photoelectron pulses, the multiplier chain must exhibit both high gain and good (i.e., Poisson) statistics.

A significant improvement in SNR, results when the photocathode quantum efficiency η is increased. At present the peak value of η for the S-20 cathode is 0.35; doubling η to 0.7 would improve SNR_a by a factor of 1.4. The ideal photomultiplier, for which $\eta = 1$, would have an $\text{SNR}_\perp$ equal to the square root of $\bar{n}_p$. The present value of $\eta = 0.35$ degrades the ideal SNR_a by a factor of 0.59. Considerable improvement can be expected with the development of photocathode materials of increased sensitivity.

The application of these equations to present photomultipliers indicates that the available photocathode quantum efficiency is the principal degrading influence on SNR_a. Values of η less than 1 also decrease the multiple-photon input-pulse resolution of a photomultiplier. High dynode gains (δ greater than 6) do not significantly degrade the input signal-to-noise ratio of photoelectrons provided the dynode statistics are nearly Poisson.

OTHER SOURCES OF NOISE IN PHOTOMULTIPLIER TUBES

Within a photomultiplier there are sources of noise that are not associated directly with the processes of photoelectric conversion and electron multiplication. These sources can, in general, be separated into two groups: (1) those that are not correlated with and (2) those that are correlated with the signal pulse.

Non-Correlated Noise Sources

The materials used to fabricate the internal structure and the glass envelope of a

photomultiplier may contain amounts of certain radioactive elements that decay and give off gamma rays or other high-energy particles. If one of these emitted particles strikes the photocathode or one of the first few dynodes, it will produce an anode dark pulse. The size of the anode pulse may be equivalent to one or more photoelectrons emitted at the photocathode. These pulses are randomly emitted. In tube manufacture this type of emission is minimized through the careful selection of materials.

Analytically, the fluctuations resulting from non-correlated random sources add in quadrature to those of the signal. Because they are random, the dark-pulse variances σ_{dp}^2 are proportional to the average dark-pulse rate $\bar{n}_{dp}$, as follows:

$$\sigma_{dp}^2 = \bar{n}_{dp} \qquad \text{G-77}$$

The total anode variances are given by:

$$\sigma_a^2 = (\eta\bar{n}_p + \bar{n}_{dp}) \cdot \left[\bar{m}_k^2\left(1 + \frac{1}{\delta - 1}\right)\right] \qquad \text{G-78}$$

where $\eta\bar{n}_p$ and $\bar{n}_{dp}$ are the average single-photoelectron and the average single-dark-emitted electron numbers observed in a time τ. The factor $\bar{n}_{dp}$ sets a real limit on the anode signal-to-noise ratio. Again, in those instances where the incoming radiation signal comprises more than one photon, coincidence techniques can be employed to reduce the effect of randomly emitted electrons originating at the cathode.

Electrons may originate at dynodes well along in the multiplier chain. At the anode, these electrons appear as fractional-photoelectron pulses. Such pulses also result from interstage skipping, generally near the beginning of the chain. With good statistics in the chain, the fractional pulses may be discriminated against because the single-electron peak in the pulse-height spectrum stands out sharply.

Correlated Noise Sources

A gas atom or molecule within the photomultiplier may be ionized by a photoelectron pulse, This ionization may occur at the first-dynode surface or in the vacuum between the photocathode and the first dynode. The positive ion thus created travels backward to the cathode where it may release one or more electrons from the photocathode. Because there is a time delay in the ion-emitted electron pulse equal to the time of flight of the ion to the photocathode, the resulting pulse, usually referred to as an afterpulse, occurs after the true signal pulse at the anode. Afterpulses are caused mainly by hydrogen ions and their occurrence can be minimized in tube processing.

Primary electrons produce photons as well as secondary electrons within the dynodes of the multiplier chain. Despite the low efficiency of this process, some of the emitted photons may eventually reach the photocathode and release additional electrons. A time delay is observed corresponding to the transit time for the regenerated electron pulse to reach the point of origin of the light. Depending upon the type of dynode multiplier cage, this time may be of the order of 20 nanoseconds. Most of the photons comprising the light feedback originate in the region of the last few dynodes or of the anode.

If the voltage across the tube is increased, the dark-pulse rate also increases and usually produces some observable light near the anode region, a fraction of which is fed back to the photocathode. The result of this positive feedback. is that, at a certain voltage, the photomultiplier becomes unstable and allows the output dark-pulse rate to increase to an intolerably high level. The voltage at which this increase occurs is generally above the recommended maximum operating voltage.

Not every signal pulse initiates an afterpulse. Therefore, coincidence techniques, using more than one photomultiplier, can be employed in some instances to eliminate this source of noise as well as the uncorrelated sources discussed above.

If correlated noise sources cannot be eliminated by time discrimination or other means, an analytical treatment for the total variance would follow the form given by Eq. G-12.

NOISE AND THE BANDWIDTH OF THE OBSERVATION

At high counting rates, noise calculations are performed with the average and variance

of the photoelectron current rather than with individual photoelectron pulses. The expressions which have been developed for signal-to-noise ratio by consideration of the average number of events in a time τ and the variance from average may be converted to expressions of signal-to-noise ratio involving currents and bandwidth, B, by considering the reciprocal nature of the observation time and the bandwidth.

Noise equivalent bandwidth B may be defined[133] as follows:

$$B = \frac{1}{A_m^2} \int_0^\infty |H(j\omega)|^2 \, df \qquad \text{G-79}$$

where $H(j\omega)$ is the complex frequency transfer response of the circuit, and A_m is the maximum absolute value of $H(j\omega)$. The "circuit" in this case counts pulses in a time τ. The network transfer function is the Laplace transform of the impulse response. The impulse response is a rectangular pulse of width τ, like a camera shutter. For this case,

$$H(j\omega) = \frac{1}{j\omega}(1 - e^{-j\tau\omega}) \qquad \text{G-80}$$

and A_m is found to be equal to τ. The noise equivalent bandwidth is then readily found to be

$$B = 1/2\tau. \qquad \text{G-81}$$

It is of interest to compare this relation with the equivalent noise bandwidth for exponential impulse response as in an RC circuit; in this case

$$B = 1/4RC \qquad \text{G-82}$$

From Eq. G-25, the SNR for a random photon flux is given by

$$SNR_p = \sqrt{I_p \tau} \qquad \text{G-83}$$

where I, is the average photon arrival rate and τ is the time interval of the count. When $\tau = 1/2B$ is substituted,

$$SNR_p = \sqrt{I_p/2B} \qquad \text{G-84}$$

In the case of the photocathode electron current,

$$SNR_{p.e.} = \sqrt{\frac{\eta I_p}{2B}} = \sqrt{\frac{i}{2eB}} \qquad \text{G-85}$$

where i is the photocathode emission current in amperes and e is the charge of the electron. If the signal current is considered as i, the noise in the bandwidth B for the photocurrent is the familiar shot noise formula $(2eiB)^{1/2}$.

The equation for the photon noise squared is given by

$$I_{pN}^2 = 2\, I_p B \qquad \text{G-86}$$

The photocurrent noise squared is given by

$$I_{peN}^2 = 2\eta e^2 I_p B \qquad \text{G-87}$$

Both these equations involve the photon "current" I,.

If the photons are not randomly emitted, Eq. G-86 must be modified. In the case in which the variance in the photon current is given by σ_p^2, the equation becomes

$$I_{peN}^2 = 2e^2 B \left[\eta I_p (1 - \eta) + \frac{\sigma_p^2 \eta^2}{\tau}\right] \qquad \text{G-87a}$$

For a randomly emitted photon, the noise current squared at the anode is given by

$$\Delta I_{aN}^2 = 2e^2 \eta \delta^{2k} I_p B. \qquad \text{G-88}$$

where the multiplier chain is assumed to be composed of k high-gain dynodes exhibiting Poisson statistics, each with an average gain δ.

At the anode, the input resistance and capacitance of a preamplifier generate a noise current squared given by

$$i_n^2 = 4kTgB \cdot \left[1 + R_n g + \frac{4\pi^2}{3} \cdot \frac{R_n}{g} B^2 C^2\right] \qquad \text{G-89}$$

where g = l/R is the shunt conductance in the anode lead, C is the shunt capacitance, B is the bandwidth, k is Boltzmann's constant, T is the absolute temperature, and R_n is the equivalent noise resistance of the preamplifier input. The total noise current squared through R is $\Delta I_{aN}^2 + i_n^2$, and SNR_a is given by

$$SNR_a = \eta\delta^k I_p e \left[2e^2\eta\delta^{2k} I_p B + 4k\,TgB \cdot \left(1 + R_n g + \frac{4\pi^2}{3}\frac{R_n}{g} B^2 C^2\right)\right]^{-1/2} \quad \text{G-90}$$

To maintain the input SNR, ΔI_{aN}^2 must be greater than i_n^2. For example, with $\Delta I_{aN}^2 = 10\ i_n^2$, and R = 100 ohms, C = 100 picofarads, R_n = 100 ohms, T = 300 K, and $B = 10^6$ Hz, at room temperature,

$$i_n^2 = 3.2\ 10^{-16}\ \text{amperes}^2 \quad \text{G-91}$$

With $\eta = 0.3$ and $\delta^k = 10^6$,

$$I_p = 10 i_n^2 / (\,2e^2\eta\delta^{2k}B\,) \quad \text{G-92}$$

or

$$I_p \cong 2 \times 10^5 \text{ photons per second}$$

The value of I, shown in Eq. G-92 is the lower limit for the average photon current and makes the squared anode-current fluctuation greater than the squared noise current in the photomultiplier preamplifier input by a factor of ten. The resulting value of the average photon current corresponds to a photoelectric current of about 10^{-14} ampere, or about 6×10^4 photoelectrons per second. In cases in which the dark current is effectively higher than 6×10^4 photoelectrons per second, the photomultiplier sensitivity limit is set by the dark current and not by the preamplifier noise. It is the noise-free gain of the multiplier chain which increases the rms photocurrent shot noise by a factor of δ^k and permits the low-input-level operation. See also Fig. 65 in Chapter 4, **Photomultiplier Characteristics.**

PULSE COUNTING STATISTICS*

In utilizing a photomultiplier in a "photon" counting mode, individual anode pulses initiated by electrons from the photocathode are counted. Because the count at very low light levels originates from both photoemission and thermionic emission, two separate counts are required: one in the light and one in the dark. In determining the photoelectron count rate, the statistics of the measurement are improved by increasing the count time. The present discussion recommends the optimum time division between the dark and the light counts.

Let the average photoemission and thermionic emission rates be I_{pe} and I_{te}, respectively. Let the time for the count in the light be τ_p and the time for the dark count be τ_d. The total counts in the light and dark measurements are then:

$$n_p = (I_{pe} + I_{te})\tau_p \quad \text{G-93}$$

$$n_d = I_{te}\tau_d. \quad \text{G-94}$$

The variances for the light and dark measurements are given by

$$\sigma_p^2 = n_p \quad \text{G-95}$$

$$\sigma_d^2 = n_d. \quad \text{G-96}$$

The final "signal" which is a measure of I, is given by

$$S = \frac{n_p}{\tau_p} - \frac{n_d}{\tau_d} \quad \text{G-97}$$

Assume that the times of the counts are accurately determined so that the respective variances of τ_p and τ_d are negligible. By the use of Eq. G-21 for multiplication (by the reciprocal of the count times), the variance of each term in G-97 is then

$$\sigma^2\left(\frac{n_p}{\tau_p}\right) = \frac{n_p}{\tau_p^2} \quad \text{G-98}$$

$$\sigma^2\left(\frac{n_d}{\tau_d}\right) = \frac{n_d}{\tau_d^2}. \quad \text{G-99}$$

For the variance of a difference, using Eq. G-11,

$$\sigma_s^2 = \frac{n_p}{\tau_p^2} + \frac{n_d}{\tau_d^2} \quad \text{G-100}$$

The signal-to-noise ratio in the determination of I, is then given by

$$SNR = \frac{\left(\frac{n_p}{\tau_p} - \frac{n_d}{\tau_d}\right)}{\left[\frac{n_p}{\tau_p^2} + \frac{n_d}{\tau_d^2}\right]^{1/2}} \quad \text{G-101}$$

*Measured signal-to-noise ratios are similar for pulse-counting or for current -measurement techniques.[134] Baum[135] has shown that in some cases, pulse counting can have an advantage of the equivalent of a factor of 1.2 in quantum efficiency.

The expression for the noise (σ_s) in G-101 is to be minimized with respect to the division of times τ_p and τ_d. Let the total time be $\tau = \tau_p + \tau_d$. Substitute for τ_p and for n_p and nd from G-93 and G-94:

$$\sigma_s = \left[\frac{I_{pe} + I_{te}}{\tau - \tau_d} + \frac{I_{te}}{\tau_d}\right]^{1/2} \qquad \text{G-102}$$

and differentiate with respect to τ_d, considering the other quantities as invariant. Setting $\delta\sigma_s/\delta\tau_d = 0$, we have for the maximum SNR condition:

$$\frac{\tau_p}{\tau_d} = \left[\frac{I_{pe} + I_{te}}{I_{te}}\right]^{1/2} \qquad \text{G-103}$$

The implication of Eq. G-103 is as follows: For example, if the signal count is much less than the dark count, about equal times should be spent for both readings. If the signal count and dark count are about equal, $\tau_p = \sqrt{2}\tau_d$.

PULSE-HEIGHT RESOLUTION IN SCINTILLATION COUNTING

In scintillation counting, for the case of a K_2CsSb photocathode and a NaI:Tl scintillator, the typical photoemission yield is approximately 8 photoelectrons per keV of gamma-ray energy absorbed in the crystal- or 125 eV per photoelectron. The peak of the emission spectrum for NaI:Tl is approximately at 415 nm which corresponds to a photon energy of 3 eV. The quantum efficiency of the bialkali photocathode for the blue spectrum of the scintillator is approximately 25 per cent. If the crystal were 100 per cent efficient in converting gamma-ray energy to light energy, one would expect a photoelectron for every 12 eV. Thus, the conversion efficiency of the crystal is about 10 per cent.

The statistics of the pulse-height distribution, therefore, involve both the crystal and the photomultiplier processes. On the other hand, if the conversion efficiency of the crystal were 100 per cent, the photoelectric conversion of the gamma-ray would yield essentially a constant number of photons per conversion and the crystal would then not contribute to the statistical process.

Let the average number of photons exiting from the scintillator onto the photocathode per photoelectrically converted gamma-ray be m_c with a variance of σ_c^2. Assume the average quantum efficiency of the photocathode to be η. The variance of the photoemission process is as before (Eq. G-28):

$$\sigma^2 = \eta - \eta^2 \qquad \text{G-104}$$

Now, using G-15 and G-16 for a cascaded event, the average number of photoelectrons per pulse is

$$n_p = m_c\eta \qquad \text{G-105}$$

and the variance in the number of photoelectrons per pulse is

$$\sigma_p^2 = \eta^2\sigma_c^2 + m_c(\eta - \eta^2) \qquad \text{G-106}$$

It is instructive to consider the signal-to-noise ratio at each stage of the photomultiplier. For the photocurrent in the pulse, using G-105 and G-106:

$$\text{SNR} = \left[\frac{m_c\eta}{1 - \eta + \eta\sigma_c^2/m_c}\right]^{1/2} \qquad \text{G-107}$$

For the current pulse leaving the first dynode, assuming a secondary emission ratio of δ_1 and a variance of δ_1 (for Poisson statistics), again using G-15 and G-16:

Average electrons per pulse $= \delta_1 m_c\eta$

Variance in this number =

$$\delta_1^2[\eta^2\sigma_c^2 m_c(\eta - \eta^2)] + m_c\eta\delta_1$$

SNR (pulse out of first dynode) =

$$\left[\frac{m_c\eta}{1 - \eta + \dfrac{\eta\sigma_c^2}{m_c} + \dfrac{1}{\delta_1}}\right]^{1/2} \qquad \text{G-108}$$

Similarly, for the pulse out of the second dynode:

Average electrons per pulse $= \delta_1\delta_2 m_c\eta$

Variance in this number =

$$\delta_1^2\delta_2^2[\eta^2\sigma_c^2 + m_c(\eta - \eta^2] + m_c\eta\delta_1\delta_2^2 + m_c\eta\delta_1\delta_2$$

SNR (pulse out of second dynode) =

$$\left[\frac{m_c\eta}{1-\eta+\frac{\eta\sigma_c^2}{m_c}+\frac{1}{\delta_1}+\frac{1}{\delta_1\delta_2}}\right]^{1/2} \qquad \text{G-109}$$

If a tube having k stages of equal secondary emission is considered, δ:

Average electrons per pulse $= \delta^k m_c\eta$

Variance in this number $= \delta^{2k} m_c\eta\left[1-\eta+\frac{\eta\sigma_c^2}{m_c}+\frac{1}{\delta-1}\right]$

SNR (anode pulse) =

$$\left[\frac{m_c\eta}{1-\eta+\frac{\eta\sigma_c^2}{m_c}+\frac{1}{\delta-1}}\right]^{1/2} \qquad \text{G-110}$$

In pulse-height resolution measurements it is common to refer to the **Full-Width-Half-Maximum (FWHM)** which may be related to the SR as follows:

FWHM $= 2.355/\text{SNR}$

$$= 2.355\left[\frac{1-\eta+\frac{1}{\delta-1}}{m_c\eta}+\frac{\sigma_c^2}{m_c^2}\right]^{1/2} \qquad \text{G-111}$$

The first term in the brackets represents the relative variance of the photomultiplier contribution and the second term is the relative variance of the crystal contribution.

One might expect σ_c^2 to have a magnitude about equal to m_c, the number of photons per pulse. In this case,

$$\text{FWHM} = 2.355\left[\frac{1+\frac{1}{\delta-1}}{m_c\eta}\right]^{1/2} \qquad \text{G-112}$$

Actually, the crystal statistics are worse than the above assumption. This question is discussed in more detail in Chapter 4, **Photomultiplier Characteristics** in the section on "Pulse Counting."

SUMMARY

The more important expressions relating to signal and noise discussed in this Appendix are summarized below. Beginning at the input to the photomultiplier, the signal is followed through the tube, and the variance and the SNR associated with the signal are noted.

Photon flux: Conditions: random emission, Poisson statistics. Terminology: average number, $\bar{n}_p$; observation time interval, τ; average rate of emission, I_p photons per second; variance in photon number, σ_p^2.

$$\bar{n}_p = I_p\tau$$
$$\sigma_p^2 = I_p\tau = \bar{n}_p$$
$$\text{SNR} = \bar{n}_p/\sigma_p = \sqrt{I_p\tau} = \sqrt{\bar{n}_p}$$

Photoemission from a photocathode: Conditions: photon flux as above; Terminology: quantum efficiency, η; average number of photoelectrons emitted in time τ, $\bar{n}_{p.e.}$; variance in photoelectron number, $\sigma_{p.e.}^2$.

$$\bar{n}_{p.e.} = \eta I_p\tau$$
$$\sigma_{p.e.}^2 = \eta I_p\tau$$
$$\text{SNR}_{p.e.} = \sqrt{\eta I_p\tau}$$

Dark emission from a photocathode: Terminology: average number of thermionic electrons in time τ, $\bar{n}_{th}$; variance in dark emission number, σ_{th}^2.

$$\sigma_{th}^2 = \bar{n}_{th}$$

Combined dark and photoemission from the photocathode: Terminology: average total electron emission number in time τ, $\bar{n}_{p+t}$.

$$\bar{n}_{p+t} = \bar{n}_{p.e.} + \bar{n}_{th} = \eta I_p\tau + \bar{n}_{th}$$
$$\sigma_{p+t}^2 = \eta I_p\tau + \bar{n}_{th}$$
$$\text{SNR}_{p+t} = (\eta I_p\tau + \bar{n}_{th})^{1/2}$$

Photoemission determined from total emission: Conditions: dark emission determined over a time large with respect to τ, so that the variance in the measurement is negligible; dark emission to be subtracted from total emission to determine photoemission .

$$\bar{n}_{p.e.} = \bar{n}_{p+t} - \bar{n}_{th} = \eta I_p \tau$$
$$\sigma^2_{p.e.} = \eta I_p \tau + \bar{n}_{th}$$
$$SNR_{p.e.} = \frac{\eta I_p \tau}{(\eta I_p \tau + \bar{n}_{th})^{1/2}}$$

(Also, see section above on Pulse Counting Statistics for cases in which the dark emission count is not determined over a long time interval.)

Multiplier chain with single electron input: Terminology: number of stages, k; average gain and variance of the j^{th} stage, δ_j, σ_j^2; total gain and variance of the multiplier chain, $\bar{m}_k$, σ^2_{mk}.

$$\bar{m}_k = \delta_1 \cdot \delta_2 \cdots \delta_k$$
$$\sigma^2_{mk} = (\bar{m}_k)^2 \left\{ \frac{\sigma_1^2}{\delta_1^2} + \frac{\sigma_2^2}{\delta_1 \delta_2^2} + \cdots \frac{\sigma_k^2}{\delta_1 \cdot \delta_2 \cdots \delta_{k-1} \cdot \delta_k^2} \right\}$$

$$SNR_k = \frac{\bar{m}_k}{\delta_{mk}} = \left\{ \frac{\sigma_1^2}{\delta_1^2} + \frac{\sigma_2^2}{\delta_1 \delta_2^2} + \cdots \frac{\sigma_k^2}{\delta_1 \cdot \delta_2 \cdots \delta_{k-1} \cdot \delta_k^2} \right\}^{-1/2}$$

Photomultiplier tube: Terminology: average number of electrons collected at the anode, $\bar{n}_a$; variance in this number, σ_a^2,

$$\bar{n}_a = \eta \cdot \bar{n}_p \cdot \bar{m}_k$$
$$\sigma_a^2 = \eta n_p (\bar{m}_k^2 + \sigma_{mk}^2)$$
$$SNR_a = \sqrt{\eta \bar{n}_p} / [1 + \sigma_1^2/\delta_1^2 + \sigma_2^2/(\delta_1 \cdot \delta_2^2) + \cdots + \sigma_k^2/(\delta_1 \cdot \delta_2 \cdots \delta_{k-1} \cdot \delta_k^2)]^{1/2}$$

Photomultiplier tube: Conditions: Each stage is identical and has Poisson statistics.

$$\bar{n}_a = \eta \bar{n}_p \bar{m}_k$$
$$\sigma_a^2 = \eta \bar{n}_p \bar{m}_k^2 \left[1 + \frac{1}{\delta - 1} \left(1 - \frac{1}{\delta^k} \right) \right]$$
$$\cong \eta \bar{n}_p \bar{m}_k^2 \delta / (\delta - 1)$$
$$SNR_a \cong [\eta \bar{n}_p (\delta - 1)/\delta]^{1/2}$$

Photomultiplier tube: Conditions: $\delta >> 1$.

$$SNR_a \cong \sqrt{\eta \bar{n}_p}$$

Photomultiplier tube: Conditions: Each stage identical with exponential statistics.

$$SNR_a = [\eta \bar{n}_p (\delta - 1)/2\delta]^{1/2}$$

Photomultiplier tube: Conditions: high-gain dynodes assumed, high photon-counting rates, output circuit noise contributions included. Terminology: charge on the electron, e; bandwidth, B; Boltzmann's constant, k; temperature, T, (degrees Kelvin); equivalent noise resistance of the input of the preamplifier that processes the anode signal, R_n; shunt conductance in the anode lead, g; shunt capacitance in the anode lead, C.

$$SNR_a = \eta \delta^k I_p e \left[2e^2 \eta \delta^{2k} I_p B + 4k\, TgB \left(1 + R_n g + \frac{4\pi^2}{3} \frac{R_n}{g} B^2 C^2 \right) \right]^{-1/2}$$

Photomultiplier tube: Conditions: high-gain dynodes assumed, gain and output current sufficient so that circuit noise components can be neglected. Terminology: photocathode emission current, i.

$$SNR_a = \left(\frac{\eta I_p}{2B} \right)^{1/2} = \left(\frac{i}{2eB} \right)^{1/2}$$

Photomultiplier tube and scintillator: Conditions: scintillations resulting from gamma-ray photoelectric excitation in the crystal; equal gain per stage assumed. Terminology: full width half maximum, FWHM; photocathode quantum efficiency, η; secondary emission gain per stage, δ; average number of photons incident on the photocathode in each scintillation, $\bar{m}_c$; variance in the number of photons in each scintillation, σ_c^2.

FWHM = 2.355/SNR

$$FWHM = 2.355 \left[\frac{1 - \eta + \frac{1}{\delta - 1}}{\bar{m}_c \eta} + \frac{\sigma_c^2}{\bar{m}_c^2} \right]^{1/2}$$

The first term inside the brackets is the relative variance associated with the photomultiplier; the second term is the relative variance associated with the scintillator.

REFERENCES

127. T. Jorgensen, "On Probability Generating Functions," **Am. J. Phys.,** Vol. 16, p 285 (1948); E. Breitenberger , "Scintillation Spectrometer Statistics," Prog. Nuc. **Phys.,** Vol. 4, (Ed. O.R. Frisch, Pergamon Press, London, p. 56 (1955); William Feller, An In**troduction to Probability Theory and Its Applications,** Vol. 1, John Wiley and Sons, Third Edition (1968).

128. R.H. Brown and R.Q. Twiss, "Interferometry of the intensity fluctuations in light," **Proc. Royal Soc. London,** Vol. 243A, p 291 (1958).

129. W. Shockley and J.R. Pierce, "A theory of noise for electron multipliers," Proc. IRE, Vol. 26, p 321 (1938); V.K. Zworkykin, G.A. Morton, L. Malter, "The secondary emission multiplier-a new electron device," **Proc. IRE,** Vol. 24, p 351 (1936).

130. **G.A.** Morton, H.M. Smith, and H.R. Krall, "Pulse height resolution of high gain first dynode photomultipliers," **Appl. Phys.** Lett., Vol. 13, p 356 (1968).

131. **L.A.** Dietz, L.R. Hanrahan and **A.B.** Hance, "Single-electron response of a porous KCl transmission dynode and application of Polya statistics to particle counting in an electron multiplier," **Rev. Sci. Inst.,** Vol. 38, p 176 (1967).

132. J.R. Prescott, Nuc. **Instr. Methods, A** statistical model for photomultiplier single-electron statistics," Vol. 39, p 173 (1966).

133. M. Schwartz, **Information Transmission, Modulation, and Noise,** McGraw-Hill, p. 207 (1959).

134. F. Robben, "Noise in the measurement of light with photomultipliers," **Appl. Opt.,** Vol. 10, No. 4, pp 776-796, (1971).

135. W.A. Baum, "The detection and measurement of faint astronomical sources," **Astronomical Techniques,** Edited by W.A. Hiltner, The University of Chicago Press, (1962).

Index

Absorptance 18,125
Absorption coefficient 18
Acceptor. 125
Acceptor levels 14
After pulse 57, 125
Aging 58, 75
Air pressure and photomultiplier operation 76
Angle of incidence and photoemission 39,92
Angle of polarization and photoemission .. 39,40
Angstrom unit 125
Anode 3,34,125
Anode current maximum 50
Anode pulse current maximum 47
Anticoincidence circuit. 125
Applications list. ..... Appendix A
Argon arc lamp. 153
Astronomy, application to 5,112
Avalanche photodiodes 8

Background counts 12 5
Band bending 14
Bandwidth and noise spectrum . 59,125,170,171
Basing 88
Beta radiation, effect on photomultiplier 44
Black-body radiation 148
Bleeder 125
Box-andgrid dynode structure 28

Cage 125
Calibration, standard lamp. 92
Candela 125,139
Capacitors, by pass. 84
Carbon-arc lamp 153
CAT scanner ..... See CT-scanner
Cerencov radiation 19,57,92,97,126
Channel multiplier 32,126
Channel number 126
Circular cage 4,27
Coincidence counter., ... 72
Collection efficiency 27
Collection uniformity 41
Color temperature 126,139
Color-temperature standard. 149
Compton effect 93
Conduction band 126
Connections, terminal 88
Constant-fraction triggering 99
Cooling photomultipliers 74
Count 12 6
Counting efficiency 126
Count-rate stability 52,96
Crossed-field photomultiplier 33
Crosstalk 12 6
Cross talk in liquid scintillation counting 73
Cryostats for photomultipliers. 54
CT-scanner 6,7,102,125
Curie 12 6
Current-voltage characteristic 36

Darkcurrent 4,8,16,126
Dark current and noise 54
Dark current and temperature 8
Dark current, increase following exposure to fluorescent lamps 43,58
Dark current, sources of 19,53
Dark noise pulse spectrum 59
Dark noise reduction with cooling 50,54,58
Degaussing 46
Delayline 12 6
Delta function 59,63,126
Densitometry 105
Detectivity 56,90, 126
Deuterium lamp 151
Differential cooling 74
Discriminator, pulse height 126
Discriminator setting 68
Donor 126
Dynamic compression of output signal 87
Dynode ..... .
Dynode, Cs-Sb 96
Dynode, Cu-Be 98
Dynode, GaP:Cs 68,83
Dynode glow. 56
Dynode voltage control 83

EADCI (Equivalent Anode Dark Current Input). 55, 127
E^2B ..... ,
Einstein 10
Electron affinity 13,127
Electron multiplier. 127
Electron optics 26-35
Electron resolution (See also Pulse-height resolution, single electron) 127
Electron volt 20, 127
Electrostatic focus 4
Energy diagram 10, 13,14,94
Energy distribution, photoelectrons 12
ENI (Equivalent Noise Input) 8,9,55,127
Environmental effects 74
Environment, high humidity 76
Environment, pressure 76
ERMA 15,16,127
Escape depth 13,18

Fall time. 62,127
Fatigue 50,51,127
Fatigue and dynode materials 51
Feed back. 4
Fermi-Dirac energy distribution function .. 11,13
Fermilevel 10,11,13,127
Fiber-optic communication systems. 8
Field emission 60
Filters, narrow bandpass color 92,158
Filters, neutral density 91
Fluorescent lamp 154

Fluorometry 106
Flying-spot scanner. ..... .115,127
Focussing electrode ..... .127
Focussing-electrode voltage ..... .42
Foot candle 127
Foot Lambert 127
Forbidden band ..... .13,127
FWHM (Full Width at Half Maximum) . .63,64,127

Gain 3,9,127
Gain control 83
Gain, maximum 75
Gain, variation with temperature ..... .49
Gain, variation with voltage ..... .44
Gamma radiation and glass discoloration .... .43
Gamma-ray camera 6,100,128
Generating functions ..... .160
Glass, browning of ..... .19,77
Glass charging effects ..... .56
Glass, properties of. ..... .19
Glass transmission ..... .19
Ground potential 75

Headlight dimmer 6
Helium penetration ..... .57,76,90
Hertz (Hz) 128
History of photomultiplier development 3-6
Hofstadter 5
"Hysteresis" (cyclic instability) ..... .47,52,127

Illuminance ..... .128,140
Illuminated area, photocathode. ..... .92
Insulator charging ..... .47,52
IPA's (Integrated Photodetection Assemblies) .80
Irradiance 126

JEDEC 13 2
Johnson noise 61

Lambert's cosine law ..... .128,141
Laplace's equation ..... .27
Laser range finding 8,113
Lasers 155-157
Lasers, Nd:YAG 8
Leading edge timing 9 6
Leakage, ohmic ..... .53
Life expectancy..... 3
Light chopper. ..... .92
Light emitting diodes, (LED's) 8,158
Light level for photomultiplier use. ..... .89,90
Light level reduction methods ..... .90,91
Light pipe 95,128
Light shielding ..... .75
Light sources for testing. ..... .158
Linearity..... 4 7
Linearity and photocathode resistivity ..... .47
Linearity and voltage divider current. ..... .82
Linearity measurement. ..... .49
Linearity, pulse measurement of ..... .86
Liquid scintillation counting ... .69,72,87,97,128
Lithium fluoride ..... .19
Lumen(lm)..... 128
Luminance.. ....128.14 0
Luminous efficacy ..... .128
Luminous Intensity ..... .128,129
Lux..... 128

Magnetic defocussing system (reduction of effective photocathode area) 110, 111
Magnetic fields and gain 45
Magnetic focus 3
Magnetic shields 46, 76, 90
Magnetization of photomultipliers 46
Mercury lamp 151, 153
Microchannel-plate photomultiplier ... 33, 65, 128
Mirrors, spherical 91
Moisture condensation 76, 90
Monochromator 92, 143, 144
Mounting 89
Multichannel analyzer 128

NEA (Negative Electron Affinity) . 5, 14, 17, 22, 128
NEP (Noise Equivalent Power) 8, 9, 55, 128
Neutral-density filters 91
Neutral density screens 91
Neutron detection 93
Nit 128
Noise and secondary emission 164
Noise in signal 61, 129
Noise output 58, 128
Noise reduction 58
Noise sources, photomultiplier 169
Noise spectrum 59
Noise, statistical theory ..... Appendix G
Nuclear radiation 77

Ohmic leakage 19
Oil-well logging 71, 99
Opal glass 91
Opaque photocathode 17, 129, 132
Optical enhanced photoresponse 40
Overload protection 87
"Overshoot" 51

Pair production 93
Peak-to-valley 68, 69, 70, 129
Phonon scattering 13, 14
Photocathode 3, 4, 15
Photocathode area 8
Photocathode capacitance 37
Photocathode characteristics, table 16
Photocathode current, maximum 37
Photocathode, damage by ionic transport 42, 43, 56, 57
Photocathode, exposure to uv 43
Photocathode, pulse current maximum 37
Photocathode resistivity 36, 37, 43, 90
Photocathode stability 42
Photocathode thickness 17
Photocathode type: Ag-O-Cs 4, 15
Photocathode type: Cs_3Sb 4, 15, 16
Photocathode type: K_2CsSb 5, 15, 16
Photocathode type: Na_2KSb 5, 15, 16
Photocathode type: Na_2KSb:Cs 4, 15, 16
Photocathode type: Rb_2CsSb 15, 16
Photocathode, undercoating for 37, 83
Photocathode uniformity 40
Photocell 7, 129
Photoconductivity 13
Photoelectron 3
Photoemission noise 161
Photoemission, theory 10, 13
Photographic film, quantum efficiency of 5

Photography, automatic exposure control 7
Photometer, color balancing for color prints .. 105
Photometer, logarithmic 106
Photometric units 139
Photomultiplier 129
Photomultiplier as a photodiode 83
Photon counting 66, 109–112, 129
Photon noise 161
Photopic vision 129, 138
Planck's equation 148
Plateau 70, 129
Poisson distribution 164
Polarized light and photoemission 39
Polution monitoring 7
Polya statistics 164
Positron 93
Positron camera 104
Potential, bulb 56
Potting 89
Power supply ground 81
Power supply requirements 80
Pre-pulse 35
Pulse counting 66
Pulse counting statistics 172
Pulsed operation 113
Pulse-height analyzer 129
Pulse-height-distribution, background 67, 96, 110, 111
Pulse-height-distribution, ^{137}Cs 69
Pulse-height-distribution, differential 66, 67
Pulse-height-distribution, ^{55}Fe 69
Pulse-height-distribution, integral 67, 68
Pulse-height distribution, single electron 59, 67, 112
Pulse-height-distribution, tritium 72
Pulse height vs count rate 52
Pulse-height resolution 69, 129, 173
Pulse-height-resolution and temperature 100
Pulse-height spectrum 69
Pulse-height stability 53
Pulse jitter 64, 129
Pulse width 64, 129
Pyroelectric detector for radiation calibration 144

Quantum Efficiency (Q.E.) 11, 129, 143

Rad 129
Radar jammer 5
Radiance 129
Radiant energy sources 148
Radiant intensity 129
Radioactive contaminants 97
Radioactive isotopes in photomultipliers 57
Raman spectroscopy 108
Reflectance 18, 129
Refrigerated operation 50, 74
Regenerative effects and dark current .. 20, 54–57
Rem 129
Resistance network as an analogue computer . 27
Resistance per square 36, 129
Responsivity 130, 142
Richardson equation 20
Ringing 85
Rise time 3, 62, 64, 130
Roentgen 130
Rubber dam, electron-optical analogue 4, 26
Ruggedization 77

Sapphire windows 19
Scintilation counting 5, 69, 92, 130
Scintillation process 93, 94
Scintillator coupling 95
Scintillator material: BGO (bismuth germanate) 6, 103
Scintillator material: $CdWO_4$ 103
Scintillator material: glass 68
Scintillator material: NaI:Tl 5, 94
Scintillator statistics 69, 70, 95
Scotopic vision 130, 137, 138
Secondary electron 3
Secondary electron, energy distribution 23
Secondary emission 21, 130
Secondary emission noise 164
Secondary emission ratio, δ 21
Secondary emitter: Ag-O-Cs 5, 22
Secondary emitter: BeO:Cs 5, 23
Secondary emitter: Cs_3Sb 5, 22
Secondary emitter: GaP:Cs 5, 22
Secondary emitter: K_2CsSb 22
Secondary emitter: MgO 5, 22, 23
Secondary emitter: Na_2KSb:Cs 22
Secondary emitter: Rb-Cs-Sb 22
Selection criteria for photomultipliers 80
Semiconductor energy-band model 13
Semitransparent photocathode 17, 130, 132
Shield potential 56, 75, 81
Shock and vibration 76
Shot noise 60
Signal-to-noise and bandwidth 62
Signal-to-noise ratio 8, 60, 169, 171–175
Signal output compression 87
Signal voltage output, maximizing 86
Silicon p-i-n diode vs photomultiplier 8, 9, 80
Simon, R.E. 5
Single-electron counting 68
Smoke detectors 8
S-numbers 16, 132
Socket 86
Solid-state photodetectors 6
Sommer, A.H. 4
Sound on film 3
Space charge 47, 86
Spectral absorptance, semi-transparent photocathodes 17
Spectral absorption, semi-transparent photocathodes 18
Spectral emissivity 148
Spectral luminous efficacy 130, 137
Spectral matching factor 146
Spectral response: Ag-O-Cs 15, 17
Spectral response, alkali metals 12
Spectral response, Bi-alkali 15
Spectral response: Cs_3Sb 15
Spectral response designation 132
Spectral response difference; photocathode vs anode 145
Spectral response: ERMA 15
Spectral response: GaAs:Cs 17
Spectral response: $In_{18}Ga_{82}As$:Cs 17
Spectral response: K_2CsSb 15
Spectral response: Na_2KSb 15
Spectral response: Na_2KSb:Cs 15, 17
Spectral response: Rb_2CsSb 15

Spectral response, range for photomultipliers 80
Spectral response, source-detector matching . 143
Spectrometry 5, 7, 104
Spectrometry, absorption 107
Spectrophotometry 105
Speed of response 8, 80
Spot size 92
Stability, photomultiplier 9, 49
Storage, photomultiplier 43, 75, 90
Stray light 75
Super-market check-out system 117

Tea-cup dynode 29, 42, 96, 130
Temperature and plateau characteristic 71
Temperature, maximum for photomultiplier 8, 49, 74
Temperature, minimum for photomultiplier 50
Temperature, photocathode resistivity variation with 37
Temperature, spectral response variation with 38
Thermionic emission 19, 54
Thermopile, for radiation calibration 144
Time-domain reflectometer 86
Time jitter 130
Time lag, photoemission and secondary emission 24, 63
Time resolution 33, 65
Time resolution statistics 66
Time response 32
Time spectroscopy 98
Time-to-amplitude converter (TAC) 130
Tomography 102
Transit time 32, 62, 63
Transit-time difference 32
Transit-time spread 130
Transmission-mode photocathode 130
Transmittance 18, 130
Tritium 72
Tungsten-halogen lamps 144, 149
Tungsten-halogen lamps, spectral irradiance of 152
Tungsten lamps 148
Tungsten lamps, spectral irradiance of 150

Ultraviolet radiation, damage to photocathode from 43

Voltage dividers for pulsed operation 83
Voltage divider, resistance values for 82
Voltage dividers, tapered 86
Voltage maximum 75
Voltage pulsing, photomultiplier 113
Voltage stability requirement 80

Work function 10, 11, 20, 131

Xenon arc lamp 153
X-radiation, glass discoloration resulting from 43
X-ray scanner 102

Zero-crossover timing 98
Zirconium concentrated arc lamp 151